ISTANBUL TECHNICAL UNIVERSITY ★ GRADUATE SCHOOL OF SCIENCE ENGINEERING AND TECHNOLOGY

INVESTIGATION OF SORPTION INDUCED PLASTICIZATION IN POLYMERIC CO_2 SEPARATION MEMBRANES

Ph.D. THESIS

Sadiye VELİOĞLU

Department of Materials Science and Engineering

Materials Science and Engineering Programme

NOVEMBER 2014

ISTANBUL TECHNICAL UNIVERSITY ★ GRADUATE SCHOOL OF SCIENCE ENGINEERING AND TECHNOLOGY

INVESTIGATION OF SORPTION INDUCED PLASTICIZATION IN POLYMERIC CO_2 SEPARATION MEMBRANES

Ph.D. THESIS

Sadiye VELİOĞLU
(521082006)

Department of Materials Science and Engineering

Materials Science and Engineering Programme

Thesis Advisor: Prof. Dr. Ş. Birgül TANTEKİN-ERSOLMAZ
Thesis Co-Advisor: Assoc. Prof. Dr. M. Göktuğ AHUNBAY

NOVEMBER 2014

İSTANBUL TEKNİK ÜNİVERSİTESİ ★ FEN BİLİMLERİ ENSTİTÜSÜ

**POLİMERİK CO_2 AYIRMA MEMBRANLARINDA
PLASTİZASYONUN İNCELENMESİ**

DOKTORA TEZİ

**Sadiye VELİOĞLU
(521082006)**

Malzeme Bilimi ve Mühendisliği Anabilim Dalı

Malzeme Bilimi ve Mühendisliği Programı

**Tez Danışmanı: Prof. Dr. Birgül TANTEKİN-ERSOLMAZ
Tez Eş-Danışmanı: Doç. Dr. Göktuğ AHUNBAY**

KASIM 2014

Sadiye VELİOĞLU, **a Ph.D.** student of ITU **Graduate School of Science Engineering and Technology** student ID **521082006,** successfully defended the **thesis/dissertation** entitled "**INVESTIGATION OF SORPTION INDUCED PLASTICIZATION IN POLYMERIC CO$_2$ SEPARATION MEMBRANES**", which she prepared after fulfilling the requirements specified in the associated legislations, before the jury whose signatures are below.

Thesis Advisor :   **Prof. Dr. Ş. Birgül TANTEKİN-ERSOLMAZ** ....
İstanbul Technical University

Co-advisor :   **Assoc. Prof. Dr. M. Göktuğ AHUNBAY** ....
İstanbul Technical University

Jury Members :   **Prof. Dr. Hüsnü ATAKÜL** ....
İstanbul Technical University

Prof. Dr. Oğuz OKAY ....
İstanbul Technical University

Prof. Dr. Türkan HALİLOĞLU ....
Boğaziçi University

Prof. Dr. Pemra DORUKER ....
Boğaziçi University

Assoc. Prof. Dr. Seda KESKİN-AVCI ....
Koç University

Date of Submission : 29 August 2014
Date of Defense   : 28 November 2014

To my spouse and daughter,

FOREWORD

Finally, I would like to thank with all my heart to my darling. This doctorate would not have been possible without the unselfish support of my loving husband, Murat VELİOĞLU. He has shouldered so many responsibilities during my PhD studies and made this process a success.

September 2014   Sadiye VELİOĞLU

TABLE OF CONTENTS

ABBREVIATIONS

2,6-DAT : 2,6-diaminotoluene
4MPD, TeMPD: 2,3,5,6-tetramethyl-1,4-phenylene-diamine
4PDA : 2,4,5,6-trimethyl-1,4-phenylene-diamine
6BpB : 6FDA/BTDA-pBAPS
6FDA : 4,4-hexafluoroisopropylidene-diphthalic anhydride
6FmDA : 3,3'-hexafluoroisopropylidene dianiline
6FpDA, 6FAP: 4,4'-(hexafluoro-isopropylidene) dianiline
6pBD : 6FDA-pBAPS/DABA
6pBmP : 6FDA-pBAPS/mPDA
BADS : 4,4'-bis(3-aminophenoxy)- diphenyl sulfone
BCDA : bicyclo(2.2.2)-oct-7-ene-2,3,5,6-tetracarboxylic dianhydride
bis-APAF : 2,2-bis-(4-carboxyphenyl) hexafluoropropane
BPADA : 2,2-bis[4-(3,4-dicarboxyphenoxy) phenyl]propane dianhydride
BPDA : 3,3',4,4'-biphenyltetracarboxylic dianhydride
BTDA : 3,3-4,4-benzophenone tetracarboxyclic dianhydride
CED : Cohesive Energy Density
CH$_2$Cl$_2$: Dichloromethane
COMPASS : Condensed-phase Optimized Molecular Potentials for Atomistic Simulation Studies
DABA : 3,5-diamino benzoic acid
DAM : 2,4,6-trimethyl-m-phenylene diamine
DANT : 1,5-diaminonaphthalene
DBTF : 3,5-diaminobenzotrifluoride
DDBT : 3,7-diamino-2,8(6)-dimethyldibenzothiophene sulfone
DMA : Dynamic Mechanical Analyzer
DMAc : Dimethylacetamide
DMDA : 2,2-dimethyl-1,3-(4-aminophenoxy) propane
DMF : Dimethylformamide
DPX : 2,5-dimethyl-p-phenylenediamine
DSC : Differantial Scaning Calorimetry
DSDA : 3,3',4,4'-biphenylsulfone tetracarboxylic dianhydride
Durene : 2,3,5,6- tetramethyl-1,4-phenylenediamine
FAV : Fractional Accessible Volume
FFV : Fractional Free Volume
FTIR : Fourier Transform Infrared Spectroscopy
GC : Gas Chromatogram
GPC : Gel Permeation Chromatography
HQDPA : 1,4-bi(3,4-dicarboxyphenyl) benzene dianhydride
IGA : Intelligent Gravimetric Analyser
MC : Monte Carlo
MD : Molecular dynamics
MDA : 4,4'-methylenedianiline

mDDS	:	3,3'-diaminodiphenyl sulfone
MDI	:	4,4'-diphenyl-methane diisocyanate
mMPD	:	2-methyl-m-phenylenediamine
MOCA	:	4,4'-methylene bis(2-chloroaniline)
MOMDA	:	3,3',dimethoxy -4,4'-diaminediphenylmethane
mPDA	:	1,3-phenylenediamine
MSD	:	Mean Square Displacement
μVT	:	Grand canonical ensemble
NDA	:	1,5-naphthalene
NMP	:	N-methyl-2-pyrrolidone
NPT	:	Isothermal-isobaric ensemble
NVE	:	Microcanonical ensemble
NVT	:	Canonical ensemble
ODA	:	4,4-oxydianiline
o-DCB	:	Ortho-dichlorobenzene
ODPA	:	4,4'-oxydiphthalic anhydride
P	:	Permeability
pBAPS	:	bis [4-(4-aminophenoxy) phenyl] sulfone
PIs	:	Polyimides
PMDA	:	Pyromellitic dianhydride
pPDA	:	1,4-phenylenediamine
PVA	:	Polyvinyl alcohol
PTMSP	:	poly(1-trimethylsilyl-1-propyne)
RDF, g(r)	:	Radial Distribution Function
RTCF	:	Root Time Correlation Function
RU	:	Repeat Unit
SiDA	:	(3,4-dicarboxyphenyl) dimethylsilane dianhydride
SRCs	:	Sorption Relaxation Cycles
TDI	:	2,4-toluene-diisocyanate
Tg	:	Glass Transition Temperature
TGA	:	Thermogravimetric Analysis
THF	:	Tetrahydrofurane
TMMDA	:	Tetramethyl methylenedianiline
TR	:	Thermally-Rearranged
TST	:	Transition State Theory
WAXD	:	Wide Angle x-ray Diffraction
σ|ϕ|	:	Standard deviation of the dihedral angle distribution of dianhydride-diamine linkage based on the absolute value
α	:	Selectivity

LIST OF FIGURES

INVESTIGATION OF SORPTION INDUCED PLASTICIZATION IN POLYMERIC CO$_2$ SEPARATION MEMBRANES

SUMMARY

Understanding the factors effecting the separation properties of membranes is important for membrane industry. Most commercial gas separation membranes are prepared from glassy polymers which are affected by highly sorbing gases. Plasticization is a pressure dependent phenomena and occurs when the concentration of gases, such as CO$_2$, H$_2$S, and condensable hydrocarbons, such as propylene and propane, in glassy polymers is high enough to cause swelling in the polymer, i.e. disrupt chain packing and increase fractional free volume (FFV) and inter-segmental mobility. Hence, the selectivity of the membrane decreases significantly due to the loss in size discrimination ability. Moreover, plasticization often results in higher gas flux but lower mixed gas selectivities, particularly at high pressures, therefore it is important to test membranes with mixed gas compositions.

The relative increase in permeability and plasticization pressure vary from polymer to polymer, highlighting the continuing need to explore plasticization in greater depth as new materials are developed. A fundamental understanding of penetrant induced plasticization is needed to design high performance membranes. Considering the difficulties associated with high pressure separation experiments, advances in molecular modelling can be a remarkable tool to quantitatively investigate penetrant induced plasticization and understand the physics behind it.

In this thesis, molecular simulation techniques were used to estimate the degree of CO$_2$ induced plasticization in various 4,4-hexafluoroisopropylidene-diphthalic anhydride based polyimides (PIs), co-PIs and a thermally rearranged polymer known as polybenzoxazole. The structural properties, such as glass transition temperature, FFV and its distribution, d-spacing, and cohesive energy density, along with sorption isotherms were investigated to understand the dynamics of these polymeric membranes and compared with experimental results. The sorption simulations were carried out in the Grand Canonical Monte Carlo ensemble. To reproduce the CO$_2$-induced plasticization effect, sorption-relaxation cycles (SRCs) were applied until the CO$_2$ concentration converges. The increase in the FFV of the resulting polymer structure was considered as the extent of plasticization.

Results indicate that the FFV of the swollen PI or the increase in FFV after SRCs depend on two factors: (1) the backbone flexibility which was defined by using dihedral distribution of dianhydride-diamine linkage and (2) particular interactions between CO$_2$ and defined sorption sites in polymer repeat unit which was supported by radial distribution functions (RDFs) in this study. For instance, the linkages which are present in the backbone of polymer chain such as –SO$_2$– and –O– may lead to an increase in polymer flexibility and hence the plasticization effect. On the other hand, the side groups such as –CF$_3$, –CH$_3$ and –COOH may affect the polymer backbone with different interactions between CO$_2$ and decrease the plasticization effect. This

proposal may lead to an efficient screening of suitable combinations of diamine and dianhydride pairs among hundreds that are resistant to sorption-induced plasticization.

POLİMERİK CO$_2$ AYIRMA MEMBRANLARINDA PLASTİZASYONUN İNCELENMESİ

ÖZET

Membranların ayırma özelliklerine etki eden faktörlerin belirlenmesi membran endüstrisi için çok önemlidir. Ticari gaz ayırma membranlarının çoğu camsı polimerlerden üretilmektedir ve bu polimerler yüksek miktarlarda adsorbe olabilen gazlarla etkileşime girerek membran özelliklerinin değişmesine sebep olan plastizasyona maruz kalmaktadır. Plastizasyon basınca bağlı bir olaydır ve CO$_2$, H$_2$S ve propan, propilen gibi hidrokarbonların konsantrasyonlarının poliimid gibi camsı polimerlerde yeterince yüksek olduğu durumlarda polimer matrisinin şişmesi nedeniyle oluşmaktadır. Böylece polimerin serbest hacmi ve segmentel hareketliliği artarak polimer zincirindeki birbirine yakın segmentler arasındaki etkileşim azalmaktadır. Bunun sonucunda membranın boyut ayırım yetisini kaybetmesinden dolayı membran geçirgenliği artmakta ve seçiciliği düşmektedir. Plastizasyon yüksek basınçlarda, yüksek gaz akış hızlarında gaz karışımları için daha düşük seçicilik değerlerinin elde edilmesine neden olmaktadır. Bu yüzden her zaman saf gazlar yerine gaz karışımları için testler yapmak daha doğru sonuçlar verecektir.

Polimerlerin yapılarına bağlı olarak plastizasyon basınçları ve geçirgenliklerdeki artış miktarları değişmektedir. Yeni malzemeler geliştirildikçe, gaz ayırma performansını etkilediğinden dolayı plastizasyon basıncının belirlenmesi giderek önem kazanmaktadır. Plastizasyonun etkisini azaltarak sürdürülebilir membran performansı elde etmek için bazı özel önlem veya stratejiler gereklidir. Moleküler modellemedeki ilerlemeler CO$_2$'in polimerler üzerindeki plastizasyon etkisinin incelenmesinde ve altındaki fiziğin anlaşılmasında kullanılabilir.

Bu çalışmada, 4,4-(heksafloroizopropiliden) difitalik dianhidrit bazlı poliimidler, kopoliimidler ve polibenzoksazol olarak bilinen ısıl işlemle kimyasal yapısı düzenlenebilen poliimidlerde CO$_2$ plastizasyonu probleminin moleküler simülasyon yöntemleri ile incelenmesi ve moleküler yapı ile plastizasyon arasındaki ilişkilerin ortaya çıkarılması amaçlanmıştır. Elde edilen poliimid yapıları için dönüş yarıçapı, x-ışını spektrumu, kohesiv enerji yoğunluğu, kısmi serbest hacim (FFV) ve camsı geçiş sıcaklığı polimerik membran malzemelerinin dinamiğini anlamak için hesaplanmış ve deneysel verilerle karşılaştırılmıştır. Grand Kanonik Monte Carlo simülasyonları yardımıyla adsorpsiyon simülasyonu gerçekleştirilmiştir. CO$_2$'in adsorpsiyonundan kaynaklanan plastizasyon etkisini görebilmek için adsorpsiyon-dengeleme adımları (SRCs), bir önceki yapı ile en son yapı arasındaki şişme oranı değişmeyinceye kadar uygulanmıştır. FFV değerindeki artış, plastizasyon etkisinin bir göstergesi olarak kullanılmıştır.

Moleküler yapı ile plastizasyon arasındaki ilişkinin ortaya çıkarılması için öncelikle üç farklı poliimid yapısı çalışılmıştır. 35°C ve 10 bar'da yapılan CO$_2$ adsorpsiyon ölçümlerinde, CO$_2$ adsorpsiyon kapasitesi ile şişen polimerin FFV değeri orantılıdır.

Diğer bir deyişle, aynı FFV değerine sahip olan poliimidler aynı CO_2 konsantrasyonuna sahiptirler. Polimer zincirindeki bazı adsorpsiyon birimleriyle CO_2 betkileşimlere girerek polimerin konfigürasyonunu değiştirmekte ve FFV değerinde artışa sebep olarak poliimidin plastize olmasını sağlamaktadır. Ayrıca bu sonuç, serbest hacim dağılımından da elde edilebilmektedir. Poliimidlerin başlangıçtaki hacim dağılımları farklılık gösterirken CO_2 adsorpsiyonundan sonra hacim dağılımları aynı olmuştur. RDF'ler de poliimidlerin plastizasyona karşı olan dayanıklılıklarının, CO_2'in polimer zincirindeki dianhidrit ile diamin arasındaki bağa ulaşılabilirliği ile ilişkili olduğunu göstermektedir.

Aynı poliimidler de 25°C ve 1.13 bar'da propan ve propilen adsorpsiyon ölçümleri yapıldığında CO_2 gibi bir ilişki görülmemiştir. Propan ve propilenin farklı adsoprsiyon bölgelerini tercih ettiği görülmüştür. Bu yüzden plastizasyonda FFV değerlerinin yanında adsorplanan gaz molekülleri ile polimer yapısında moleküllerin birbirleri ile olan etkileşimlerinin de adsorpsiyonda etkin rol oynadığı görülmüştür.

Son yıllarda yapılan çalışmalarda, polimerik membran film dökümü sırasında kullanılan çözücünün membran performansında etkili olduğu kanıtlanmıştır. Farklı çözücüler kullanılarak farklı gaz geçirgenlik ve seçicilik değerleri elde edilmiştir. Bunun nedenin ise çözücülerin farklı kaynama noktasına sahip olmalarından dolayı polimerin istenilen konsigürasyonuna alabilmesi için yeterli süreye izin verip vermemesinden kaynaklandığı iddia edilmektedir. Ayrıca polimer matrisi içerisinde kalan çözücülerinde plastizasyona sebep olarak membranın farklı performans sergilemesine sebep olduğu gözlenmiştir. Yapılan çalışmalarda, üstün kurutma çalışmalarına rağmen belli oranda çözücünün polimerin içine hapsolduğu bulunmuştur. Ayrıca az miktarda polimer içine hapsolan çözücünün antiplastizasyon özelliği gösterdiği görülmüştür. Bu tez kapsamında 6FDA-DAM ve 6FDA-ODA polimerlerine ağırlıkça % 1, 2 ve 4 NMP ve THF çözücülerinin etkisi incelenmiştir. Yüksek çözücü içeriğinde CO_2 ve çözücü sayesinde FFV değerlerinde çok daha fazla artış görülmüştür. Çok az çözücünün bile ayırma performansında değişikliklere sebep olduğu doğrulanmıştır. Ayrıca her iki polimerde de NMP çözücüsünün CO_2 ile farklı etkilerden (plastize ve anti-plastize) dolayı yarış halinde olduğu, % FFV artış değerlerindeki minimumdan gözlenebilmektedir.

Yapı-geçirgenlik ilişkilerinin deneysel olarak belirlenmesi oldukça zahmetli, masraflı ve zaman alan bir süreç olduğundan bu ilişkinin teorik olarak belirlenebilmesi potansiyel membran malzemelerinin ortaya çıkarılmasına olanak vermektedir. Daha önce Park ve Paul tarafından bazı polimerlere uygulanmış olan grup katkısı yöntemi ile Alentiev v.d. tarafından poliimidlere uygulanmış olan grup katkısı yöntemi kopoliimidlere uygulanarak, geçirgenlik ve seçiciliklerinin hesaplanması amaçlanmıştır. Bunun için literatürde sentezlenmiş olan kopoliimidlere ait deneysel geçirgenlik değerleri belirlenmiş ve bu kopoliimidlerin geçirgenlikleri ve ideal seçicilikleri söz konusu grup katkısı yöntemleri ile hesaplanmıştır. Her iki yöntem de kopoliimidlere uygulanabilmiş ancak Alentiev v.d. tarafından önerilmiş olan grup katkısı yönteminin deneysel değerlere daha yakın sonuçlar verdiği görülmüştür. Daha sonra farklı monomer kombinasyonları yapılarak yeni 2200 tane kopoliimid için Alentiev v.d. yönteminin grup katkısı yöntemiyle H_2, O_2, He, CO_2, N_2, ve CH_4 geçirgenlikleri ve O_2/N_2, CO_2/CH_4, H_2/CO_2, H_2/N_2, ve CO_2/N_2 seçicilikleri hesaplanmıştır. Özellikle CO_2 gaz ayrımı için üstün performans gösteren kopoliimidler belirlenmiştir.

Bu kısımda, bir önceki bölümde seçilmiş olan 6FDA/BTDA-pBAPS, 6FDA-pBAPS/mPDA ve 6FDA-pBAPS/DABA kopolimidlerinin plastizasyon davranımı incelenmiştir. Bilindiği gibi membranların endüstriyel alanda kullanılabilmesi için üstün performanslarının yanında plastizasyona karşı dirençli olması da istenmektedir. Üç kopoliimid arasında 6FDA/BTDA-pBAPS en yüksek CO_2 ve CH_4 adsorpsiyon katsayısına sahiptir, bu da 6FDA/BTDA-pBAPS kopoliimidinin plastizasyon davranımı modellendikten sonra elde edilen kısmi serbest hacmin en yüksek olduğunu göstermektedir. Kopoliimid matrislerinin FFV değerleri dengeleme sonrası aynıyken, plastizasyon davranımı modellendikten sonra değişmiştir. 6FDA-pBAPS/DABA kopoliimidi en düşük FFV'a sahiptir. Bunun nedeni yüksek Tg'ye sahip olmasından da anlaşıldığı gibi sert bir iskelete sahip olmasıdır. RDF'ler incelendiğinde, bütün kopoliimidlerde pBAPS diaminindeki sülfon grubu CO_2 tarafından en çok tercih edilen sorpsiyon bölgesidir. CO_2'in bu bölgeye tercihi en çok 6FDA/BTDA-pBAPS kopoliimidinde gözükürken, en az 6FDA-pBAPS/DABA kopoliimidinde görülmüştür. Diğer tercih edilen bölgeler ise dianhidritlerdeki azot ve oksijen gruplarıdır. 6FDA-pBAPS/DABA kopoliimidinde diğer kopoliimidlere nazaran DABA diaminindeki oksijen grubu da CO_2 için önemli bir sorpsiyon bölgesidir ve bu grup polimer zincirinin sertliğini arttırmaktadır.

En son kısımda ise ısıl işlemle yapısı değiştirilmiş polimerlerin plastizasyon davranımı incelenmiştir. Temelde bu polimerler polibenzoksazollerdir, fakat bir çok çözücüde çözünemememelerinden dolayı membran alanında uzun yıllar boyunca kullanılmamışlardır. Ancak bazı poliimidlerin ısıl işelmle reaksiyona girip bu polimerlere dönüştüğü keşfedilmiş ve ilk önce poliimid sentezleyip, film oluşturup daha sonra termal işleme tabi tutarak bu polimerler elde edilmiştir. Yüksek gaz ayırma performanslarından dolayı ilgi görmüşlerdir. Bu polimerlerde, diamin ile dianhidrit arasında yer alan bağdaki azot atomu poliimidlerdeki gibi ana zincirde değil, beşli halkanın içerisinde yer almaktadır. Simülasyon çalışmalarında CO_2'in azot atomuna olan afinitesi bu polimerde poliimidlere göre daha azdır. Hem CO_2 affinitesisn daha az olması hem de bu polimerlerin zincir iskeletinin sert olmasından dolayı plastizasyona karşı daha dayanıklı olduğu ve 40 atm'de bile poliimidlere kıyasla çok az FFV değerinde artış olduğu yapılan simülasyon çalışmasında görülmüştür.

Sonuç olarak, platizasyonu incelerden FFV değerindeki artış önemli bir parametre olarak kullanılmıştır. Şişmiş poliimid yapısının FFV değerinin veya SRCs adımlarının sonunda elde edilen FFV değerindeki artışın iki faktöre bağlı olduğunu göstermektedir. Bunlar, dianhidrit ile diamin bağının dihedral açısının dağılımı yardımıyla gözlenilen polimer iskeletinin esnekliği ve radyal dağılım fonksiyonu ile desteklenen, CO_2 ile polimerin tekrarlanan birimindeki adsorpsiyon gruplarının etkileşimidir. Örneğin, $-SO_2-$ ve $-O-$ gibi grupların polimer zincirinin iskeletinde yer alması esneklik kazandırarak plastizasyonu arttırırken, $-CF_3$, $-CH_3$ ve $-COOH$ gibi yan grupların varlığı da çeşitli etkileşimlerle polimer zincirine etkileyerek plastizasyon etkisini azaltmaktadır. Bu bulgu, birçok dianhidrit ve diamin arasından, CO_2'in adsorpsiyonundan kaynaklı plastizasyona dayanıklı en uygun bileşimi incelememizi sağlayabilir.

1. INTRODUCTION

Membrane based gas separation processes are getting attention in separation of many commercially important gas pairs such as O_2/N_2, CO_2/CH_4, H_2/CH_4, H_2/N_2, CO_2/N_2, H_2/CO_2 and olefins/paraffins. The outstanding properties of membrane-based gas separation processes that attract the gas separation industry are the low capital and operating costs, low energy requirements, and ease of operation.

In commercial applications, it is desirable that gas separation membranes should exhibit high permeability and selectivity as well as thermal, mechanical, and chemical resistance. While the most important criterion is the selectivity of membrane, other criteria are also required for a membrane material to succeed, and become commercially viable. Synthesizing membrane materials that provide these criteria is a major goal of membrane research. Among various polymeric membrane materials in gas separation area, aromatic polyimides (PIs) draw attention due to their outstanding thermal and chemical stability, and good mechanical properties. Polyimide membranes also govern selectivity towards separation of commercially important gas pairs such as O_2/N_2, CO_2/CH_4, H_2/CH_4, H_2/N_2 and propylene/propane.

Recently, CO_2/CH_4 separation become important in natural gas purification. While the natural gas is fed to pipeline, gas composition should be in some limits. Due to this limitation, purification of natural gas becomes an essential process. The large amount of CO_2 in natural gas not only reduces the energy content of the mixture, but also CO_2 is acidic thus, likely to induce corrosion of pipelines. In addition to CO_2/CH_4 gas separation, CO_2/N_2 gas separation is also important for the reduction of greenhouse gas emissions by the capture of CO_2 from flue gases followed by underground sequestration. Another CO_2 separation process is the CO_2 removal from syngas which is the product of coal gasification process and mainly contains H_2. As a result, CO_2 comes up with an essential hazardous gas that should be removed from gas mixtures before or after use in many processes. However, the use of polymeric gas separation membranes for CO_2 and hydrocarbon separations is limited by plasticization-induced selectivity losses in feeds with significant partial pressures of

CO_2 and C_3+ hydrocarbons [1-3]. Altough polyimides high selectivity and permeability properties, plasticization is the main drawback of PIs as well.

The key to controlling plasticization is to control the membrane swelling, since it is related to the increase in polymer chain segmental mobility facilitated by the penetrant gas (such as CO_2) sorption. As the the interaction between the polymer segments and the penetrant gas increases, gas permeability increases and selectivity decreases.

In recent years, studies about gas separation membrane plasticization has increased significantly in the literature. Several approaches for stabilizing membranes against plasticization, along with some practical constraints has been introduced. The accepted opinion is that plasticization should be minimized by proper molecular design of the membrane materials in order to overcome the permselectivity reduction. A fundamental understanding of penetrant induced plasticization is needed to achieve this. Advances in molecular modeling provide an opportunity to quantitatively investigate penetrant induced plasticization and understand the physics behind it. Only a few simulation studies investigating plasticization have been reported in the literature while there are many experimental studies.

In this chapter, an overview of the polymeric gas separation membranes and polyimides is provided. Theory and methods employed for gas separation are presented follwed by further description of sorption induced plasticization effect. Finally, the organization of dissertation is clarified.

1.1 Polymeric Gas Separation Membranes

A membrane is a thin barrier between two phases, through which differential transport occurs under a variety of driving forces across the membrane. Driving force can be pressure, chemical potential, electrical potential and temperature difference. Feed gas is separated into two gas streams that are rich from one of the gas components as shown in Figure 1.1. Membrane modules may be packaged as flat sheets (plate-in-frame or spiral wound), tubes, or hollow fibers.
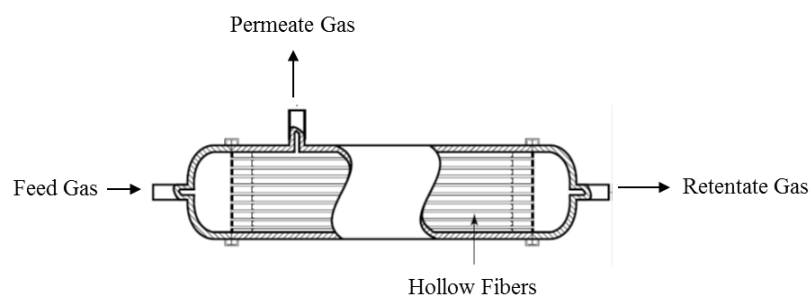
Figure 1.1 : A schematic representation of hollow fiber module [4].

Gas separation has become a major industrial application of membrane technology only during the past 20 years, but the study of gas separation has a long history. Recently, gas separation membranes have reached the high sailing rates. The main reason of this increase is that membrane separation processes are more efficient, cheaper and easier to handle than traditional separation processes such as cryogenic distillation, adsorption and filtration. Mainly polymeric gas separation membranes get the share of ındustrial use due to their ability to form stable, thin, defect-free, low cost membranes that can be packaged into high-surface area modules. Polymeric gas separation membranes are used in many areas such as obtaining high purity N_2 from air, air production with high oxygen concentration, CO_2 separation from natural gas and CO_2, He recovery, volatile organic compounds separation from light gases, and organic solvent separation from air. Application of the membrane technology is expanding rapidly and further growth is likely to continue for the next 10 years or so.

Gas transport in polymeric gas separation membranes is governed by the solution-diffusion mechanism: gas molecules are first adsorbed by the polymer on the feed side of the membrane, and then they diffuse across the membrane cross-section via transient gaps in the polymer matrix, and are desorbed from the other surface of the membrane. The performance of a polymeric gas separation membrane is dependent on the permeability and selectivity properties of the polymer it is manufactured from. Permeability is related to diffusion coefficient which represents the mobility of gas molecules in the polymeric material and sorption coefficient which represents the thermodynamic effect. Selectivity is a measure of the efficiency of a membrane to separate one gas from another. While high permeability decreases the need for large membrane area, high selectivity enables obtaining high purity products.

3

Polymeric gas separation membranes have generally high permeability and low selectivity or vice verse. Despite the focused attempts at tailoring membrane structure to obtain desirable separation properties, polymers seem to have reached a productivity/selectivity trade-off. A permeability-selectivity trade-off curve was described by Robeson in 1991 [5] and revisited in 2008 [6] for O_2/N_2, H_2/N_2, He/N_2, H_2/CH_4, He/CH_4, CO_2/N_2, H_2/CO_2 and CO_2/CH_4 gas pairs. Figure 1.2 shows the upper-bound for CO_2/N_2, H_2/CO_2 and CO_2/CH_4 gas pairs, with selectivity versus permeability of faster-permeating gas. Robeson put all the ideal transport properties of polymers in a graph and defined a so-called upper-bound, which shows the upper limit for the performance of polymeric membranes. Heterogeneous membranes, surface modified membranes and molecular sieve membranes are not taken into the group of polymeric materials employed for constituting the upper bound correlation. It should be noted that several of the polymers constituting the majority of the population within the adjacencies of the upper bound line have structural characteristics that start approaching molecular sieving type structures. Polyimides can be given as an example to that kind of polymeric materials. A benzoxazole phenylene structure which is employed with a solid state thermal transformation of a polyimide is an example for a new type of molecular sieving structures with remarkable CO_2/CH_4 separation shown in Figure 1.2 a) with blue dots [7]. The thermal transformation yielded insoluble and infusible polymers with molecular sieving pore dimensions.
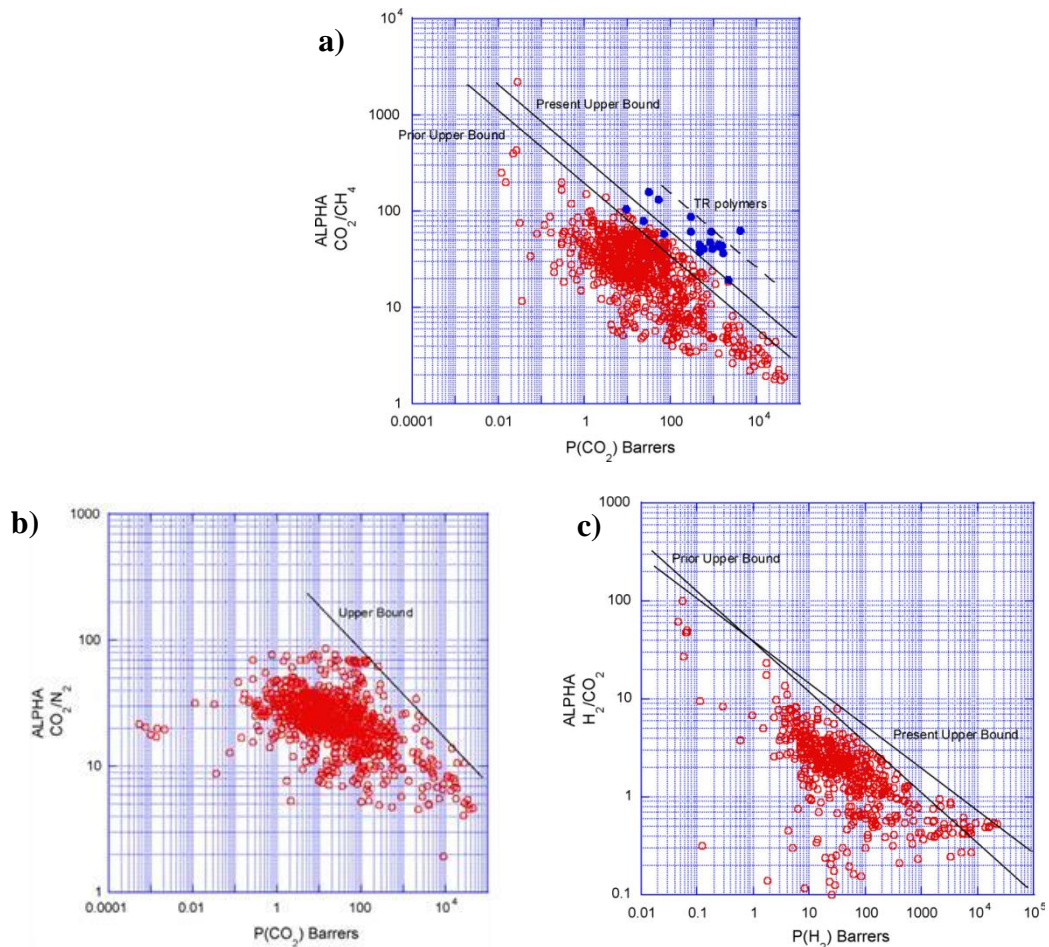
Figure 1.2 : Robeson trade-off maps [6] for a) CO_2/CH_4, b) CO_2/N_2 and c) H_2/CO_2 separation applications. Prior and present upper bounds refer to the upper bounds of Robeson presented in 1991 and 2008 respectively.

1.2 Polyimides

Aromatic engineering polymers such as polysulphones, polycarbonates and polyimides have a big potential of application in the membrane-based gas separation area. Polyimides are thermally stable polymers that are often based on rigid aromatic backbones. Moreover, polyimides attract attention within the polymeric membranes due to their outstanding chemical stability and good mechanical properties. The chemistry of polyimides is in itself a vast area with a large variety of monomers available and several methodologies available for synthesis. The properties of polyimides can be dramatically altered by minor variations in the chemical structure of diamine or dianhydride and by isomeric attachment of the diamines.

Polyimides are synthesized by the reaction of two monomers (dianhydride and diamine) in a solvent and by dehydration of this solution (polyamic acid) by thermal

5

or chemical imidization. If this procedure is carried out with three or more monomers instead of two then copolyimides are synthesized [8]. Polyimides are characterized with imide group, -CONCO-, in the backbone as shown in Figure 1.3.
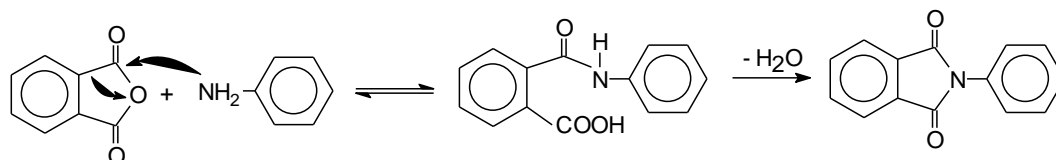
Figure 1.3 :   Generalized reaction mechanism of imide formation [8].

Aromatic polyimides are mainly chosen in membrane based gas separation due to their high performances. First aromatic polyimide was synthesized by Marstin Boent and first commercial polyimide, Kapton, was produced by the DuPont company. The development of materials by Dow, Ube and DuPont/Air Liquide with improved selectivities has made membrane separation much more competitive. This application of membranes has expanded very rapidly and captured more than one-half of the market for N_2 separation systems within the next few years.

There are many polyimide synthesis methods such as the classic two-step method, one-step method for high temperature solution polymerization, synthesis via derivatives of poly(amic acid)s, synthesis via Diester-diacid derivatives, aromatic nucleophilic displacement polymerization, polymerization of diisocyanates and dianhydrides, synthesis by transimidization [4]. However, two-step method is the most preferred method, because it yields powder with high solubility in many solvents or film polyimide membranes. This method provided the first such solvent-based route to process these polyimides.

1.3   Theory and Background

There are three commonly effective mechanisms (Figure 1.4) for transport of gaseous species within membranes: Knudsen diffusion, molecular sieving, and solution-diffusion. In dense polymeric membranes, gas transport occurs via the solution-diffusion mechanism [4, 9]. The solution-diffusion model assumes that the pressure within a membrane is uniform and also chemical potential gradient across the membrane is expressed only as a concentration gradient. Gas molecules are first sorbed by the polymer on the feed side of the membrane, and then they diffuse across

the membrane cross-section via transient gaps in the polymer matrix, and are desorbed from the other surface of the membrane.
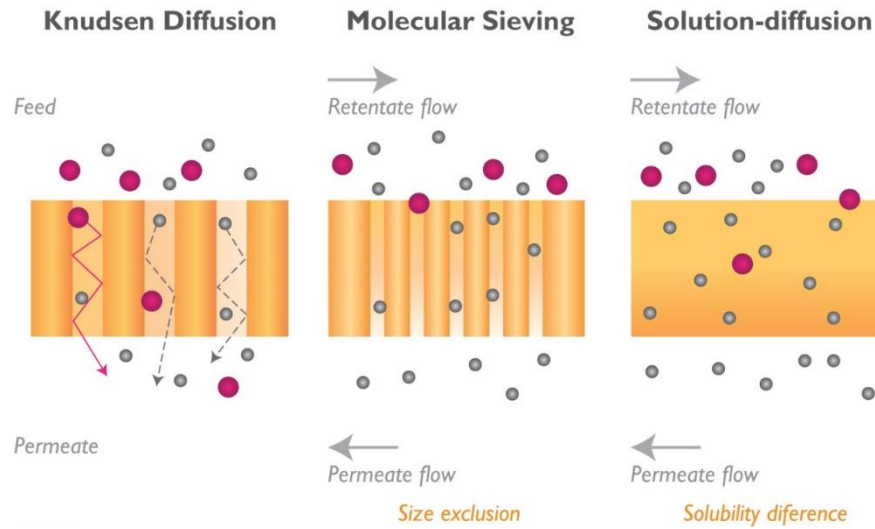
Figure 1.4 : Generalized three most common possible mechanisms for gas separation with membranes: (a) Knudsen diffusion (b) molecular sieving (c) solution-diffusion, adapted from [10].

In commercial applications, gas separation membranes should exhibit high permeability and selectivity as well as thermal, mechanical, and chemical resistance. Permeability of a gas in a membrane is equal to the product of the effective diffusivity (D) and sorption coefficient (S):

$$P = D \times S \tag{1.1}$$

and it is a measure of the productivity of a membrane. High permeability is needed for low investment and operation costs in membrane systems since the required membrane area and driving force would be reduced. Permeability values are typically reported in Barrers, $10^{-10} \frac{ss(STP).cm}{cm^2.cmHg.s}$.

Selectivity is a measure of the efficiency of a membrane to separate one gas from another. The ideal selectivity (i.e. pure gas feeds) between two gases A and B is defined as the ratio of their permeabilities,

$$\alpha_{AB} = \frac{P_A}{P_B} = \frac{D_A S_A}{D_B S_B} \tag{1.2}$$

For mixed gas feeds the separation factor can be calculated from,

$$\alpha_{AB} = \frac{(y_A / y_B)}{(x_A / x_B)} \qquad (1.3)$$

where x_i is the mole fraction of component i on the upstream side and y_i is the mole fraction of component i on the downstream side, as measured by gas chromatography.

Rubbery polymers are in a hypothetical thermodynamic equilibrium liquid state and their gas sorption obeys the Henry's law. On the other hand, sorption of gas molecules in a glassy polymer is determined by the inherent condensability of the penetrant gas molecule, the polymer-penetrant interactions and the amount of free volume in the polymer. Glassy polymers are typically assumed to be in a non-equilibrium state containing two components; a hypothetical liquid state and a solid state. Over the past three decades, sorption of gas molecules in glassy polymers has been described by the dual-mode sorption model [11-13]. The first environment pertains to the densely packed, amorphous regions of the polymer, which can be modeled using Henry's Law at low and intermediate pressures. The second environment exists in the form of microvoids created when the polymer is cooled from above its glass transition temperature. These microvoids are modeled using Langmuir sorption model. When these two effects are combined, the dual mode model can be depicted as in Figure 1.5 and expressed by:

$$C = k_D p + \frac{C'_H bp}{1 + bp} \qquad (1.4)$$

where C is the penetrant concentration, p is the pressure, k_d is the Henry's Law constant, b is the hole affinity constant for Langmuir sorption, and C'_H is the Langmuir sorption capacity. The ratio of the penetrant concentration to pressure is defined as the sorption coefficient:

$$S = \frac{C}{p} = k_D + \frac{C'_H b}{1 + bp} \qquad (1.5)$$

8
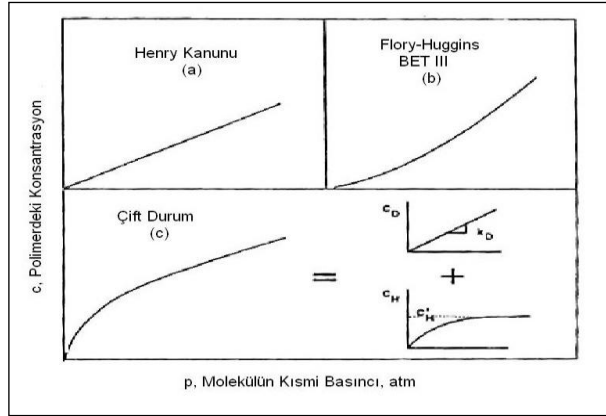
Figure 1.5 : Schematic representation of (left) Henry's sorption (right) Langmuir sorption and (bottom) dual mode sorption [14].

In all polymeric materials, the diffusion coefficient decreases with increasing molecular size of penetrant molecule, because large molecules interact with more segments of the polymer chain than do small molecules. Therefore, the mobility selectivity always favors the passage of small molecules over large ones. However, CO_2 is the only exception within the other gaseous species. Although it has a kinetic diameter smaller than O_2, it has a smaller diffusion coefficient than O_2 due to the polarity interaction with polymer structure. Penetrant-polymer interaction is not the only parameter that affects the diffusivity, but also fractional free volume (FFV) or a pore size of a polymer and flexibility of a polymer backbone are important factors.

1.4 Plasticization

Sorption induced volume swelling and plasticization is a serious concern limiting the use of PIs as membrane materials for gas separation involving CO_2, H_2S and condensable hydrocarbons such as propylene and propane. Plasticization is a pressure dependent phenomenon and occurs when the concentration of these gases in glassy polymers, such as PIs, is high enough to cause swelling in the polymer, i.e. disrupt chain packing and increase fractional free volume (FFV) and inter-segmental mobility [1-3]. The upturn pressure in the permeability versus pressure plot is known as the plasticization pressure depicted in Figure 1.6. The selectivity decreases significantly at this point due to the loss in size discrimination ability, therefore it is important to test membranes with mixed gas compositions. In the case of the

9

CO_2/CH_4 separation, the permeation of CH_4 is accelerated due to the CO_2-induced swelling of the polymer matrix and as a consequence the polymer permselectivity is deteriorated.
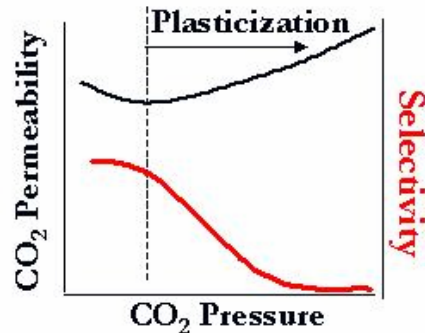
Figure 1.6 : Typical membrane response to plasticization via CO_2 [3].

In general, the CO_2-permeability characteristics of glassy polymers can be classified to three categories, which are represented in Figure 1.7 [3]. While Type (I) CO_2-permeation behavior fits to polymers without large substituents on the backbone, such as polysulpfone (PSF) and polycarbonate (PC), Type (II) is monitored mainly in polyimides. Polyacrylates, such as polyethyl-methacrylate (PEMA), cellulose acetate (CA), polymethyl-methacrylate (PMMA) and polystyrenes which containing large side groups on the main chain show Type (III) trend can be regarded as typical.
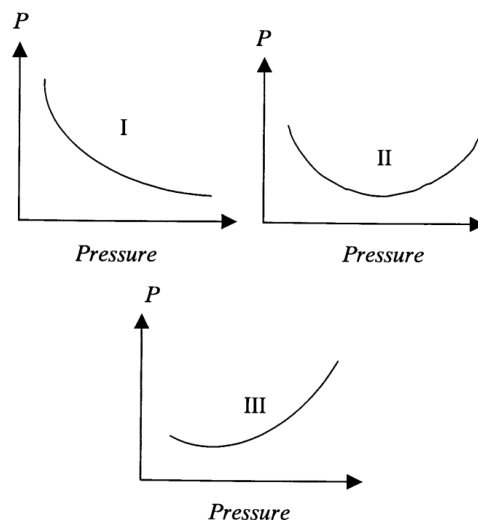
Figure 1.7 : Representation permeability (P) of several glassy polymers to CO_2 [3].

Plasticization pressure also can be accepted as the indication of the stability of polymeric membrane materials. Plasticization pressures for some glassy polymers

that are used for gas separation membranes have been reported in decreasing order as: polysulphone (PSF) > bisphenol A polycarbonate (BPAPC) > polyetherimide (PEI) > polyethersulphone (PES) > bisphenol Z polycarbonate (BPZ-PC) > copolyimide (P84) > poly(2,6-dimethyl-p-phenylene) oxide (PPO) > tetramethyl bisphenol A polycarbonate (TMBPA-PC) > Matrimid® 5218 (BTDA-DAPI) (3,3'4,4'-benzophenon tetracarbocyclic dianhydride and diamino-phenylindane) > cellulose acetate (CA) > cellulose triacetate (CTA) [1]. Therefore, it was claimed that all polymers need a similar CO_2 concentration to swell or plasticize, but require different feed pressures to reach it [1]. While Matrimid has initially high selectivity, it displays low plasticization pressure compared to polymeric material family that it belongs. As a consequence, there is need for further studies to understand and reduce the effect of plasticization in order to obtain a sustainable membrane performance.

There are many experimental studies about the effect of plasticization on polyimides [15-38]. These studies mainly investigate the plasticization dependencies of various parameters such as membrane thickness [15-17], membrane type (symmetric, asymmetric) [18, 19], physical aging [16], operation conditions [20-23], solvent type [24, 25], fabrication form of a membrane (hollow fiber or flat sheet), and some solutions to reduce its effect such as cross-linking [26-32], blending [33], thermal treatment [15, 19, 25, 34], filler addition [35-38], etc.

Rather than permeability measurements at high feed pressures, a variety of techniques have been utilized to quantify and investigate the effect of plasticization on glassy polymers on exposure to gas at high pressures. For example, some of them are in situ spectroscopic ellipsometry by means of swelling or dilation increase [15, 39], wide angle X-ray (WAXD) measurements and dilatometry by means of the increase in an average intersegmentel spacing (d-spacing) in the polymer [40], fourier transform infrared spectroscopy (FTIR) by means of vibrational changes with the interaction of CO_2 and polymer [41], differential scanning calorimetry (DSC) by means of the difference in glass transition temperature (Tg) [1] and dynamic mechanical analyzer (DMA) by means of the shifts in the first and secondary relaxations to low temperatures [42].

Aromatic polyimides are stiff-chain amorphous polymers and there are only a limited number of molecular simulation studies on the transport properties of gases in polyimides in the literature [43-50]. The details of these molecular simulation studies will be introduced in subsequent relevant chapters.

1.5 Research Objectives

The main objective of this thesis is to understand the relationships between the structure and plasticization behavior of 4,4-hexafluoro isopropylidene-diphthalic anhydride (6FDA) based polyimide membranes in order to estimate their degree of plasticization induced by CO_2, propane and propylene sorption, for proper membrane material selection. The effect of the observed plasticization and the associated relaxations in the polyimide matrix was assessed by means of the change in the local structure and free volume of a polyimide. The effect of polymer structure and mechanism of structural relaxations are aimed to be understood, as they are the factors that influence solubility and mobility of the plasticizing penetrant. In particular,

I. In Chapters 3 and 4, molecular simulation techniques will be used to estimate the degree of plasticization of 6FDA-based PI membranes induced by sorption of CO_2, propane and propylene. The 6FDA-based PIs exhibit high gas permeability and low chain packing density as a result of the blockage of the rotation of phenyl rings by $-C(CF_3)_2-$ linkage [9] and membranes with commercially attractive selectivities may be obtained by changing the diamine structure. 2,4,6-trimethyl-m-phenylene diamine (DAM) and 4,4-oxydianiline (ODA) were selected as the diamine groups. 6FDA-DAM and 6FDA-ODA PIs have a strong potential for O_2/N_2, CO_2/CH_4 and C_3H_6/C_3H_8 separation applications [13]. To gain a deeper insight on structure-plasticization relationship of polyimides, a third 6FDA-based PI, 6FDA-2,5-dimethyl-p-phenylenediamine (DPX) will be included in the study. Based on the relationship between the glass transition temperature (Tg) and the degree of plasticization, 6FDA-DPX with a Tg value in between those of 6FDA-DAM and 6FDA-ODA, is expected to manifest a degree of plasticization in between the other two PIs, as well. This work aims to compare the characteristic properties of membrane structures and dynamics at the

molecular level, as well as the early stages of CO_2, C_3H_6 and C_3H_8 sorption and plasticization in three 6FDA-based glassy polymers.

II.   In Chapter 5, the change in the CO_2 sorption capacity of PI membranes, as a function of residual solvent type and amount will be investigated. A certain amount of solvent used in the membrane fabrication process is usually left in the membrane and is very difficult to remove due to the extremely low diffusion coefficient of solvents in glassy polymers. Therefore it is important to know the effect of this residual solvent on membrane performance and plasticization phenomenon. Residual solvent in known to plasticize the polymer structure at high concentrations and antiplasticize at low concentrations. This work, to the best of our knowledge, is the first to investigate the change in the CO_2 sorption capacity of polymers or plasticization as a function of residual solvent type via molecular simulation. It is aimed to show the competition between CO_2 and residual solvent at molecular level, by means of fractional free volume change. A low-boiling-point solvent, tetrahydrofurane (THF) (b.p. 66ºC), and a high-boiling-point solvent, n-methyl-2-pyrrolidone (NMP) (b.p. 202ºC), is selected to study the effect of residual solvent.

III.   In Chapter 7, molecular simulation techniques will be used to estimate the degree of plasticization of novel copolyimide (co-PI) membranes induced by sorption of CO_2. The selection of the copolyimide structures will be based on the use of group contribution methods presented in Chapter 6, in which the permeability coefficients of H_2, O_2, He, CO_2, N_2, and CH_4 gases for more than 2200 possible copolyimide structures will be estimated by the group contribution method of Alentiev et al. [51]. The copolyimide structures whose predicted permselectivities are located well above the upper bound of Robeson's permeability-selectivity diagrams for CO_2/CH_4 separation application will be selected for plasticization study. The selected copolyimides also will be synthesized and characterized by Gel Permeation Chromatography (GPC), Differential Scanning Calorimetry (DSC), Dynamic Mechanical Analysis (DMA), Thermogravimetric Analysis (TGA), wide angle X-Ray Diffraction (XRD) and permeability ans sorption measurements. This work, to the best of our knowledge, will be the first to synthesize these

novel copolyimide structures. The experimental results on structural, mechanical and separation properties will be compared with those estimated via molecular simulation methods.

IV.   A new class of polymers, thermally-rearranged (TR) aromatic polyimides, has recently been studied by Park et al. [7] as a promising membrane material for gas separation processes. They show high permeability and selectivity in combination with exceptional thermal and chemical resistance characteristics. In particular, they exhibit much higher plasticization pressures indicating that they are more plasticization resistant than any other polymers. The thermal conversion step applied to certain PIs produces fundamental changes in molecular connectivity and conformation that change free volume shape and distribution. In Chapter 8, we aim to analyze TR polymers by the help of molecular simulation to understand why they are more resistant to platicization. We will first analyze the linkage flexibility due to the change from PI (6FDA-2,2-bis-(4-carboxyphenyl) hexafluoropropane (bisAPAF)) to TR-polyimide. Then, the objective is to understand how the CO_2 sorption capacity and plasticization change with the thermal rearrangement.

1.6   Organization of the Dissertation

The dissertation contains nine chapters and three appendices (A1-3). Chapter 1 gives background on polymeric gas separation membranes, polyimides, membrane transport, sorption and plasticization. In Chapter 2 molecular simulation methods and the methodology used for the simulation of plasticization effect are described. The effects of CO_2 and C_3H_6/C_3H_8 sorption induced plasticization on the selected polyimide structures are explored in Chapter 3 and 4 respectively. Chapter 5 describes the effect of residual solvent on the swelling of polyimide matrix and CO_2 plasticization. Chapter 6 discusses the group contribution methods that are used to predict the permeability coefficients of polymers and includes the application of these group contribution methods to the copolyimide structures in order to predict their gas transport properties. The prominent copolyimide structures that were identified in Chapter 6 are further investigated in Chapter 7 for CO_2 sorption induced plasticization effect via molecular simulation. The simualtion results are compared with experimental permeation and sorption behavior to understand the relationship

between plasticization and polymer structure. The sorption and plasticization behavior of TR polymers and its precursor polyimide are explored in Chapter 8. FFV and dihedral angle changes in polymer matrices are monitored to understand how these parameters are related to morphology and plasticization. Finally, in Chapter 9, conclusions are presented along with recommendations for future work.

2.   MOLECULAR SIMULATION METHODS

Molecular modeling applies numerical methods and theoretical models to model the molecular behavior. Molecular simulation is the numerical experiment that is based on the observed molecular modeling. The feature that distinguishes molecular simulation from other computing methods is that the molecular coordinates of the system are evolved in accordance with a rigorous calculation of intermolecular energies or forces. Today, molecular simulation methods are used widely by researchers in many disciplines such as computational chemistry, computational biology and material science. The most known feature of the molecular simulation methods is to describe the molecular systems at atomic level. The most important benefit of the molecular simulation method is to include all atoms in the system into the calculations during simulation while reducing the system complexities. Molecular simulation methods are mainly used to gain insight about the structure, dynamics and thermodynamic properties of inorganic, biological and polymeric systems. This chapter includes a brief review of statistical ensembles, force fields and methods used in molecular simulations.

2.1   Statistical Ensembles

Before the summary of methods used in molecular simulation, it is better to review the statistical ensembles, which are constituted to precisely represent the experimental system and obtain accurate results. A statistical ensemble is a collection of various states of the system which differ the positions and the velocities of the component particles. In molecular simulation, many configurations are obtained and the average of this system is taken account to carry out the desired measurements. There are several different types of statistical ensembles, depending on the type of system and the conditions, which are listed on Table 2.1 [52].

Before giving the details of statistical ensembles used in molecular simulation, it is better to look at the history of them. First of all, the canonical ensemble, in which the number of particles, temperature and volume are constant, was produced for original Monte Carlo (MC) simulations by Metropolis et al. [53] in 1953. After two decades, McDonald reported MC calculations for binary mixtures on an isothermal-isobaric (NPT) ensemble [54]. In 1980, Valleau and Cohen [55] conducted MC calculations in the grand canonical (μVT) ensemble. Later on, Ray developed techniques for MC simulations in the microcanonical ensembles in 1991 [56]. It is very difficult to obtain different type of statistical ensembles for Molecular Dynamics (MD) method due to the fact that the equations of motion lead naturally to the microcanonical (NVE) ensemble. In 1980, Andersen conducted MD simulations on NVT and NPT ensembles by introducing additional degree of freedom [57]. Nose was able to control the temperature by adding additional terms to the Hamiltonian of the system [58]. Studies on this area are in progress. In 1995, Lo and Palmer formulated an alternative Hamiltonian for MD simulations in the grand canonical ensemble [59].

Table 2.1: Summary of common statistical ensembles [52].

Ensemble	Constraints	Partition Function (Z)	P_i
Microcanonical	N, V, E	$\sum_i \delta(E_i - E)$	$\dfrac{\delta(E_i - E)}{Z_{NVE}}$
Canonical	N, V, T	$\sum_i e^{-\beta E_i(N,V)}$	$\dfrac{e^{-\beta E_i(N,V)}}{Z_{NVT}}$
Grand Canonical	V, T, μ	$\sum_i e^{\beta N \mu} Z_{NVT}$	$\dfrac{e^{-\beta(E_i - \mu N)}}{Z_{VT\mu}}$
Isothermal-Isobaric	N, P, T	$\sum_i e^{\beta p V_i} Z_{NVT}$	$\dfrac{e^{-\beta(E + PV_i)}}{Z_{NPT}}$

In the formulations of statistical ensembles presented in Table 2.1, Z represents the total number of states found in each ensemble. β, Boltzman factor which acts a weighting factor to all the energies, is calculated with the Equation 2.1 where k is the Boltzman constant and T is temperature.

$$\beta = \frac{1}{kT} \tag{2.1}$$

Each ensemble is associated with a characteristic thermodynamic function. For instance, entropy (S) can be obtained directly from the microcanonical partition function.

$$S = k \ln Z_{NVE} \tag{2.2}$$

Ensembles like NPT and NVT can represent experiments more naturally since they constrain measurable quantities like pressure and temperature. This means that the configurations controlled by the partition function are related to macroscopic properties. It can be shown that the Helmholtz function (A) is associated with the canonical ensemble.

$$A = -kT \ln Z_{NVT} \tag{2.3}$$

Similarly, the NPT ensemble that additionally constraints the pressure of the system but relaxes the volume constraints, is related to the fundamental quantity called Gibbs free energy, G.

$$G = -kT \ln z_{NPT} \tag{2.4}$$

whereas, the appropriate thermodynamic function for the grand canonical ensemble is pressure (P).

$$PV = -kT \ln Z_{\mu VT} \tag{2.5}$$

2.2   Force Fields

The heart of the molecular simulation processes is the force field. A force field is a set of equations (often parameterized using quantum level calculations) that describe the potential energy of a molecular system. Potantial energy ($V(\mathbf{r}_p)$) is a function of cartesian coordinates ($\mathbf{r}_p$) of all atoms in the molecule. An accurate force field should represent the structural, thermodynamic and dynamic properties of the system in the thermodynamic equilibrium conditions. Most force fields contain energy contributions for both bonded (intramolecular) and non-bonded (intermolecular) interactions as expressed in

$$E_{Total} = E_{Bonded} + E_{Nonbonded} \tag{2.6}$$

where E_{Bonded} is the energy related to the bonded interactions and $E_{Nonbonded}$ is the nonbonded interactions. These energies are subdivided into more specific interactions.

The bonded interactions are defined by

$$E_{Bonded} = E_{Bond} + E_{Angle} + E_{Torsion} + E_{Inversion} + E_{Crossterms} + E_{Restraints} \tag{2.7}$$

where E_{Bond} is bond stretching, E_{Angle} is angle bending, $E_{Torsion}$ is the intrinsic torsion potential, $E_{Inversion}$ is the energy associated with one atom having three single bonds with three other atoms, $E_{Crossterms}$ is the energy associated with mixed term interactions such $Bond_1$-$Bond_2$ or $Bond_1$-$Angle_1$-$Bond_2$ and $E_{Restraint}$ is the energy associated with an restraint derived externally to the system. Typically, harmonic functions are used for modelling bonds, angles and torsions. Another commonly used function is the Morse potential, which considers complete dissociation when the atoms of a bond are largely separated.

The non-bonded interactions are defined by

$$E_{Nonbonded} = E_{Repulsion-Dispersion} + E_{Coulombic} \tag{2.8}$$

where $E_{Coulombic}$ is coulombic interactions, and $E_{Repulsion-Dispersion}$ is the electron dispersion effect, typically modeled by van der Waals interactions. Van der Waals interactions account for the repulsion of electronic clouds at close range and the attraction of induced dipoles at longer range. The most popular functional form for van der Waals interactions due to its computational advantages and efficiency is the 12-6 Lennard-Jones potential,

$$E_{LJ} = \sum_{\substack{i,j \\ i<j}} 4\varepsilon_{ij} \left(\left(\frac{\sigma_{ij}}{r_{ij}} \right)^{12} - \left(\frac{\sigma_{ij}}{r_{ij}} \right)^{6} \right) \tag{2.9}$$

where r_{ij} is the distance between atoms i and j, ε_{ij} is the well depth, or maximum attractive energy, and σ_{ij} is the collision diameter at which there is no interaction energy.

While the attractive part of the van der Waals forces takes care of interactions between induced dipoles, a model for electrostatic interactions is needed to account for the attraction of permanent dipoles or multipoles inherent to the species in a system. Partial point charges are a convenient way to represent the electrostatic surface of molecules that generates dipoles and higher order multipoles. Coulomb's law can then provide the energy between atomic charges, q_i separated by a distance r_{ij} as

$$E_{Coulombic} = \frac{q_i q_j}{4\pi\varepsilon_0 |r_{ij}|}$$ **(2.10)**

where ε_0 is the vacuum permittivity.

Several different force fields have been developed for different systems and their parameters along with their validation are reported in the literature. In general, parameterization takes place by tuning each kind of interaction with the common goal of reproducing certain experimental properties. If we classify some of the common force fields found in professional molecular modelling programs into two groups, first group is comprised of Chemistry at HARvard Macromolecular Mechanics (CHARMM) [60, 61], DREIDING [62, 63], GROMOS [61] and GROningen Machine for Chemical Simulations (GROMACS); and second group is formed from Condensed-phase Optimized Molecular Potentials for Atomistic Simulation Studies (COMPASS) [61], Polymer-Consistent Force Field (PCFF) [63, 64] and Consistent Valence Force Field (CVFF) [63, 65].

In this work, the COMPASS force field was adopted for controlling the movements and potential energy among polymeric, solvent and penetrant molecules. The total energy of the COMPASS force field can be classified into three categories: (1) bonded contributions of energy terms based on the polymeric chain coordinates, (2) cross-effect energy terms between coupled terms based on the polymeric coordinates and (3) non-bonded energy terms, including both van der Waals and Coulombic electrostatic force:

$$E_{Total} = E_b + E_\theta + E_\phi + E_\chi + E_{bb'} + E_{b\theta} + E_{b\phi} + E_{\theta\theta'} + E_{\theta\phi} + E_{\theta\theta'\phi} + E_{Elec.} + E_{LJ}$$

$$= \sum_b \left[K_2(b-b_0)^2 + K_3(b-b_0)^3 + K_4(b-b_0)^4 \right] +$$

$$\sum_\theta \left[H_2(\theta-\theta_0)^2 + H_3(\theta-\theta_0)^3 + H_4(\theta-\theta_0)^4 \right] +$$

$$\sum_\phi \left[V_1(1-Cos\,\phi) + V_2(1-Cos\,2\phi) + V_3(1-Cos\,3\phi) \right] + \sum_\chi K_\chi(\chi-\chi_0)^2 +$$

$$\sum_{b,b'} F_{b,b'}(b-b_0)(b'-b_0') + \sum_{b,\theta} F_{b,\theta}(b-b_0)(\theta-\theta_0) +$$

$$\sum_{b,\phi}(b-b_0)\left[F_{b,\phi}^{(1)}(Cos\,\phi) + F_{b,\phi}^{(2)}(Cos\,2\phi) + F_{b,\phi}^{(3)}(Cos\,3\phi) \right] +$$

$$\sum_{\theta,\theta'} F_{\theta,\theta'}(\theta-\theta_0)(\theta'-\theta_0') + \sum_{\theta,\phi}(\theta-\theta_0)\left[F_{\theta,\phi}^{(1)}(Cos\,\phi) + F_{\theta,\phi}^{(2)}(Cos\,2\phi) + F_{\theta,\phi}^{(3)}(Cos\,3\phi) \right] +$$

$$\sum_{\theta,\theta',\phi} F_{\theta,\theta',\phi}(\theta-\theta_0)(\theta'-\theta_0')\phi(\phi-\phi_0) + \sum_{i,j}\frac{q_i q}{r_{i,j}} + \sum_{i,j}\varepsilon_{ij}\left[2\left(\frac{r_{ij}^0}{r_{ij}}\right)^9 - 3\left(\frac{r_{ij}^0}{r_{ij}}\right)^6 \right]$$

(2.11)

where b, θ, ϕ and χ represent bond length, bond angle, dihedral angle or out-of-plane angle formed by pairs, triplets and quadruplets, respectively.

2.3 Molecular Dynamics (MD)

Molecular dynamics which is one of the methods used in molecular simulations is a powerful technique to compute the equilibrium and dynamical properties of a classical many-body system. In this method, Newton's equation of motion is solved to describe the natural trajectory of a system through a set of 2N differential equations where N is the number of atoms. This can be written as:

$$m_i \frac{d^2 r_i(t)}{dt^2} = F_i(t), \quad (i = 1, 2,..., N) \tag{2.12}$$

where m_i is the mass and r_i is the Cartesian position for atom i. The equation of motion can also be expressed in terms of different coordinates systems as needed. The most expensive part of a molecular simulation is the determination of forces. The force field of the system can be used to determine the force on atom i, F_i by

$$F_i = -\nabla_i E(r_1, r_2,..., r_N) \tag{2.13}$$

Once the equation of motion has been integrated in time, a set of configurations describing a trajectory are obtained. By analyzing this trajectory, properties can be

obtained. Equation of motion produces the NVE ensemble correctly as the total energy and density are maintained constant throughout the simulation. Reproducing other ensembles such as the NPT and NVT ensembles require additional implementations to the basic equation of motions such as introducing degrees of freedom that account for thermal and/or pressure control. In the literature there exist a variety of methodologies for performing MD simulations under isochoric of isothermal conditions [66]. Most of these constitute a reformulation of the Lagrangian equations of motion to include the constraints of constant T and/or P. The two mostly used methods for MD simulations under constant T or/and P are the Nosé-Hoover [67, 68] and the Berendsen [69] methods. The Grand-Canonical ensemble [55] allows one to thermally average over a system which is able to exchange both energy and particles with its environment. The probability distribution function for the Grand-Canonical Ensemble can be derived by considering the closed system consisting of a subsystem and its larger environment. The probability distribution for the total closed system is calculated in the Micro-Canonical Ensemble. It is assumed that the number of particles and the energy can be uniquely partitioned into contributions from either the subsystem or its environment.

A common feature of all molecular dynamics algorithms is that the positions of molecules are evolved with time by integrating the equation of motion. Mathematically, the equation of motion represents a set of initial value type differential equations. In principle, these equations can be solved by using any standard finite difference algorithm. However, in practice, many commonly used algorithms are computationally too expensive because they require multiple force evaluations. In literature, some finite difference algorithms have been developed and specifically tuned for applications to molecular dynamics. These methods can be categorized as the integration of the equation of motion, Gear predictor-corrector methods [70] and Verlet predictor methods [71].

The most popular and applied algorithm is the Verlet predictor method [71] and its many subsequent modified methods. In common with the corrector-predictor algorithm, the starting point for the Verlet algorithm is a Taylor series expansion:

$$r(t + \Delta t) = r(t) + \frac{dr}{dt}\Delta t + \frac{1}{2!}\frac{d^2 r}{dt^2}\Delta t^2 + ...$$

(2.14)

$$r(t - \Delta t) = r(t) - \frac{dr}{dt}\Delta t + \frac{1}{2!}\frac{d^2 r}{dt^2}\Delta t^2 + ...$$

(2.15)

When equations 2.14 and 2.15 are added and arranged, the below equation is obtained:

$$r(t + \Delta t) = 2r(t) - r(t - \Delta t) + \frac{1}{2!}\frac{d^2 r}{dt^2}\Delta t^2$$

(2.16)

Equation 2.16 is generally known as Verlet's algorithm. It enables to advance the position of the molecules without calculating their velocities. However, the velocities are required to determine kinetic energy. They are obtained from:

$$v(t) = \frac{r(t + \Delta t) - r(t - \Delta t)}{2\Delta t}$$

(2.17)

The Verlet method is compact, easy to implement, time reversible, and it conserves energy even for long time steps. A minor disadvantage about this algorithm is not self starting. In addition, the main disadvantages of the Verlet algorithm are that it does not handle velocities well and its numerically precision is not optimal. It should be noted that the velocities calculated by equation 2.17 are the current velocities rather than the velocities corresponding to the new time step. As result, the calculated velocities lag behind the calculated positions by one time interval. These deficiencies have been addressed by various modified methods such as Leap-Frog Verlet Algorithm [72], Velocity-Verlet Algorithm [73] and Beeman Modification [74].

2.4 Monte Carlo (MC)

The Monte Carlo method is a stochastic strategy that relies on probabilities. In this algorithm, several configurations of a system are generated by randomly modifying the atom positions as well as their orientations and conformations. Efficient sampling

of a given probability distribution is essential to reproduce the correct ensemble. In contrast to MD methods no momentum contribution is required in MC simulations and thus, time dependent quantities cannot be determined through the use of these stochastic algorithms. Ensemble configurations are generated by constructing a Marov chain [75]. A Markov chain is a sequence of trials in which the outcome of successive trials depends only on the immediate predecessors. In a Markov chain, a new state will only be accepted if it is more 'favorable' than the existing state. In the context of a simulation using an ensemble, this usually means that the new trial state is lower in energy. The Metropolis method was introduced as a Markov process in which a random walk is constructed in such a way that the probability of visiting a particular point r^N is proportional to the Boltzmann factor $\exp[-\beta E(r^N)]$. There are many ways to construct such a random walk. In the approach introduced by Metropolis et al. [53], the following scheme is proposed:

1. Select a particle at random, and calculate its energy $E(r^N)$.

2. Give the particle a random displacement; $r'^N = r^N + \Delta$, and calculate its new energy $E(r'^N)$.

3. Accept the move from r^N to r'^N with probability as:

$$acc(o \rightarrow n) = \min\left(1, \exp\left(-\beta[E(r'^N) - E(r^N)]\right)\right) \qquad \textbf{(2.18)}$$

This method is generally clarified with the help of the simple example in Figure 2.1. In this figure [76], two ways to measure the depth of the river Nile are compared, by conventional quadrature (left) and by Metropolis sampling; that is, the construction of an importance-weighted random walk (right). In the conventional quadrature scheme, the value of the integrand is measured at a predetermined set of points. In contrast, in the Metropolis scheme, a random walk is constructed through that region of space where the integrand is nonnegligible. In this random walk, a trial move is rejected if it takes you out of the water, and is accepted otherwise. After every trial move (accepted or not), the depth of the water is measured.
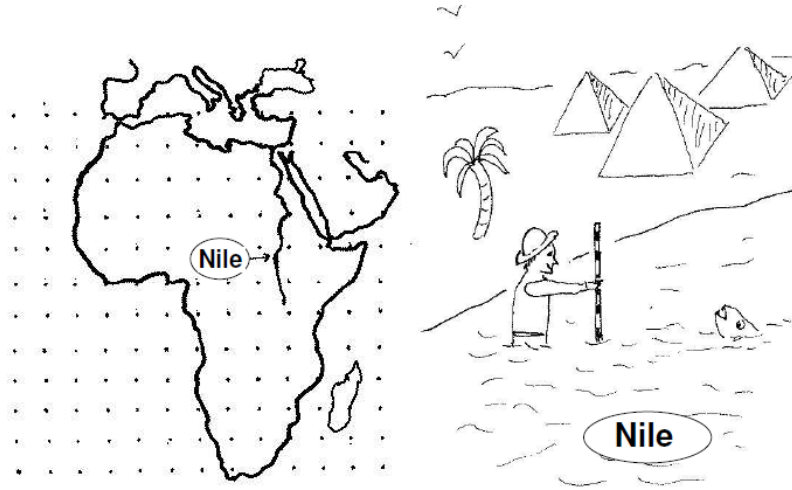
Figure 2.1 : Measuring the depth of the Nile: a comparison of conventional quadrature (left), with the Metropolis scheme (right) [76].

The transition matrix is denoted in order to determine the probability to perform a trial move from o (old state) to n (new state) by α(o→n); where α is usually referred to as the underlying matrix of Markov chain. The next stage is the decision to either accept or reject this trial move.

$$\pi(o \rightarrow n) = \alpha(o \rightarrow n) \text{ X } acc(o \rightarrow n) \qquad (2.19)$$

In the original Metropolis scheme, α is chosen to be a symmetric matrix (acc(o→n) =acc(n→o)). However, there are several examples where α is not symmetric. If α is symmetric, Equation 2.19 can be rewritten in terms of the acc(o→n):

$$N(o) \text{ X } acc(o \rightarrow n) = N(n) \text{ X } acc(n \rightarrow o) \qquad (2.20)$$

From Equation 2.20 follows

$$\frac{acc(o \rightarrow n)}{acc(n \rightarrow o)} = \frac{N(n)}{N(o)} = \exp\{-\beta[E(n) - E(o)]\} \qquad (2.21)$$

Again, many choices for acc(o→n) satisfy this condition (and the obvious condition that the probability acc(o→n) cannot exceed 1). The choice of Metropolis et al. is

$$\begin{aligned} acc(o \rightarrow n) &= N(n)/N(o) \quad if \quad N(n) < N(o) \\ &= 1 \quad\quad\quad\quad if \quad N(n) \geq N(o) \end{aligned} \qquad (2.22)$$

There are other choices for acc(o→n) are possible, but the original choice of Metropolis et al. appears to result in a more efficient sampling of configuration space than most other strategies that have been proposed in the literature.

26

2.5 Methodology for Molecular Simulation of Polyimide Matrices

All simulations in this thesis were carried out using the *Accelrys Materials Studio 5.0* simulation package [77] with all molecular interactions being modeled using the COMPASS force field [78], which was shown to be efficient in reproducing density-related properties in polymers by Heuchel et al. [48]. The default charge set parameters of the force field were used in the simulations. Details of the force field are provided in the Section 2.2. All-Atom model was used to represent the gas molecules. The Van der Waals interactions were calculated by pair-wise addition, with the cut-off distance being set to the half of the simulation cell length, which varies between 38 and 40 Å, with an energy spline to zero, and Ewald summation method was used to calculate the electrostatic interactions. The calculations were performed on multi-core PCs and high performance clusters.

2.5.1 Construction and Characterization

In modeling polymers, chain length is an important factor to reproduce polymer properties accurately. Heuchel et al. [48] reported that larger simulation cells are necessary for stiff chains in comparison to rubbery materials in order to see possible heterogeneities in the distribution of free volume elements, and used 60 to 80 repeat units (about 4500 atoms) in their models for simulating several PIs including 6FDA-DAM and 6FDA-ODA. Neyertz and Brown [49] compared polymer models containing 4150, 6225, and 56025 atoms in their calculation of sorption and diffusivity coefficients of helium in ODPA-ODA, and concluded that polymer model of 4150 atoms (83 repeat units) provided satisfactory accuracy in the simulations. Similarly, Zhang and coworkers [79] used 72 repeat units to model 6FDA-ODA chain.

In this thesis, PI chains were constructed from 60 and 80 repeat units. Dianhydride and diamine moieties were constructed and linked followed by geometry optimization to create polymer repeat units. The PI chains were then built by connecting these repeat units with each other and a final geometry optimization was carried out. A cubic simulation cell with a side of 38-40 Å for each model PI matrix was constructed from a single chain using the *Amorphous Cell* module of the software package. To avoid ring catenation and spearing problems, the starting

density of the simulation cells was selected as low as 0.1 g/cm^3, and 200-300 Si atoms or 200-500 methanol molecules were added randomly into the PI matrix following the work of Heuchel *et al.* [48]. After construction of the simulation cell, these extra atoms were deleted, and the simulation cells were equilibrated by applying a series of MD runs using the *Forcite* module as described by Heuchel et al. [48]:

1. Compression by a 5-50 ps MD run in the *NPT* ensemble (fixed number of particles, pressure and temperature) at high pressure (5000 bar).

2. Annealing by subsequent MD runs in the *NVT* ensemble (fixed number of particles, volume and temperature) at 327ºC and at 27ºC, each about for 20-100 ps.

3. Relaxation by a 20-100 ps *NPT*-MD run at 1 bar. If the final density was lower than the experimental density of the PI, first and second steps were repeated.

4. Equilibration by a 300-500 ps *NVT*-MD run.

The time step in the MD simulations was adopted as 1fs, and the temperature and pressure were controlled through Berendsen thermostat and barostat [69], respectively.

Once the model PI matrices were constructed, the x-ray scattering pattern and d-spacing, dihedral distribution, cohesive energy density (CED), fractional free volume (FFV) and glass transition temperature (Tg) of each PI were estimated and compared with the available data in the literature. Accurate estimation of these structural properties is crucial to predict separation performance of the PI membranes.

The d-spacing is a measure of the average intermolecular distance of polymer chains and is related to the FFV of the polymer. The d-spacing and FFV values are two important properties determining the diffusivity and sorption, thus the permeability of the gases in the polymer matrix [80]. The d-spacing (*d*) can be obtained from the x-ray patterns through the Bragg's equation,

$$\lambda = 2dSin\theta \qquad\qquad \textbf{(2.23)}$$

where λ and 2θ represent the wavelength and scattering angle, respectively.

The distribution of dihedral angle (C-N-C-C) on the diamine-dianhydride linkage is one of the indicators of the polymer rigidity. When 6FDA based PIs are considered, a wider dihedral distribution indicates lower backbone rigidity, thus a lower Tg. The x-

ray scattering patterns and dihedral distributions were estimated using *Forcite Analysis* tools available in the software.

Cohesive energy density (CED) is an indication of the strength of intermolecular forces and is defined as the energy needed to remove the molecule from its nearest neighbors divided by the total volume of the moved molecule, and for a single chain polymer is defined as

$$CED = \frac{E_{inter}}{V} = \frac{E_{non-PBC} - E_{PBC}}{V}$$

(2.24)

where E_{PBC} and $E_{non-PBC}$ are non-bonded energies of the polymer chain calculated with and without periodic boundary conditions, respectively, and V is the volume of the simulation cell. Alternatively, the solubility parameter, δ, which is the square root of the CED, is also frequently used in the analyses. E_{PBC} was calculated using a cut-off set to the half of the simulation box (~19 Å), whereas a 100-Å cut-off was used to evaluate $E_{non-PBC}$ in order to count all parts of polymer matrix. When the polymer matrix has a closed packed structure, the CED and δ value increases but the FFV and diffusivity decrease [81].

The FFV is an indicator of the openness of a polymer matrix and the penetrant concentration in polymers scales usually with the FFV of the material. [9]. The FFV values of the model PI matrices were estimated by the following equation:

$$FFV = \frac{V - 1.3V_w}{V}$$

(2.25)

where V_w is the van der Waals volume of the PI chain. The V_w is calculated directly using *Atom Volumes & Surfaces* [82, 83] tool of the simulation software, instead of using the Bondi method [84]. The sorption-induced FFV increase is as a measure of polymer plasticization. As the amount of sorbed penetrant increases, the polymer chains are forced apart to accommodate penetrant molecules. At the same time, penetrant molecules can facilitate chain motion. Both mechanisms act to reduce the separation performance of a polymer membrane [85]. Therefore, prediction of the sorption-induced FFV increase can provide information on plasticization tendency of polymeric membrane materials.

The analysis of the sorption-induced changes in FAV besides the free volume allows measuring sorption-induced conformational changes in the polymer chains as

recently reported Chang et al. [86, 87] because the FAV estimation excludes the dead volume and gives a more realistic prediction of available free volume for gas molecule transport. FAV is estimated from the *Solvent* task simulation by using different probe radii to detect the available vacancy inside the simulation cell. The interaction between the probe atom and polymer atoms was ignored during the FAV simulation. The FAV distribution in PI matrices was calculated by increasing the probe radius gradually form 0 to 3.2 Å.

The glass transition temperatures of the polymers were estimated by observing the volume change of the simulation cells during cooling down [88] from 700 K with an interval of 20-25 K. A 300-ps NVT and 700-ps NPT molecular dynamics were performed between each temperature jump to calculate the density of equilibrated structures. The glass transition temperatures were determined from the plots of specific volume versus temperature, which are provided in the Appendix 1. The intersection of the best fit lines to the data points of the rubbery and glassy phases yielded the Tg values of the PI structures.

2.5.2 Sorption simulations

The *Sorption* module of the software was used to simulate sorption of CO_2, CH_4, N_2, and O_2 gases in PI matrices. The Sorption calculations were carried out in the Grand Canonical Monte Carlo (GCMC) ensemble at fixed temperature, volume and chemical potential using the Metropolis Algorithm [53]. Simulation temperature and pressure values were chosen based on the experimental studies in the literature in order to compare the results, but the general conditions are 35ºC and 10 bar for CO_2 and CH_4; 35ºC and 2 bar for N_2 and O_2.

Experimental gas sorption coefficients of polymeric membranes were calculated via Equation 1.5 and are reported in units of [cm^3 (STP)/cm^3.bar], which corresponds to the ratio of the volume of the adsorbed gas molecules at standard temperature and pressure to the volume of the PI matrix and the working pressure. The volume of the sorbed gas molecules in this study was calculated as the product of the number of molecules and the molar volume of the ideal gas at STP.

To reproduce sorption-induced volume swelling and plasticization, *Sorption-Relaxation Cycles (SRCs)* were applied until the sorption coefficients converge: At each cycle, the polymer matrix was loaded with sorbate molecules corresponding to

its equilibrium capacity at the considered pressure using GCMC calculations, and then *NVT* and *NPT*-MD simulation runs were applied for up to 200-500 ps to obtain an equilibrated matrix. Next, SRCs were repeated until CO_2 concentration converges to its equilibrium value. This procedure (Figure 2.2) yielded the equilibrium volume and concentration of the system at the imposed temperature and pressure.
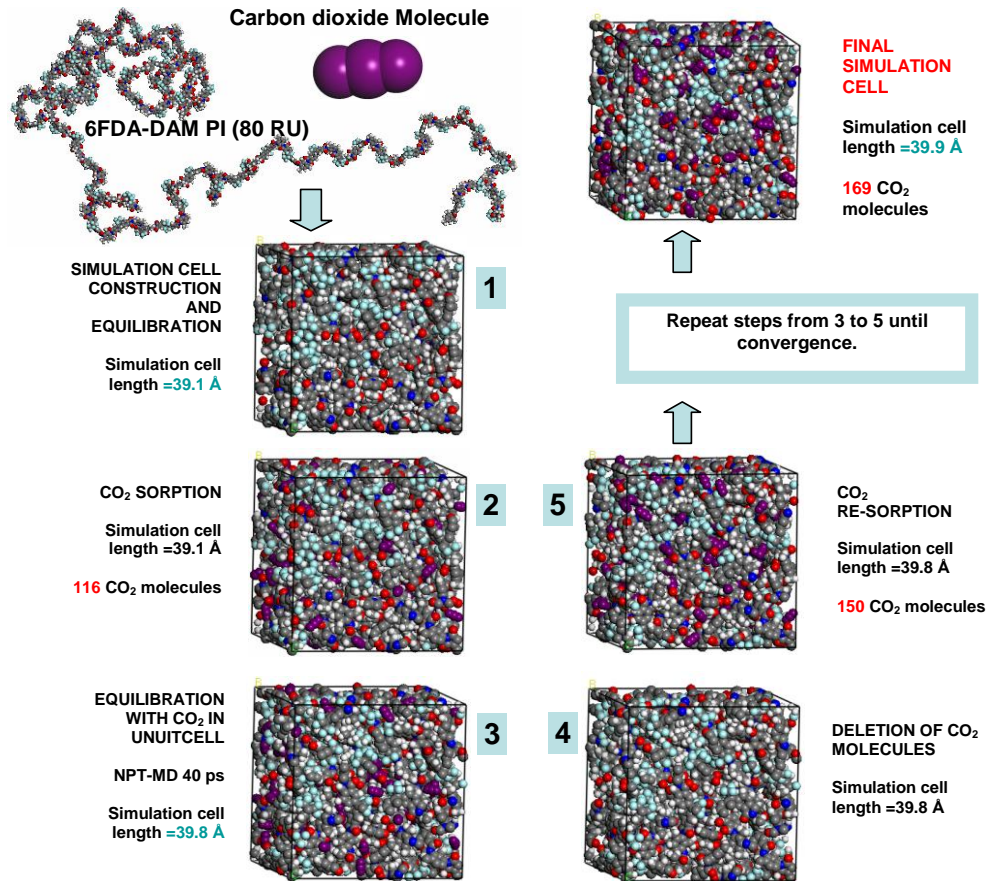
Figure 2.2 : Illustration of the Sorption Relaxation Cycles (SRCs) procedure used in CO_2 sorption on 6FDA-DAM at 10 bars and 35°C.

Ideal selectivity for a binary mixture of gases A and B ($\alpha_{A/B}$) is defined as the ratio of the pure gas permeability coefficients which is also expressed as the product of diffusion and sorption selectivities in Equation 1.2.

Ideal sorption selectivities of O_2/N_2, and CO_2/CH_4 gas pairs in the PI matrices were evaluated by calculating the ratio of the estimated sorption coefficients of the relevant gases. However, actual selectivities may differ significantly from ideal values due to plasticization and competitive sorption [81]. To reproduce these effects, actual mixed gas sorption selectivities were also calculated for mixtures of CO_2/CH_4 (P_{CO2}:P_{CH4} = 50:50) which have a strong potential for commercial gas separation applications.

3. CO$_2$-INDUCED PLASTICIZATION IN FLUORINATED POLYIMIDE MEMBRANES

3.1 Introduction

Aromatic polyimides (PIs) are an important group of polymers with outstanding thermal and chemical stability, and good mechanical properties, which make them very attractive as membrane material for membrane based gas separation [89]. They are synthesized by the reaction of dianhydride and diamine monomers, which govern selectivity towards separation of commercially important gas pairs such as O$_2$/N$_2$, CO$_2$/CH$_4$, H$_2$/CH$_4$, H$_2$/N$_2$ and propylene/propane. Hence, selection of an appropriate monomer pair is crucial for the preparation of membranes with high selectivity for a specific application. There are numerous studies in the literature reporting PIs synthesized using different dianhydride/diamine combinations [90-94]. The interdependence of chemical structures and gas transport properties [95] provides an opportunity of specific tailoring of the molecular structure to obtain desired separation performance for specific applications.

Sorption induced volume swelling and plasticization is a serious concern limiting the use of PIs as membrane material for gas separation involving CO$_2$, H$_2$S and condensable hydrocarbons such as propylene and propane. Plasticization is a pressure dependent phenomenon and occurs when the concentration of these gases in glassy polymers, such as PIs, is high enough to cause swelling in the polymer, i.e. disrupt chain packing and increase fractional free volume (FFV) and inter-segmental mobility [96-103]. The upturn pressure in the permeability versus pressure plot is known as the plasticization pressure. The selectivity decreases significantly at this point due to the loss in size discrimination ability, hence it is important to test membranes with mixed gas compositions. In the case of the CO$_2$/CH$_4$ separation, the permeation of CH$_4$ is accelerated due to the CO$_2$-induced swelling of the polymer matrix and as a consequence the polymer permselectivity is deteriorated. Therefore, plasticization should be minimized by proper molecular design of the membrane

materials in order to overcome the permselectivity reduction. A fundamental understanding of penetrant induced plasticization is needed to achieve this. Advances in molecular modeling provide an opportunity to quantitatively investigate penetrant induced plasticization and understand the physics behind it. Only a few simulation studies investigating plasticization have been reported in literature [79, 104, 105].

In this work, we used molecular simulation techniques to estimate the degree of plasticization of 4,4-hexafluoroisopropylidene-diphthalic anhydride (6FDA)-based PI membranes induced by CO_2 sorption. The 6FDA-based PIs exhibit high gas permeability and low chain packing density as a result of the blockage of the rotation of phenyl rings by $–C(CF_3)_2–$ linkage [9] and membranes with commercially attractive selectivities may be obtained by changing the diamine structure. 2,4,6-trimethyl-m-phenylene diamine (DAM) and 4,4-oxydianiline (ODA) were selected as the diamine groups due to the strong potential of 6FDA-DAM and 6FDA-ODA PIs for O_2/N_2, CO_2/CH_4 and C_3H_6/C_3H_8 separation applications [106]. To gain a deeper insight on structure-plasticization relationship of PIs, a third 6FDA-based PI, 6FDA-DPX (DPX: 2,5-dimethyl-p-phenylenediamine) was also considered in the study. Based on the relationship between the glass transition temperature (Tg) and the degree of plasticization, 6FDA-DPX with a Tg value in between those of 6FDA-DAM and 6FDA-ODA (Figure 3.1), was expected to manifest a degree of plasticization in between the other two PIs, as well.
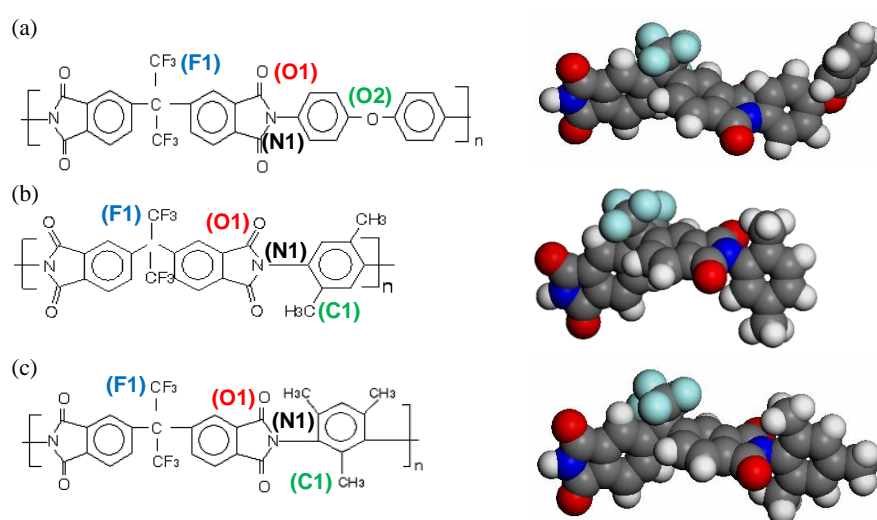
Figure 3.1 :   Structures of constructed repeat units for (a) 6FDA-ODA, (b) 6FDA-DPX and (c) 6FDA-DAM . Typical sorption sites are shown in parenthesis.

The penetrant concentration in polymers scales usually with the FFV of the materials [9]. Previous studies established that the FFV in some glassy polymers tends to increase with an increase in the Tg [80]. This tendency was observed in various 6FDA-based PIs by Shimazu et al [81], who reported that PIs with two $-CF_3$ groups at the diamine moiety exhibit an increased FFV similar to that of 6FDA-DAM, which has three $-CH_3$ groups, and 6FDA-Durene, which has four $-CH_3$ groups, although their Tg values are lower than those of 6FDA-DAM and 6FDA-Durene. They concluded that the introduction of the $-CF_3$ functional group is effective in increasing the FFV, even if the chain stiffness is not very rigid in comparison with the PIs with three or four $-CH_3$ substituents on the phenylene linkage at the diamine moieties. They also reported that PIs with a $-CONH-$ linkage at the diamine moiety exhibits a remarkably decreased FFV with a high Tg, which was explained by the presence of a charge transfer complex in some PIs which acts as a factor decreasing the FFV with increasing Tg.

Aromatic PIs are stiff-chain amorphous polymers and there are only a limited number of molecular simulation studies on the transport properties of gases in PIs in the literature [43-50]. Smith et al. [43] analyzed the motion of CO_2 gas molecules inside 6FDA-4PDA (2,4,5,6-trimethyl-1,4-phenylene-diamine) and 6FDA-ODA polyimide matrices in simulation cells containing . They used simulation cells were created using the soft-core method, with short (11 segments) chains. They concluded that the calculated diffusivities were unrealistic due to the shortcomings in their model. Zhang and Mattice [44] were studied diffusion of two small penetrant molecules, O_2 and N_2, in the bulk amorphous polyimide of 3,3′,4,4′-benzophenonetetracarboxylic dianhydride and 2,2-dimethyl-1,3-(4-aminophenoxy) propane (BTDA-DMDA) with molecular dynamics simulations. They claimed that although the thermal fluctuations of the polymer matrix play an important part in the diffusion process, conformational relaxation of the polymer chains may not be important for estimating the diffusion coefficient. Their finding indicates that the local packing of the amorphous polymer tends to shield some of the atoms from close contact with the diffusant molecules in the diffusion process. Hofmann and coworkers studied molecular simulation of gas transport in several PIs, a poly(amide-imide) and a variety of siloxane polymers [45, 46, 96]. They calculated diffusion and sorption coefficients of O_2, N_2, and H_2 gases in these polymers by the help of the

transition state Gusev-Suter MC method [107], and they nearly reproduced experimental results. In the subsequent studies, Hoffman and coworkers calculated also diffusion and sorption coefficients for O_2, N_2, CH_4 and CO_2 gases in ten different PIs [47, 48]. In a similar work, Neyertz and Brown [49] evaluated the transport properties of 4,4'-oxidiphthalic dianhydride-4,4-oxydianiline (ODPA-ODA) PI by using a combination of MD and MC simulation methods. They tested the dependence of calculated gas permeation coefficient in glassy polymers by constructing simulation cells of different number of repeat units of ODPA-ODA. They reported that the permeation characteristics of helium were independent of the chain length. Chang and coworkers [50] analyzed the free volume morphology and gas diffusion mechanism of seven different aromatic PI membranes composed of various diamines and dianhydrides via MD technique. Their FAV and free volume morphology analyses showed that the existence of the 6FDA group contributes to the formation of larger, continuous, and more circular effective free volume elements for gas passage and also supplies more sites for gas sorption.

Studies that focused on CO_2-induced plasticization in PIs are rare. Neyertz and coworkers [104] studied volume dilation of 6FDA based polyimides loaded with different CO_2 amounts. They performed MD simulations in order to calculate CO_2 diffusivity in the polymer matrices. They employed also a novel method "trajectory-extending Kinetic Monte Carlo [108]" that increases the time scales in diffusivity simulations by three orders of magnitude. Diffusivity simulations showed that CO_2 molecules moves by a combination of oscillations within available free volumes in the polymer matrix associated with occasional jumps from one site to another. The absence of long-lived interactions with the polymer matrices and with the other penetrants indicates that CO_2 molecules are highly mobile and free to access any part of the free volume. In another recent study, Zhang and coworkers [79] carried out both experimental measurements and molecular simulation runs to examine CO_2-induced plasticization of 6FDA-ODA. They concluded that the imide group was the preferential sorption sites, followed by the ether and CF_3 groups. With increasing CO_2 loading, the PI exhibits a depressed glass transition temperature, a dilated volume and an increased fractional free volume which are the indication of plasticization effect. They concluded also that the plasticization could be suppressed

by substituting the ether groups in the PI chains which exhibit a significant effect on plasticization.

3.2 Simulation Method

All simulations in this work were carried out according to methodology described in Section 2.5. Simulation temperature and pressure values were chosen based on the experimental studies in the literature: 35ºC and 10 bar for CO_2 and CH_4; 35ºC and 2 bar for N_2 and O_2. These conditions correspond to the experimental study of Tanaka et al. [99, 109], who calculated sorption coefficients for both PIs from isothermal sorption measurements instead of obtaining them indirectly by calculating the ratio of permeability to diffusivity. The two other experimental data sets in the literature belong to Yeom et al. [101] who obtained them indirectly by using the ratio of permeability to diffusivity in 6FDA-DAM and Koros and Coleman [100] who obtained sorption coefficients by isothermal sorption measurements for 6FDA-ODA.

3.3 Results and Discussion

3.3.1 Characterization of the Model PI Matrices

The structural properties of 6FDA-DAM, 6FDA-DPX and 6FDA-ODA models estimated in this work and comparison to data reported in the literature are presented in Table 3.1. The d-spacing values were obtained from the computed x-ray patterns through Equation 2.3. These patterns are in very good agreement with the experimental data as can be seen in Figure 3.2; consequently, calculated d-spacing values coincide with the experimental values. 6FDA-based PIs with the bulky -$C(CF_3)_2$- group in their structure generally have d-spacing values larger than those of PIs of other dianhydrides [109]. A large d-spacing value shows that polymeric chain has high free volume and polymer is not closed-packed; hence a polymer with high d-spacing value have a high gas sorption coefficient and thus a high permeability coefficient value. The d-spacing value depends both on the dianhydride and diamine type. Among the three PIs considered in this study, 6FDA-DAM has the highest d-spacing value due to three –CH_3 groups connected to the phenyl ring in the DAM moiety, which increases the free volume of the polymer.

Table 3.1: Comparison of estimated properties of PIs with previously reported data.

Properties		6FDA-DAM	6FDA-DPX	6FDA-ODA
d-spacing (Å)	Literature	6.56[a]	----	5.66[b]
	This work	6.61	6.22	5.81
FFV	Literature	0.189[c]	0.177	0.162[c]
	This work	0.271	0.257	0.221
Tg (°C)	Literature	377[d]	331[d]	304[d]
	This work	370	328	302
δ (J/cm^3)$^{1/2}$	Literature	22.3[c], 26.4[e], 15.7[f]	22.9[c], 26.8[e]	23.1[c]
	This work	14.0	15.7	17.4
Density (g/cm^3)	Literature	1.340[c]	1.386[c]	1.434[c]
	This work	1.240	1.286	1.348

[a]Ref. 97, [b]Ref. 98, [c]Ref. 81, [d]Ref. 101, [e]Ref. 99, [f]Ref.111.
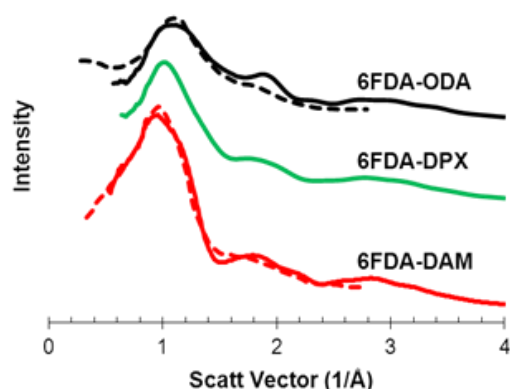
Figure 3.2 : Calculated X-ray Scattering Patterns (solid lines) of 6FDA-DAM, 6FDA-DPX and 6FDA-ODA in comparison with experimental data (dashed lines [97, 98]).
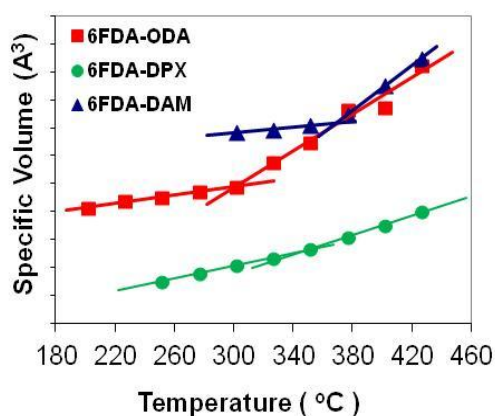
Figure 3.3 : Glass transition temperature of 6FDA-ODA, 6FA-DPX and 6FDA-DAM PIs at 1 bar.

Shimazu et al. [81] reported that introducing –CH$_3$ substituents in phenylene group decreases CED (thus δ) and increases FFV due to the restriction of efficient packing by steric hindrance, yielding a lower CED and a higher FFV for 6FDA-DAM with respect to 6FDA-DPX. On the other hand, replacing the phenylene group by a

diphenylether linkage, as in the case of 6FDA-ODA has an opposite effect. The comparison of the δ values against our ones indicates a quantitative disagreement as we calculated lower values for all three PIs. However, it should be noted that previously reported δ or CED in the literature, which were calculated either with group contribution methods [81, 99, 110] or through molecular simulations [111] varies within a relatively large range, as summarized in Table 3.1. Therefore, our estimations are in the right order of magnitude.

Similarly, the FFV values calculated in this study agree qualitatively with previous reports, although our values are lower, which may be due to direct calculation of the Van der Waals volumes instead of using the Bondi method [81, 99, 110, 111]. On the other hand, Zhang et al. [79] reported a FFV value of 0.210 for 6FDA-ODA by calculating the van der Waals volume in their molecular simulation study, which agrees well with our results. Considering the flaws of Bondi method described by Yampolskii and Shantarovich [9], such as unrealistic assumption of a unified packing density factor of 1.3 for all polymers or the additive scheme of computing V_w of repeat units that ignores conformational distinctions, our results reflect satisfactorily the fact that 6FDA-DAM has a higher free volume than 6FDA-DPX and 6FDA-ODA.

The FFV in some glassy polymers tends to increase with an increase in the Tg because of increasing chain stiffness. This tendency can be observed for the three PIs, as well. Estimated Tg values (Figure 3.3) of the three PIs are in very good agreement with available experimental results as shown in Table 3.1. As can be seen from the dihedral distributions of the diamine-dianhydride linkages shown Figure 3.4, the flexibility of 6FDA-DAM is significantly restricted due to three methyl substituent compared to the flexibility of the 6FDA-DPX with two methyl substituent, which in turn is more sterically hindered with respect to the flexibility of diphenylether-connected 6FDA-ODA. This difference in the flexibility correlates with the differences in Tg, FFV and δ values. To quantify the linkage flexibility, we calculated the standard deviation of the dihedral angle distribution based on the absolute values, $\sigma|\phi|$. Figure 3.5 shows variations in the Tg, FFV and δ as a function of $\sigma|\phi|$, reflecting the correlations discussed above.
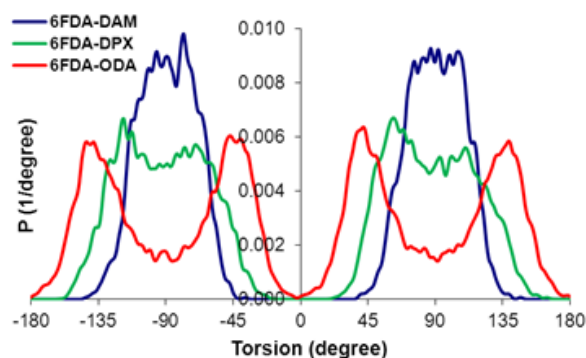
Figure 3.4 :   Dihedral distribution of the dianhydride–diamine linkage (C-N-C-C) in 6FDA-polyimides.
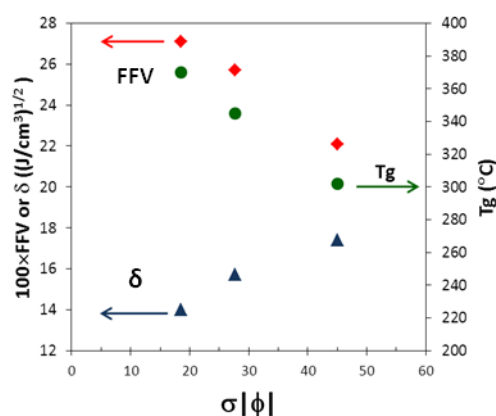
Figure 3.5 :   Correlation among the FFV, solubility parameter (δ), glass temperature (Tg) and flexibility of the diamine-dianhydrade linkage in 6FDA-polyimides.

Overall, the estimated structural properties agree quantitatively well with the experimental data, such as glass transition temperature, and d-spacing. However, some disagreement exists with respect to the literature values of FFV and CED which had been calculated with group contribution methods.

3.3.2 Sorption simulations

GCMC simulations to predict the sorption of CO_2, CH_4, N_2, and O_2 gases in the model PI matrices were carried out at different temperature and pressures as described in the previous chapter. It is well-known in the literature [112, 23] that while light gases such as CH_4, N_2, and O_2 do not plasticize polymer membranes, CO_2 induces strong plasticization. Previous simulation studies reported in the literature [79, 104, 105] on CO_2 plasticization estimated sorption-induced volume swelling and FFV increase at experimentally obtained equilibrium concentrations, i.e. they calculated the number of CO_2 molecules in the simulation cell corresponding to the experimental concentration value and examined the dilation of the polymer matrix

containing these CO_2 molecules. In this study, equilibrium concentrations and corresponding sorption coefficients of CO_2 were calculated through the sorption-relaxation cycles (SRCs) as described in section 2.5, thus in a purely predictive manner. Figure 3.6 shows the convergence of the CO_2 concentration in the three PIs through the SRCs. These cycles provided an estimation of the extent of CO_2 induced volume swelling and plasticization in the membrane materials. In accordance with the differences in the flexibility of diamine-dianhydride linkages, the sorption-induced volume swelling is the highest in 6FDA-ODA as presented in Table 3.2, which indicates that this PI underwent a much more significant plasticization than the other two PIs. These results agree with the expectation based on the fact that 6FDA-ODA has the most flexible backbone due to the presence of the diphenylether moiety.
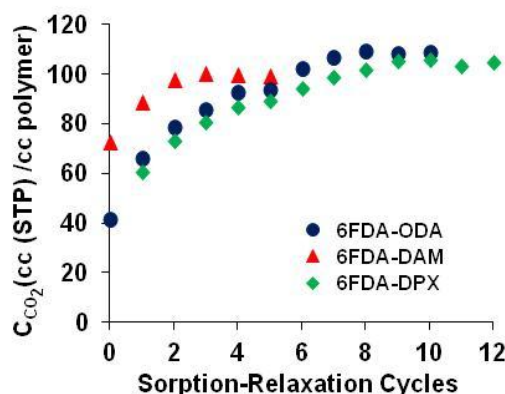
Figure 3.6 : Increase in the CO_2 concentration (C_{CO_2}) in 6FDA-DAM, 6FDA-DPX and 6FDA-ODA due to sorption induced plasticization at 35°C and 10 bar.

Table 3.2: Relationship between the backbone flexibility ($\sigma|\phi|$), glass transition temperature (Tg), FFV increase and CO_2 sorption.

| | $\sigma|\phi|$ | Tg(°C) | FFV | | | S_{CO_2}* |
			initial	final	% increase	
6FDA-DAM	18.5	370	0.271	0.316	16.5	9.866
6FDA-DPX	27.7	345	0.257	0.309	20.2	10.35
6FDA-ODA	45.1	302	0.221	0.323	45.9	10.74

*cc(STP)/cc polymer.bar.

It was also observed that CO_2 concentration depends strongly on the FFV of the swollen membranes at the considered pressure. Figure 3.7 compares the concentration with respect to the FFV at the initial and final sorption steps in the SRCs. Thus, the comparable FFV values of both polymers after plasticization resulted in similar concentration values. This observation agree well with the

findings of Neyertz at al. who reported that sorbed CO_2 molecules interact weakly with each other and the polymer chain [104].
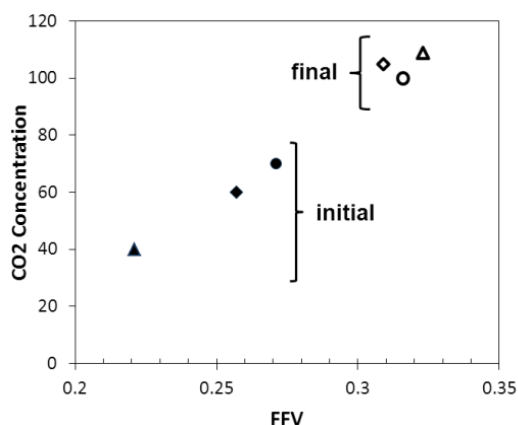
Figure 3.7 : CO_2 concentration at the initial and the final steps of the SRCs in 6FDA-DAM (circles), 6FDA-DPX (diamonds) and 6FDA-ODA (triangles).

The flexibility of the PI chains can be compared to the dihedral angle distribution of the diamine-dianhydride linkage as discussed early in this section. The correlations between $\sigma|\phi|$ and other structural properties can also be extended to the degree of plasticization, reflected by the FFV increase, as illustrated in Figure 3.8. These correlations may be used to predict the FFV increase, whence the degree of plasticization, of the PIs as a function of $\sigma|\phi|$. Consequently, the CO_2 concentration in the swollen PI may be also predicted without any sorption simulation, if the concentration depends primarily on the FFV of the swollen matrix, which appears to be the case for 6FDA-polyimides. But for a more accurate description of correlation we need data for additional polyimides.
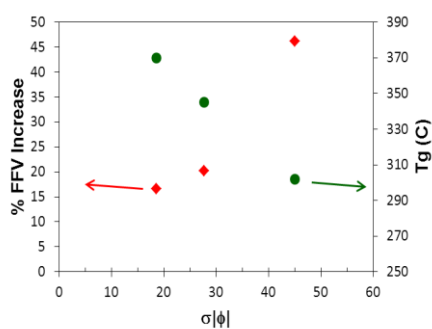
Figure 3.8 : Correlation between the backbone flexibility ($\sigma|\phi|$) and FFV increase and glass transition temperature (Tg) in 6FDA-polyimides.

Table 3.3 compares the sorption coefficients of O_2, N_2, CO_2 and CH_4 gases estimated in this simulation study with the experimental sorption coefficients reported in the literature [99-102, 48, 106, 109, 114], as well as with the simulated sorption

coefficients calculated by Heuchel et al. [48]. Since sorption coefficients mainly depend on the critical temperatures of adsorbed gases, solubility coefficients are also presented as a function of critical temperature of gases in Figures 3.9 and 3.10. The calculated sorption coefficients of these light gases in the polyimides are generally in good agreement with the experimental data reported in the literature. Furthermore, the sorption coefficients calculated in this study are in better agreement with the available experimental data than those obtained by simulations of Heuchel et al. [48] who applied the Transition State Theory (TST) in their calculations ignoring the structural relaxations of polymers. The TST assumes that the polymer chain is stationary within the unit matrix, while each atom in the chain oscillates at its fixed position. It can be seen from Table 3.3 that while the sorption coefficients of CO_2 and CH_4 are affected by this assumption, those of O_2 and N_2 are not. Hence, their sorption coefficients for CO_2 were higher as much as one order of magnitude for 6FDA-DAM and two orders of magnitude for 6FDA-ODA compared to the experimental data. On the other hand, the O_2 and N_2 sorption coefficients in 6FDA-ODA and 6FDA-DAM estimated by Heuchel et al. and this study agree quite well with each other but they are slightly higher than all the experimental data reported in Table 3.3. The data clearly indicates that O_2 and N_2 sorption coefficients are independent of the feed pressure, i.e. simulation/experimental results at different pressures are comparable.

Table 3.3:   Sorption coefficients of light gases in 6FDA-ODA, 6FDA-DAM and 6FDA-DPX.

PI	Sorption Coefficient (cm³ (STP) / (cm³ bar))				Sorption Selectivity (α_S)		
	CO_2[a]	CH_4[a]	O_2[b]	N_2[b]	CO_2/CH_4	O_2/N_2	
6FDA-ODA	10.74	1.952	3.266	2.242	5.50	1.46	This Study
	151.0	14.00	3.700[a]	2.400[a]	10.8	1.54	Sim.[48]
	4.104	1.216	0.912	0.502	3.38	1.82	Exp.[109]
	4.890	1.322	1.030	0.542[a]	3.70	1.90	Exp.[100]
	7.752	1.125	1.284[a]	0.585[a]	6.89	2.19	Exp.[101]
	7.098[c]	1.550[c]	0.530[c]	0.523[c]	4.58	1.01	Exp. [113]
6FDA-DAM	9.866	3.372	4.331	3.216	2.93	1.35	This Study
	68.00	8.600	2.800[a]	1.900[a]	7.91	1.47	Sim.[48]
	6.080	1.976	1.216	0.988	3.08	1.23	Exp.[99]
	13.680	5.320	3.800[a]	2.204[a]	2.57	1.72	Exp.[101]
	21.052	6.612	2.356	1.520	3.18	1.55	Exp.[102]
	6.069[d]	2.030[d]	1.264[d]	1.028[d]	2.99	1.23	Exp.[106]
6FDA-DPX	10.350	3.273	4.200	3.220	3.16	1.30	This Study
	5.016	1.748	1.216	0.988	2.87	1.23	Exp.[99]

[a] at 35°C and 10 bar;   [b] at 35°C and 2 bar unless otherwise stated; [c] at 30°C and 1 bar; [d] at 35°C and 1.5 bar.
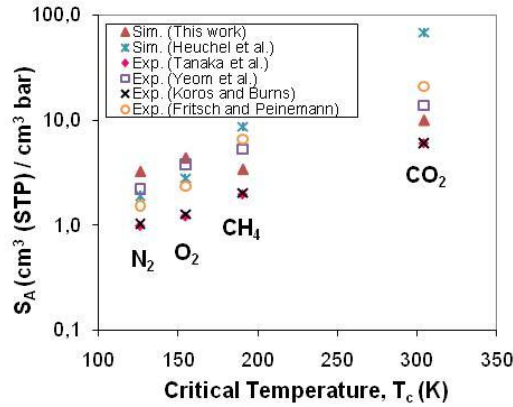
Figure 3.9 :   Comparison of simulated O_2, N_2, CO_2 and CH_4 sorption coefficients in 6FDA-DAM with the experimental data.
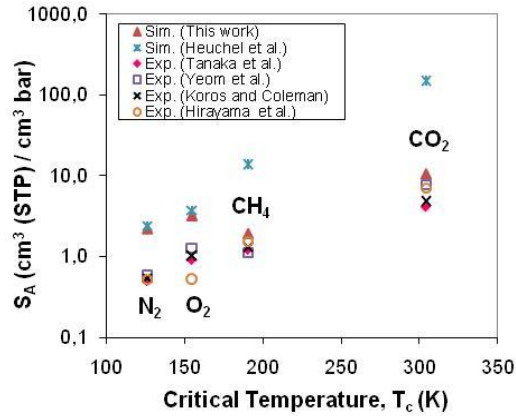
Figure 3.10 : Comparison of simulated O_2, N_2, CO_2 and CH_4 sorption coefficients in 6FDA-ODA with the experimental data.

Next, binary gas sorption simulations were carried out. In real binary gas separation processes, both gases are in the same flow and in contact with each other. Since it is generally difficult to measure sorption selectivities for such systems, it is common to measure pure gas sorption coefficients and calculate the ideal sorption selectivity, which is calculated by taking the ratio of pure gas sorption coefficients. However, ideal and true selectivities may differ significantly due to the combined effect of the competition between the penetrants, gas phase non-ideality, plasticization phenomena, and gas polarization. Table 3.4 compares the simulated ideal and true sorption selectivities of 6FDA-ODA and 6FDA-DAM for O_2 and N_2 ($P_{O_2}:P_{N_2}$ = 21:79) at 35°C and 2 bar, and for CO_2 and CH_4 ($P_{CO_2}:P_{CH_4}$ = 50:50) at 35°C and 10 bar. For non-plasticizing O_2/N_2 pair, variation between ideal and true selectivities is mild as expected. However, very strong departures from ideal selectivities were obtained in the case of binary mixtures of CO_2/CH_4. To estimate ideal and true sorption selectivities of these gas pairs in the two PIs here, the SRC procedure was repeated for each binary mixture. The SRCs were not applied to the case of pure CH_4 sorption, since it was assumed that pure CH_4 does not have any plasticizing effect on the polyimides.

Table 3.4: Single and binary gas ($P_{CO_2}:P_{CH_4}$ = 50:50 for CO_2/CH_4 and $P_{O_2}:P_{N_2}$ = 21:79 for O_2/N_2) sorption coefficients and selectivities of light gases and hydrocarbons in 6FDA-ODA and 6FDA-DAM.

PI		S(CO_2)	S(CH_4)	α_S(CO_2/CH_4)	S(O_2)	S(N_2)	α_S(O_2/N_2)
6FDA-DAM	Pure	9.866	3.372	2.93	4.331	3.216	1.35
	Mixed	13.87	1.678	8.27	4.607	3.013	1.53
6FDA-ODA	Pure	10.744	1.952	5.50	3.266	2.242	1.46
	Mixed	11.713	0.753	15.6	3.288	2.145	1.53

The strong variation between ideal and true selectivities of the CO_2/CH_4 gas pair can be better understood in terms of FFV changes upon sorption. Table 3.5 shows the change of FFV of 6FDA-DAM and 6FDA-ODA due to plasticization. The increase in the FFV of 6FDA-ODA is nearly three times larger than that of 6FDA-DAM, which is less flexible. This behavior is well consistent with our earlier findings. Plasticization effect of CO_2/CH_4 mixed gas is smaller than CO_2 pure gas in both PIs because of lower CO_2 partial pressure and, thus its lower concentration. The increase in the FFV is a function of the CO_2 concentration for each polyimide.

Table 3.5: CO_2-induced FFV increase in 6FDA-DAM and 6FDA-ODA at T = 35°C and P_{total} = 10 bar

Sorbed Species	6FDA-DAM (FFV = 0.271)			6FDA-DPX (FFV=0.257)			6FDA-ODA (FFV=0.221)		
	C^a	FFV	% increase	C^a	FFV	% increase	C^a	FFV	% increase
CO_2	98.66	0.316	16.5	104.8	0.309	20.2	107.4	0.323	45.9
CO_2/CH_4	69.35/8.39	0.311	14.5	---	---	---	58.57/3.77	0.242	9.6

^{a} cc (STP) / cc polymer.

3.3.3 Sorption-induced accessible free volume increase

The analysis of the sorption-induced changes in FAV instead of free volume is a more useful approach to measure sorption-induced conformational changes in the polymer chains as recently reported Chang et al. [50, 87] because the FAV estimation excludes the dead volume and gives a more realistic prediction of available free volume for gas molecule transport. FAV is estimated from the *Connolly* task simulation by using different probe diameters to detect the available vacancy inside the simulation cell. The interaction between probe atom and polymer atoms was ignored during the FAV simulation. Probe size is chosen until 3.2 Å because gaseous molecules are ranging between this region.

Figure 3.11 compares the FAV distribution as a function of probe size for the three polyimides before and after saturation with CO_2. The analysis shows that FAV distributions, which are distinct for each of the empty PI matrices, become similar in all three matrices upon sorption, indicating the sorption capacity depends primarily on the free volume. The increase in the FAV can be seen for a probe radius above 0.8 Å; and much more significantly above 1.65 Å, which is the kinetic radius of CO_2. The change in the FAV distribution is more drastic for 6FDA-ODA due to its higher chain flexibility.
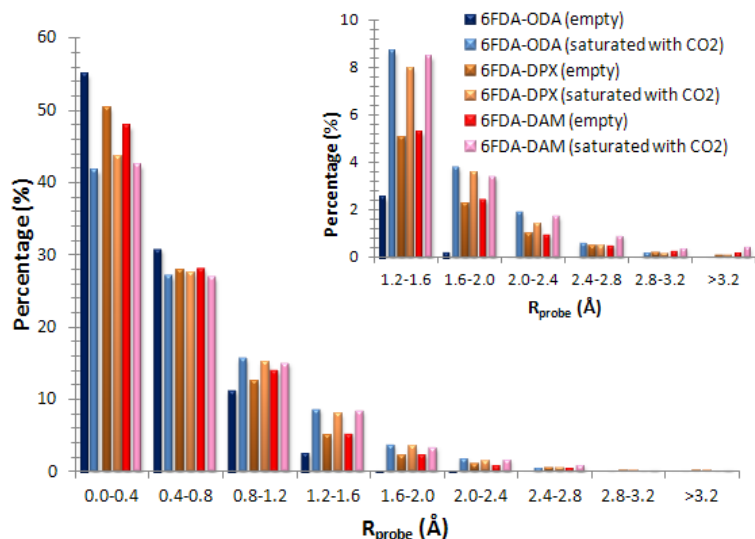
Figure 3.11 : Fractional accessible volume distribution in empty 6FDA-DAM and 6FDA-ODA before and after saturation with CO_2.

3.3.4 Radial distribution functions

RDFs can be used for an in-depth analysis of atomic interactions between penetrants and the PI matrices. Based on the location and intensity of the peaks in the RDF, one can determine the preferential sorption sites on the polymer chain for a particular sorbate. Figure 3.12 presents the RDFs of CO_2 molecules calculated at the corresponding equilibrium concentration at 10 bar and 35 °C around the typical atoms (sorption sites) of the three PIs that are shown in Figure 3.1.
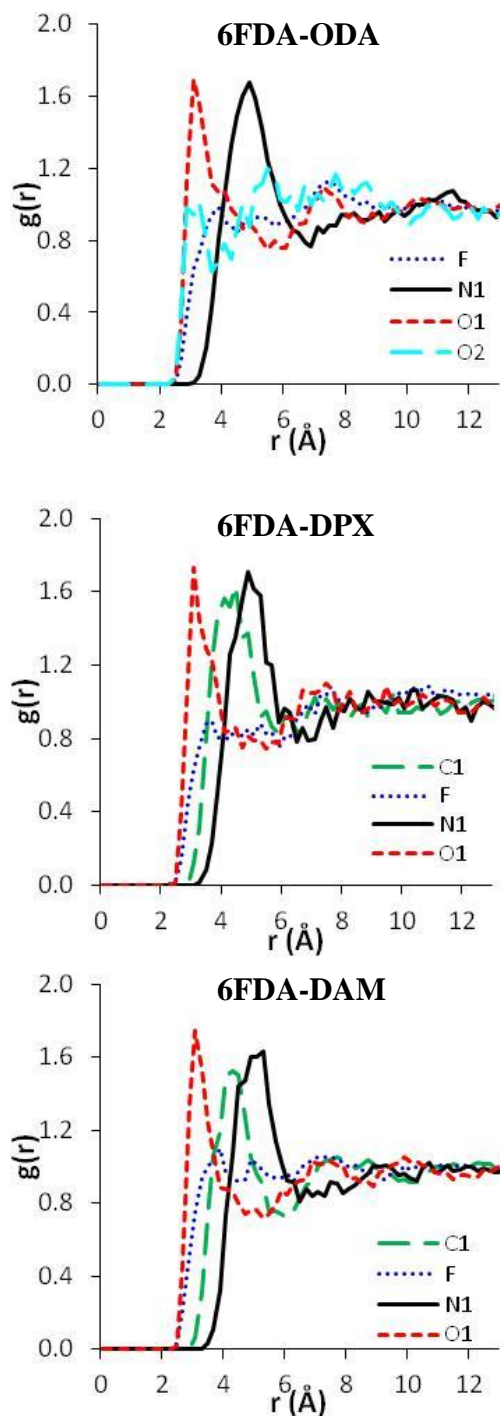
Figure 3.12 : Radial distribution functions (g(r)) of CO_2 in 6FDA-ODA, 6FDA-DPX and 6FDA-DAM.

The typical atoms on the 6FDA-ODA polymer chain are the oxygen and nitrogen in the imide, the fluorine in the $-CF_3$ group, and the oxygen in the ether linkage (labeled as O1, N1, F, and O2, respectively). For 200 CO_2 molecules at the equilibrium concentration, the distinct peaks at 3.0 and 4.9 Å in the RDFs indicate that the oxygen and nitrogen in the imide are the preferential sorption sites for CO_2, but the fluorine atoms are not. Furthermore, the intensity of the peaks for the interactions of

CO_2 with the ether linkage (O2) is relatively lower indicating weaker attraction. This may be due to the fact that the phenyl rings on each side of the ether linkage restrict the access of CO_2 molecules to the O atom in the linkage. These conclusions agree well with the findings of Zhang and coworkers [79], despite the difference in their number of sorbed CO_2 molecules (80 CO_2 molecules in the simulation cell), with the exception of the interactions with the F atoms. Their RDF for the F atoms indicates that these sites are secondary sorption sites, i.e. CO_2 molecules populate these sites at that loading when the preferential sites are all occupied. The RDF agrees reasonably with what we calculated for a loading of 67 CO_2 molecules at the initial stage of the sorption. The difference in the interaction with F atoms may be due to the different force field (polymer consistent force field [114]) and chain model construction employed in their simulations. As the loading increases further to 200 CO_2 molecules, these sites become less preferred.

For 6FDA-DPX and 6FDA-DAM the same typical atoms on the polymer chains were selected due to their similar chemical structures: The oxygen and nitrogen in the imide, the fluorine in the -CF_3 group, and the carbon in –CH_3 group of the diamine (labeled as O1, N1, F, and C1, respectively). While 6FDA-DAM contains one more methyl group than 6FDA-DPX, the numbers of CO_2 molecules dissolved are similar for both PIs. The RDFs indicate that O1, N1 and C1 sites are preferential sorption sites in both PIs. However, the N1 sites in 6FDA-DPX have relatively higher affinity for the CO_2 molecules with respect to the N1 sites in 6FDA-DAM, which act as a favorable sorption site in lieu of the missing methyl group. Furthermore, the diamine-dianhydride linkages in both PIs are similarly accessible to the sorbate molecules, and it is the steric effect of the three methyl groups that increases the plasticization resistance of 6FDA-DAM by reducing the linkage flexibility.

When the RDFs and the degree of plasticization resistance of the three PIs are compared, it may be suggested that the occupation of the sorption sites on the PI backbone by CO_2 molecules promotes plasticization by increasing the chain mobility. The interaction of CO_2 molecules with the O2 site in 6FDA-ODA exhibits this effect very strongly. Since there is no such sorption sites on the backbone of 6FDA-DPX and 6FDA-DAM, and the accessibility of N1 sites to CO_2 molecules is more restricted, and the plasticization of these two PIs is limited.

The change in the CO_2-polymer interactions due to plasticization in 6FDA-ODA can be revealed by comparing RDFs in the initial and final stages of the SRCs (with 67 and 200 CO_2 molecules/simulation cell, respectively). Figure 3.13 shows that there is no significant difference in the RDFs of the CO_2-O1 and CO_2-N1 in the saturated 6FDA-ODA polymer simulation cell at the beginning and at the end of the SRC procedure. The relative shift in the RDF of CO_2-F may also be explained by the change in the chain conformation due to the increased CO_2 loading. However, there is a considerable decrease in the second peak of the RDF of CO_2-O2 whereas the first one remains unchanged. This may be explained by the reorientation of the ether linkage during CO_2 sorption due to the higher flexibility of the backbone (the C-N-C-C linkage). Since both the position and the intensity of the first peak are unchanged, we may conclude that at the closest distance the CO_2 molecules can access to the O2 site remains same but the number of molecules in the next shell decreases due to the change in the chain conformation as explained above. Figure 3.14 shows the change in the dihedral angle distribution of the ether linkage as a result of increased CO_2 loading. The most probable conformations corresponding to the distributions can be seen in the figure as well. The reorientation weakens the charge-transfer complexes formed between the oxygen atoms and the phenyl rings as suggested by Zhang et al. [79] and decreases the plasticization resistance of the polyamide, since these complexes act as local physical crosslinks to suppress larger scale perturbations in the packing in the vicinity of a sorbed penetrant due to sorption of other penetrants in the neighborhood.
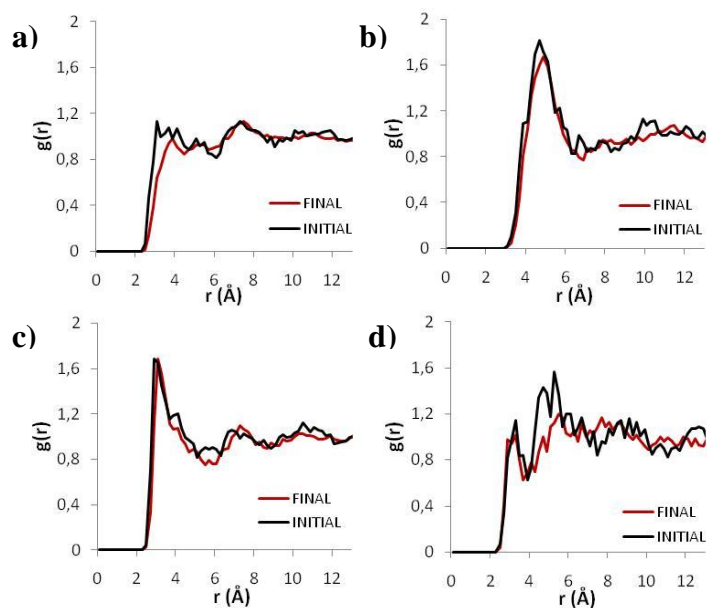
Figure 3.13 : Radial distribution functions g(r) of CO_2 around a) F, b) N1, c) O1, and d) O2 atoms in 6FDA-ODA at the initial and final stages of the sorption process.
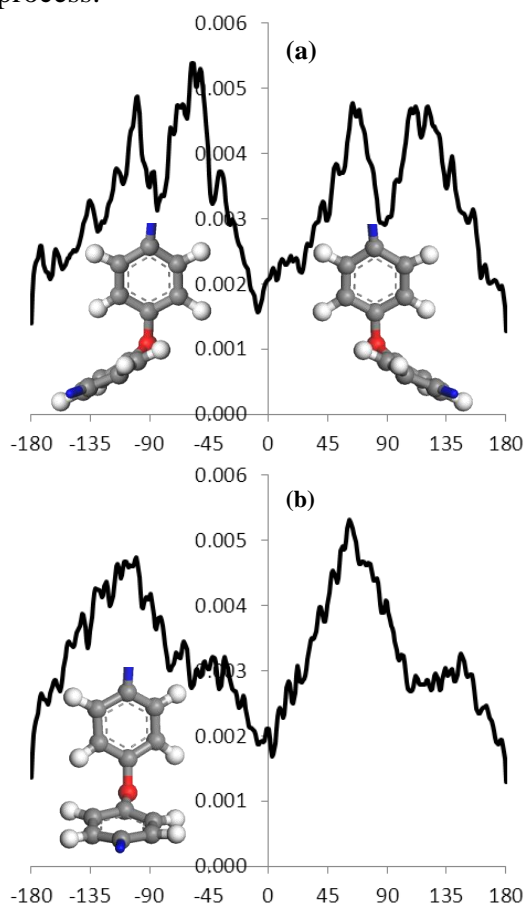
Figure 3.14 : Dihedral angle distributions of the ether linkage (-C-O-C-C-) and the most probable conformations of the diphenyl ether segment in 6FDA-ODA a) before (empty unit cell) and b) after (unit cell saturated with CO_2 the SRCs.

The RDFs before and after the SRCs in 6FDA-DAM and 6FDA-DPX are shown in the Appendices A1 and A2. The lack of significant changes in the RDFs with respect to 6FDA-ODA indicates that the reorientation of the ether linkage in the ODA moiety due to the mobility of the backbone is the principle factor for the stronger plasticization of 6FDA-ODA. The change in the chain conformation due to this linkage leads also rearrangement of the CF_3 groups which explains the change in the CO_2-F RDF in 6FDA-ODA, whereas no such change was observed in 6FDA-DAM and 6FDA-DPX.

In summary, the analysis of the RDFs indicates that the plasticization of PIs is due to strong interactions between the sorbate molecules and the backbone sorption sites. These sites are more accessible to sorbate molecules at the initial stages of the sorption; however due to the rearrangement of the polymer chain with increasing sorbate concentration, their accessibility decreases. Thus, if the concentration of the plasticizing component varies strongly between unary and binary sorption cases, i.e. if the concentration depends strongly on the partial pressure, then the nature of interactions will change with the amount of the gas in dissolved in the polymer, and this may lead to a significant difference between ideal sorption selectivity and actual selectivity for a given gas pair, as reported in the literature [23, 115].

The analyses hint that plasticization of these membrane materials may be reduced by the addition of properly selected antiplasticizing agents that would compete against the CO_2 molecules for occupying the preferred sites on the backbone such as N1 and O1, and restrict reorientation of the backbone. Furthermore, removal of these preferred sites on the backbone may also reduce plasticization. In fact, thermally rearranged polyimides, which are reported to be resistant to plasticization, lack these sites as can be seen in Figure 3.15 illustrating thermal rearrangement from hydroxyl-containing polyimide to polybenzoxazole [116]. Simulation work on plasticization behavior of thermally rearranged polymers is in progress in our group.
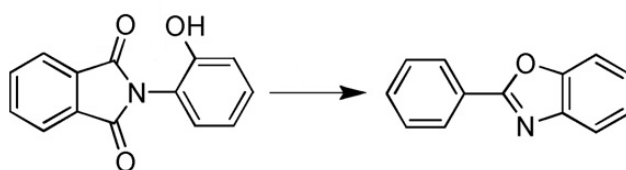
Figure 3.15 : Thermal rearrangement from hydroxyl-containing polyimide to polybenzoxazole [116].

3.4 Summary

In this study, three PIs, 6FDA-ODA, 6FDA-DPX and 6FDA-DAM, are analyzed to identify the relationship between the polymer structure and plasticization using Monte Carlo and molecular dynamics simulations. The structural properties, i.e. d-spacing, fractional free volume (FFV), cohesive energy density and glass transition temperature, of the PIs were estimated in good agreement with the experimental data, which indicates that molecular simulation can be used successfully to characterize various PI structures.

Simulation of the sorption process of CO_2 successfully reproduced the plasticization behavior in the PIs through the sorption-relaxation cycles. Estimated sorption coefficients of these gases in both PIs are within the same order of magnitude with the experimental data in the literature. Results indicate that the CO_2 sorption capacities of the PIs at 35°C and 10 bar are proportional the FFV of the swollen PI, with similar FFV values yielding similar CO_2 concentrations. Thus, the sorption of the CO_2 molecules induces configurational changes in the polymer backbone through the particular interactions with the sorption sites, leading to an increase in the FFV associated with swelling and plasticization. These conclusions may also be supported through the analyses of the accessible free volume distributions in the PIs: while each PI exhibited distinct distribution when unoccupied, the distributions became similar upon CO_2 sorption. Furthermore, the analysis of the RDFs suggests that the plasticization resistance of the PIs correlates with the accessibility of the CO_2 molecules to the diamine-dianhydride linkages on the polymer chain.

The extent of CO_2-induced FFV increase resulting from swelling and plasticization is controlled by the backbone flexibility. Simulations showed that the flexibility of the PI chains can be compared based on the distribution of the absolute values of the dihedral angles of the diamine - dianhydride linkage. Therefore a correlation may be proposed between the FFV increase and the standard deviation of the dihedral angle distribution. This relationship may be used to predict the FFV increase, whence the degree of plasticization, of the PIs as a function of this standard deviation. Consequently, the CO_2 concentration in the swollen PI may also be predicted, assuming that the concentration depends primarily on the FFV of the swollen matrix. This may lead to an efficient screening of suitable combinations of diamine and

dianhydride pairs among hundreds that are resistant to sorption-induced, which is a major problem for their use in commercial gas separation applications as membrane materials. With the accurate estimation of the diffusivities and hence permeabilities of the PIs in the future work, the simulation methodology applied here can be used to predict the effect of plasticization on transport properties of gases in different polyimides and also copolyimides for which there are no experimental data to explore their potential use as membrane material.

4. PROPYLENE/PROPANE PLASTICIZATION IN FLUORINATED POLYIMIDE MEMBRANES

4.1 Introduction

Among various polymeric membrane materials in gas separation area, aromatic polyimides (PIs) are an important group of polymers with outstanding thermal and chemical stability, and good mechanical properties [89]. They are synthesized by the reaction of dianhydride and diamine monomers, which govern selectivity towards separation of commercially important gas pairs such as O_2/N_2, CO_2/CH_4, H_2/CH_4, H_2/N_2 and propylene/propane. Numerous extensive experimental studies have been reported in the literature about PIs synthesized using different dianhydride/diamine combinations [90-94]. Hence, due to the interdependence of chemical structures and gas transport properties [95], selection of an appropriate monomer pair is crucial for the preparation of membranes with high selectivity for a specific application. For example, polyimides with large substituents such as 4,4-hexafluoroisopropylidene-diphthalic anhydrides (6FDA) containing two bulky CF_3 groups; 2,4,6-trimethyl-m-phenylene diamine (DAM) and 1,2,4,5-tetramethylbenzene (TeMPD) diamines containing three and four CH_3 groups, respectively; 4,4'-hexafluoroisopro-pylidene dianiline (6FpDA) diamine containing two bulky CF_3 groups, have been considered due to the increase of the polymer's fractional free volume (FFV) resulting in a rise in permeation rates for olefin/paraffin separation [81, 99, 117-123].

In membrane based gas separation processes, sorption induced volume swelling and plasticization appear to be a serious concern, limiting the use of PIs as membrane material for gas separation involving CO_2, H_2S and condensable hydrocarbons such as propylene (C_3H_6) and propane (C_3H_8). Plasticization is a pressure dependent phenomena and occurs when the concentration of these gases in glassy polymers, such as PIs, is high enough to cause swelling in the polymer, i.e. reduce chain alignment and increase inter-segmental mobility and FFV [117-121]. The upturn pressure obtained in the plasticization in the permeability versus pressure plot is

known as the plasticization pressure. At this point due to the loss in size discrimination ability, there would be a significantly high selectivity decrease, therefore it is important to test membranes with mixed gas compositions. In the case of C_3H_6/C_3H_8 separation, the sorption-induced swelling phenomena allow C_3H_8 to diffuse at an increased rate relative to that in unplasticized polymer, which decreases the membrane selectivity. Staudt-Bickel and Koros [117] observed plasticization of the membrane with pure propylene by the upturn in permeability values around a propylene upstream pressure of 3 bar. They further tried to define plasticization effect with a 50:50 mixed gas propylene/propane permeation test. The mixed gas selectivity decreases to 7 from 13 which is the pure gas selectivity. Propylene and propane, both being condensable, tend to plasticize polymeric membranes, even at partial pressures as low as 2 bar [121].

Therefore, plasticization has to be minimized by proper molecular design to overcome the permselectivity reduction, which requires a fundamental understanding of penetrant induced plasticization. Only a few experimental studies investigating plasticization effect of propane and propylene in polyimides have been reported in literature [117-121, 124-129]. While rubbery polymers have very low selectivity (1-2) especially for propylene/propane separations, Das and Koros summed up all transport properties of polyimides and showed that polyimides have high selectivity (10-30) [121]. Among all these studies, 4,4-hexafluoroisopropylidene-diphthalic anhydride (6FDA)-based polyimides were preferred for propane and propylene separation due to their best performances. Mainly the observed plasticization pressure among these studies was between 2 and 5 atm. In order to suppress plasticization, cross-linking and thermal treatment were used. Visser and Wessling [127] and Das and Koros [121] investigated binary mixture of propylene and propane and concluded that when both components of a binary mixture show autoplasticization, facilitated plasticization can be observed if process parameters or material properties cause high degree of swelling.

Advances in molecular modeling provide an excellent opportunity to quantitatively investigate penetrant induced plasticization and understand the mechanisms behind it. However, there is not any molecular simulation study that focused on propane and propylene-induced plasticization in polyimides, while a significant amount of research has been done on polymers such as polystyrene, poly[1-(trimethyl silyl)-1-

propyne] (PTMSP) and poly(vinyl alcohol) (PVA) for propylene/propane separations [130-132]. Although all these polymers were rubbery and easy to simulate compared to rigid glassy polymers such as polyimides, computer simulation studies overestimated the solubility coefficients nearly by one order of magnitude.

In this study, molecular simulation techniques were used to estimate the degree of plasticization of 6FDA-based PI membranes induced by sorption of propane and propylene molecules. The 6FDA-based PIs exhibit high gas permeabilities and low chain packing densities as a result of the blockage of the rotation of phenyl rings by $-C(CF_3)_2-$ linkage [9] and membranes with commercially attractive selectivities may be obtained by changing the diamine structure. PIs such as 6FDA-DAM, 6FDA-DPX and 6FDA-ODA (Figure 3.1 in Chapter 3) have a strong potential for O_2/N_2, CO_2/CH_4 and C_3H_6/C_3H_8 separation applications [106]. In Chapter 3 on CO_2-sorption induced plasticization of these three PIs [133]; the structural properties, such as glass transition temperature (T_g), FFV and its distribution, d-spacing, radius of gyration, and cohesive energy density, along with sorption isotherms were investigated from simulations to understand the dynamics of polymer chains and penetrants and the comparison was made with the experimental data available in the literature to provide an insight to polyimide structure-plasticization. In this current chapter, we extend our methodology to examine the plasticization phenomena in propane/propylene separation.

The propane and propylene concentrations in polymers scale usually with the FFV of the materials [81, 99, 117-123]. Tanaka et al. [118] showed that 6FDA-based polyimides have higher performances for propylene/propane separation than BPDA-based polyimides due to the larger FFV of the 6FDA compared with BPDA polyimides. As a result of the reduced molecular interactions and steric hindrance of CF_3 groups, 6FDA-based PIs show larger FFV compared with BPDA. Similarly, in their other study, Tanaka et al. [99] reported that PIs with DAM and Durene (Durene: 2,3,5,6-tetramethyl-1,4-phenylenediamine) diamines, which has three and four $-CH_3$ groups respectively, also possess larger FFV than other diamines such as ODA and DDBT due to the rigidity and non-polar structure of the polymer chains, as well as the bulkiness of the methyl groups which causes inefficient packing of the polymers chains.

Thousands of diamine-dianhydride combinations can be suggested as potential membrane materials, but only a limited number of them are synthesized and characterized for gas separation applications until now. However, molecular simulation techniques offer an opportunity to predict the structure-property relationships without wasting time and money in case of failure.

4.2 Simulation Method

All simulations in this work were carried out according to methodology described in Section 2.5. Sorption simulations of propane (C_3H_8) and propylene (C_3H_6) in PI matrices were carried out by the *Sorption* module of the software with the Grand Canonical Monte Carlo (GCMC) ensemble at fixed temperature, volume and chemical potential using the Configurational Bias Method [76]. Simulation temperature and pressure values were chosen based on the experimental studies in the literature: 25ºC and 1.13 bar for C_3H_8 and C_3H_6. These conditions correspond to the experimental study of Shimazu et al. [81, 123], who calculated sorption coefficients for PIs with the pressure decay method with a pirani pressure transducer, instead of obtaining them indirectly by calculating the ratio of permeability to diffusivity. Furthermore Burns and Koros [122] were performed gas sorption measurements using a dual volume sorption apparatus [21] for only 6FDA-DAM PI at 35ºC and 2 bar.

Ideal sorption selectivities of C_3H_6/C_3H_8 gas pair in the PI matrices were evaluated by calculating the ratio of the estimated sorption coefficients of the relevant gases. However, actual selectivities may differ significantly from ideal values due to the plasticization and competitive sorption [103, 134]. Difficulty in transport mechanism occurs when a second gas is present in the feed stream. If there is not any plasticization, the adsorption of both components will be lower than the single gas adsorption due to the competitive sorption. But if one of the gasses has a plasticization effect on polymer matrices, the transport phenomena will get even worse to understand. In mixed gas experiments, permeability can decrease or increase compared to single gas experiments. When both gases of binary mixture plasticize the polymer matrices, which is called facilitated plasticization, the mass transport also turns to even more complex case to work out. To reproduce these

effects, actual mixed gas sorption selectivities were also calculated for mixtures of C_3H_6/C_3H_8 ($P_{C6H6}:P_{CH6H8} = 50:50$) in PIs.

4.3   Results and Discussion

4.3.1 Sorption simulations

The equilibrium concentrations and corresponding sorption coefficients of C_3H_6 and C_3H_8 were calculated through the sorption-relaxation cycles (SRCs) as described in Section 2.5 in a purely predictive manner. Figure 4.1 shows the convergence of the C_3H_6 and C_3H_8 concentrations in the three PIs through the SRCs. These cycles provided an estimation of the extent of C_3H_6 and C_3H_8 induced volume swelling and plasticization in the membrane materials.
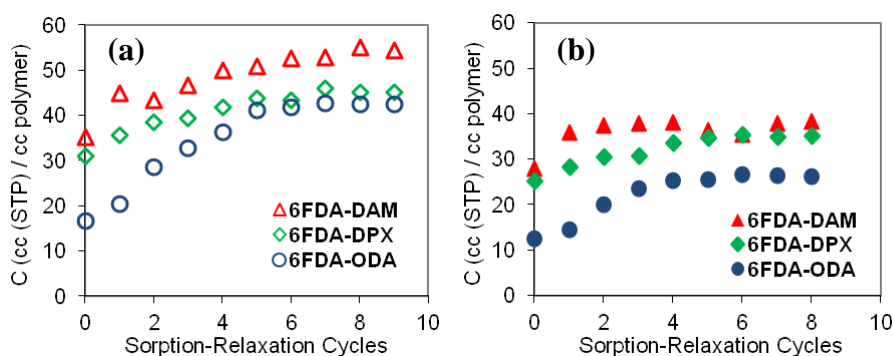
Figure 4.1 : Increase in the a) propylene and b) propane concentration in 6FDA-DAM, 6FDA-DPX and 6FDA-ODA due to sorption induced plasticization at 25°C and 1.13 bar.

The sorption coefficients for these species estimated at 25°C and 1.13 bar through the SRC procedure, are presented in Table 4.1 along with ideal and real selectivities. Comparison with the experimental data [81, 123] shows that there is a systematic overestimation of the sorption coefficients for both hydrocarbons. However, the experimental and calculated selectivities are in good agreement. For all three PIs in single gas sorption, it takes few SRC runs to reach the steady state. However, it needs more SRC runs to reach steady sate in mixed gas sorption due to mutual plasticization effects of propylene on propane and hence the lower adsorption rate at which the sorption of propane changes in time compared to that of propylene. The same tendency was observed by Visser and Wessling [127] that experimental C_3H_6/C_3H_8 mixed gas measurements for asymmetric P84/Matrimid blend membrane reach steady state at a relatively long time.

Table 4.1: Single and binary ($P_{C_3H_6}:P_{C_3H_8}$ = 50:50) gas sorption of propylene /propane and corresponding C_3H_6/C_3H_8 selectivities in PIs.

PI			$S^a_{C_3H_6}$	$S^a_{C_3H_8}$	α_S
6FDA-DAM	Single	This work	48.389	33.182	1.46
		Experimental [81]	36.632	28.424	1.29
		Experimental [122]	16.708	13.261	1.26
	Binary	This work	59.949	29.100	2.06
6FDA-DPX	Single	This work	40.649	31.340	1.30
		Experimental [123]	22.653	-----	------
	Binary	This work	48.838	24.601	1.99
6FDA-ODA	Single	This work	37.974	23.169	1.64
		Experimental [81]	17.784	11.780	1.51
	Binary	This work	30.357	19.476	1.56

^{a} cm^3 (STP) / cm^3.bar.

Simulations revealed that the increase in the FFV was larger for both gases in 6FDA-ODA, due to its higher backbone flexibility. As illustrated in Figure 4.2, the cross-section diameter and as well as the kinetic diameter value of C_3H_6 is larger than that of C_3H_8 due to the sp^2 carbon in C_3H_6 which is bigger than the sp^3 carbon in C_3H_8. However, the molecular length between the mass center of hydrogen atoms at the ends of C_3H_6 (3.75 Å) is shorter than that of C_3H_8 (4.35 Å) and also has a flat structure [135]. Hence, propylene, with its relatively smaller size, induces more significant increase in the FFV than propane in all PIs as can be seen in Table 4.2, which agrees with previous reports in literature [81].

Propylene : $CH_2=CH-CH_3$ Propane : $CH_3-CH_2-CH_3$
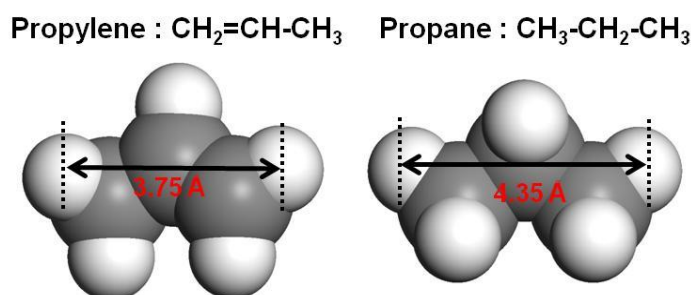
Figure 4.2 : Simulated molecular dimension of propylene and propane.

Table 4.2: The FFV increase in PIs at T = 25°C and P_{total} = 1.13 bar due to single C_3H_6 and C_3H_8 gases and their binary mixture.

Sorbed Species	6FDA-DAM (FFV = 0.271)			6FDA-DPX (FFV=0.257)			6FDA-ODA (FFV=0.221)		
	C^a	FFV	% increase	C^a	FFV	% increase	C^a	FFV	% increase
C_3H_6	54.68	0.305	12.5	45.463	0.283	10.12	42.56	0.257	16.3
C_3H_8	37.50	0.282	3.8	35.051	0.277	7.78	26.27	0.239	8.2
C_3H_6/C_3H_8	33.87/16.44	0.301	10.8	27.31/13.76	0.274	6.61	17.15/11.0	0.237	7.3

[a] cc (STP) / cc polymer.

Comparison of hydrocarbon and CO_2 sorption behaviors of three PIs shows that while the CO_2 sorption capacity of PIs correlates with the FFV of the swollen PI, with similar FFV values yielding similar CO_2 concentrations, no such relationship was obtained for propane and propylene. The decorrelation between the FFV and sorption capacity is especially more significant for propane than propylene. To better analyze the sorption characteristics, further analyses were carried out on sorption induced changes on fractional accessible volumes (FAVs) and radial distribution functions (RDFs).

4.3.2 Sorption-induced accessible free volume increase

The analysis of the sorption-induced changes in FAV instead of free volume is a more useful approach to measure sorption-induced conformational changes in the polymer chains as recently reported Chang et al. [86, 87]. FAV is estimated from the *Solvent* task simulation by using different probe diameters (D_{probe}) to detect the available vacancy inside the simulation cell.

Figure 4.3 present the propane- and propylene- induced changes in the FAV distribution due to sorption for PIs. The change in the FAV induced by sorption is more significant for 6FDA-ODA due its higher flexibility. It is noteworthy that the increase in FAV due to propylene sorption is observed for $D_{probe} > 1.6$ Å, whereas the increase due to propane sorption is observed for $D_{probe} > 2.4$ Å. The analysis shows that FAV distributions, which are distinct for each of the empty polyimide matrices, do not become similar in all three matrices upon sorption of C_3H_6 and C_3H_8, indicating the sorbate-polymer interactions have a more significant role on sorption capacity than free volume of the swollen polymer matrix itself, as opposed to CO_2 sorption [133], where the sorption capacity depends primarily on the free volume. The role of the sorbate-polymer interactions can be better understood with the help of RDFs.
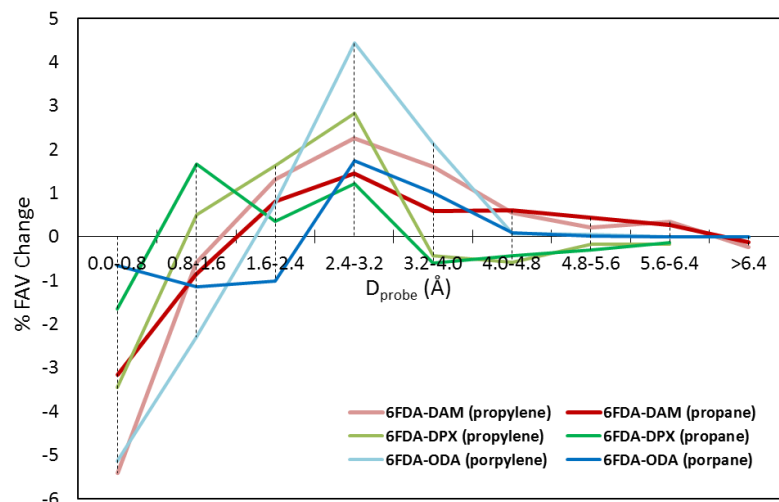
Figure 4.3 : Sorption induced changes (%) in FAV distributions in polyimides.

4.3.3 Radial distribution functions

RDFs can be used for an in-depth analysis of atomic interactions between penetrants and the PI matrices. The RDF (g(r)) describes in general how the atomic density, ρ, varies as a function of the distance, r, from one particular atom with respect to bulk density, ρ_b.

$$\rho(r) = \rho_b\, g(r) \tag{4.1}$$

It should be noted that g(r) should approach 1 for large r values. At very short distance, the radial distribution function must be zero, because two atoms cannot occupy the same space. Peaks are observed when distance between two atoms are larger than the nearest interaction distance (e.g. the van der Waals diameter (σ) in case of spherical particles), because the neighboring atoms try to diffuse into the region occupied by the one at the origin. The remaining atoms in the first peak causes a lack of particles in the adjacent region, explaining the minimum of $g(r)$ around r = 2σ.

RDFs can be used for an in-depth analysis of atomic interactions between penetrants and the polyimide matrices. Based on the location and intensity of the peaks in the RDF, one can determine the accessibility and affinity of the sorption sites on the polymer chain for a particular sorbate. The RDFs of pure and binary propane and propylene sorption around the four typical atoms such as the oxygen and nitrogen in the imide, the fluorine in the -CF$_3$ group, and the oxygen in the ether linkage (labeled as F1, N1, O1 and O2, respectively) in the saturated 6FDA-ODA and, instead of O2,

the carbon of –CH$_3$ groups in the diamine (labeled as C1) for the saturated 6FDA-DPX and 6FDA-DAM are presented in Appendix 3 of Figures A3-14. In order to prevent complexity, the initial and final stages of all PIs' RDFs did not present here and the results were summarized below an in Table 4.3.

Table 4.3: Summary of favorite sorption sites at T = 25°C and P$_{total}$ = 1.13 bar due to single and binary C$_3$H$_6$ and C$_3$H$_8$ penetrant sorption.

		Favorite Sorption Sites		
		6FDA-DAM	*6FDA-DPX*	*6FDA-ODA*
Single	Propylene	N1>C1≈O1>F1	N1≈C1≈O1>F1	O1>N1>O2≈F1
	Propane	N1>C1≈O1>F1	N1>C1>O1>F1	N1>O1≈O2>F1
Binary	Propylene	N1≈O1>C1>F1	C1>N1>O1>F1	O2>N1>O1>F1
	Propane	N1>C1≈O1>F1	C1>N1>O1>F1	N1>O1≈O2>F1

The RDF analyses of single gas sorption simulations suggest that propane molecules prefer to occupy sites around the nitrogen atoms of the imide groups. Propane molecules display significantly higher affinity to all sorption sites in 6FDA-ODA except fluorine atoms, while it has preference to nitrogen and carbon atoms with a small difference in 6FDA-DPX. However, only nitrogen atoms are dominant in the interaction with pure propane in 6FDA-DAM. On the other hand, while propylene molecules favor the oxygen atoms of dianhydride (the side chain) in 6FDA-ODA, causing the promotion of small local motions, the nitrogen is still the most preferential sorption site for 6FDA-DAM and 6FDA-DPX as in the case of propane sorption, by a small margin right before carbon and oxygen side groups.

Comparison of the RDFs for propane at the initial and final stages of SRCs shows that there are not any remarkable changes in the RDF diagrams of 6FDA-DAM, while there is an increase in the interaction of side groups (O1) with pure propane in 6FDA-ODA and 6FDA-DPX. Hence, the substantial increase in the FFV (6FDA-ODA > 6FDA-DPX > 6FDA-DAM) and plasticization can be identified easily for propane sorption. These results correlate with the backbone rigidity of the polymers.

The comparative RDF analysis for propylene for the final and initial stages of SRCs shows on the other hand that there is an increase affinity to all side groups in 6FDA-DAM while its preference rises only in oxygen groups of 6FDA-DPX. This observation agrees with the FFV increase after propylene sorption in 6FDA-DAM, which is higher than 6FDA-DPX as shown in Table 4.2. This indicates that

propylene molecules favor those side groups that are easily accessible rather than forming interactions with more sheltered parts of the polyimide. For instance, oxygen (O2) and nitrogen atoms in the backbone of PI chain lose intensity after propylene adsorption with the SRCs procedure due to the hindered interactions between the penetrant and polymer backbone.

In the case of the propane-propylene mixture sorption, propane molecules have again the strongest interaction with nitrogen atoms in the imide group of all three polyimide structures. However, the most preferential sorption site varies for the propylene molecules according to the diamine monomer of polyimide. Propylene has the affinity to oxygen atoms of the polyimide backbone in 6FDA-ODA, carbon atoms of diamine side groups in 6FDA-DPX and nitrogen and oxygen atoms in 6FDA-DAM.

In summary, the analysis of the RDFs clearly displays that there is strong interactions between the penetrants and the backbone sorption sites, which results in the plasticization of PIs. These sites are more accessible to penetrants at the initial stages of the sorption; however due to the rearrangement of the polymer chain with increasing sorbate concentration, their accessibility decreases. Consequently, it is an expected outcome to obtain differences between ideal sorption selectivity and actual selectivity for a given gas pair. If the concentration of a gas in a mixture at its partial pressure differs significantly than the concentration of the same gas at a pressure equal to the total feed pressure of the mixture, important deviations from ideal selectivities can be observed as reported in the literature [115].

4.3.4 Rotational Time Correlation Function

To quantify the linkage flexibility, in Chapter 3 [133], the standard deviation of the dihedral angle distribution based on the absolute values, $\sigma|\varphi|$ was calculated. To further characterize the mobility of three PIs, the mobility of the diamine-dianhydride linkage were examined through the Rotational Time Correlation Functions (RTCF) analysis. For this purpose, vectors connecting the carbon atoms in the 5-member ring of dianhydride (*C*-N-C-C) and phenyl ring of diamine (C-N-C-*C*) were defined. Molecular motions cause differences in molecule orientation and these reorientations with time can be described by the time correlation functions,

$$P_2(t) = \frac{3}{2}\langle(\boldsymbol{u}(t_0).\boldsymbol{u}(t_0-t))^2\rangle - \frac{1}{2}$$

(4.2)

where $\boldsymbol{u}(t)$ denotes a unit vector characterizing the orientation at a time, t. The more rigid polymer structure means that the RTCF decays slower.

Figure 4.4 shows that RTFC of empty PI matrices and those saturated with propane and propylene. Comparison of the RTFC for empty matrices show that the decay of the RTFCs correlates with $\sigma|\varphi|$, that is, the more wide-spread the dihedral angle of the linkage, the faster the decay, hence the more flexible the polymer chain. When $\sigma|\varphi|$ values of empty and saturated matrices were compared (not presented here), the clear representation could be obtained. Hence RTCFs (Figure 4.4) explicitly reveal the differences in the chain flexibility of PIs for the empty and the saturated matrices with penetrant molecules. For matrices saturated with propylene penetrants, there is similar tendency between the FFV increase and the vector decay. 6FDA-ODA has the highest increase in FFV as well as the more wide-spread the dihedral angle of the linkage and hence the fastest decay in RTCF. 6FDA-DPX follows the 6FDA-ODA PI. On the other hand, the difference in FFV increase and the decay rate of the defined vector between 6FDA-DPX and 6FDA-ODA in propane sorption is closer to the each other than between 6FDA-DPX and 6FDA-DAM PIs. For matrices saturated with propylene molecules, the decay rate for 6FDA-DAM and 6FDA-DPX in RTCFs were not proportional with the FFV increase.

Moreover, same graphs also were shown in PI-based graphs separately in Figure 4.5. Saturated matrices with both hydrocarbon molecules of 6FDA-DPX, with propane of 6FDA-DAM and propylene of 6FDA-ODA PIs show the fastest decay rates than the empty matrices, which is the evidence of the plasticization and swelling of PIs with the penetrant concentration increase. However, in 6FDA-ODA, the matrix saturated with propane is the slowest one and in 6FDA-DAM, the matrix saturated with propylene is almost same with empty matrix. This may be the indication of the occurrence of some blocking in the movement of PI chain when the matrix saturated with penetrant molecules. 6FDA-DPX has the same decay rate in both hydrocarbons of RTCFs as well as closer FFV increase.
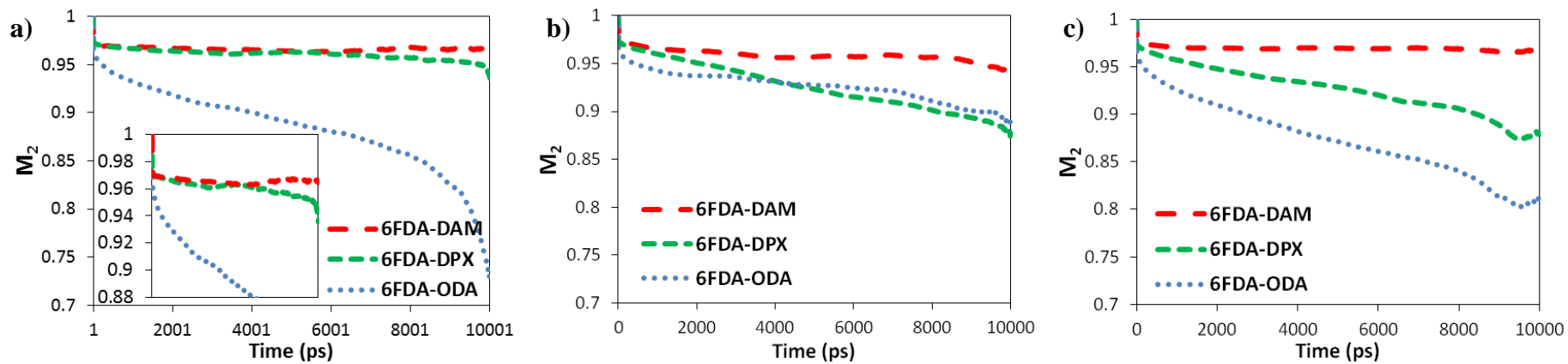
Figure 4.4 : RTCF of a) empty and the saturated b) propane and c) propylene PI matrices.
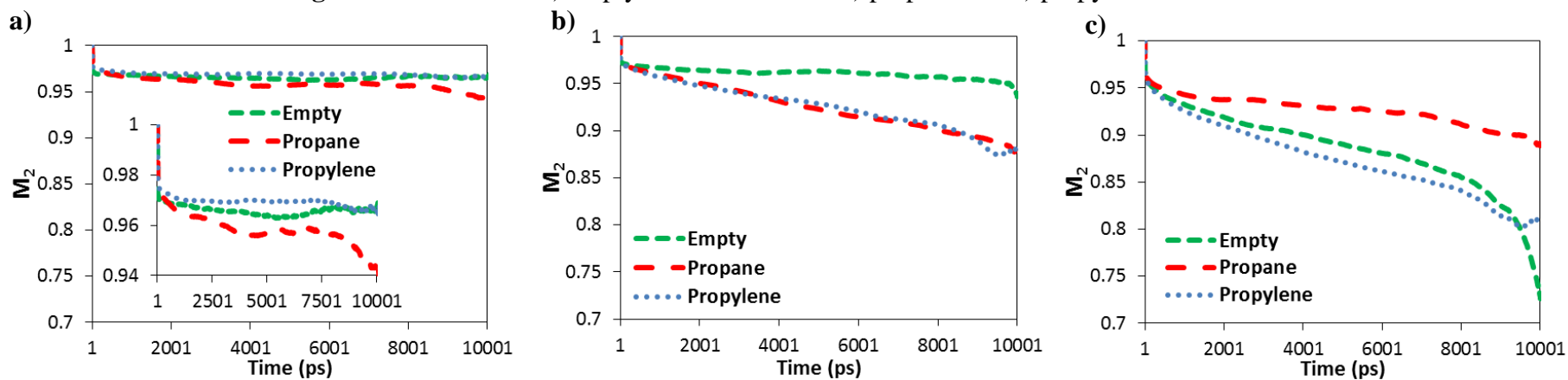
Figure 4.5 : RTCF of a) 6FDA-DAM, b) 6FDA-DPX and c) 6FDA-ODA PI matrices.

4.3.5 Mean Square Displacement

In polymeric membranes, a gas molecule can jump from one void to another as a result of the opening and closing of voids in the polymer matrix, leading to gas diffusion. The mobility of propane and propylene was estimated by the mean-squared displacement (MSD) of the gas molecules

$$MSD(t) = \frac{1}{N}\sum_{i=1}^{N}\left\langle\left|r_i(t) - r_i(0)\right|^2\right\rangle \tag{4.3}$$

where N is the number of gas molecules and $r_i(t)$ is the position of the ith molecule at time t. MSD was calculated from the ensemble average $\langle\ldots\rangle$ of the trajectory. In this study, the number of molecules of each gas at the saturated state were used to calculate MSDs which were performed for 10-ns of each PIs to provide the longer time period for further discussion.

Figure 4.6 shows the MSD diagrams of the propane and propylene molecules in PI membranes during a 10-ns MD duration. The MSDs of propane and propylene in 6FDA-DAM are higher in comparison to the 6FDA-DPX and 6FDA-ODA PIs. The MSDs suggest that the free volume in the polymers allows for the transport of species inside the membrane structure. Therefore, it can be seen that penetrant displacement is proportional to the FFV of PIs and a measure of diffusivity. For instance, MSD of propane in 6FDA-DAM and 6FDA-DPX PIs are close to the each other, while propane molecules in 6FDA-ODA show more restricted movements due to closed-packed structure of 6FDA-ODA PI. When FFV parameters of these PI matrices after penetrant saturation are compared, the same relationship can also be seen in the final FFVs.
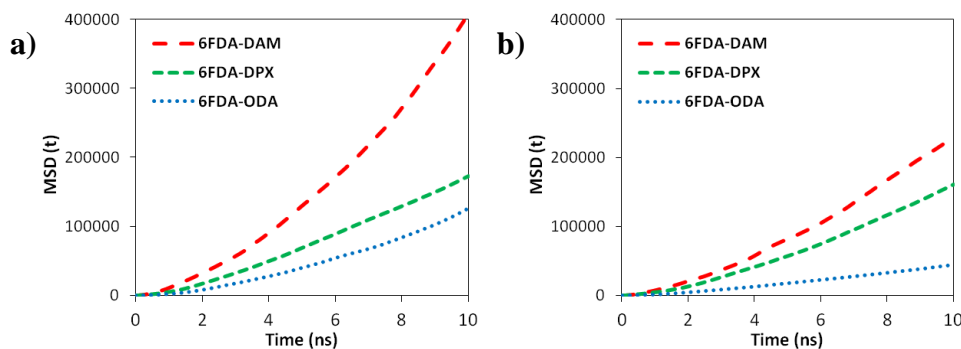
Figure 4.6 : MSD of a) propylene and b) propane in PI matrices.

4.4 Summary

In this study, we considered three PIs, 6FDA-ODA, 6FDA-DPX and 6FDA-DAM, and analyzed the relationship between polymer structure and plasticization using Monte Carlo and molecular dynamics simulations. Simulation of the sorption process of propane and propylene, which are known as strong plasticizers for PIs, successfully reproduced the plasticization behavior in 6FDA-ODA, 6FDA-DPX and 6FDA-DAM through the sorption-relaxation cycles. Estimated sorption coefficients of these gases in all PIs are within the same order of magnitude with the experimental data in the literature. Sorption simulations for binary gas feed can be used to predict the plasticization behavior at different feed compositions. Ideal sorption selectivities are comparable to binary feed selectivities since both propane and propylene are plasticizing gases.

Propylene affects the O1 site which is bulky group in 6FDA-ODA, hence FFV increase is large. But when N1 site which is in backbone, is the most preferential sorption site, FFV increase become smaller.

Results indicate that the CO_2 sorption capacity of both PIs at 35°C and 10 bar depends on the FFV of the swollen PI, with similar FFV values yielding similar CO_2 concentrations. Thus, particular interactions between CO_2 and sorption sites have limited differential contribution on sorption capacity, as supported also by the RDFs [133]. However, no such relationship was obtained for propane and propylene at 25°C and 1.13 bar due to changing site preferences, indicating the strength of sorbate-site interactions is significant on sorption capacity, as well as the FFV. These conclusions may also be supported through the analyses of the accessible free volume distributions in all PIs: while each PI exhibited distinct distribution when unoccupied, the distributions became similar upon CO_2 sorption. However the distributions were again different than each other in the case of propane and propylene sorption.

Sorption-induced plasticization of PIs is a major problem for their use in commercial gas separation applications as membrane materials. Since there are hundreds of combinations of diamine and dianhydride pairs, it is a time consuming task to determine the appropriate ones to prepare PIs resistant to plasticization. Molecular

simulation is a prominent tool to investigate the structure-plasticization relationship of the PIs at the atomistic scale. With the accurate estimation of the diffusivities and hence permeabilities of the PIs in the future work, the simulation methodology applied here can be used to predict the effect of plasticization on transport properties of gases in different polyimides and also copolyimides for which there are no experimental data to explore their potential use as membrane material.

5. CO₂-INDUCED PLASTICIZATION IN THE PRESENCE OF RESIDUAL SOLVENT IN POLYIMIDE MEMBRANES

5.1 Introduction

Previous experimental studies on gas permeabilities of polyimide membranes showed that the presence of the residual solvent in the membrane has a significant effect on the membrane free volume size distribution, and it alters the gas sorption behavior and gas permeability [105, 136, 137]. While a small amount of solvent in membrane acts as an anti-plasticizing agent, larger amounts exhibit an opposite effect [137]. Besides that it has been revealed that the solvent used in the casting influences the resulting structure of the membrane [138-141]. Nevertheless, molecular simulation methods were previously used to investigate the effect of the residual solvents on free volume changes of the polyimides [142, 143].

Joly et al. focused to determine how the gas permeation properties of 6FDA–mPDA polyimide affected from five different type of residual solvent remaining after membrane fabrication [136]. They observed an increase in the permeability and solubility coefficients with the reduction in residual solvent and concluded that the solvents characterized by a high molar volume such as NMP leave more important imprints in the polymeric membrane material [136]. Macchione et al. investigated the thermal, mechanical and transport properties of Hyflon® AD dense membranes, depending on the residual solvent content [105]. They confirmed their results with thermal analysis which shows that there is a 60ºC reduction in Tg when 0.17 weight fraction of the residual solvent presents in Hyflon® AD dense membranes [105]. Macchione et al. [105] suggest that residual solvent plasticizes the polymer and strongly affects its permeability properties and reduces the membrane's permselectivity. Similar study was performed by Fu et al. [137] who search the effects of residual solvent on the gas sorption and transport properties of a novel 6FDA/PMDA-TMMDA polyimide membrane. The most prominent conclusion they were argued that the role of the residual solvent changed from plasticization to

antiplasticization when the residual solvent content was lower than a critical value [137]. Molecular study done by Chang et al. [142] confirmed the physical properties and changes that were obtained from experimental study. They addressed the differences in the energy and RDF analyses, which show that the presence of residual solvent tends to promote the flexibility of polymer [142]. Moreover, they claimed that the effect of the residual solvent on the sorption properties is suppressed at higher feed pressures due to the sorption competition between the gas and solvent molecules [142]. Another molecular simulation study performed by Zhang et al. [143], simulates the microstructure and permeation in polymer of intrinsic microporosity (PIM-1) membranes which are closely related to residual solvent during membrane fabrication. Their results in FFV and large-size voids in PIM-1/solvent membranes decrease as $CH_3OH > CHCl_3 > H_2O$, consistent with positron annihilation lifetime spectroscopy measurements [143].

The objective of this study is to apply molecular simulation techniques to understand the relationships between the structure and plasticization behavior of 6FDA-based polyimide (PI) membranes in order to estimate their degree of plasticization induced by CO_2 sorption, for proper membrane material selection. In this context, the effect of the residual solvent type and amount on plasticization is also investigated. In this study, we investigated the change in the CO_2 sorption capacity of these membranes such as 6FDA-DAM and 6FDA-ODA as a function of residual solvent type and amount. A low-boiling-point solvent, tetrahydrofurane (THF) (b.p. 66ºC), and a high-boiling-point solvent, n-methyl-2-pyrrolidone (NMP) (b.p. 202ºC), were selected for this purpose.

For all matrices, the structural properties, such as fractional free volume, d-spacing, and cohesive energy density (CED), along with sorption isotherms are investigated from simulations to understand the interactions between polymer chain - solvent - penetrant. Sorption induced changes in the polymer matrices were investigated through radial distribution function (RDF) and fractional accessible volume analyses (FAV). There are only two molecular simulation studies in open literature investigating the solvent effect. But these do not include the polymers studied here. However, simulated results were compared with the experimental studies present in the literature by means of trend and similarity. This work, to the best of our knowledge, is the first to investigate the change in the CO_2 sorption capacity of

polymers or plasticization as a function of residual solvent type via molecular simulation.

5.2   Simulation Method

Simulation procedure applied to polyimides was same as that of used in our previous Chapters. 6FDA dianhydride, DAM and ODA diamine moieties were constructed and linked followed by geometry optimization to create 6FDA-DAM and 6FDA-ODA repeat units shown in Figure 3.1. A cubic simulation cell with a side of 39-41 Å for each model PI matrix was constructed from a single chain and solvents, NMP or THF (Figure 5.1) introduced into polymer matrices at 4 wt % using the Amorphous Cell module of the software package. Equilibration by applying a series of molecular dynamics runs while solvent molecules are in the polymer matrices was same as pure PIs.
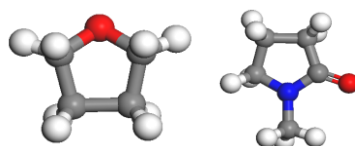
Figure 5.1 : Structures of solvents (a) THF and (b) NMP.

Simulation temperature and pressure values were chosen based on the experimental studies in the literature: 35ºC and 10 bar for CO_2 and CH_4. Sorption-induced volume swelling and plasticization is a common behavior also in PIs which include residual solvents. Besides CO_2 induced swelling, there is also plasticization due to the presence of residual solvent in polymer at high solvent concentration. Furthermore there is competition between the effects of plasticization at high CO_2 concentration and anti-plasticization at low residual solvent concentration. To reproduce these effects sorption-relaxation cycles (SRCs) were again applied until the sorption coefficients converge. Solvent molecules were randomly deleted in order to obtain 2, 1 and 0 wt % of solvents in polymer matrices and again SRCs were applied.

5.3   Results and Discussion

5.3.1 Characterization of polyimides containing residual solvent

Structural properties of PI models which include different amounts of NMP and THF solvents calculated by molecular simulation methods, and their comparison to

experimental data available in the literature are presented in Table 5.1 and 5.2, respectively. It should be noted that there is no information in the literature on the amount of residual solvent present in the membranes of which the experimental results are reported and comparison should be done with extra care. Unfortunately, no other data was found in the literature.

When CED values of 6FDA-DAM and 6FDA-ODA polymer matrices containing 4 wt % either THF or NMP were compared, the THF containing polymers have more closed packed structure in their initial states before CO_2 sorption. CED change is much more prominent in the presence of THF than NMP for both PIs when results for 0 wt % and 4 wt % of solvent contents are compared. This is expected, because if THF solvent has significant effect on the structure strength, then when it is removed, there will be much more difference in CEDs compared to those of with NMP solvent. However, we should also pay attention to the fact that these results are due to the effect of presence of both CO_2 and the solvent, not only the solvent.

Table 5.1 : Comparison of estimated properties of PIs which include **NMP** with experimental data.

	Density (g/cm³)	FFV (Initial)	FFV (Final)	% Increase	CED (MCal/m³)
6FDA-DAM					
Experimental	1.340[a,b]	0.189[a]	---		119[a]
Pure	1.240[c]	0.271	0.316	16.5	57
0 %	1.254	0.263	0.314	19.4	49
1 % (5 NMP)	1.254	0.260	0.305	17.3	50
2 % (9 NMP)	1.253	0.258	0.297	15.1	52
4 % (18 NMP)	1.267	0.246	0.297	20.7	53
6FDA-ODA					
Experimental	1.434[a,b]	0.162[a]	---		128[a]
Pure	1.348[c]	0.221	0.323	45.9	88
0 %	1.332	0.230	0.271	17.8	64
1 % (5 NMP)	1.344	0.223	0.238	6.73	65
2 % (10 NMP)	1.351	0.214	0.242	13.1	67
4 % (20 NMP)	1.360	0.203	0.234	15.3	76

[a] Ref. 7, [b] at 23ºC, [c] at 35ºC.

Table 5.2 : Comparison of estimated properties of PIs which include **THF** with experimental data.

	Density (g/cm^3)	FFV (Initial)	FFV (Final)	% Increase	CED (MCal/m^3)
6FDA-DAM					
Experimental	1.340[a,b]	0.189[a]	---		119[a]
Pure	1.240[c]	0.271	0.316	16.5	57
0 %	1.255	0.263	0.290	10.3	54
1 % (6 THF)	1.269	0.251	0.278	10.8	58
2 % (12 THF)	1.265	0.251	0.278	10.8	59
4 % (25 THF)	1.251	0.252	0.295	17.1	67
6FDA-ODA					
Experimental	1.434[a,b]	0.162[a]	---		128[a]
Pure	1.348[c]	0.221	0.323	45.9	88
0 %	1.316	0.239	0.275	15.1	63
1 % (7 THF)	1.332	0.227	0.279	22.9	66
2 % (14 THF)	1.339	0.219	0.279	27.4	69
4 % (27 THF)	1.361	0.200	0.272	36.0	85

[a] Ref. 7, [b] at 23ºC, [c] at 35ºC.

The differences in the initial FFV of the samples with between 0 and 4 wt % solvent content are as follows: 6FDA-ODA + THF (%19.5) > 6FDA-ODA + NMP (%13.3) > 6FDA-DAM + NMP (%6.9)> 6FDA-DAM + THF (%4.4).

This indicates that 6FDA-ODA polyimide affected more from the residual solvent due to its flexible backbone as we concluded in Chapter 3. 6FDA-DAM polyimide has a more rigid backbone compared to 6FDA-ODA and so its free volume changed only slightly and also residual solvent type is not dominant as we compare the initial FFV of PIs with NMP and THF.

Figure 5.2 shows % FFV increase with residual solvent content for both PIs. Comparison of fractional free volume increase after CO_2 sorption provides information on the extent of plasticization. It is very obvious that there is a competition between penetrant gas, CO_2 and the solvents in both PIs due to the minimum in the curve. At some solvent contents, the anti-plasticization effect of solvent is dominant and there is reduction in % FFV increase, but at high solvent concentrations, plasticization effects of both solvent and CO_2 are combined together. It can be concluded from Figure 5.2 that CO_2 is the winner in the competition between CO_2 and THF in 6FDA-ODA PI because of regular increment in % FFV increase. Fu et al. [137] reported that the effect of residual solvent may change from plasticization to anti-plasticization when the residual solvent content in the

membrane is lower than 1.5 wt%. Our findings also show the same conclusion with Fu et al [137]. Based on the results of Fu et al. [137], it clearly seems that complete removal of the residual solvent in the membrane is very difficult. They annealed their membranes at high temperatures but there is still 0.87 wt % of residual solvent in the membrane. Due to the presence of the residual solvent in the polymer matrix, the comparison of the experimental results with molecular simulation results based on solvent free PIs will exhibit some disagreement.
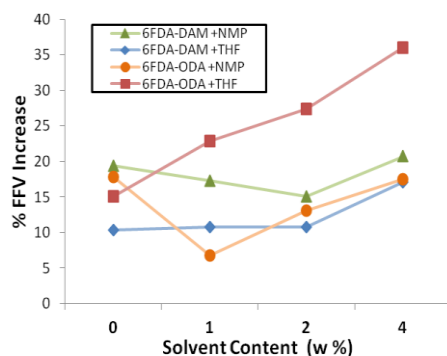
Figure 5.2 : FFV change with residual solvent content.

X-ray patterns of PIs for each solvent type are given in Figure 5.3. Figure 5.3 shows that while x-ray patterns of 6FDA-DAM for each solvent type are similar; there are differences in the x-ray patterns of 6FDA-ODA for each solvent type, especially in the region between 0.5-1 scattering vectors. There is an increase in the intensity of 0.5-1 scattering vector region of x-ray pattern with the decrease of solvent amount. Due to the high solvent content, x-ray pattern of 6FDA-ODA for 4 wt % for each solvent type has a narrow peak. But when solvent molecules removed, free volume, due to the absence of solvent molecules, is not closed packed enough and between 0.5-1 scattering vectors, a new shoulder is observed in the x-ray pattern. This may indicate that there are apparent conformational changes in 6FDA-ODA. Calculated d-spacing values for each PI while the solvent molecules are present, coincide with the experimental values.
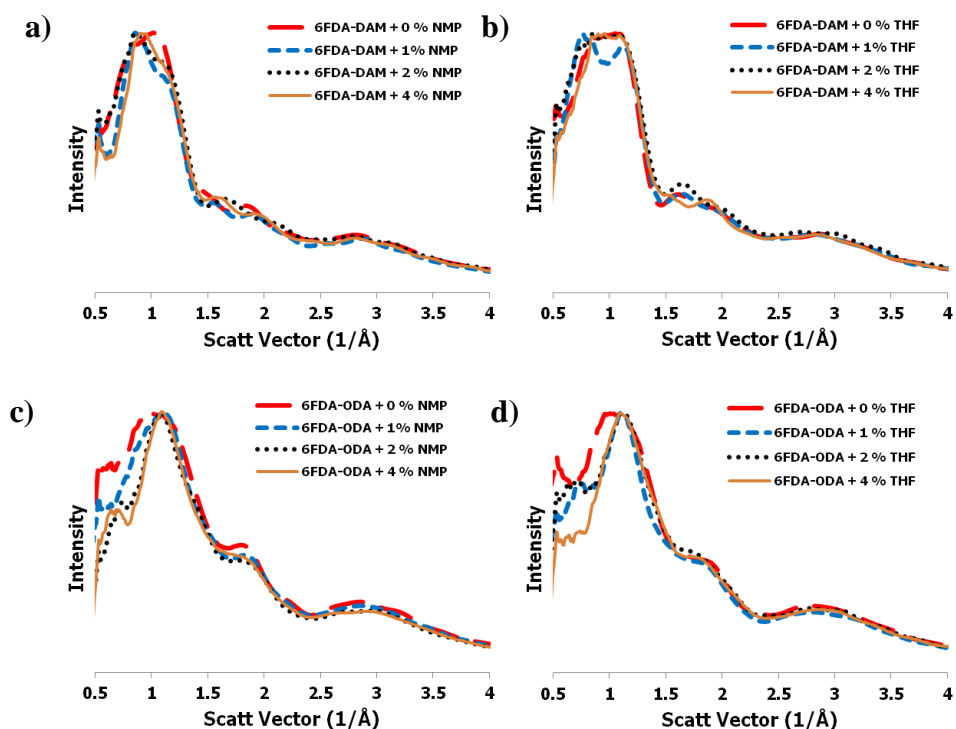
Figure 5.3 : X-Ray spectrum of a) 6FDA-DAM+NMP, b) 6FDA-DAM+THF, c) 6FDA-ODA+NMP and d) 6FDA-ODA+THF.

The FFV in some glassy polymers tends to increase with an increase in the Tg because of increasing chain stiffness. This tendency can also be observed for the two PIs here. The difference in the flexibility correlates with the differences in Tg, FFV and δ values. To quantify the linkage flexibility, we calculated the standard deviation of the dihedral angle distribution based on the absolute values, $\sigma|\phi|$. Figure 5.4 shows variations in $\sigma|\phi|$ as a function of the solvent amount. Between 0 and 4 wt% THF content in both PIs, there is a small increase in the standard deviation of the dihedral angle distribution whereas there are no changes between the different NMP solvent amounts.
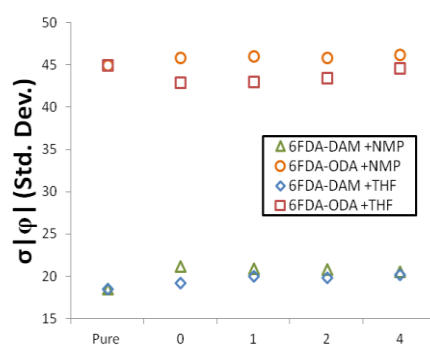
Figure 5.4 : Correlation among the solvent type and flexibility of the diamine-dianhydrade linkage in 6FDA-polyimides.

77

Overall, the estimated structural properties agree well with the experimental data (such as glass transition temperature and d-spacing) quantitatively. However, some disagreement exists with respect to the experimental values [81] of FFV which had been calculated with group contribution methods.

5.3.2 Sorption predictions

GCMC simulations to predict the sorption of CO_2 and CH_4 gases in the model PI matrices were carried out at 35ºC temperature and 10 bar pressure. Table 5.3 and 5.4 show the sorption coefficients of CO_2 and CH_4 gases and ideal sorption selectivities estimated by molecular simulation. Gas sorption decreases and density increases with the increase in solvent amount in PIs. The decrease in gas solubility might be caused by the saturation of the sorption sites, which result in not enough space for gas sorption. It is clearly seen from Table 5.3 and 5.4 that gas sorption is controlled by the type and amount of solvent molecules in the membrane.

Table 5.3 : Sorption coefficients of light gases in PIs which include NMP.

	6FDA-DAM			6FDA-ODA		
	$S(CO_2)$	$S(CH_4)$	α_s	$S(CO_2)$	$S(CH_4)$	α_s
Experimental	6.080	1.976	3.08	4.890	1.322	3.70
Pure	9.866	3.372	2.93	10.74	1.952	5.50
0 %	10.406	3.267	3.19	8.567	2.701	3.17
1 %	9.354	2.796	3.35	6.809	2.669	2.55
2 %	9.083	2.981	3.05	6.782	1.797	3.77
4 %	9.117	2.552	3.57	6.025	1.436	4.20

Table 5.4 : Sorption coefficients of light gases in PIs which include THF.

	6FDA-DAM			6FDA-ODA		
	$S(CO_2)$	$S(CH_4)$	α_s	$S(CO_2)$	$S(CH_4)$	α_s
Experimental	6.080	1.976	3.08	4.890	1.322	3.70
Pure	9.866	3.372	2.93	10.74	1.952	5.50
0 %	8.698	2.993	2.91	9.091	2.852	3.19
1 %	8.226	3.058	2.69	9.194	2.276	4.04
2 %	8.161	2.524	3.23	7.852	2.060	3.81
4 %	8.210	2.519	3.26	7.825	1.451	5.39

Figure 5.5 summarizes Tables 5.3 and 5.4 and shows the relationship between residual solvent content and CO_2 sorption coefficient, and ideal sorption selectivities. Gas sorption decreases and ideal sorption selectivity mainly increases with the increase in residual solvent amount in PIs, which correlate well with the experimental results [105, 136]. The sorption selectivity of PI matrices constructed

without any solvent in the beginning are slightly smaller for 6FDA-DAM and relatively bigger for 6FDA-ODA compared to those with solvent included. This may be the evidence that flexible PIs may be affected more from residual solvent. Moreover, the annealed and the residual solvent-free (which is in fact unrealistic) matrices cannot have the same sorption properties.
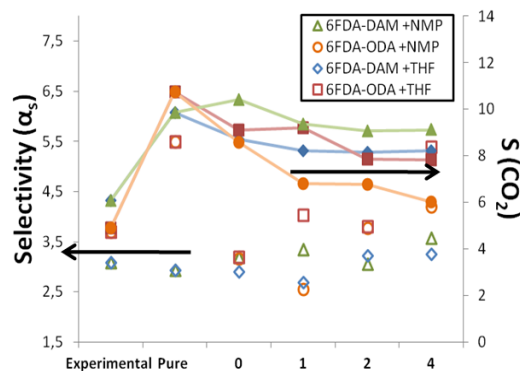
Figure 5.5 : Change of sorption coefficient and ideal sorption selectivities with the residual solvent amount in 6FDA-polyimides.

5.3.3 Sorption-induced accessible free volume increase

The analysis of the sorption-induced changes in FAV was carried out according to previous Chapters. Figure 5.6 compares FAV distribution as a function of probe size for each polyimide before CO_2 saturation. The analysis shows that residual solvent apparently influence the free volume size distribution, which affect the gas transport properties. There are considerable differences in accessible free volume distribution of 6FDA-ODA when NMP and THF solvents are present in polyimide matrix, compared to that of 6FDA-DAM polyimide.

There was free volume greater than 81-86% for 6FDA-ODA and 76-79% for 6FDA-DAM in the range between 0.0 and 0.8 Å probe size. So this means that 6FDA-DAM mainly has a higher effective free volume and this high effective free volume compared to 6FDA-ODA benefits the sorption phenomenon after gas enters the membrane matrix. Generally, polyimides with 0 wt % solvent content has a higher percentage of free volume in the range of 0.8-1.6 Å probe size, while the membrane with 4 wt% solvent content has mainly higher percentage of free volume between 0.0 and 0.8 Å probe size. So this means that polyimides with 0 % solvent content will contain more effective free volume for CO_2 passing through and have high sorption capacities.
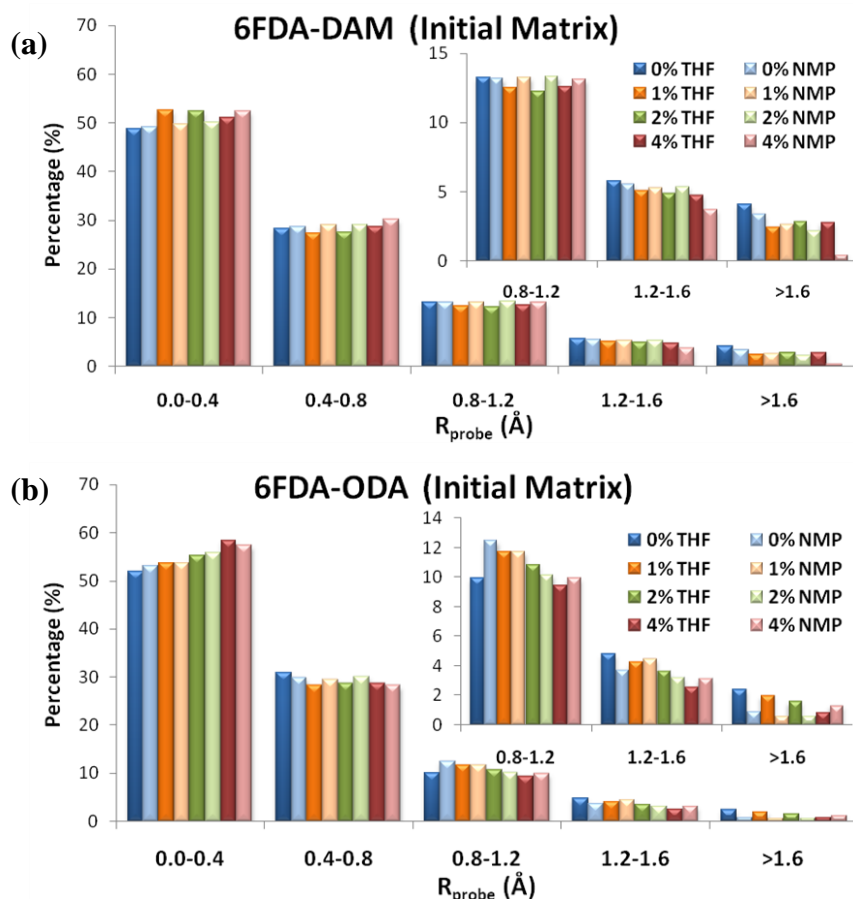
Figure 5.6 : FAV distribution in (a) 6FDA-DAM and (b) 6FDA-ODA PIs before CO_2 saturation.

The initial accessible free volumes before CO_2 sorption are smaller than those of the swelled polyimides at the end of the SRC procedure. However, for 6FDA-ODA with 1 wt% NMP content in 1.2-1.6 Å probe radius, accessible free volume before and after SRCs is slightly different. Despite CO_2 plasticization effect, the accessible free volume decreased very little possibly due to the anti-plasticization effect of residual solvent.
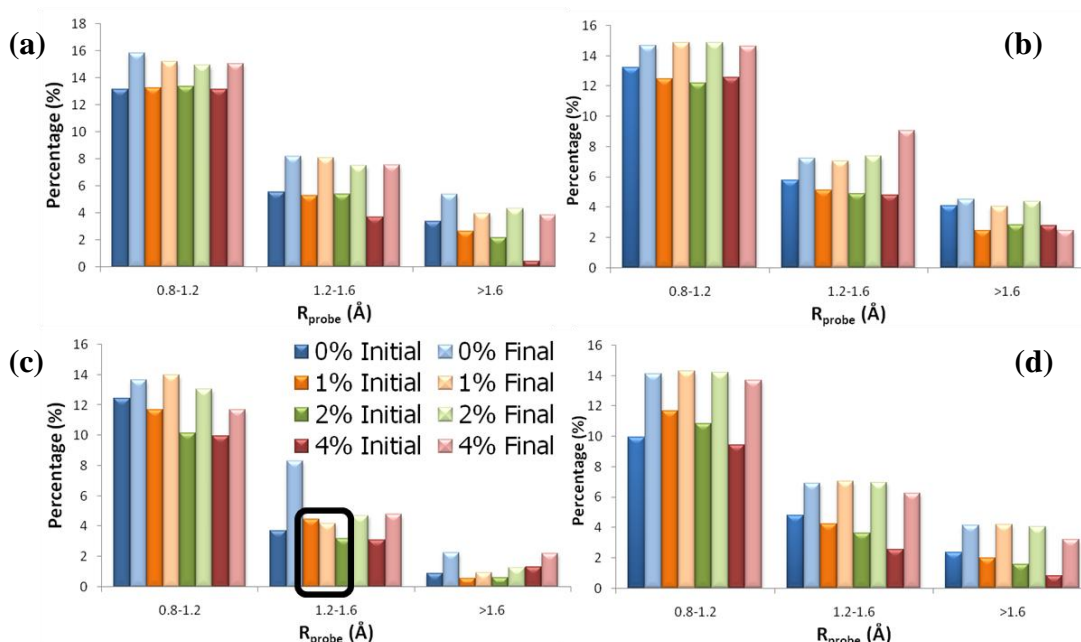
Figure 5.7 : FAV distribution for 6FDA-DAM PI with (a) NMP and (b) THF and 6FDA-ODA PI with (c) NMP and (d) THF before and after saturation with CO_2.

5.3.4 Radial distribution functions

RDFs are used for an in-depth analysis of atomic interactions between penetrants and the PI matrices. Figure 5.8 presents the RDFs of CO_2 around five typical atoms of monomers in PI chains: the oxygen and nitrogen in the imide, the fluorine in the -CF_3 group, the oxygen in the ether linkage and carbon in the –CH_3 groups of DAM diamine (labeled as O1, N, F, O2 and C respectively). The fluorine in the -CF_3 group is the least preferential sorption site in each PIs, but the others are the most preferential sorption sites as seen in Figure 5.8. Not all residual solvent types and amounts are presented here, because most preferential sorption sites for both PIs are always the same.
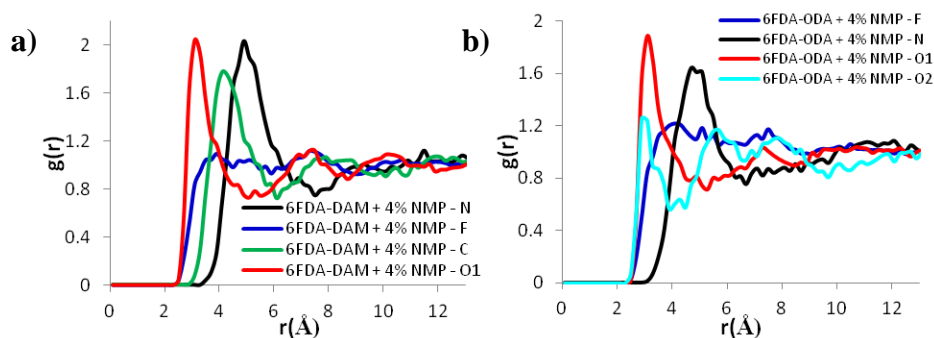
Figure 5.8 : Radial distribution functions (g(r)) of CO_2 in a) 6FDA-DAM and b) 6FDA-ODA PIs.

In 6FDA-DAM, the intensity and the position of g(r) of CO_2 for different amount of residual solvents (THF and NMP) change very slightly in all groups as seen in Figure 5.9, which represents only interactions with N group. This also may be the indication of rigidity of 6FDA-DAM polymer chain.
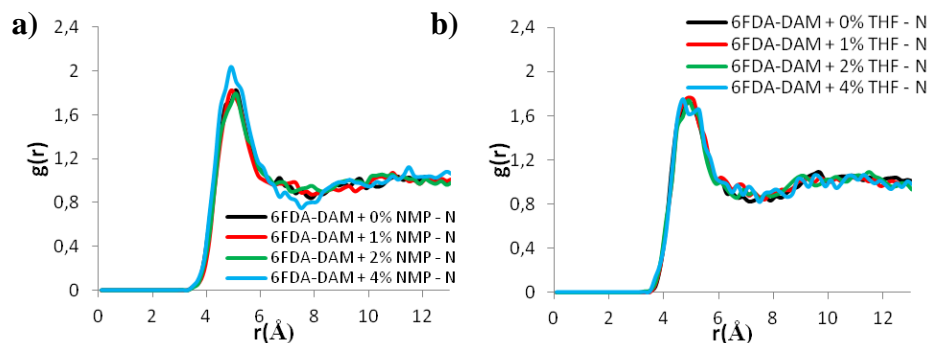
Figure 5.9 : Radial distribution functions (g(r)) of CO_2 in 6FDA-DAM for N sorption site while a) NMP and b) THF are present.

In 6FDA-ODA, the intensity and the position of g(r) of CO_2 for different amount of residual solvents (THF and NMP) also change very slightly in all groups except O2 as seen in Figure 5.10. It was found that the gas solubility coefficients increased when the PI membranes contain less residual solvent. This might be caused by the sorption site competition between gas and solvent molecules. This can be seen in Figure 5.10, as the amount of residual solvent increases, the intensity of g(r) of CO_2 decreases at some point and later it again increases for both solvents, because O2 group is the preferential sorption site for both CO_2 and residual solvents (NMP and THF) and there is competition between them. 6FDA-ODA PI is much more affected from residual solvent and also from CO_2 plasticization compared to 6FDA-DAM due to the changes in g(r) of O2 group which is in the backbone of polymer chain.
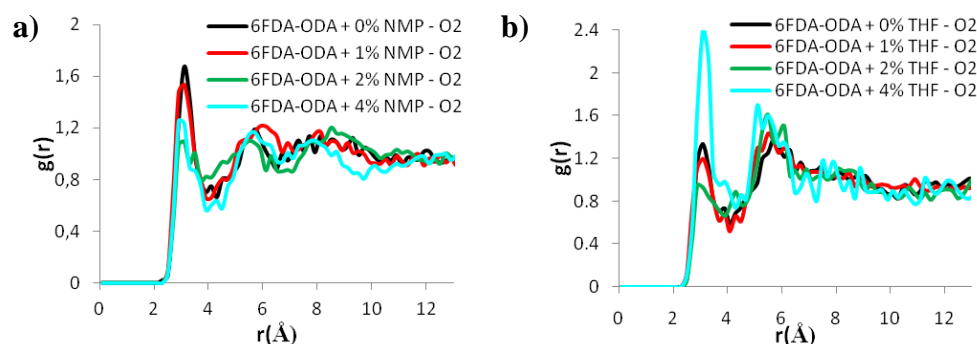
Figure 5.10 : Radial distribution functions (g(r)) of CO_2 in 6FDA-ODA for O2 sorption site while a) NMP and b) THF are present.

82

Figure 5.11 and 5.12 show very clearly the preferential sorption sites of residual solvents in both two PIs.
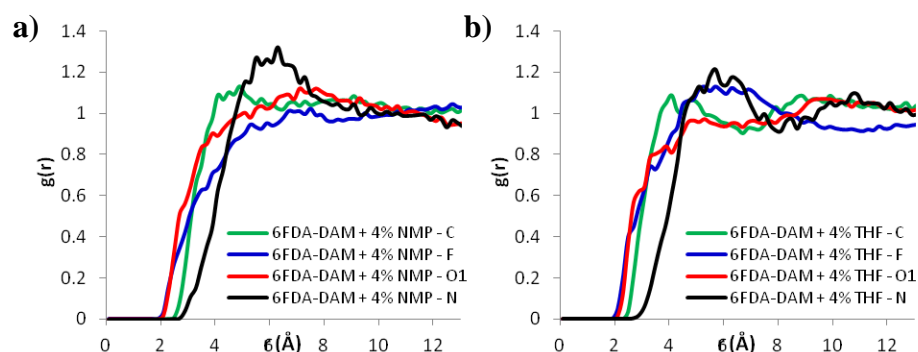
Figure 5.11 : Radial distribution functions (g(r)) of a) NMP and b) THF in 6FDA-DAM PIs.
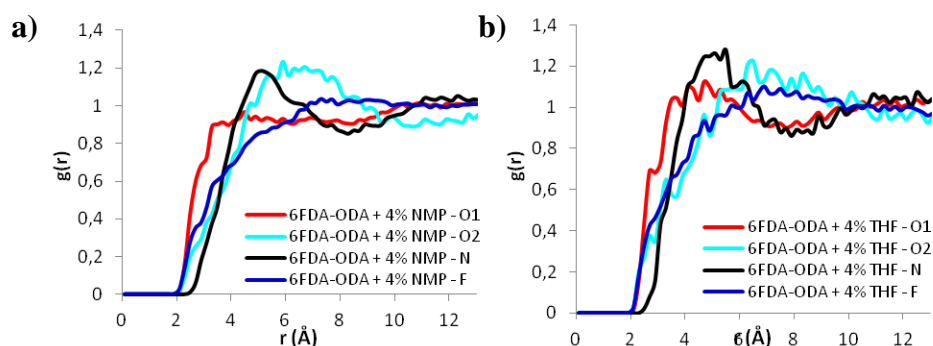
Figure 5.12 : Radial distribution functions (g(r)) of a) NMP and b) THF in 6FDA-ODA PIs.

5.4 Summary

Estimated structural properties of 6FDA-DAM and 6FDA-ODA polyimides were used to identify the characteristic differences in polyimides containing residual solvent. This allows one to clarify the effect of residual solvent on structural properties since most literature havee not report the amount of residual solvent when reporting the structural data.

Estimated sorption coefficients of CO_2 and CH_4 in both PIs containing residual solvent are within the same order of magnitude with the experimental data found in the literature. Even if a small amount of residual solvent is present in polymeric membrane material, the separation properties are affected considerably. Thus, the agreement between the experimental and predicted sorption coefficients of PIs containing residual solvent is much better than that between the experimental and predicted values of PI matrices containing no residual solvent. In 6FDA-DAM and

6FDA-ODA, residual solvents reduce CO_2 sorption capacity and alter CO_2/CH_4 selectivity.

CO_2 solubility in PIs is solely a function of the FFV of the plasticized PIs. A correlation between the dihedral angle distribution and the FFV increase as well as the final CO_2 concentration may be established. Relationship between backbone rigidity and plasticization resistance is altered in the presence of solvents.

Solvent-sorbate-polymer interactions are complex and therefore molecular simulation runs take a tremendous amount of time. Thus, only one simulation run for each parameter was carried out in this work. In order to confirm the results presented in this chapter, simulations should be repeated at least one more time.

6.   PREDICTION OF GAS PERMEABILITY COEFFICIENTS OF COPOLYIMIDES BY GROUP CONTRIBUTION METHODS

6.1   Introduction

Membrane based gas separation processes are getting attention in separation of many commercially important gas pairs. Aromatic engineering polymers such as polysulfones, polyimides, and polycarbonates are widely used as membrane materials. Polyimides are attractive for membrane based gas separation due to their outstanding thermal and chemical stability, and good mechanical properties. Preparation of polyimide membranes with high permselectivity is important for the separation of commercially important gas pairs such as O_2/N_2, CO_2/CH_4, CO_2/N_2, and H_2/CO_2.

Polyimides are synthesized by the reaction of two monomers (dianhydride and diamine) in a solvent and by dehydration of this solution (polyamic acid) by thermal or chemical imidization. If this procedure is carried out with three monomers instead of two then copolyimides are synthesized. There are large number of studies reported in the literature on the synthesis of polyimides with limited separation performance for commercial applications [4, 144]. Copolyimides allow us to optimize the separation properties by using two different polyimides which have different permeability and selectivity properties, such as one having high permeability-low selectivity and the other having low permeability-high selectivity. Apart from tailoring the separation properties of two homopolyimides by combining them at a defined ratio, copolyimides also give an opportunity to synthesize plasticization resistant, robust membrane materials with the judicious selection of the monomers such as using a cross-linkable diamine. While plasticization effect can be minimized by the help of cross-linking, separation properties can be optimized with the use of suitable homopolyimides. Plasticization is a serious concern limiting the use of PIs as membrane material for gas separation involving CO_2, H_2S and condensable hydrocarbons such as propylene and propane.

The thermal, mechanical and separation properties of polyimides strongly depend on their chemical structure, i.e. a slight modification of their chemical structure may often result in a significant change in properties. Thus, development of structure-property relationships for polyimides may provide a guideline for designing polyimides and copolyimides having desirable end-use properties. There are detailed experimental studies in the literature focusing on the effect of polymer chemical structures on transport properties resulting in a large amount of data on the gas permeation parameters [4, 144]. This data can be used to develop relationships which will be then used to predict the permeation parameters of polymers that have not been investigated or prepared yet. This provides an opportunity for the synthesis of novel polymers with desired properties.

There are group contribution methods in the literature, such as the methods of Robeson et al. [145] and Park and Paul [146], developed for predicting the gas permeability coefficients of glassy polymers based on the experimental data for 65 and 105 glassy polymers prepared from 24 and 41 structural subunits, respectively. There is also group contribution method of Alentiev et al. [51] developed specifically to predict the permeability coefficients of polyimides using a database including about 120 polyimides prepared from 9 dianhydrides and 70 diamines. These methods have been tested for several polyimide structures, but no predictive studies for copolyimides have been reported. Considering the structural complexity of copolyimides, predicting their permeation parameters is a more difficult task. Moreover, there are other factors that influence the permeability values such as polymer synthesis, film formation procedure, solvent type, annealing conditions, etc. which are all reflected to the conformation of the polymer chain. For example, the effect of solvent type on the gas permeability values has been investigated in the last decade [137, 147]. In light of foregoing findings, the prediction of structure-property relationship of copolyimides is hard but important for designing new membrane materials.

The objective of this study is to design copolyimides with better separation properties than the upper bound performance of currently available polymers. Hundreds of different copolyimide structures can be proposed, however, the experimental analysis of the separation properties of all these structures is a tedious and time-consuming task. The group contribution methods can predict the

permeability coefficients and ideal separation factors for the proposed structures. In this study, the group contribution methods of Park and Paul and Alentiev et al. first will be used to predict the permeability coefficients for 30 different copolyimides that have been synthesized in the literature and have gas permeability data available. After it is shown that the group contribution methods can be applied to predict the permeability and selectivity values of copolyimides within reasonable error for the available data, one of these methods will be used to predict the permeability coefficients of H_2, O_2, He, CO_2, N_2, and CH_4 gases at 35°C for more than 2200 proposed copolyimide structures whose subunit increments are available. The value of 35°C is chosen due to the fact that the majority of the available data in the literature have been reported at this temperature. The diamine/diamine or dianhydride/dianhydride ratios are also varied as 50/50, 25/75, and 75/25. The ideal selectivity values are calculated for O_2/N_2, CO_2/CH_4, H_2/CO_2, H_2/N_2, and CO_2/N_2 separation applications and the results are evaluated in terms of the selectivity-permeability plots to propose copolyimide structures with separation properties better than the upper bound performance of current polymers. However, it should also be noted that we can only propose copolyimide structures whose monomer data is available in the database. This study is the first to use group contribution methods to predict the gas permeability coefficients of copolyimides.

6.2 Group Contribution Methods

Group contribution methods are based on several assumptions. First, polymer structure is assumed to be represented as a sum of several subunits which have a certain increment into the property in question; second, the increments are assumed to be constant for the whole set of complex structures, and third, the properties of complex molecules are assumed to be represented as sums of the corresponding increments after accounting for weight factors [148].

There are many group contribution methods developed to predict numerous properties of polymers such as glass transition temperature, melting point, cohesion energy, heat capacity, etc. [149, 150]. Besides the prediction of characteristic properties, group contribution methods also have been used to predict the transport properties of polymers. Salame [151] was the first to use the group contribution method to predict the permeability coefficients of polymers based on cohesive

energy density and FFV assigning parameter values based on the polymer repeat units. Later on, Park and Paul applied the group contribution method to predict permeability coefficients of aromatic polymers [146]. The empirical factors for 41 different structural units were determined from a permeability database of 102 polymers. At the same time period, Robeson et al. [145, 152] proposed a group contribution method based on solving a least squares fit of a large data base of polymers containing aromatic units in the main chain. They assumed that the permeability of copolymers followed a logarithmic relationship with the permeability of the homopolymers. Different normalization parameters, such as molecular mass, van der Waals volume, molecular volume, etc. were used in these studies. For instance, Robeson et al. [145, 152] used volume fraction of comonomers or homopolymer comprising the copolymer in their permeability predictions of aromatic polymers, such as polycarbonates, polyarylates, polysulfones, polyimides, aromatic polyamides, poly(aryl ketones), poly(aryl ethers). Another method was proposed by Alentiev et al. [148] in which the polymer structure was subdivided into a number of groups (building blocks) and predictions were based on the chemical structure of the repeat units with the groups chosen to be specific atoms and their bond configurations. In a subsequent study, Alentiev et al. applied group contribution method to polyimides considering a polyimide as an alternating copolymer of a dianhydride and a diamine [51] and calculated permeability values for dianhydrides and diamines using a basic set of 120 homopolyimide structures and multiple linear regression method. A different method was developed by Meares [153] which gives the relationship between the activation energy of diffusion and cohesive energy times the square of the gas diameter. Meares [153] used this predicted activation energy to calculate the diffusivity and permeability coefficients of polymers.

In this work, two of the above mentioned group contribution methods are used for prediction of permeability coefficients and ideal selectivities of copolyimides. Method of Park and Paul [146] is developed for polymers generally and used to predict permeability coefficients of different polymer types, i.e. polycarbonates, polysulfones, polyesters, polyether ketones, polyimides, etc., whereas method of Alentiev et al. [51] is specifically developed for polyimides.

6.2.1 Method of Park and Paul

This method involves an empirical modification of a free volume scheme that has been used by Bondi [84]. The group contribution correlations were developed using a database of over 105 glassy polymer structures whose specific volume (at 30ºC) and permeability to various gases (at 35ºC) are believed to be known very well. Park and Paul [146] assumed that permeability coefficient (P) depends on the fractional free volume of the polymer and the fractional free volume changes with the gas type [146].

$$P = A_m \exp\left(\frac{-B_m}{FFV}\right) \tag{6.1}$$

A_m and B_m are constants for a particular gas in Equation 6.1 and fractional free volume, FFV, is defined as

$$(FFV)_m = \left[V - (V_0)_m\right]/V \tag{6.2}$$

where V represents the volume of the polymer which is obtained at the temperature of experiments and V_0 represents the volume occupied by the polymer chain which is calculated from the Van der Waals volumes, $(V_w)_k$, of the various groups in the polymer structure in Equation 6.3.

$$(V_o)_m = \sum_{k=1}^{K} \gamma_{mk} (V_w)_k \tag{6.3}$$

Here, the γ_{mk} is the set of empirical factors to be determined that depend on the gas type (m) and group number (k) into which the repeat unit structure of the polymer is separated. V in Equation 6.2, is defined as

$$V = \sum_{k=1}^{K} \beta_k (V_w)_k$$

$$\tag{6.4}$$

where β depends on the type of group k. Empirical factors for 41 different structural units were determined from this study.

6.2.2 Method of Alentiev et al.

This method is developed specifically to predict the gas (He, H_2, O_2, N_2, CO_2, CH_4) permeability coefficients of polyimides at 35°C using the database at the Russian

Academy of Sciences, Institute of Petrochemical Synthesis which includes about 120 polyimide structures prepared from 9 dianhydrides and 70 diamines. Since polyimides are the products of polycondensation reaction of diamines and dianhydrides, they are considered as alternating co-polymers with a regular structure consisting of diamines and dianhydrides that can be used as sub-units for the predictions. For a set of M polyimides, the system was solved for the best values of the group contributions of the dianhydride (x_j) and diamine (y_k) to obtain the best fit of the experimental P_i value using the method of multiple linear regression such as:

$$x_1 + y_1 = \log P_1$$
$$x_2 + y_2 = \log P_2$$
$$x_2 + y_1 = \log P_n$$
$$x_j + y_k = \log P_z \qquad\qquad \textbf{(6.5)}$$

Here all linear lines represent polyimides. If there are different experimental values of the same polyimide, these are included into linear system as an independent equation. The obtained linear system has been solved by using multiple linear regression and the dianhydride and diamine contributions have been calculated. Naturally there is not enough data for all the combinations of dianhydrides and diamines. But there is enough data of "homopolyimide" combinations to evaluate the group contribution of all dianhydrides and diamines.

Alentiev and his coworkers suggested the use of Equation 6.6 in order to calculate the gas permeability coefficients of polyimides [51].

$$\log P_m = \log M_{jm} + \log N_{km} + C_m \qquad\qquad \textbf{(6.6)}$$

In this equation, P, M_j, N_k, m, C_m are the permeability coefficient, dianhydride group contribution, diamine group contribution, gas type and constant which depends on the gas type respectively. The method of Alentiev et al. uses molar content and not molar volume in predicting permeabilities. It was accepted that diamine and dianhydride structures have same molar volumes, which may be the factor that influence the predictions. On the other hand, the method of Park and Paul uses molar volume but it has not yielded accurate predictions for copolyimides in this study due to small increments [146].

6.2.3 Methodology and Data Used

The methodology used in this study involves two steps:

1. In order to test the predictive ability of the chosen group contribution methods (method of Park and Paul and method of Alentiev et. al.) for copolyimides, we first used the specific increments these methods assigned for the subunits, to predict the permeability coefficients of several gases for 31 different copolyimides for which gas permeability data are reported in the literature. Table 6.1 lists all the copolyimide structures which have permeability and selectivity data for their dense membranes available in the literature. Table 6.1 also presents the names of dianhydrides and diamines used in constructing the copolyimides, the ratio of the dianhydride or diamine pairs, and experimental gas permeability values for these copolyimides. The dianhydride/diamine ratio for a copolyimide is always 50/50, in other words, total dianhydride and total diamine mole numbers are the same, but the mole ratio between dianhydrides or between diamines can be varied as 25/75, 50/50 and 75/25. The copolyimide structures were assumed as alternating polyimides of two dianhydrides and one diamine or one dianhydride and two diamines. For unequal diamine or dianhydride feed (25/75 and 75/25), the polyimide permeability values were multiplied by the appropriate dianhydride/dianhydride and diamine/diamine ratios.

   The column which shows the solvent type in Table 6.1, reveals that there are many different solvents used in membrane formation. Shao et al. [147] prepared membranes using three different solvents and obtained different H_2, O_2, N_2, CO_2, CH_4 permeabilities of the same copolyimide (6FDA/PMDA-TMMDA). This clearly shows the importance of solvent type and how much it can change the transport properties of copolyimides. The other parameters such as residual solvent and membrane or dense/film preparation procedure also influence the polymer structure and hence their permeability coefficients. In some studies, the permeability unit was reported as GPU; in order to convert it to Barrer, GPU was multiplied with the average film thickness [166-168]. However, the thickness of the selective layer is not known with high accuracy in case of asymmetric membranes, so this will also bring another source of error.

It should also be noted that the experimental errors involved in the databases used in the methods of Park and Paul or Alentiev et. al. and any error in the subunit values due to insufficient or incorrect data in their databases reduce the accuracy of their predictions. While comparing the predicted and experimental results, these effects should be considered as the limitations of group contribution methods.

The method of Park and Paul is applied to copolyimides directly since the repeat units are divided into structural units and the γ_{mk}, β_k, and V_W values in Equations 6.3 and 6.4 assigned to these units are used to predict the FFV and permeability values of the polymer. Park and Paul suggest that the repeat unit must be divided into groups as large as possible. The division of the repeat unit of a copolyimide into structural units is shown in Figure 6.1 as an example. When FFV of a copolyimide is calculated, the coefficients which are related to the ratio between the pair of dianhydride or diamine are multiplied with V and V_0 values of the structural unit in the repeat unit. Empirical factors in Table 6.1 of the study of Park and Paul were used to predict permeability coefficients of copolyimides.
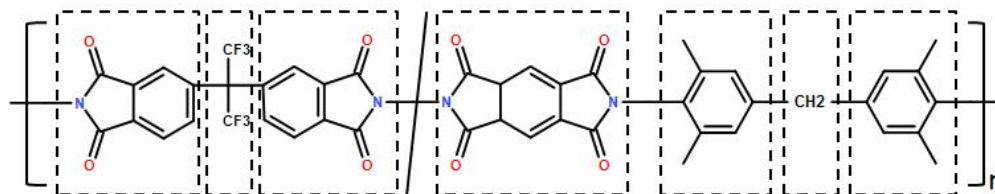
Figure 6.1 : Division of 6FDA/PMDA-TMMDA copolyimide into groups for the method of Park and Paul [146].

For the method of Alentiev et al. the Equation 6.6 is modified for copolyimides taking into account the ratio between the pairs of dianhydride or diamine as follows:

$$\log P_m = \left[\left(Ratio_{dianhydride1}\right)\log M_{1m} + \left(Ratio_{dianhydride2}\right)\log M_{2m}\right] + \log N_m + C_m \quad \textbf{(6.7)}$$

$$\log P_m = \log M_m + \left[\left(Ratio_{diamine1}\right)\log N_{1m} + \left(Ratio_{diamine2}\right)\log N_{2m}\right] + C_m \quad \textbf{(6.8)}$$

In the above equations, we have assumed that the additivity rules also govern the copolyimides. Specific increments characteristic for certain dianhydrides (M_m, M_{1m} and M_{2m}) and diamines (N_m, N_{1m} and N_{2m}), and the gas constant (C_m) for mth gas were also taken from the work of Alentiev et

al. (Table 3.1 in ref. 5) and applied to equations 6.7 and 6.8. Some missing decimal points were corrected in this table. The results of the predictions of both methods are evaluated for their predictive capability for copolyimides by comparison to the experimental data.

2. Based on the evaluations of step 1 described above, one of these group contribution methods will be chosen and used to predict the permeability coefficients of H_2, O_2, He, CO_2, N_2, and CH_4 gases at 35°C for more than 2200 proposed copolyimides based on known dianhydride and diamine structures. The value of 35°C is chosen due to the fact that the majority of the available data in the literature including the databases used in both methods have been reported at this temperature. The diamine/diamine or dianhydride/dianhydride ratios are also varied as 25/75, 50/50 and 75/25. The ideal selectivity values are calculated for O_2/N_2, CO_2/CH_4, H_2/CO_2, H_2/N_2, and CO_2/N_2 separation applications and the results are evaluated in terms of the selectivity-permeability plots to propose copolyimide structures with separation properties better than the upper bound performance of current polymers.

Table 6.1: Experimental permeability data available in the literature for copolyimides.

Copolyimide						Permeability Coefficient (Barrer[a])					
Dianhyd.-1	Dianhyd.-2	Diamine-1	Diamine-2	Solvent	Ratio[b]	H_2	O_2	N_2	CH_4	CO_2	Ref.
6FDA	PMDA	TMMDA	—	CH$_2$Cl$_2$		240	45.0	11.7	13.3	187	
				NMP	(1:6)	210	35.4	8.76	8.99	144	[147]
				DMF		130	21.2	5.16	5.35	88.6	
6FDA	—	4MPD	DABA	NMP	(4:1)	—	—	—	5.62	129.3	[154]
6FDA	—	NDA	Durene	NMP	(3:1)	—	16.9	3.25	1.65	70.0	[155]
					(1:1)		29.6	6.67	3.93	96.4	
					(1:3)		75.8	19.1	12.9	274	
6FDA	BPDA	DDBT	—	NMP	(1:1)	120	13.1	2.6	1.48	71	[156]
6FDA	—	Durene	2,6-DAT	NMP	(3:1)	374	64.8	16.2		220	[157]
					(1:1)	243	36.9	8.44	—	117	
					(1:3)	169	21.3	4.33		67.3	
BPDA	SiDA	ODA	—	DMAc	(8:2)	3.3	0.154	0.018			[158]
					(6:4)	6.21	0.326	0.040	—	—	
					(4:6)	8.78	0.503	0.060			
					(2:8)	9.63	0.621	0.074			
BTDA	—	TDI	MDI	NMP	(8:2)	—	0.24	0.024	—	0.99	[159]
6FDA	—	Durene	pPDA	CH$_2$Cl$_2$	(8:2)	343	64.81	16.88		230	[160]
					(1:1)	212	33.8	7.74	—	126	
					(2:8)	114	13.91	2.81		59.26	
6FDA	—	Durene	mPDA	CH$_2$Cl$_2$	(8:2)		60.39	15.05		223	[161]
					(1:1)	—	21.89	4.60	—	71.8	
					(2:8)		6.49	1.10		21.3	
BTDA	—	ODA	pPDA	NMP	(1:1)	—	0.053	0.01	0.01	0.213	[162]
BTDA	6FDA	ODA	—	NMP	(2:8)	—	0.597	0.077	0.083	2.559	[162]
BTDA	—	ODA	DAM	NMP	(4:6)	—	0.407	0.067	0.066	1.7	[162]
6FDA	—	6FpDA	DABA	NMP	(2:1)	—	11.5	2.17	1.02	45	[163]
6FDA	—	DAM	DABA	NMP	(2:1)	—	18	4.36	4.17	113	[163]
6FDA	—	Durene	mDDS	CH$_2$Cl$_2$	(3:1)	195	27	5.91		84.7	[164]
					(1:1)	71.6	6.26	1.09	—	19.8	
					(1:3)	28.1	1.8	0.26		5.12	
6FDA	—	mPDA	DABA	CH$_2$Cl$_2$	(9:1)	—	1.71	0.25	0.1	6.53	[2]
6FDA	—	mPDA	mMPD	NMP	(7:3)	—	1.26	0.21	0.19	6.0	[165]
6FDA	—	mPDA	DAM	NMP	(7:3)	—	1.30	0.23	0.13	7.22	[165]
BTDA	6FDA	mMPD	—	NMP	(1:1)	—	1.46	0.22	0.10	6.59	[165]
BPDA	6FDA	ODA	—	NMP	(3:7)	—	2.87	0.44	0.25	13.4	[165]
BPDA	—	ODA	DAM	NMP	(5:5)	—	0.94	0.15	0.11	3.32	[165]
6FDA	—	ODA	DDS	THF	(8:2)	10.64	2.205	0.608	—	30.76	[166]
					(6:4)	10.91	2.250	0.675		31.73	
6FDA	—	ODA	MDA	THF	(8:2)	10.51	1.890	0.473	—	20.36	[166]
					(6:4)	61.88	6.053	1.283		45.02	
6FDA	—	ODA	BADS	THF	(8:2)	7.088	1.125	0.293	—	11.32	[166]
					(6:4)	18.36	3.510	0.833		33.86	
6FDA	BTDA	MDA	—	THF	(9:1)	3.825	0.90	0.225	—	10.80	[167]
6FDA	BPADA	MDA	—	THF	(9:1)	36.90	4.950	1.125	—	75.60	[167]
6FDA	—	ODA	DABA	THF	(8:2)	19.44	1.495	0.230	—	13.34	[168]
					(6:4)	6.670	2.300	0.345		10.93	
6FDA	—	ODA	DANT	THF	(9:1)	10.70	1.61	0.345	—	17.37	[168]
					(8:2)	6.210	1.15	00.230		15.53	
6FDA	—	6FAP	3MPA	THF	(1:1)	—	12	2.66	2.03	73	[169]
6FDA	—	DAM	mPDA	NMP	(3:1)	239.19	38.87	8.86	5.79	195.16	[170]
					(1:1)	139.69	18.08	3.59	2.07	88.25	
					(1:3)	47.86	3.64	0.58	0.29	15.66	
6FDA	—	DAM	MOCA	NMP	(3:1)	258.4	41.85	9.36	6.24	204.31	[171]
					(1:1)	97	11.66	2.27	1.22	53.02	
					(1:3)	56.14	6.05	1.05	0.57	23.80	

6.3 Results and Discussion

The comparison between the experimental and theoretical H_2, O_2, N_2, CO_2 and CH_4 gas permeability coefficients for the copolyimides given in Table 6.1 is presented in Figure 6.2, whereas Figure 6.3 shows the comparison between the experimental and theoretical H_2/CO_2, O_2/N_2, CO_2/N_2 and CO_2/CH_4 ideal selectivity values of these copolyimides. The dashed lines in Figure 6.2 show the deviation of the predictions from experimental data in logarithmic scale as half and one order of magnitude such that one order of magnitude corresponds to ten times higher or lower than the experimental value. The comparison of selectivity coefficients is a more challenging test due to the risk of error propagation since ideal selectivity is calculated as the ratio of the permeability coefficients.
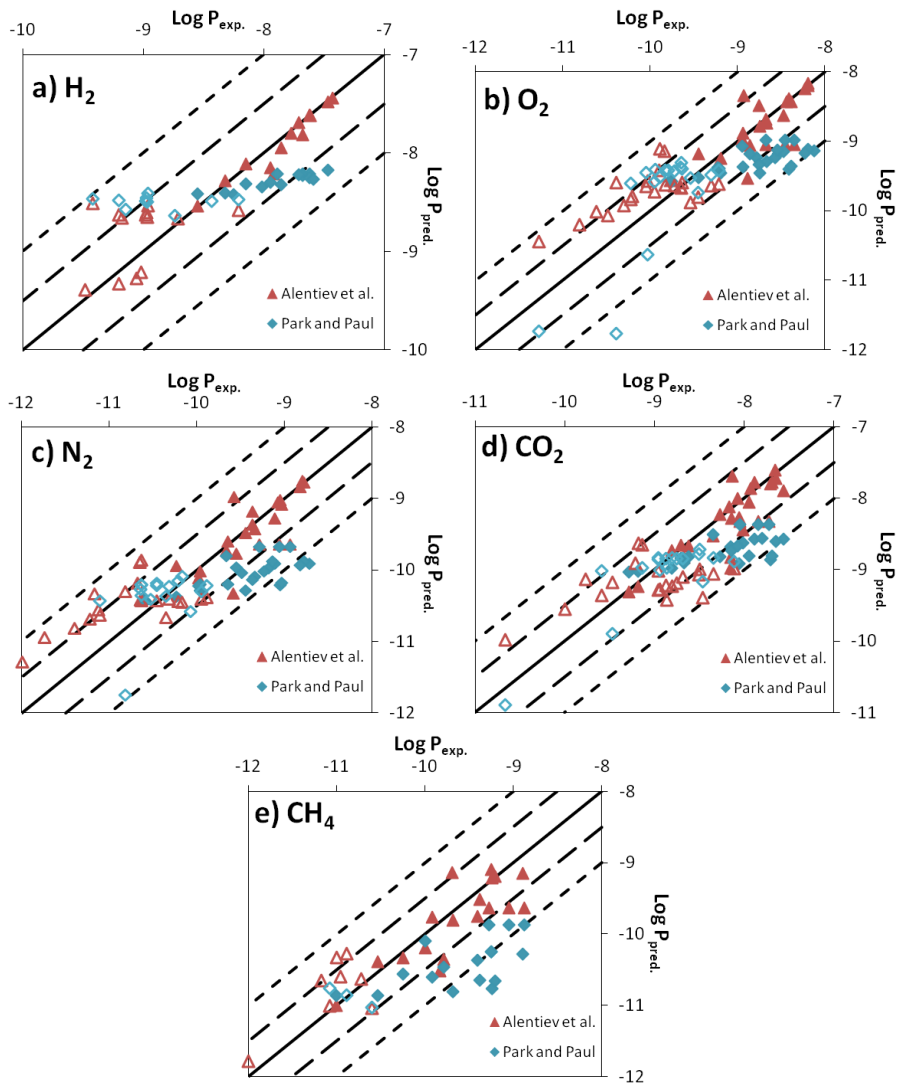
Figure 6.2 : Comparison of experimental and predicted gas permeability coefficients for the methods of Park and Paul (blue diamonds) and Alentiev et al. (red triangles). Full diamonds and triangles show the permeability data measured at 35ºC. (a) H_2, (b) O_2, (c) N_2, (d) CO_2, and (e) CH_4 (Figure displays the lower left quadrant of the Cartesian coordinate system).
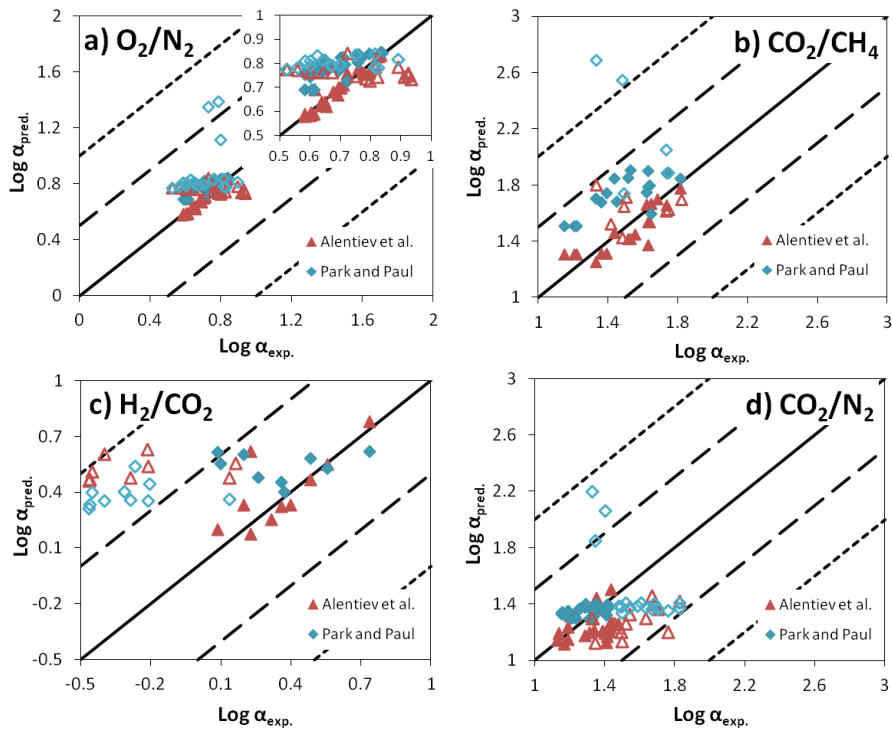
Figure 6.3 : Comparison of experimental and predicted ideal selectivities for the methods of Park and Paul (blue diamonds) and Alentiev et al. (red triangles). Full diamonds and triangles show the data of copolyimides which permeabilities were measured at 35ºC. (a) O_2/N_2, (b) CO_2/CH_4 and (c) H_2/CO_2, (d) CO_2/N_2.

As seen from Figures 6.2 and 6.3, the gas permeability coefficients calculated by the method of Alentiev et al. are within one order of magnitude of the experimental values whereas the deviations are generally more for the method of Park and Paul. The unfilled symbols in these figures belong to the data reported for temperatures other than 35°C and hence the deviations for these copolyimides are higher. The least deviation (0.75 %) for the method of Alentiev et al. is obtained for H_2, N_2, and O_2 permeability coefficients of 6FDA-Durene/2,6-DAT copolyimide. The deviations in selectivity were smaller than the deviations in permeability coefficients in the method of Alentiev et al. except H_2/CO_2 selectivity.

Figure 6.4 shows average percent relative error in permeability and selectivity predictions for different gas types and gas pairs, respectively. The percent relative error was calculated as the ratio of the difference between the experimental and predicted values divided by the experimental value multiplied by 100. The average percent relative error was calculated by averaging the values of relative percent error of all copolyimides for each gas type or gas pairs. Since some of the available experimental data was measured at temperatures different than 35ºC, the error

analysis for the data at 35ºC is reported separately. Large errors were mostly due to the temperature difference between the experimental data and the predictions. The predictions of method of Alentiev et al. exhibited an average error of 38% for permeability coefficients and 18% for selectivity values of copolyimides at 35ºC. The method of Park and Paul exhibited an average error of 68% for permeability coefficient values and 53% for selectivity values at 35ºC. Figure 4 indicates that the method of Alentiev et al. gives better predictions for copolyimides discussed here. This is somewhat expected since the method of Alentiev at al. is developed specifically for polyimides, as opposed to the method of Park and Paul which predicts for a wide variety of polymers, such as polysulfones and polycarbonates.
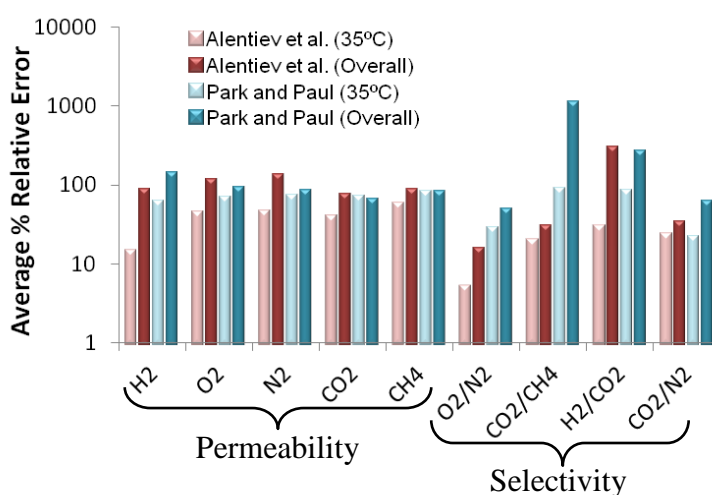
Figure 6.4 : Average percent relative error for permeability coefficients and ideal selectivities calculated by the methods of Park and Paul [146] and Alentiev et al. [51].

The predictions from both methods tend to give underestimated values for high permeable membranes and overestimated values for low permeable membranes. This behavior is most dominant in the method of Park and Paul. The reason for this large deviation in the method of Park and Paul may be due to the division of the repeat unit of a copolyimide into too small groups rather than dividing into diamine and dianhydride as in the method of Alentiev et al. It is known from the literature [172] that when a copolyimide is constructed from two polyimides, its charge distribution along the polymer chain will change and hence the intra- and inter-molecular interactions in the copolyimide will be different than its homopolyimides. As more subunits are used in constructing the copolyimide, as in the method of Park and Paul, we suspect that we highly eliminate the negative or positive effect of these interactions on the polymer chain and hence the predicted coefficients converge

approximately to the same value. It is known that polyimides or copolyimides are diffusive selective. Hence, the increase in permeability is relevant to increase in diffusivity. A high diffusion coefficient is usually due to high fractional free volume (FFV). Moreover, if one copolyimide has high FFV, its intra- and inter-molecular interactions are weaker compared to the copolyimide with low FFV. This means that high permeable membranes have high FFV and weaker interactions or vice versa. So if a highly permeable copolyimide structure is divided into many subunits, we eliminate many weak interactions and obtain a copolyimide with strong inter- and intra-molecular interactions than the actual polymer and therefore obtain underestimated predicted values. A similar argument can be made for the low permeable polymer. Another reason for this deviation may come from the connectivity of these many subunits. The gas permeation properties of glassy polymers are much more sensitive to chemical structure of their repeat unit and hence configurations of subunits. The contributions of some subgroups (symmetric side groups, bulky groups directly or with a spacer connected to the main chain, or linear substituents) to the separation properties can change in different polymers due to the different neighborhood. For instance, one diamine can be in a different configuration when connected to the different dianhydrides.

Based on the results of this analysis, the method of Alentiev et al. is chosen in this study to predict the permeability coefficients of H_2, O_2, CO_2, N_2, and CH_4 gases at 35°C for more than 2200 possible copolyimide structures whose monomers' data are available in the study of Alentiev et al. The diamine/diamine or dianhydride /dianhydride ratios were also varied as 25/75, 50/50 and 75/25. The ideal selectivity values were calculated for O_2/N_2, CO_2/CH_4, CO_2/N_2 and H_2/CO_2 separation applications.

6.3.1 Predictions for copolyimides of two dianhydrides and one diamine

The permeability coefficients for copolyimides with two dianhydrides and one diamine calculated by Equation 6.7 are presented in the form of selectivity-permeability diagrams for O_2/N_2, CO_2/CH_4, CO_2/N_2 and H_2/CO_2 gas pairs in Figure 6.5. These figures also show the 1991 and 2008 polymer upper-bound lines as defined by Robeson [5, 6] and the commercially attractive region. Copolyimides shown in Figure 3.5 contain 6FDA as the first dianhydride; one of the 8 dianhydrides

as the second dianhydride; and one of the 70 diamines, all of which had permeability values reported by Alentiev et al. [51]. The choice of 6FDA as one of the dianhydrides is due to the general consensus in the literature that 6FDA based polyimides have more preferable gas separation properties for most of the commercially important gas pairs. A general observation common to all graphs is the fact that very few copolyimides have separation properties above even the 1991 upper bound line. For O_2/N_2 and CO_2/CH_4 separations, any copolyimides could not be located above the 2008 upper bound, but for H_2/CO_2 separation, there are two groups of copolyimides which are located above the 2008 upper bound. Some of the copolyimides offer selectivity values as high as 47 and permeability values as high as 204 Barrer for H_2/CO_2 separation that is located way above the 2008 upper bound. However, for CO_2/N_2 separation none of the copolyimides exceeded the 2008 upper bound. Robeson did not report an upper bound line for CO_2/N_2 in 1991. Figure 6.5 indicates that, as the ratio of 6FDA was increased, its copolyimides exceed the upper bound and form a group.
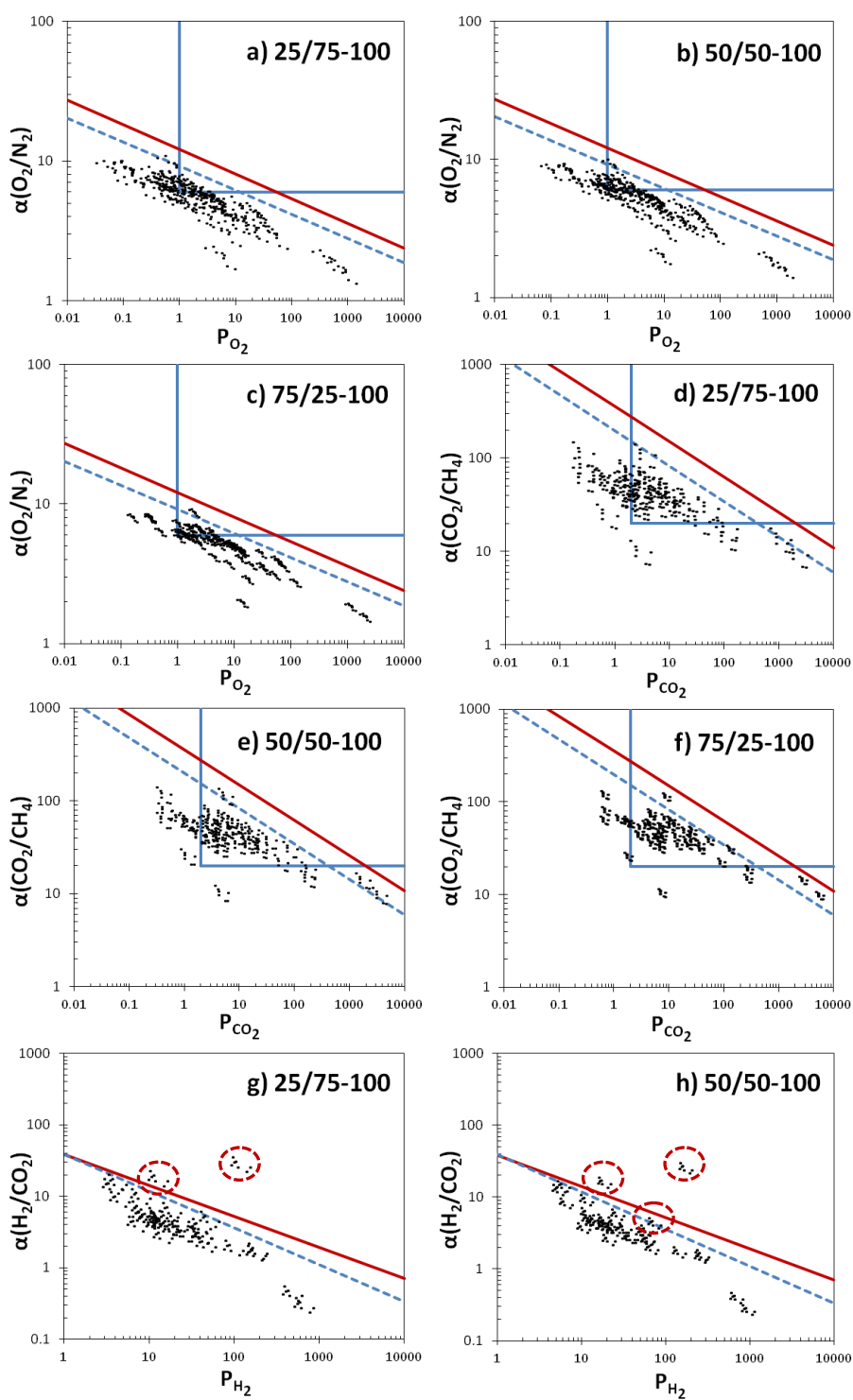
Figure 6.5 : Selectivity-permeability diagrams for O_2/N_2 pair for dianhydride ratios (a) (25:75), (b) (50:50) and (c) (75:25), CO_2/CH_4 pair for dianhydride ratios (d) (25:75), (e) (50:50) and (f) (75:25), H_2/CO_2 pair for dianhydride ratios (g) (25:75), (h) (50:50) and (i) (75:25) and CO_2/N_2 pair for dianhydride ratios (j) (25:75), (k) (50:50) and (l) (75:25).
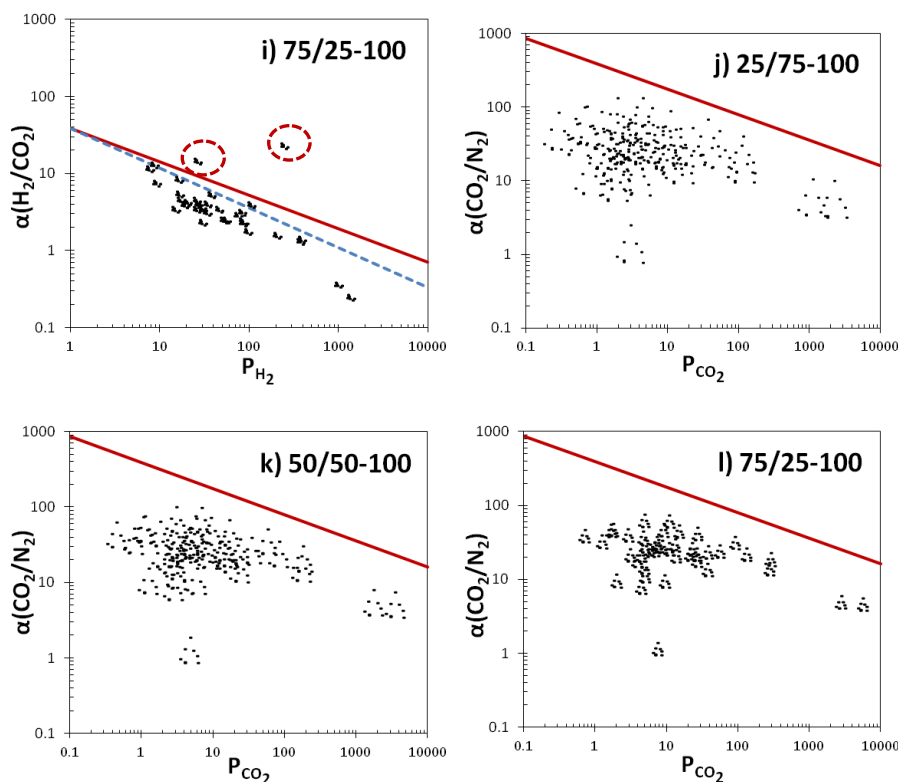
Figure 6.5 (devam): Selectivity-permeability diagrams for O_2/N_2 pair for dianhydride ratios (a) (25:75), (b) (50:50) and (c) (75:25), CO_2/CH_4 pair for dianhydride ratios (d) (25:75), (e) (50:50) and (f) (75:25), H_2/CO_2 pair for dianhydride ratios (g) (25:75), (h) (50:50) and (i) (75:25) and CO_2/N_2 pair for dianhydride ratios (j) (25:75), (k) (50:50) and (l) (75:25).

Table 6.2 presents all of the copolyimides that are located above the 1991 upper bound in Figure 6.5. All combinations of the 1st dianhydride, 2nd dianhydride and diamine that are given in Table 3.2 yielded permeability values above the 1991 upper bound. Moreover, for H_2/CO_2 separation, all monomer combinations that are represented in bold in Table 6.2 yield the permeability values of copolyimides above the 2008 upper bound and these copolyimides are marked with dashed circles in Figure 6.5.

Table 6.2: Copolyimide structures with two dianhydrides and one diamine, located above the 1991 upper bound.

Gas Pair	1st Dianhydride	2nd Dianhydride	Diamine
O_2/N_2	6FDA	PMDA	DABA
		BPDA	
		BTDA	
		ODPA	
		DSDA	
		SiDA	
		BPADA	
		HQDPA	
CO_2/CH_4	6FDA	PMDA	pBAPS
		BPDA	DBTF
		BTDA	MOMDA
		ODPA	
		DSDA	
		SiDA	
		BPADA	
H_2/CO_2	6FDA	PMDA	6FmDA
		BPDA	DANT
		BTDA	DDBT
		ODPA	
		DSDA	
		SiDA	
		HQDPA	

6.3.2 Predictions for copolyimides of one dianhydride and two diamines

The predicted separation properties of copolyimides with one dianhydride and two different diamine types and three different ratios calculated by the method of Alentiev et al. are shown in the form of selectivity-permeability diagrams in Figure 6.6. Copolyimides shown in Figure 6.6 involve dianhydrides, 6FDA, BPDA, BTDA, PMDA; mPDA, ODA, DAM, DABA, 2,6-DAT and Durene as the first diamine; and 64 different diamines as the second diamine, all of which had permeability values reported by Alentiev et al [51].
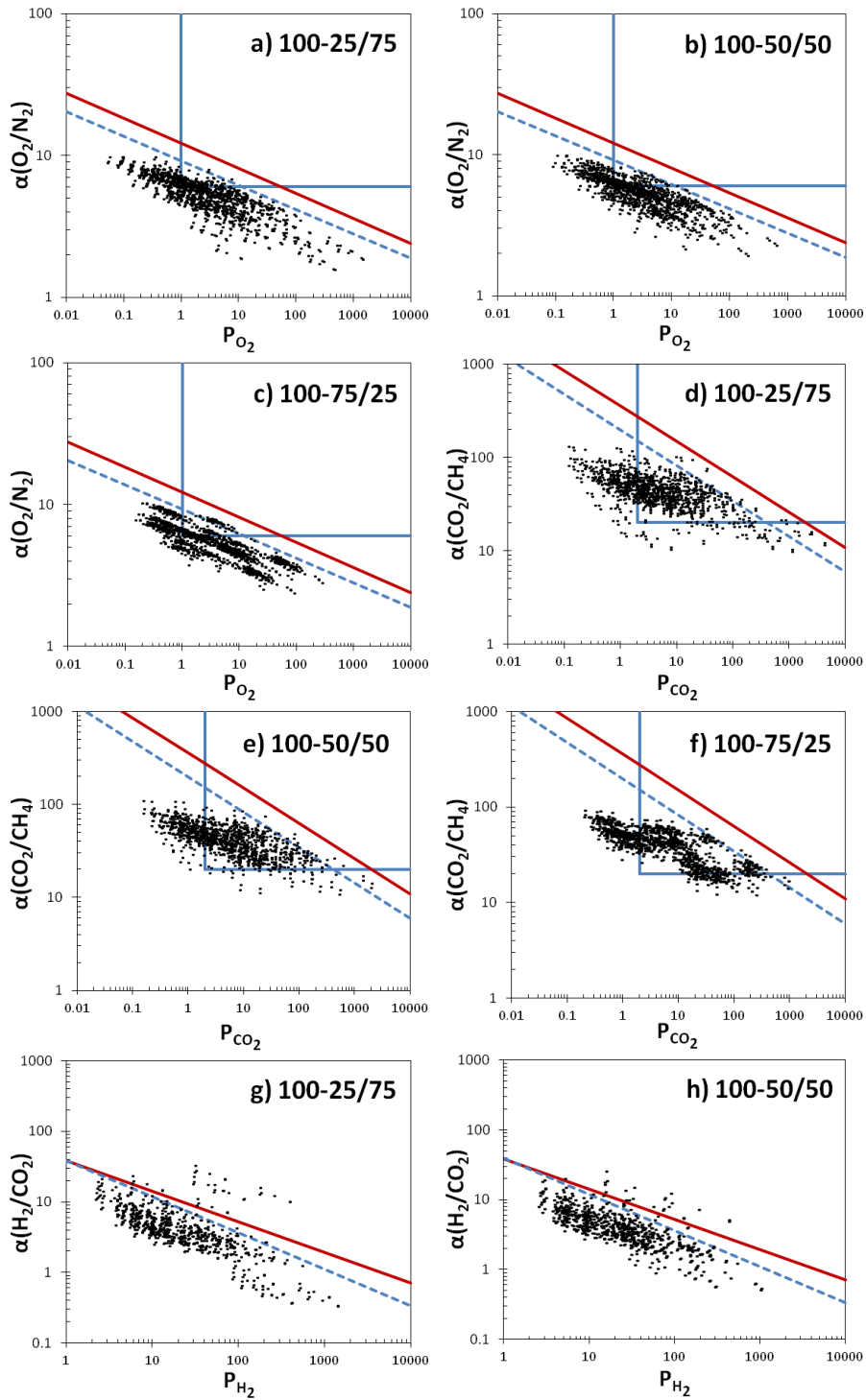
Figure 6.6 : Selectivity-permeability diagrams for O_2/N_2 pair for diamine ratios (a)
(25:75), (b) (50:50) and (c) (75:25), CO_2/CH_4 pair for diamine ratios (d)
(25:75), (e) (50:50) and (f) (75:25), H_2/CO_2 pair for diamine ratios (g)
(25:75), (h) (50:50) and (i) (75:25) and CO_2/N_2 pair for diamine ratios
(j) (25:75), (k) (50:50) and (l) (75:25).
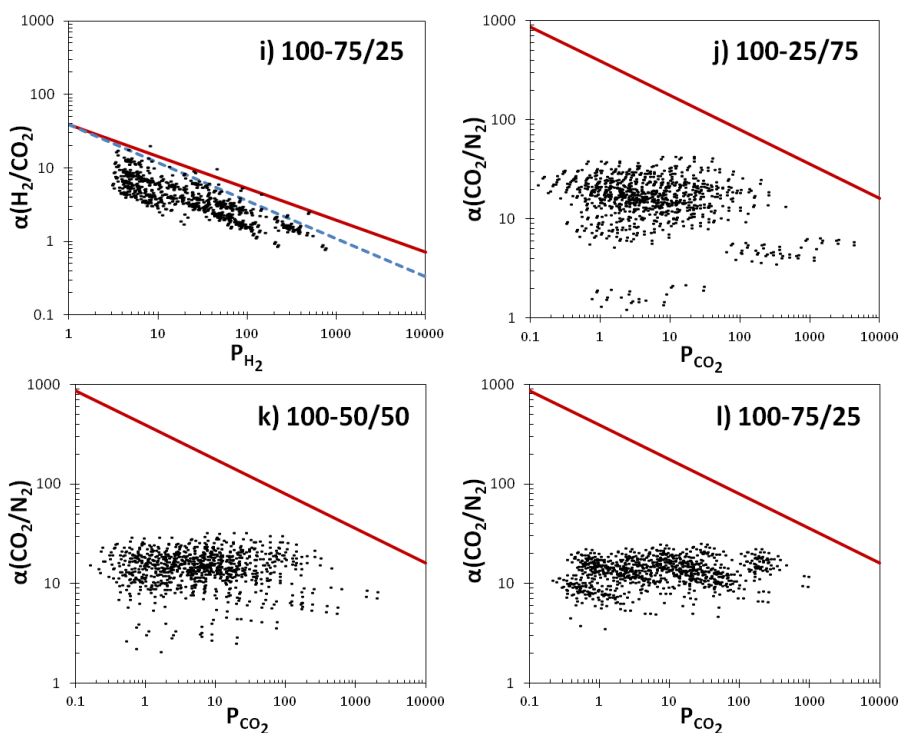
Figure 6.6 (devam): Selectivity-permeability diagrams for O_2/N_2 pair for diamine ratios (a) (25:75), (b) (50:50) and (c) (75:25), CO_2/CH_4 pair for diamine ratios (d) (25:75), (e) (50:50) and (f) (75:25), H_2/CO_2 pair for diamine ratios (g) (25:75), (h) (50:50) and (i) (75:25) and CO_2/N_2 pair for diamine ratios (j) (25:75), (k) (50:50) and (l) (75:25).

The predicted permeability and ideal selectivity values for the copolyimides considered in this study are all below the 2008 upper bound, except for separation of H_2/CO_2 gas pair. On the other hand, there are several copolyimides that are located above the 1991 upper bound, i.e. 80, 108 and 113 structures for O_2/N_2, CO_2/CH_4 and H_2/CO_2 separations, respectively. As the ratio of the first diamine is increased, the spread in selectivity decreases for these gas pairs. For CO_2/N_2 separation, the predicted copolyimides mainly collected on the higher permeability (1-1000 Barrer) end of data below the 2008 upper bound. This agrees well with the trend of experimental data as displayed by Robeson in his analysis to find the 2008 upper bound line for this gas pair. Robeson was not able to determine an upper bound line for CO_2/N_2 in 1991 due to lack of clear correlation between the upper bound protocol and the data that was used.

Table 6.3 shows some of the copolyimides that are located above the 1991 upper bound. All combinations of the 1st dianhydride, 1st diamine and 2nd diamine that are given in Table 6.3 yield permeability values above the 1991 upper bound except

H_2/CO_2 separation (above the 2008 upper bound). Although the separation properties of more than 2200 copolyimides with different monomer ratios have been predicted in this study, only a limited number of them exceeded the 1991 upper bound and only a few of them exceeded the 2008 upper bound. Four of the copolyimides listed in Table 6.2 and 6.3 have experimental permeability and selectivity values available in the literature [2, 156, 163]. This provided an opportunity to test the predictive capability of the method of Alentiev et al. modified for copolyimides. Table 6.4 and 6.5 show the comparison of the experimental and predicted permeability and selectivity coefficients of these four copolyimides, respectively. While 6FDA/BPDA-DDBT is a promising membrane polymer for H_2/CO_2 separation, the other three copolyimides (6FDA-DABA/6FpDA, 6FDA-DABA/DAM and 6FDA-DABA/mPDA) exhibit high permselectivity for O_2/N_2 and CO_2/CH_4 separation.

Table 6.3: Copolyimide structures with one dianhydride and two diamines, located above the 1991 upper bound.

Gas Pair	1st Dianhydride	1st Diamine	2nd Diamine
O_2/N_2	6FDA	DABA	mPDA
			DAM
			6FmDA
			6FpDA
			MOCA
CO_2/CH_4	6FDA	pBAPS	mPDA
		pDDS	DAM
			DABA
H_2/CO_2	6FDA	mPDA	6FmDA
	BTDA	ODA	DANT
		DAM	
		DABA	
		2,6-DAT	
		Durene	

Table 6.4: Comparison of predicted and experimental permeability coefficients of the copolyimides located near the 1991 upper bound.

Copolyimide	Predicted Permeability Coefficient (Barrer)					Experimental Permeability Coefficient (Barrer)					
	H_2	O_2	N_2	CH_4	CO_2	H_2	O_2	N_2	CH_4	CO_2	Ref.
6FDA/BPDA-DDBT(1:1)	61.4	2.86	0.46	0.30	14.8	120	13.1	2.6	1.48	71	[156]
6FDA-DABA/6FpDA(1:2)	75.8	10.6	1.85	0.63	29.1	—	11.5	2.17	1.02	45	[163]
6FDA-DABA/DAM(1:2)	187	32.0	6.56	3.02	87.0	—	18	4.36	4.17	113	[163]
6FDA-DABA/mPDA(1:9)	24.2	2.65	0.39	0.097	5.77	—	1.71	0.25	0.1	6.53	[2]

Table 6.5: Comparison of predicted and experimental selectivities of the copolyimides located near the 1991 upper bound.

Copolyimide	Predicted Ideal Selectivity				Experimental Ideal Selectivity				Temp. (°C) / Pressure (atm)
	O_2/N_2	CO_2/CH_4	CO_2/N_2	H_2/CO_2	O_2/N_2	CO_2/CH_4	CO_2/N_2	H_2/CO_2	
6FDA/BPDA-DDBT(1:1)	6.22	49.33	32.17	4.15	5.04	47.97	27.31	1.69	35 / 1
6FDA-DABA/6FpDA(1:2)	5.73	46.19	15.73	—	5.30	44.12	20.74	—	35 / 2
6FDA-DABA/DAM(1:2)	4.88	28.81	13.26	—	4.13	27.10	25.92	—	35 / 2
6FDA-DABA/mPDA(1:9)	6.79	59.48	14.79	—	6.84	65.30	26.12	—	35 / 3.74

Figure 6.7 shows the "trade-off" for O_2/N_2, CO_2/CH_4 and CO_2/N_2 separations. For O_2/N_2 and CO_2/CH_4 separations, experimental and predicted copolyimide transport properties are nearby the 1991 upper bound. However, for CO_2/N_2 separation, separation properties of these copolyimides are far from the 2008 upper bound, which was mainly observed for all predicted copolyimides in this study for this gas pair. While the predicted permeability coefficients are generally below the experimental values for all gas pairs, selectivity values for O_2/N_2 and CO_2/CH_4 separations are in close agreement with the predicted ones. Considering the simplicity of the group contribution method used here, the complexity of the copolyimide structures, and the variation in membrane preparation protocols, the agreement we have obtained here is rather remarkable. It should also be noted here that all permeability measurements for these four copolyimide structures were conducted at 35ºC and low pressures below typical plasticization pressures.
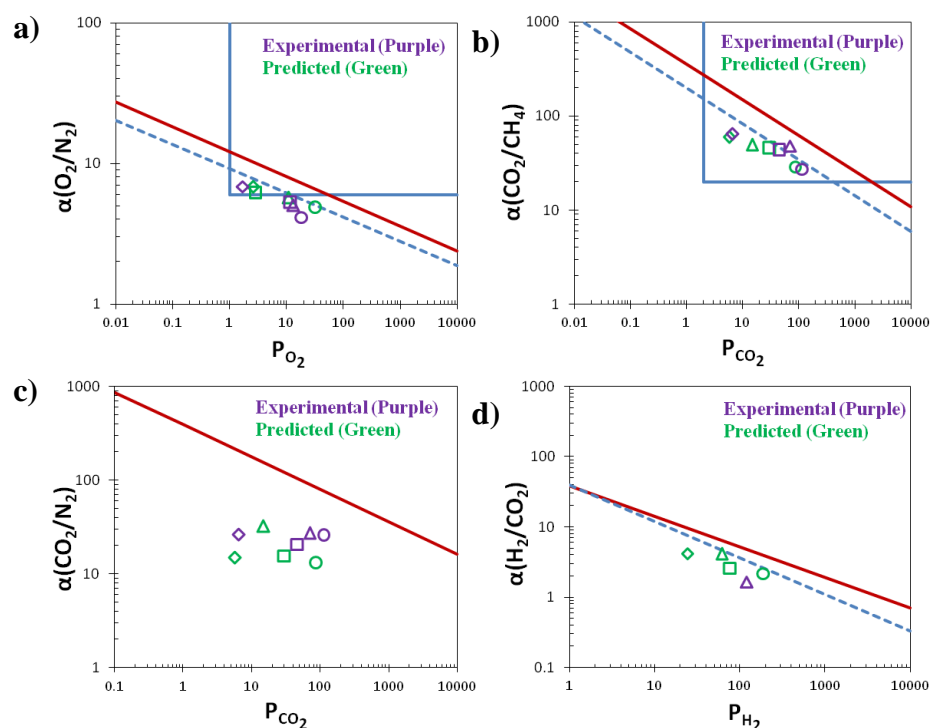
Figure 6.7 : Selectivity-permeability diagrams for (a) O_2/N_2, (b) CO_2/CH_4, (c) CO_2/N_2 and (d) H_2/CO_2 gas pairs. (6FDA/BPDA-DDBT, triangle (Δ); 6FDA-DABA/6FpDA, square (□); 6FDA-DABA/DAM, circle (O), 6FDA-DABA/mPDA, diamond (◊)).

6.4   Summary

Two different group contribution methods, method of Park and Paul [146] and method of Alentiev et al. [51] were examined in terms of their applicability to

copolyimides. To the best of our knowledge, this is the first study which investigates group contribution methods to predict the permeability of gases for copolyimides. All permeability predictions were made at 35°C. Large deviations were observed in case of experimental data obtained at different temperature values. The predictions of the method of Alentiev et al. exhibited less error than the method of Park and Paul for the copolyimides which have data available in the literature and therefore was chosen as the method to carry out predictions for more than 2200 possible copolyimide structures.

The following conclusions can be drawn from this work:

1. The separation performances of the copolyimide structures predicted in this study are all below the 2008 upper bound except for H_2/CO_2 gas pair. On the other hand, there are many copolyimide structures that are located above the 1991 upper bound for all gas pairs, except CO_2/N_2 which was not included in the 1991 study of Robeson [5].

2. The comparison of the predictions of the method used here for four different copolyimide structures with the available experimental data indicated that the selectivity predictions agree with the experimental data better than the permeability predictions. The average percent relative error for selectivity predictions range between 0.7–48.8. The permeability predictions are generally under-predicted.

3. For H_2/CO_2 separation, 52 different copolyimide structures which exceed the 2008 upper bound have been identified. To ensure the reliability of the method and eliminate the any speculative results, these promising structures need to be experimentally synthesized and characterized to further test the predictive capability of the method used here.

4. The copolyimide structures that exceed the 1991 upper bound for CO_2/CH_4 separation are slightly below the 2008 upper bound. A common feature of these structures (6FDA/PMDA-p-BAPS, 6FDA/BPDA-pBAPS, 6FDA/BTDA-pBAPS, 6FDA-pBAPS/mPDA, 6FDA-pBAPS/DAM, 6FDA-pBAPS/DABA, 6FDA-pDDS/mPDA, 6FDA-pDDS/DAM and 6FDA-pDDS/DABA) is the sulphone group in one of the diamines used to build the copolyimide repeat unit.

5. The copolyimide structures that exceed the 1991 upper bound for O_2/N_2 separation are 6FDA/PMDA-DABA, 6FDA/BPDA-DABA, 6FDA/BTDA-DABA, 6FDA-DABA/mPDA, 6FDA-DABA/DAM, 6FDA-DABA/6FmDA, 6FDA-DABA/6FpDA, and 6FDA-DABA/MOCA. It is noteworthy to mention that all of these structures contain the DABA unit which contains a carboxylic acid group.

6. Development of better membrane materials is a continuing research topic. A large number of studies have been dedicated to polyimides and copolyimides for over 30 years, however, the improvement in separation properties have been only incremental as can be seen from the 2008 upper bound. Based on the results obtained for the monomers studied here, there is a limit to what copolyimides can offer for important separation applications such as O_2/N_2 and CO_2/CH_4 and no major improvement is expected. Innovative design of new monomer structures is needed to overcome the existing challenges or access applications that are not yet practiced commercially.

7. Although group contribution methods have many limitations, they enable a quick screening of a large number of polyimide and copolyimide structures. An alternative approach may be the use of molecular simulation techniques; however they take much more time to even characterize one structure. There is a need for such fast screening especially in designing new novel polyimides or monomers, or selecting continuous phase for mixed-matrix membranes [173].

In spite of all the simplifications and assumptions involved, this study has shown that group contribution methods can be used for identifying possible copolyimide structures to lead experimental studies. Some of the copolyimide structures identified here will be the primary focus of the next chapter.

7. CO$_2$-INDUCED PLASTICIZATION IN COPOLYIMIDES CONTAINING A SULFONE GROUP

7.1 Introduction

High performance polymers such as aromatic polyimides (PIs) are gaining increasing attention because of their outstanding thermal and chemical stability, and good mechanical properties [9]. Polyimides are synthesized by the reaction of two monomers (dianhydride and diamine) in a solvent and by dehydration of the polyamic acid formed. If this procedure is carried out with two or more dianhydrides and/or diamines, then copolyimides are synthesized. Copolyimides allow us to optimize the separation properties by using two different polyimides which have different permeability and selectivity properties. 6FDA-based copolyimides are of particular interest since they contain two bulky -CF$_3$ groups, have a lot of attention due to the increase of the polymer's FFV, and thus rise in permeation rates. Moreover 6FDA-based copolyimides are also important by means of processability in gas separation membranes. The high solubility of these aromatic polyimides is good from a processing standpoint, but it also means that they are sensitive to plasticization, which causes the swelling of PI matrix with the sorption of condensable gases. It is well known that the use of PIs as well as co-PIs for natural gas and hydrocarbon separations are limited by sorption induced volume swelling and plasticization. Plasticization is a pressure dependent phenomena and occurs when the concentration of these gases in glassy polymers, such as co-PIs, is high enough to cause swelling in the polymer, i.e. reduce chain alignment and increase inter-segmental mobility and fractional free volume (FFV).

A few experimental studies investigating plasticization effect of CO$_2$ in copolyimides have been reported in the literature [2, 32, 33, 90, 154, 166-168, 174-180]. However, all of these studies mainly focus on the change in plasticization pressure with the crosslinking of co-PIs in case of pure and binary gases rather than looking at the diamine and dianhydride monomer ratio variation. Only gas transport properties of

copolyimides were investigated by systematically varying the diamine or dianhydride ratios [160, 164, 169, 171, 181-188]. Staudt-Bickel and Koros [2] studied the synthesis of the uncross-linked and cross-linked 6FDA-mPD/DABA (9:1) co-polyimides in order to show the reduction due to plasticization effect caused by CO_2 induced swelling in CO_2/CH_4 separation and the effect of stabilizing the co-polyimide structure with ethylene glycol crosslink. They succeeded in reducing the swelling effect of CO_2 at least up to a pure CO_2 pressure of 35 atm [2]. The same group, in 2003, investigated the solid-state covalent cross-linking of 6FDA-DAM/DABA 2:1 with ethylene glycol, 1,4-butylene glycol, 1,4-cyclohexanedimethanol, and 1,4-benzenedimethanol and were very effective in stabilizing membranes against CO_2 plasticization up to 40 atm feed pressure [180]. A year later, they added a thermal annealing procedure to the covalent crosslinking in their previous study on 6FDA-DAM/DABA 2:1 co-PI and measured the transport properties of gas mixtures at 35°C and feed pressures up to 55 atm [90]. In 2008, Kratochvil and Koros presented a novel cross-linking approach for the same co-PI and progressed in obtaining an excellent plasticization resistance for CO_2 which renders a polyimide insoluble in typical solvents [178]. In 2011, Koros's group performed the sub-Tg thermal annealing for 6FDA-DAM/DABA (3:2) and studied simultaneous removal of CO_2 and H_2S from sour natural gas streams [179]. Bos et al. used blending of a polymer that is highly susceptible to plasticization such as Matrimid, with a polymer that hardly plasticizes such as P84 co-PI to suppress plasticization [33]. Chung et al. investigated the 6FDA-durene/mPDA co-PI up to 20 atm and reported that the permeabilities of O_2, N_2, and CO_2 decrease with an increase in the upstream pressure, however, no CO_2-induced plasticization was noticed in this testing pressure range [177]. Konietzny et al. examined the effect of swelling agent on chain distance, free volume size and orientation of functional groups of 6FDA-4MPD/6FDA-DABA (49:1) and (9:1) co-PIs containing carboxyl groups and reported that although the chain distance initially decreased slightly as seen by WAXD of film samples, FTIR experiments did not show any significant orientation changes in the co-PI chains [174].

There are not many molecular simulation studies that focus on CO_2-induced plasticization in copolyimides. Pinel et al. [189] studied the effect of increasing bicyclo(2.2.2)-oct-7-ene-2,3,5,6-tetracarboxylic dianhydride (BCDA) content in

ODPA/BCDA co-PIs as well as adding trifluoromethyl or methoxy substituents on the ODA at the molecular level. Many different analyses were performed such as cohesive energies, Hildebrand parameters and the available void spaces and these parameters were compared by changing dianhydride ratio of BCDA and diamine substituents. They found that both the BCDA moiety and the trifluoromethyl substituent on the diamine decrease chain cohesion and increase the available void space [189]. To the best of our knowledge, this will be the first simulation study examining the plasticization phenomena for CO_2/CH_4 separation in co-PIs.

In this study, molecular simulation techniques were used to estimate the degree of plasticization of 4,4-hexafluoroisopropylidene-diphthalic anhydride (6FDA)-based sulfonated copolyimide membranes induced by sorption CO_2. The selection of 6FDA/BTDA-pBAPS, 6FDA-pBAPS/DABA, and 6FDA-pBAPS/mPDA copolyimide structures was based on our previous study in Chapter 3 (Figure 3.5 and 3.6, and Table 3.2 and 3.3) [190] in which the permeability coefficients of H_2, O_2, He, CO_2, N_2, and CH_4 gases for more than 2200 possible copolyimide structures were estimated by the group contribution method of Alentiev et al. [51]. The predicted permselectivities of the above mentioned copolyimides were located well above the 1991 upper bound of Robeson diagrams for CO_2/CH_4 separation application.

The structural properties, such as glass transition temperature (T_g), FFV and its distribution, d-spacing, radius of gyration, and cohesive energy density, along with sorption isotherms were investigated from simulations to understand the dynamics of polymer chains and penetrants. Moreover, in order to make comparison and provide an insight to copolyimide structure-plasticization, the synthesis and the characteristic analysis of these co-PI membranes were also performed. Experimental sorption measurements provide us the validity of our simulation procedure. Furthermore, permeability measurements were also performed to determine the separation performance of co-PIs and plasticization behavior.

Thousands of diamine-dianhydride combinations can be suggested as potential membrane materials, but only a limited number of them were synthesized and characterized for gas separation applications until now. However, molecular simulation techniques offer an opportunity to predict the structure-property relationship without wasting time and money in the case of failure.

7.2 Simulation Method

All simulations in this study were carried out according to the methodology described in Section 2.5. Simulation procedure which was applied to polyimides was used for copolyimides. The copolyimide structure was assumed as alternating polyimides of two dianhydrides and one diamine or one dianhydride and two diamines. 6FDA and BTDA dianhydride, pBAPS, mPDA and DABA diamine moieties shown in Figure 7.1 were constructed and linked followed by geometry optimization to create 6FDA-pBAPS, BTDA-pBAPS, 6FDA-mPDA and 6FDA-DABA repeat units. The co-PI chains with appropriate dianhydride/dianhydride (3:1) and diamine/diamine (3:1) ratios were then built by connecting these repeat units with each other by using *Random Copolymer* tool and a final geometry optimization was carried out.
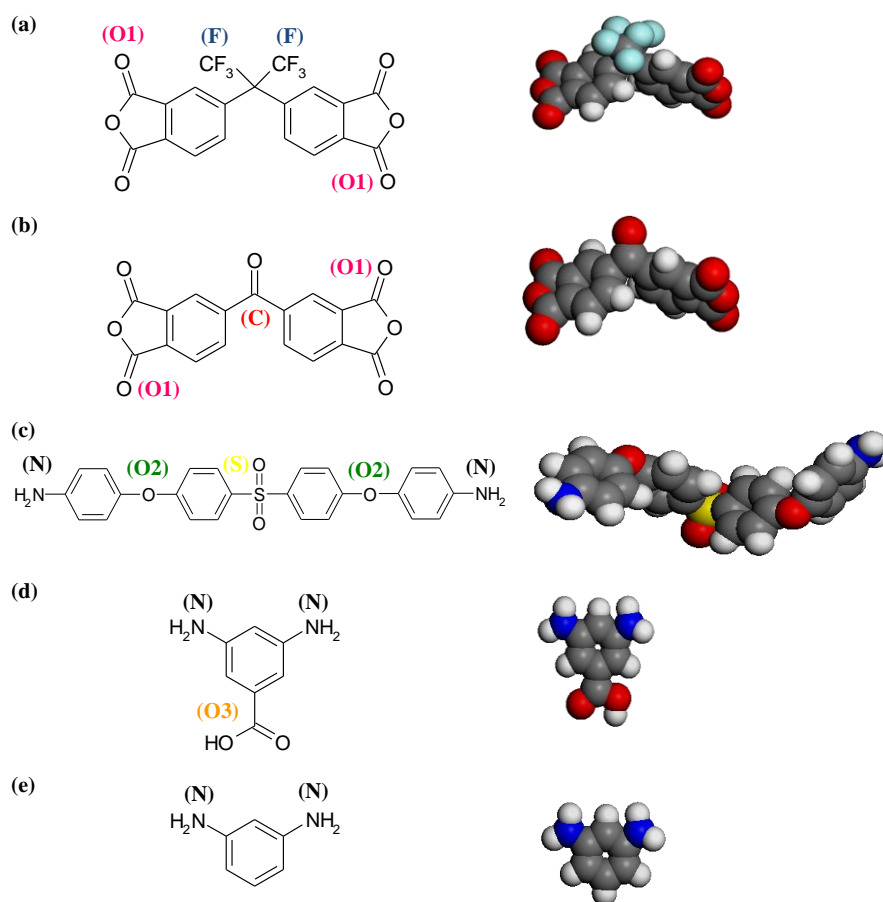
Figure 7.1 : Structures of moieties for (a) 6FDA, (b) BTDA, (c) pBAPS, (d) DABA and (e) mPDA.

Simulation temperature and pressure values were chosen based on our experimental study: 35ºC and 10 bar for CO_2 and CH_4; 35ºC and 2 bar for O_2 and N_2.

7.3 Experimental Methodology

7.3.1 Materials

The physical properties of monomers which were used in the synthesis of the selected co-PIs, 6FDA/BTDA-pBAPS, 6FDA-pBAPS/mPDA, and 6FDA-pBAPS/DABA, are given in Table 7.1.

Table 7.1 : Physical properties of monomers.

Monomer	Molecular Weight (g/mol)	Melting Point(°C)	Purity	Supplier
6FDA	444.25	244	≥99%	Aldrich
BTDA	322.23	220-223	>97%	Merck
pBAPS	432.5	194-196	≥98%	TCI America
mPDA	108.14	64-66	≥99%	Aldrich
DABA	152.15	235-238	≥98%	Aldrich

Table 7.2 shows the physical properties of solvents, dimethylacetamide (DMAc) and n-methyl-pyrrolidone (NMP), used in the polyimide synthesis and membrane formation respectively. Ortho-dichlorobenzene (o-DCB) was used exclusively as a dehydration agent in the thermal imidization step of polymer synthesis. Methanol was used as a non-solvent to precipitate and blend the polymer after it was synthesized. Table 7.3 gives the physical properties of these chemicals.

Table 7.2 : Physical properties of solvents.

Monomer	Molecular Weight (g/mol)	Boiling Point(°C)	Purity	Supplier
DMAc	87.12	165-166	≥99%	Merck
NMP	99.13	202-204	≥99.5%	Merck

Table 7.3 : Physical properties of chemicals.

Monomer	Molecular Weight (g/mol)	Boiling Point(°C)	Purity	Supplier
o-DCB	147	174	≥98%	Merck
Methanol	32.04	64-65	≥99.9%	Merck

7.3.2 Polymer Synthesis

A two-step technique was used in copolyimide synthesis. In the first step, a polyamic acid was formed in a solution of solvent (DMAc) from the reaction of a dianhydride and a diamine followed by the second step in which the polyamic acid was converted to polyimide by using a dehydration agent (o-DCB). Water evolving during reaction forms a low boiling point azeotrope with o-DCB and removed using a Dean-Stark trap. To ensure high purity of the monomers, they were sublimed under vacuum at 5-10°C below their melting points. In the polyamic acid synthesis, dianhydride and diamine monomers were added in equimolar ratio. Diamine or dianhydride ratios is scaled as 3:1. The monomer weight in the reaction solution was ~ 20%. Polyamic acid reaction was carried out at 4°C. A three-necked round bottom flask was continuously purged with a stream of nitrogen that was maintained throughout the entire reaction. DMAc and diamine were added into the flask and stirred with a mechanical stirrer, and then dianhydride was added in five equal portions at every fifteen minutes. If there were two dianhydrides in copolyimide, they were added alternately. Solution was stirred 48 hours at 4°C and the reaction was monitered by FTIR analysis. Polyamic acid reaction was completed when the FTIR peaks did not change any more and polyimide reaction step was proceded.

During the entire conversion of polyamic acid to the final polyimide a constant stream of nitrogen and constant stirring was maintained throughout the entire reaction. Polyimide reaction was carried at 180°C in an oil bath. o-DCB was added in 1:3 ratio of DMAc by mole. Water formed during the reaction was removed when it formed a low boiling point azeotrope with o-DCB using a Dean-Stark trap and condenser. The o-DCB that was removed during this process was replenished with new o-DCB via Dean-Stark trap. This is done in order to maintain a constant solvent volume in the flask. After imidization the polyimide solution was cooled and precipitated using methanol. Recovered white precipitate was filtered and then dried in a vacuum oven at 80°C for one day; 80, 150 and 210°C for one day at vacuum.

7.3.3 Membrane Formation

The formation of polymer films has been achieved by dissolving a known amount of polymer in a solvent. NMP was used as solvent in film formation. The solution was

prepared at 20 wt% polymer concentration and stirred one day with a mechanical stirrer. Before casting, the surface of a mirror was cleaned and the mirror was heated to 100°C in a furnace. The polymer solution was poured on the heated mirror surface and cast into a film by using a film casting blade and an automatic film applicator. The initial thickness was set to 500 μm. The membrane was dried for 2 hours at 80°C, which was then removed from the surface of the mirror and left hanging in an oven to evaporate in both surfaces at 80°C for one day; 80, 150 and 210°C for one day at vacuum.

7.3.4 Membrane Characterization

Following membrane preparation, standard characterization methods were employed to determine the properties of the membranes. Following morphological and thermal characterization, transport properties of membranes were investigated by permeation and sorption measurements.

7.3.4.1   Fourier transform infrared spectroscopy

Fourier transform infrared spectroscopy (FTIR) is a technique which is used to obtain an infrared spectrum of absorption, emission, photoconductivity or Raman scattering of a solid, liquid or gas. In this work, polyamic acid and polyimide reactions were monitored by Perkin-Elmer Spectrum One Fourier Transform Infrared Spectroscopy. All analysis were performed between 4000 cm^{-1} and 600 cm^{-1} wavelength. In polyamic acid reaction, characteristic adsorption peaks of amic acid which are aromatic NH-C at 3500 cm^{-1}, -OH (-COOH) at 2925 cm^{-1} and C=O (-COOH) at 1680 cm^{-1} wavelengths were monitored. Characteristic adsorption peaks of polyimide are symmetric and asymmetric C=O peaks at 1780 cm^{-1} and 1820 cm^{-1} wavelengths respectively and C-N vibration peaks around 1350-1375 cm^{-1} wavelengths.

7.3.4.2   Gel permeation chromatography

Gel permeation chromatography (GPC) separates based on the size or hydrodynamic volume (radius of gyration) of the analytes. Separation occurs via the use of porous beads packed in a column. The smaller analytes can enter the pores more easily and therefore spend more time in these pores, increasing their retention time. Conversely,

117

larger analytes spend little if any time in the pores and are eluted quickly. All columns have a range of molecular weights that can be separated. When characterizing polymers, it is important to consider the polydispersity index (PDI) as well the molecular weight. Polymers can be characterized by a variety of definitions for molecular weight including the number average molecular weight (M_n), the weight average molecular weight (M_w), the size average molecular weight (M_z), or the viscosity molecular weight (M_v).

7.3.4.3 Thermo-gravimetric analysis

Thermo-gravimetric analysis (TGA) is a technique where the mass of a sample is measured as a function of temperature or time, while the sample is subjected to a controlled temperature programme in a controlled atmosphere. A sample TGA thermogram for an elastomer shows weight loss due to desorption of gases and decomposition. In this work, TGA measurements were carried out with a Perkin-Elmer Diamond TG/DTA. About 3 mg of sample was weighed for both film and powder copolyimides, and heated from 50°C–550°C, with a rate of 10°C/min. The resultant data was used to determine the amount of moisture and residual solvent in the sample, and also as a guide for DSC measurements.

7.3.4.4 Differential Scanning Calorimetry

Differential scanning calorimetry (DSC) is a mostly preferred thermal analysis technique used for determination of glass transition (T_g), melting (T_m), crystallization (T_c) temperatures, and heat of fusion for polymeric samples. In this work, DSC measurements of samples were carried out with a Perkin-Elmer 4000 Series DSC. Experimental runs were completed on thin films and powder having an average mass of 10 mg. The heating cycle described above was applied under inert N_2 atmosphere, in order to prevent unforeseen side reactions. Tg was calculated by half-Cp extrapolation method. A heating sequence that was designed according to the TGA data was applied. The sequence was designed as follows [191]:

1. Heating the sample from 50°C to the temperature 20-30°C above Tg, at a rate of 20°C/min. The first heating step was applied to erase the sample's thermal history without inducing irreversible transitions.
2. Keeping the sample at this temperature for about 10 min, in order to evaporate the residual solvent.

3. Cooling the sample to the temperature 50-60°C below the Tg, at a rate of 30°C/min, in order to prepare the sample for the next heating cycle.

4. Without waiting, re-heating the sample to 450°C, at a rate of 20°C/min to observe the glass transition properly.

7.3.4.5 Dynamic Mechanical Analysis

Dynamic Mechanical Analysis (DMA) measures stiffness and damping, these are reported as modulus and tan delta. The storage modulus, either E' or G', is the measure of the sample's elastic behavior. The ratio of the loss to the storage is the tan delta and is often called damping. It is a measure of the energy dissipation of a material. Modulus values change with temperature and transitions in materials can be seen as changes in the E' or tan delta curves. This includes not only the glass transition and the melt, but also other transitions that occur in the glassy or rubbery plateau, shown in Figure 7.2.
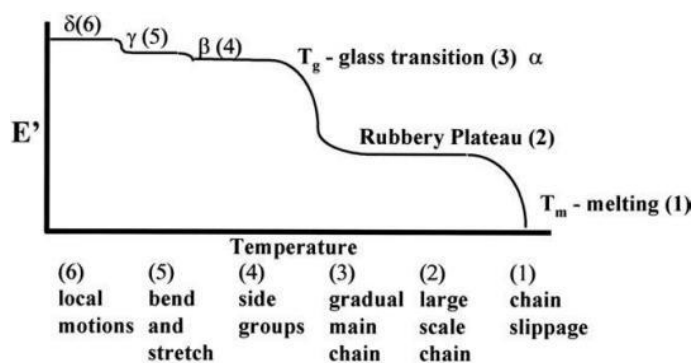
Figure 7.2 : Modulus values change with temperature and transitions in materials [192].

T_g is seen as a large drop (a decade or more) in the storage modulus when viewed on a log scale against a linear temperature scale. The value reported as the Tg varies in literature with the onset of the E' drop, the peak of the tan delta, and the peak of the E'curve being the most commonly used.

In this work, Perkin-Elmer Diamond DMA was used to characterize the glass transition, Tg and molecular transitions in the copolyimides. Experimental runs were completed on film samples having a length of 20 mm, a width of 4 mm and a nominal thickness of 0.05 mm, and heating rate was 3˚C/min.

7.3.4.6 Wide angle X-ray diffraction

Wide angle X-ray diffraction patterns of polyimide films were obtained with PAN analytical X Pert PRO diffractometer, CuKα source (λ = 1.54Å). The apparatus scanned over the range 5-60°, with a dwell time of 3 s and a step size of 0.5°. The d-spacing was calculated from Bragg's equation $n\lambda = 2d\sin\theta$, where n = 1. The average d-spacing is determined from a polynomial curve of the data in the region of the main peak.

7.3.4.7 Sorption Measurements

Intelligent gravimetric analyser (IGA) produced by Hiden Isochema, UK, was used for sorption measurements of copolymides. For static gas sorption of N_2, O_2, CO_2 and CH_4 gases, IGA-001 mode was used. Small film samples about 40 mg were cut and put the basket. The samples were first "degassed" with the small drop 50 mbar/min. in pressure to remove the sorbed gases from the samples. The heating rate was 1°C/min, and the "degassing" temperature was 250°C. The samples were kept at this temperature for 2 hours in order to get rid of solvent and water, and then allowed to cool down. The sample was heated to the measurement temperature (35°C), the weight of the "degassed" sample was tarred, and the measurement sequence was carried out between 0-9 bars, with set points at 1 bar intervals. Before the sorption of second gas, the decontamination of whole system was performed nearly 2 hours. Briefly, the working principle of IGA is as follows: The measurement chamber is pressurized to the active set point, and the deviation in weight of the sample is monitored. When the deviation reaches a minimum, equilibrium is assumed, the weight is recorded as the sorption capacity of sample (at that pressure and temperature) for the gas used, and the procedure continues with the next set point.

7.3.4.8 Permeation Measurements

The permeability measurements were carried out with an in-house constant-volume variable-pressure permeation system, shown in Figure 7.3. The permeation system mainly consists of a permeation cell, upstream and downstream transducers, data acquision system and gas chromatogram (GC). GC is used for measuring the composition of feed and permeate. Since in this part of present work, mixed feed conditions were not tested, the GC was not used. However, mixed gas measurements were also planning to perform later on in order to see plasticization effect. Before

and after measuring a sample, a leak test was applied to see the amount of gas leaking into the downstream. A sheet of aluminum with one adhesive face was used for a leak test. While the evaluation permeability of a membrane, the leak rate was subtracted from the rate of pressure increase for a measurement.
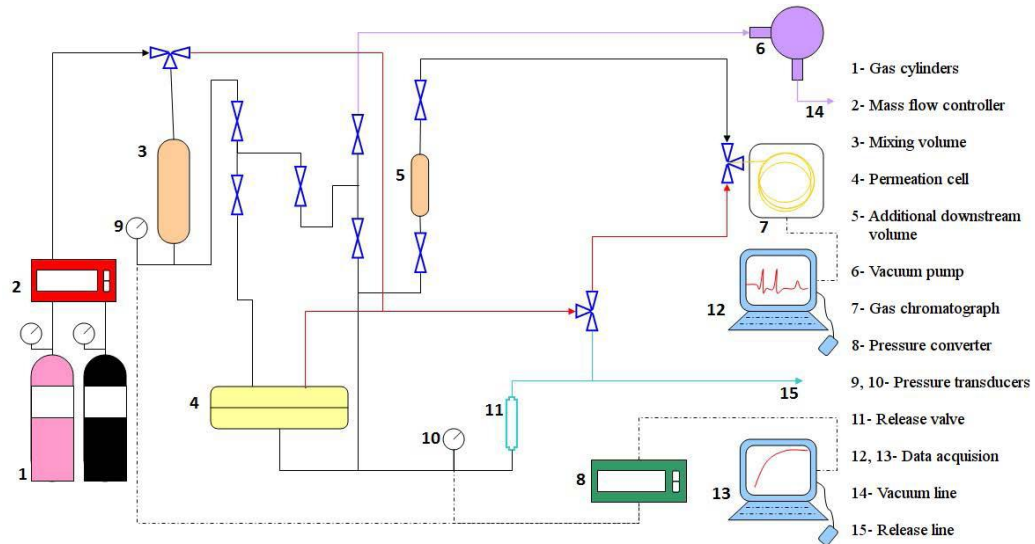
Figure 7.3 : Schematic representation of the constant-volume variable-pressure system [193].

To measure gas permeabilities, the masked membrane film was placed into the permeation cell which has O-ring on both halves and inserted into a pressure-rise permeation apparatus. In order to remove residual solvent and sorbed gases; the upstream, downstream, and the membrane were evacuated for 24 hours using a vacuum pump. After evacuation, the pressurized gas was fed to the upstream, while the change in the pressure in the downstream was constantly recorded. Until a membrane reaches steady-state or in other words, the rate of pressure increase in the downstream becoming linear was constant for three consecutive measurements, vacuum of downstream and then permeation operation were repeated many times for each gases. The permeability coefficients of gas i (N_2, O_2, CO_2 and CH_4) were calculated using Equation 7.1.

$$P_i = \frac{(m_p - m_l)Vl}{ART\Delta P} \tag{7.1}$$

where m_p is the rate of pressure increase in the downstream during permeation measurement, m_l is the rate of leak in the downstream, V is the volume of the downstream, l is the thickness of the membrane, A is the permeation area of the sample, R is the ideal gas constant, T is the temperature at which the measurement

was taken, ΔP is the pressure difference between the upstream and the downstream.N_2 and O_2 gas measurements were carried out at 35°C, 2 bar upstream pressure. CO_2 and CH_4 gas measurements were carried out at 35°C, 4 bar upstream pressure. To define CO_2 plasticization pressure of each copolyimides upstream pressure can be raised until 8.7 bar due to system limitations.

7.3.4.9 Polymer Density

Polymer film densities at 23°C were measured with a Ray-Ran advanced auto density measurement filled with aqueous zinc chloride-ethanol-water solutions. A linear calibration curve (density versus position) was established by placing glass beads of known density into the column. The beads and samples reached their equilibrium positions after a 24 h period. Each film density was measured at least twice.

7.4   Results and Discussion

For simplicity, 6BpB, 6pBmP and 6pBD, abbreviations were used for 6FDA/BTDA-pBAPS, 6FDA-pBAPS/mPDA and 6FDA-pBAPS/DABA copolyimides respectively.

7.4.1 Characterization of copolyimides matrices

For monitoring polyamic acid and polyimide formation in a one-pot synthesis method, FTIR was used. FTIR spectrums of co-PIs which have 87,000, 102,000 and 58,000 molecular weight, respectively can be seen in Figure 7.4. Amic acid characteristic adsorption peaks such as NH-C at 3525, 3522 and 3482 wavelength, O-H (-COOH) at 2934, 2933 and 2935 wavelength, C=O (-COOH) at 1633, 1635 and 1633 wavelength were disappeared in imide formation and characteristic imide peaks were appeared at 1722, 1726 and 1726 wavelengths for C=O symmetric and asymmetric stretching peaks and at 1374, 1373 and 1375 wavelength for C-N stretching peaks for 6BpB, 6pBmP and 6pBD, respectively.
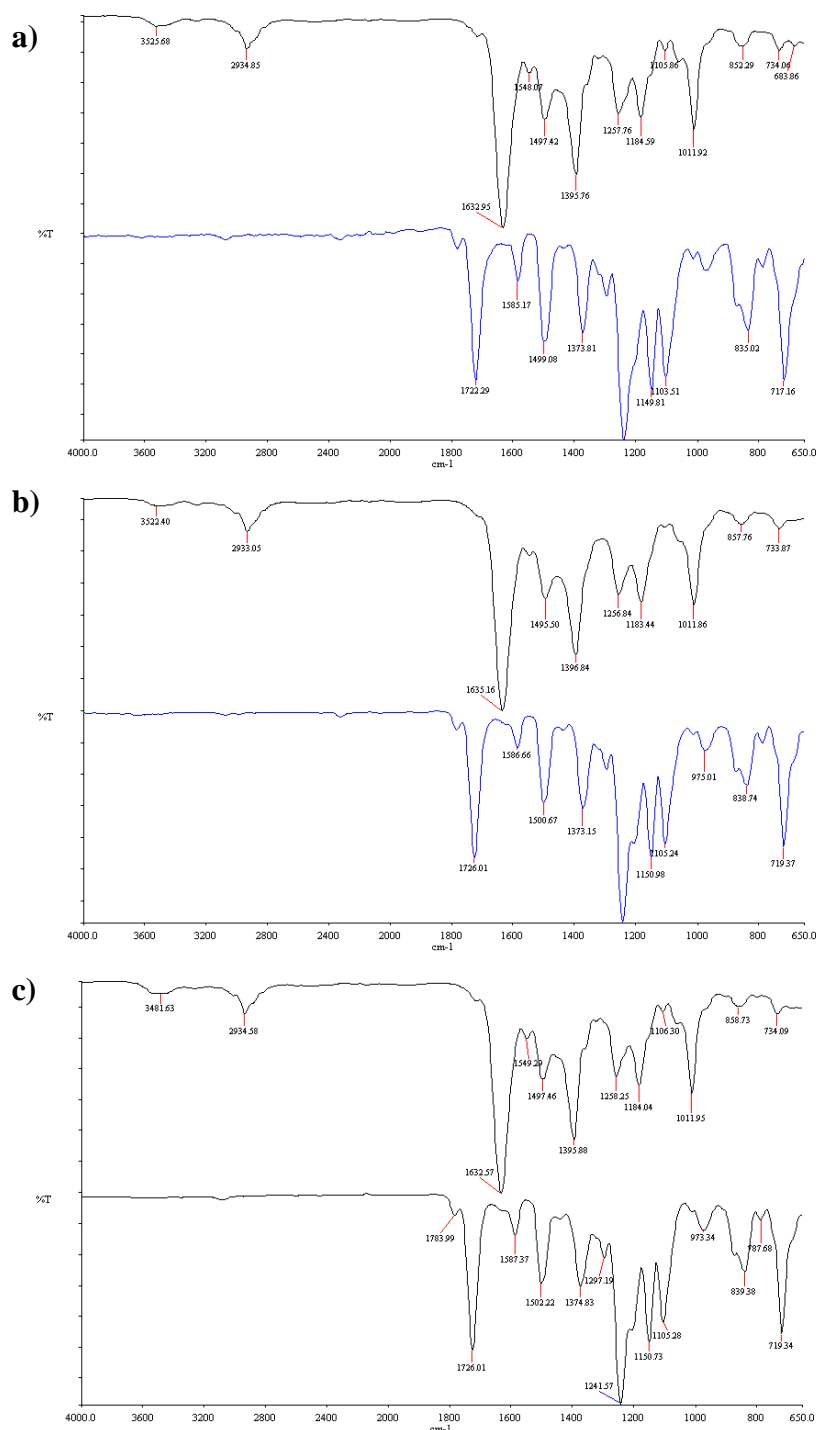
Figure 7.4 : FTIR spectrums of a) 6FDA/BTDA-pBAPS, b) 6FDA-pBAPS/mPDA and c) 6FDA-pBAPS/DABA co-PIs. (top:polyamic acid and bottom: polyimide reaction steps).

Hydrogen bonding can be followed with SO_2 stretching (1324, 1147 cm^{-1}) [194] and ether group (1232 cm^{-1}) [194, 195] in pBAPS diamine, broad weak adsorption of -OH vibration (3200-3500 cm^{-1}) of carboxylic acid group in DABA diamine [179], the OH in-plane deformation (1395-1440 cm^{-1}) of carboxyl dimers [178].

The presence of hydrogen bonding between structures can be determined by observing shifts of characteristic absorption bands to higher wavenumbers or noting changes in peak intensities. For example, Zornoza et al. were encountered that there is an increasing shift in the peak associated with the Ar- O-Ar stretching vibration at about 1235 cm^{-1} to higher wavenumbers with the SiO_2 concentration [195]. The same effect was observed by Reid et al. [194] in PSF membranes with MCM-41 30 wt % content the peak at 1232 cm^{-1} shifted to 1239 cm^{-1} upon introduction of the siliceous material. They attributed this shift to the high internal surface of mesoporous silica has -OH groups that could interact via hydrogen-bonding with the aryl ether groups of the polymer [194].

Figure 7.5 shows overlapped and split FTIR spectrums of co-PIs, respectively. The main difference between DABA and mPDA diamines is the carboxylic acid group (-COOH). Broad weak adsorption of -OH vibration (3200-3500 cm^{-1}) of carboxylic acid group in DABA diamine, which is the evidence of the presence of this group in 6pBD co-PI, can be seen clearly from Figure 7.5 a). C-N stretching peak around 1437 cm^{-1} are almost same in all co-PI FTIR spectrums. However, the nearest peak around 1463 cm^{-1}, which shows the -OH in-plane deformation, shadows the C-N stretching peak in 6pBD co-PI. This means that due to h-bonding in 6pBD co-PI, the -OH in-plane deformation peak occurs. In addition, when 6pBD and 6pBmP co-PIs were compared in Figure 7.5 b), there is a shift in SO_2 antisymmetric stretching peak from 1371 cm^{-1} in 6pBmP to 1376 cm^{-1} in 6pBD, which may be the indication of h-bonding.
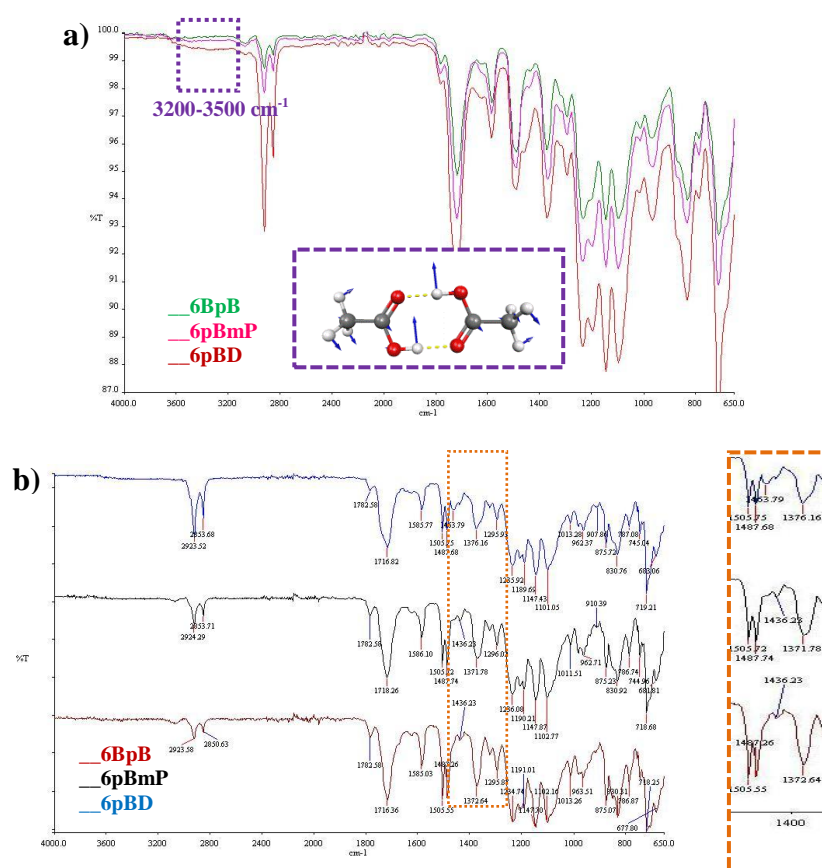
Figure 7.5 : FTIR spectrums of co-PI structures in a) overlapped version and b) slip version.

Structural properties of co-PI models calculated with molecular simulation methods and comparison to experimental results obtained in the laboratory are presented in Table 7.4. Calculated d-spacing values coincide with the experimental values. The d-spacing value depends both on the dianhydride and diamine type. Both in simulation and experiment, there was not much difference in d-spacing of co-PIs. When the second diamine (mPDA) instead of the second dianhydride (BTDA) was used, the d-spacing changed slightly. However, if we look at the x-ray patterns of co-PIs in Figure 7.6, it is clear that there was a shoulder in 6pBmP co-PIs pattern which is the indication of existence of small free volumes or different free volume distribution than 6pBB. Among the three co-PIs considered in this study, 6pBB has the highest d-spacing value. Because it has only one diamine (pBAPS) which has four phenyl rings in backbone, inhibits packing. Due to hydrogen bonding ability of –OH group in carboxylic acid of DABA diamine as mentioned in FTIR analysis, 6pBD co-PI has high density, solubility and radius gyration (Rg). It enhances the close packing and hence increases the cohesive energy of co-PI. When 6pBD and 6pBmP were

compared, this relation can be seen obviously. However, it is expected that 6pBD should have low FFV and d-spacing compared to the 6pBmP co-PI. In the next section, it will be presented clearly that with the addition of –OH groups, hydrogen bonding increased Langmuir sorption sites and decreased Henry sorption sites. Due to the increase in Langmuir sorption sites, the un-relaxed "frozen" excessive free volume present in 6pBD co-PI increased slightly.

Table 7.4 : Comparison of estimated properties of co-PIs with experimental data.

Properties		6FDA/BTDA -pBAPS	6FDA- pBPAS/mPDA	6FDA- pBPAS/DABA
T_g (ºC)	Sim.	290	280	331
	DSC[a]	276	285	287
	DMA[b]	260	277	272
d-spacing (Å)	Sim.	5.56	5.51	6.08
	Exp.	5.19	5.04	5.62
Density (g/cm^3)	Sim.[c]	1.349	1.366	1.391
	Exp.[d]	1.387	1.400	1.419
R_g(Å)	Sim.	36.6	29.0	25.6
FFV	Sim.	0.193	0.187	0.189
δ (J/cm^3)$^{1/2}$	Sim.	16.23	13.84	15.63
M_W (g/mol)	Exp.	87 000	102 000	58 000

[a] Temperatures refer to film sample.
[b] Temperatures refer to E"(T_α).
[c] at 35ºC. [d] at 23ºC.

Table 7.5 : Experimental Tg's of corresponding homopolyimides of co-PIs.

Polyimides	Tg
6FDA-mPDA	315[a], 301[b], 296[c], 286[c], 297[d], 305[e],
6FDA-DABA	348[f], 273[g], 309[h]
6FDA-pBAPS	299[i], 278[g], 282[j], 267[k]
BTDA-pBAPS	289[i],

[a]Ref.171, [b]Ref.188, [c]Ref.196, [d]Ref.197, [e]Ref.2, [f]Ref.198, [g]Ref.81, [h]Ref.199, [i]Ref.200, [j]Ref.201, [k]Ref.202.
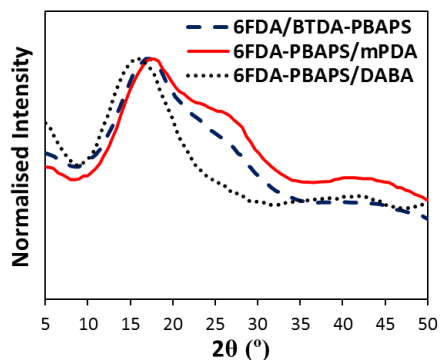
Figure 7.6 : X-Ray spectrum of co-PIs.

Characterization results of co-PIs in the simulation and the experiment were consistent in themselves.

Thermogravimetric analysis of membranes was applied in order to determine the amount of sorbed moisture and residual solvent present within the membrane. Figure 7.7 shows the TGA thermograms for co-PI membranes prepared as film where Table 7.6 lists the mass loss in these samples. All co-PIs have nearly same degradation temperature. However, 6pBD co-PI has a minor weight loss at about 300 ºC, prior to major backbone degradation at about 500 ºC, which can be seen as a small peak in the derivative weight curve of Figure 7.7. The similar thermal degradation behavior was encountered with some polymers in the literature [168, 178, 179, 184, 203] which have DABA diamine monomer in the polymer backbone. Qiu et al. [179] analyze the thermograms of 6FDA-DAM and 6FDA-DAM/DABA (3:2) polymers and realized that while there is only one peak of CO_2 fragment in 6FDA-DAM PI, 6FDA-DAM:DABA (3:2) co-PI has two CO_2 peaks. Kratochvil and Koros obtained a small mass loss in the free acid that begins at ~350°C in their research about decarboxylation-induced cross-linking of 6FDA-DAM/DABA (2:1) for enhanced CO_2 plasticization resistance [178]. There is also a two-step pattern in 6FDA-ODA/DABA (1:1) co-PI of the research of Maya et al. [184]. They observed that there is a reduction in the temperature of the weight loss peak which corresponds to the first degradation step with the theoretical content of repeat units containing ester groups in the chemical modification of co-PIs with bulky pendent groups. Kim et al. [203] also attained two major weight-loss events at temperatures of about 450 and 550°C in the thermal decomposition curve of BTDA-ODA/DABA (1:1) co-PI. They explained that the bond energy of the hydrogen bond between the carboxylic acid groups (2–8 kcal/mol) is far weaker than the covalent bonds (C=O (128 kcal/mol), C–O (86 kcal/mol), and O–H (119 kcal/mol)). Therefore, the degradation of the carboxylic acid groups in the polyimide was hardly affected by the hydrogen bonds. Xiao et al. [168] concluded in their co-PI membrane synthesis for pervaporation that the thermal stability is greatly affected by the side groups of sulfonic acid and carboxylic acid whose the pyrolysis occurs at a much lower temperature (372.2 °C). When the TGA curves of the 6pBmP and 6pBD co-PIs in this work were compared, the main difference in between these co-PIs is the carboxylic acid group in the second diamine. These carboxylic acid groups (-COOH) form weak hydrogen bonds

and hence increase the polymer packing and reduce free volume between polymer chains as indicated in the literature.
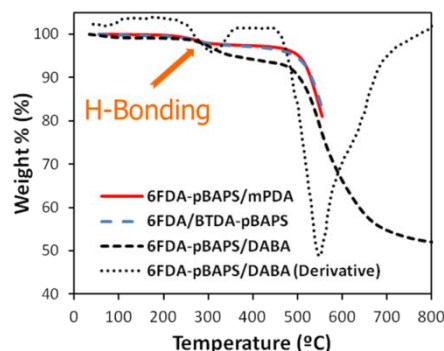
Figure 7.7 : TGA thermograms for 6BpB, 6pBmP and 6pBD membranes.

Table 7.6 : Mass Loss of 6BpB and 6pBmP co-PIs derived from TGA thermograms.

Sample	Cumulative Mass Loss at (starting from 50°C) (%)								
	100°C	150 °C	202 °C	250 °C	300 °C	350 °C	400 °C	450 °C	500 °C
6BpB	0.168	0.306	0.474	0.954	2.138	2.608	2.899	3.478	5.370
6pBmP	0.045	0.107	0.239	0.816	2.069	2.463	2.662	3.021	4.723
6pBD	0.769	0.863	0.928	1.179	2.685	4.869	5.795	6.642	9.394

Overall, the estimated structural properties agree quantitatively well with the experimental data, such as glass transition temperature, and d-spacing.

7.4.2 Experimental and simulation sorption measurements

GCMC simulations to predict the sorption of CO_2, CH_4, O_2, and N_2 gases in the model co-PI matrices were carried out. Table 7.7 shows the sorption coefficients of CO_2, CH_4, O_2, and N_2 gases estimated in molecular simulation and experimental sorption coefficients obtained from IGA measurements. The predicted sorption coefficients of these light gases in all co-PIs are generally in good agreement with the experimental data obtained by IGA. There is slight decrease in sorption selectivities of 6BpB both in experiment and simulation compared to 6pBmP co-PI due to the 75 % molar weight of pBAPS diamine in 6pBmP instead of 100 % in 6BpB co-PI. Qualitative relation between the concentration of polar moieties in the polymer and gas sorption selectivity was presented in literature [204, 205]. Koros suggested that CO_2/CH_4 sorption selectivity increases with the concentration of carbonyl or sulfonyl groups in polymer backbone [204]. The similar conclusion was done by Bondar et al. [205] that the increase in the mass density of ether linkages or carbonyl groups leads to also sorption selectivity. So this clearly explains that why

the 6BpB co-PI has high sorption selectivity compared to 6pBmP due to the high mass density of ether linkages and sulfonyl group in pBAPS diamine. However this finding can not be used to explain the relation between 6pBmP and 6pBD co-PIs due to the same concentration of pBAPS diamine. There is a decrease in all gas sorption measurements of 6pBD both in experimental and simulation due to carboxylic acid group in DABA diamine. It forms hydrogen bonds with sulfonyl and carbonyl groups and hence these groups prefer to lead hydrogen bond with –COOH rather than interact with CO_2. It can be clearly seen that there is a decrease in the peak of RDFs between CO_2 and sulfonyl group, later on this work. Lin and Freeman concluded in their study of materials selection guidelines that hydrogen bonding increases the solubility parameter to values beyond 22 $MPa^{1/2}$, which would increase the Flory-Huggins interaction parameter, χ, thereby decreasing CO_2 solubility [206].

Table 7.7 : Sorption coefficients of light gases in 6BpB, 6pBmP and 6pBD co-PIs.

PI	Sorption Coefficient* $(cm^3$ (STP) / $(cm^3$ bar))				Sorption Selectivity (α_S)		
	$CO_2{}^a$	$CH_4{}^a$	$O_2{}^b$	$N_2{}^b$	CO_2/CH_4	O_2/N_2	
6BpB	6.95	1.29	2.13	1.21	5.39	1.76	Sim.
	3.33	0.88	0.46	0.37	3.78	1.24	Exp.
6pBmP	6.75	1.18	1.88	1.19	5.72	1.58	Sim.
	3.90	1.18	0.69	0.61	3.31	1.13	Exp.
6pBD	6.44	0.93	1.76	1.14	6.92	1.54	Sim.
	3.39	1.09	0.57	0.43	3.11	1.33	Exp.

[a] at 35°C and 10 bar; [b] at 35°C and 2 bar.
  *Experimental sorption coefficients were evaluated with the Equation 1.4 by means of Henry and Langmuir constants in Table 7.8.

Table 7.8 shows the dual mode sorption constants of CO_2 for all co-PIs at 35°C, in which 6pBmP co-PI has the highest Henry constant and lowest Langmuir parameter. Due to its high Henry constant (Equation 1.4), 6pBmP co-PI shows slightly high CO_2 sorption coefficient. Dong et al. were explained in their research that in most cases, Langmuir sites adsorb a much smaller quantity of gas penetrant than Henry's sites considering that the differences in surface area available in these two sites differ by several orders of magnitude [19]. Hence it can be understand that mostly Henry constant plays an important role in sorption coefficient of glassy polymers. This conclusion is consistent with our findings. Moreover, k_D and b are related to the enthalpy of dissolution (ΔH_D) and the apparent enthalpy of hole-filling respectively, which are dependent on the nature of polymer–penetrant interaction [207]. Strongest co-PI–penetrant interactions can be observed from the highest values of k_D and b.

Table 7.8 : Dual-mode sorption parameters of CO_2 for 6BpB, 6pBmP and 6pBD co-PIs at 35°C.

	k_d (cm^3 (STP)/cm^3 polymer bar)	C_H (cm^3 (STP)/cm^3 polymer)	b (bar^{-1})
6BpB	1.473	21.26	0.676
6pBmP	2.202	18.82	0.940
6pBD	1.443	22.49	0.635

It is well-known in the literature [112, 23] that while light gases such as CH_4, N_2, and O_2 do not plasticize polymer membranes, CO_2 induces strong plasticization. Previous simulation studies reported in the literature [79, 104, 105] on CO_2 plasticization estimated sorption-induced volume swelling and FFV increase at experimentally obtained equilibrium concentrations. Figure 7.8 shows the convergence of the binary and single CO_2 concentration in the three co-PIs through the SRCs. These cycles provided an estimation of the extent of CO_2 induced volume swelling and plasticization in both membrane materials. It was also observed that CO_2 concentration depends strongly on the FFV of the swollen membranes at the considered pressure. Experimental CO_2 sorption capacities of co-PIs can be seen from sorption isotherm in Figure 7.9.
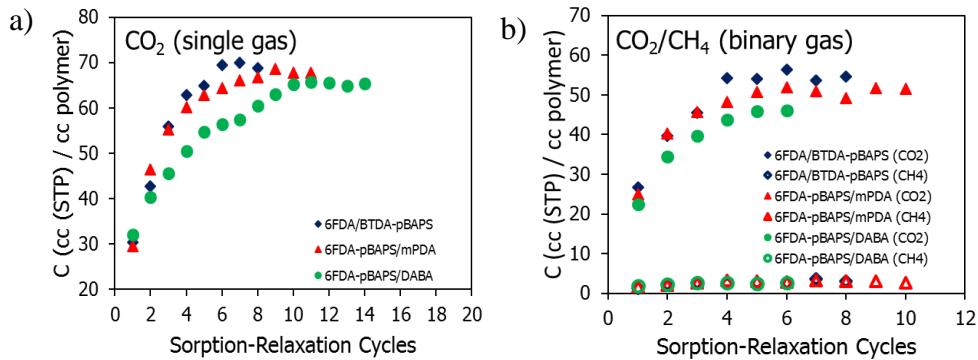
Figure 7.8 : Increase in the predicted CO_2 concentration (C_{CO_2}) in 6BpB, 6pBmP and 6pBD due to sorption induced plasticization at 35°C and 10 bar for a) single and b) binary gas systems.
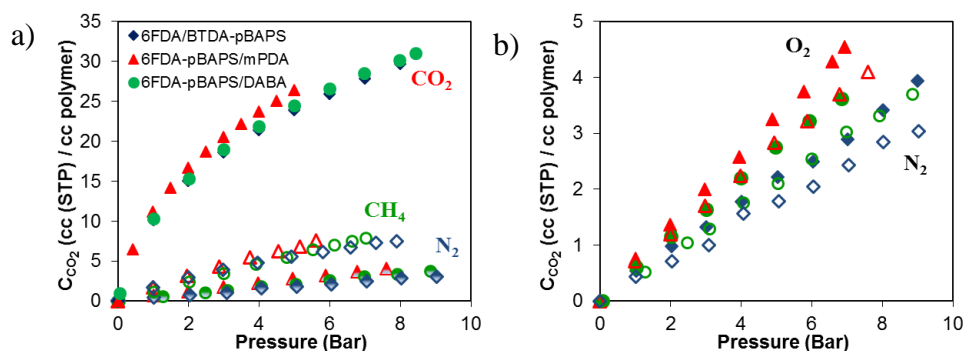
Figure 7.9 : CO_2 sorption isotherm of co-PIs obtained from IGA measurements. Symbols represent: (a) Full=CO_2, Empty=CH_4, Gradient=N_2, (b) Full=O_2, Empty=N_2.

Predicted sorption coefficients of co-PIs are in good agreement with the experimental data. Besides single gas calculations, binary gas sorption simulations for light gases were carried out. In real binary gas separation processes, both gases are in the same flow and in contact with each other. Since it is generally difficult to measure sorption selectivities for such systems, it is common to measure pure gas sorption coefficients and calculate the ideal sorption selectivity, which is calculated by taking the ratio of pure gas sorption coefficients. However, ideal and binary selectivities may differ significantly due to the combined effect of the competition between the penetrants, gas phase non-ideality, plasticization phenomena, and gas polarization. Table 7.9 compares the simulated ideal and binary sorption selectivities of co-PIs for CO_2 and CH_4 (P(CO_2):P(CH_4)= 50:50) at 35°C and 10 bar.

Table 7.9 : Single and binary gas sorption coefficients and selectivities in co-PIs.

PI		S(CO_2)	S(CH_4)	α_S(CO_2/CH_4)
6BpB	Pure	6.95	1.29	5.39
	Mixed	10.77	0.58	18.57
6pBmP	Pure	6.75	1.18	5.72
	Mixed	10.07	0.59	17.07
6pBD	Pure	5.66	0.93	6.09
	Mixed	9.07	0.51	17.78

Table 7.10 : CO_2-induced FFV increase in co-PIs.

Sorbed Species	6BpB (FFV = 0.193)			6pBmP (FFV=0.187)			6pBD (FFV=0.189)		
	C^a	FFV	% increase	C^a	FFV	% increase	C^a	FFV	% increase
CO_2	70.4	0.273	41.5	68.4	0.234	25.1	57.3	0.221	16.9
CO_2/CH_4	54.6	0.230	19.2	51.0	0.223	19.3	45.9	0.216	14.3

^{a} cc (STP) / cc polymer.

Plasticization effect of CO_2/CH_4 mixed gas is smaller than CO_2 pure gas in all co-PIs because of lower CO_2 partial pressure and, thus its lower concentration. The increase in the FFV is proportional to the CO_2 concentration, as reported by Zhang et al. [79] based on their pure CO_2 simulations. Among the three copolyimides, 6BpB provides the highest CO_2 and CH_4 single gas and CO_2/CH_4 binary gas sorption coefficients indicating that fractional free volume of 6BpB is the highest in the swollen state. FFV calculations confirm that CO_2 sorption-induced swelling is the highest (41.5%) in 6BpB. The FFV of the three copolyimides are similar before sorption. The sorption-induced increase of the FFV of 6pBD is the smallest which also agrees with the FAV analysis. This may be due to its rigid backbone indicated by its high Tg.

7.4.3 Sorption-induced accessible free volume increase

The analysis of the sorption-induced changes in FAV is similar with chapter 3. Figure 7.10 compares FAV distribution as a function of probe size for the three copolyimides before and after saturation with CO_2. The sorption-induced increase of the FFV of 6BpB is the biggest which also agrees with the FAV analysis. At probe size of 1.6-2.0 and 2.0-2.4 Å, FAV percentage of 6BpB is bigger than the other co-PIs which means that 6BpB co-PI includes many large free volumes that can enable swelling more.
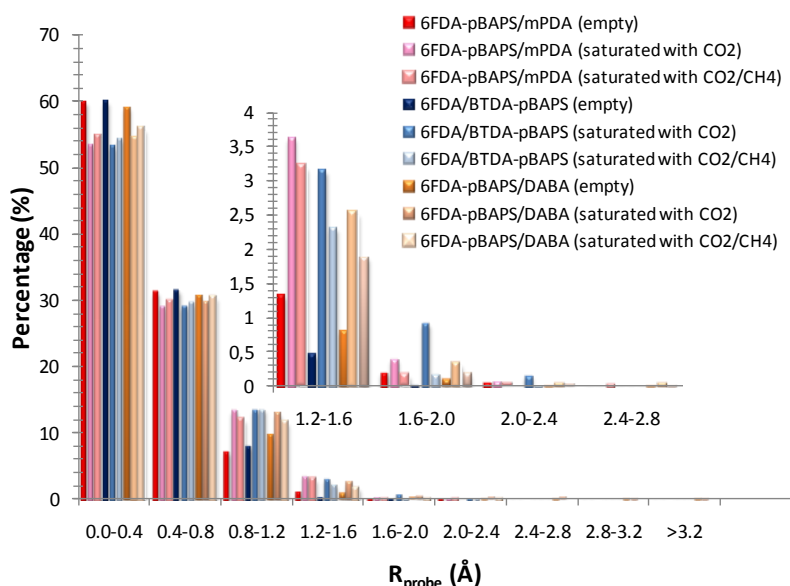
Figure 7.10 : FAV distribution in empty co-PIs before and after saturation with CO_2.

7.4.4 Radial distribution functions

RDF analysis is similar with chapters 4 and 5. Figure 7.11 presents the RDFs of CO_2 (with 118, 139 and 89 CO_2 molecules which correspond to the equilibrium concentration in 6BpB, 6pBmP and 6pBD respectively at 10 bar and 35°C) around seven typical atoms of monomers in co-PI chains: the oxygen and nitrogen in the imide, the fluorine in the -CF_3 group, the oxygen in the ether linkage, sulfone in the sulfonyl linkage, carbon in the –CO– group of BTDA monomer and single bonded oxygen of carboxylic acid (labeled as O1, N1, F, O2, S, C and O3 respectively). Sulfone group (S) in pBAPS diamine is the preferential sorption site in all three copolyimides, but its affinity to CO_2 is the highest in 6BpB and the lowest in 6pBD. N and O1 sites are also the preferential sorption sites for CO_2 for all three copolyimides. 6pBD includes an extra sorption site of O3 in DABA diamine monomer which provides more rigidity to the polymer chain. Furthermore, when the diamine moiety was changed from mPDA to DABA, the intensity of the peak for the interaction of CO_2 molecules with the nitrogen in the imide lowers and hence backbone loses its flexibility.
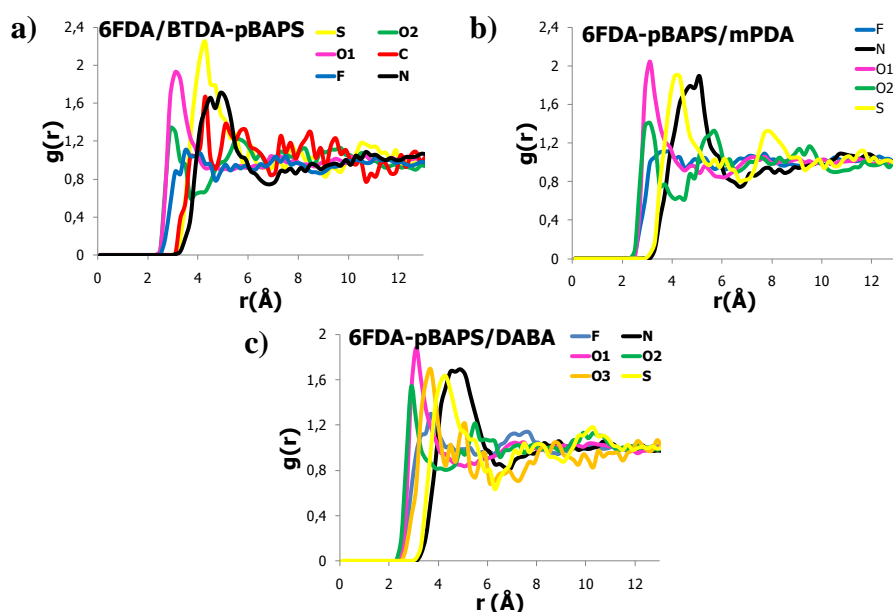
Figure 7.11 : RDFs (g(r)) of CO_2 in a) 6BpB, b) 6pBmP and c) 6pBD.

7.4.5 Permeability measurements

Table 7.11 shows the experimental permeabilities and selectivities for co-PI membranes annealed at 210°C (below Tg) and the predicted permeabilities and selectivities by the group contribution method for all co-PIs at 35ºC and 10 bar. Experimental permeabilities of 6BpB membrane for all gases exhibit smaller values

compared to 6pBmP where similar tendency was observed in the GCM. The small permeability values of 6pBmP may be associated to the presence of small d-spacing at around 3.4 Å which can be seen as a shoulder in x-ray pattern (Figure 7.6). The reason for small d-spacing value may be the mPDA monomer which is shorter compared to the pBAPS diamine. It may create extra small free volumes where CO_2 can permeate but other gases which have big kinetic diameter than 3.4 Å, cannot permeate. It must be pointed out that, although the ratio of these small d-spacing peak to the main d-spacing of co-PI is very small, the effect it has on the resultant membrane is rather significant especially in CO_2. With the change in monomer, the permeability of CO_2 showed much change compared to the other light gases, which resulted in a decrease of CO_2/CH_4 selectivity from 126 to 72.6 and 51.9 to 48.1 in the GCM and the experiment, respectively. On the other hand, for CO_2/N_2, H_2/CO_2 and O_2/N_2, the decrease in permeabilities are not more drastic as seen in Table 6.11. On the other hand, with the addition of polar group to the mPDA diamine, while the permeabilities of all gases dropped down, the selectivities increased. Yampolskii suggested in his review paper about the polymeric gas separation membranes that the introduction of the substituents that are capable to dipole−dipole interactions or can form hydrogen bonds can strongly influence the transport parameters due to increasing interchain interactions or interactions with some penetrants [208]. Plate and Yampolskii encountered that when the content of −COOH groups in polymer matrix increased 20 %, twice of permeability coefficients of hydrocarbon gases were obtained [209]. Moreover, Hirayama et al. also introduced the −COOH group in the mPDA diamine of polyimide and found that there is a decrease in permeability of O_2 from 3 Barrer to 1 Barrer with an increase in separation factor of O_2/N_2 [199].

Table 7.11 : Permeability coefficients of light gases in 6BpB, 6pBmP and 6pBD co-PIs.

PI	Permeability Coefficient (Barrer[a])					Selectivity (α)				
	CO_2[b]	CH_4[b]	H_2[b]	O_2[b]	N_2[b]	CO_2/CH_4	CO_2/N_2	H_2/CO_2	O_2/N_2	
6BpB	7.76	0.06	27.9	1.20	0.19	126	48.5	3.60	6.32	**GCM**
	6.98[c]	0.13[d]	----	1.32[e]	0.23[e]	51.9	28.6	----	5.63	**Exp.**
6pBmP	11.6	0.12	37.3	2.18	0.36	72.6	32.2	3.22	6.06	**GCM**
	9.91[c]	0.21[d]	----	1.94[e]	0.40[e]	48.1	24.9	----	4.89	**Exp.**
6pBD	9.84	0.097	36.9	2.29	0.35	101	28.1	3.75	6.46	**GCM**
	4.43[f]	0.088[d]	----	1.00[e]	0.17[e]	50.4	26.1	----	5.93	**Exp.**

[a] Barrer=10^{-10} cm³STP.cm / cm².s.cmHg; at 35°C and [b] 10 bar; [c] 8.6 bar; [d] 4 bar; [e] 2 bar, [f] 9 bar.

In 1991, Robeson [5] defined a so-called upper-bound, which represents the upper limit for the performance of polymeric membranes. Figure 7.12 shows the upper-bound for CO_2/CH_4 and O_2/N_2 gas pairs, with selectivity versus permeability of faster-permeating gas. Predictions of group contribution method of Alentiev et al. [51] for all gases in three copolyimides overestimate the measured permeability coefficients. However, these coPIs still remain in the commercially attractive region for the CO_2/CH_4 gas pair but under upper bound line as seen in Figure 7.12.
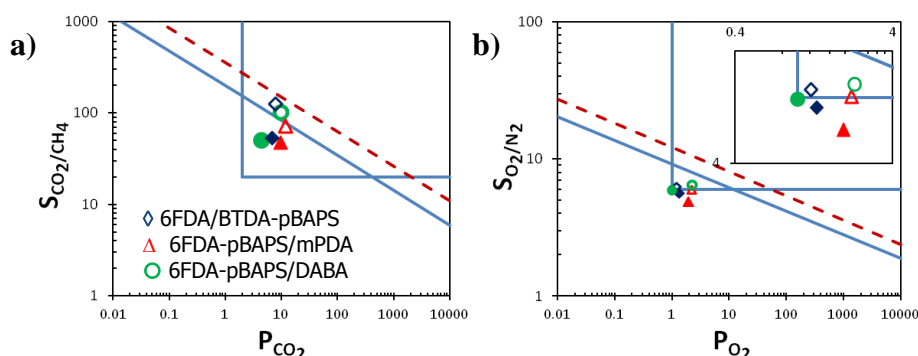
Figure 7.12 : Robeson Diagrams for a) CO_2/CH_4 and b) O_2/N_2 gas pairs. Open symbols: GCM, Full symbols: Experiment. Red line: 2008, Blue line: 1991 Robeson's upper bound.

Due to the limitations of the permeability system in our laboratories, permeation experiments were only performed up to ~9 atm. Figure 7.13 shows that three co-PIs do not show any significant sign of plasticization up to ~9 atm.
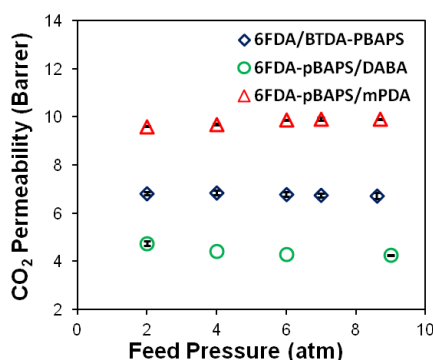
Figure 7.13 : Permeation isotherms for three co-PIs.

7.5   Summary

The structural properties of the investigated polymers were estimated in good agreement with the experimental data, which indicates that molecular simulation can be used successfully to characterize various PI structures. Simulation of the sorption process of CO_2 successfully reproduced the plasticization behavior in all polymers

through the sorption-relaxation cycles. The structural properties, i.e. d-spacing, fractional free volume (FFV), cohesive energy density and glass transition temperature, of the co-PIs were estimated in good agreement with the experimental data, which indicates that molecular simulation can be used successfully to characterize various PI structures.

The backbone flexibility is the primary factor determining the plasticization behavior of the polyimides studied here. On the other hand, when the backbone flexibility of the polyimides are similar, the functional groups attached to the backbone becomes important. Different functional groups lead to different plasticization tendencies.

The FFV of the three copolyimides are similar before sorption. The sorption-induced increase in the FFV of 6FDA-pBAPS/DABA is the smallest. This may be due to the presence of carboxylic acid groups in DABA diamine which causes H-bonding.

Sulfone group (S) in pBAPS diamine is the preferential sorption site in the three pBAPS containing copolyimides in this study, but its affinity to CO_2 is highest in 6FDA/BTDA-pBAPS and lowest in 6FDA-pBAPS/DABA. This difference may be due to the presence of carboxylic acid groups in DABA diamine which makes H-bonding. The plasticization behavior of these copolyimides was investigated experimentally and the plasticization effect was not observed up to pressure 9 atm.

8. CO$_2$-INDUCED PLASTICIZATION IN THERMALLY REARRANGED (TR) POLYMERS

8.1 Introduction

A new class of thermally-modified aromatic polyimides has recently been presented as a prominent membrane material in gas separation area. These polymers show outstanding physical properties and high separation performance that exceeds the trade-off relationships for many gas pairs. Additionally, these polymers appear to be resistant to CO$_2$-induced plasticization, which is the interest of separation of gas streams containing high level of CO$_2$. These membranes are based on soluble aromatic polyimides with ortho-positioned functional groups; exposure of the polyimides to thermal rearrangement (TR) around 400ºC leads to fully aromatic, insoluble polybenzoxazoles (PBOs) with exceptional thermal and chemical resistance characteristics. Modification of polyimide chain during the rearrangement produces fundamental changes in molecular connectivity and conformation that alter chain packing, resulting in a narrow free volume distribution and round shaped cavities.

Research about gas transport properties of TR polymers are ongoing [7, 116, 210-228]. There are a few experimental studies about TR polymers which appeared in the litearature in last five years. Most prior work, which was reported by Park et al. [7], focused on understanding the distinctive shape and distribution of cavities of TR polymers that appear to be responsible for the unprecedented gas separation performance. But an aromatic polyimide containing hydroxyl groups ortho to the imide nitrogen was firstly rearranged by Tullos and Mathias [210] to a polybenzoxazole upon heating above 400ºC in an inert atmosphere. Following studies are mostly focused on the polymer backbone modifications such as adding ether linkages, making different copolyimide compositions to be used as TR polymers [211, 212], and altering rearrangement technique to obtain TR polymers [213, 219, 224]. Other studies are focus on the influence of the polyimide synthesis route on TR polymer transport properties [116, 214-217, 221], the effect of heat

treatment on polyimide conversion to its TR polymer and hence the permeability coefficients [218, 220, 222, 223], the dehydration of biofuels via pervaporation with the use of TR-polymers [225], the effects of dope composition and thermal rearrangement conditions in order to fabricate defect-free hollow fiber membranes [226].

Although TR polymers are a hot topic in gas separation membrane area nowadays, there are only two simulation studies [227, 228]. One of them is published by Jiang et al. [227] who determined the cavity size distribution and transport properties of six recently synthesized TR polymers and their precursors. When the TR polymer and its precursor were compared, TR polymer showed high quantity in the number and size of cavities. This is consistent with the observation that the TR polymers had high permeability coefficients compared to their precursors. The other simulation study was performed by Park et al. [228] who analyzed the structure of TR polymer and its precursor. They carried out their simulation study in a broad range of temperatures in order to clarify the effect of temperature. They concluded that as the temperature increased, the change in torsional angle distribution is very low in TR polymer compared to its precursors due to its rigid and stiff polybenzoxazole linkage. Moreover, at high temperature such as 450ºC, cavities around the imide linkages became larger and hence active sites for TR reaction became free in order to obtain high conversion.

Sorption induced volume swelling and plasticization is a serious concern limiting the use of PIs as membrane material for gas separation involving CO_2, H_2S and condensable. In the case of CO_2/CH_4 separation, the TR polymers show high resistance to plasticization [7, 223]. Neither Park et al. [7] nor Sanders et al. [223] did see any evidence of plasticization in their TR polymers up to 16 atm when they measured permeability as a function of feed pressure. Except these two experimental studies, there is not any experimental or simulation study about CO_2-induced plasticization effect on TR polymers. In this study, molecular simulation techniques was used to estimate the degree of plasticization of 4,4-hexafluoroisopropylidene-diphthalic anhydride (6FDA)-2,2'-bis(3-amino-4-hydroxyphenyl)-hexafluoropropane (bisAPAF) PI membrane and its TR polymer (Thermally Rearranged Polybenzoxazole) induced by sorption CO_2. The structural properties, such as glass transition temperature (T_g), FFV and its distribution, d-spacing, radius of gyration,

and cohesive energy density, along with sorption isotherms were investigated from simulations to understand the dynamics of TR polymer and its precursor chains and CO_2 and the comparison was made with the experimental data available in the literature to provide an insight to structure-plasticization.

8.2 Simulation Method

All simulations in this work were carried out according to methodology described in Section 2.5. In this work, in brief, 6FDA-bisAPAF PI chains were constructed from 80 and 40 repeat units. Dianhydride and diamine moieties were constructed and linked followed by geometry optimization to create PI repeat units shown in Figure 8.1. For TR polymers of these PI, the chemical structures with 50% meta- and 50% para-position were constructed again from 80 and 40 RUs. The TR polymer and its precursor's chains were then built by connecting these repeat units with each other and final geometry optimization was carried out. *Amorphous Cell* module was used for the construction of cubic simulation cells with a side of 39-40 Å for one chain with 80 RUs and two chains with each 40 RUs model polymer matrices. Experimentally, conversion of PI to polybenzoxazole could not reached 100% for instance at 450ºC, 63, 76 and 86.3% conversions were obtained by Ong et al. [225], Smith et al. [222] and Kim et al. [226] respectively. However, in this study, it was assumed that 100 % conversion to TR polymer was occurred.
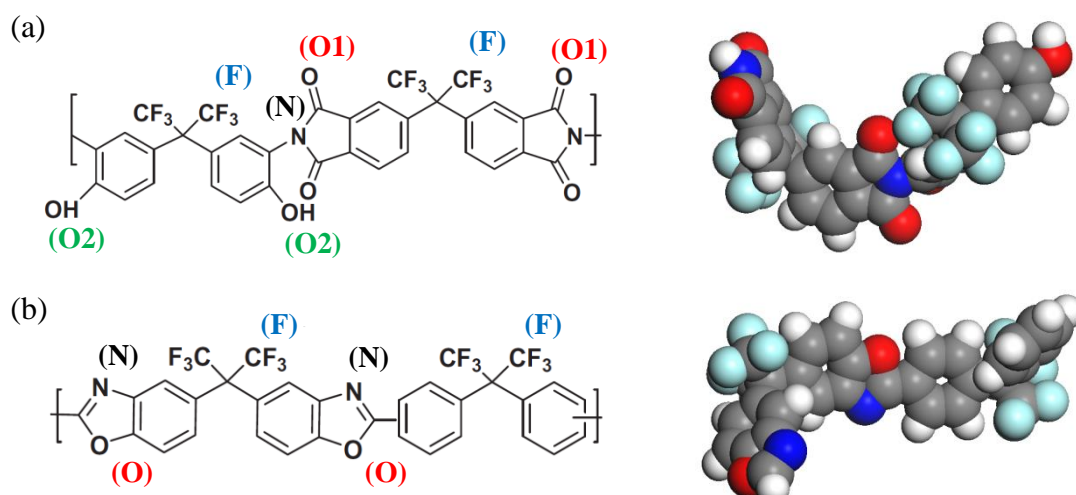
Figure 8.1 : Structures of constructed repeat units for (a) 6FDA-bisAPAF and (b) TR polymer. Typical sorption sites are shown in parenthesis.

Simulation temperature and pressure values were chosen based on the experimental studies in the literature: 25ºC and 1.0 atm. These conditions correspond to the

experimental study of Han et al. [213], who calculated sorption coefficients for TR polymers. Moreover, in order to see the plasticization pressure and understand the plasticization effect of TR polymer and its precursor, sorption calculations at 1, 10, 20, 30 and 40 atm were performed at 35ºC.

8.3 Results and Discussion

8.3.1 Characterization of model matrices

The structural properties of 6FDA-bisAPAF and its TR polymer models were calculated in this work and comparison to data reported in the literature are presented in Table 8.1. Polybezaxazoles (PBOs) were firstly synthesized in 1960s [229-231] and had attracted great attention due to their naturally rigid chain and stable thermal properties. However, while PBOs can be dissolved in strong acids, they were not dissolved in common organic solvents [230]. Hence it was very hard to prepare adequately thin membranes via traditional solution-based routes. Fortunately, thermally rearranged (TR) aromatic polyimides have recently been discovered as a new class of membrane materials for gas separation [210]. For the PI and its TR polymer considered in the present work, there are four experimental [116, 219, 220, 232] and two simulation [227, 228] studies available in the literature. Table 8.1 clearly shows that there is a wide range in all characteristic properties of both TR polymer and its precursor. This may be interpreted as that there are many factors that affect the TR polymer synthesis. For example, Han et al. investigated the effect of synthetic method to prepare polyimide precursor for the resulting TR polymer membranes [219]. There are two density, Tg, FFV and d-spacing values refer to the study of Han et al. [219]. First of data in each characteristic property belongs to the PI synthesized by thermal imidization and the second one refers to the azeotropic imidization. The differences in the synthetic method of precursor polyimides resulted in significant deviations in free volume elements, and hence in transport properties although precursors had the same structure of polybenzoxazole. Park et al. studied the effect of thermal treatment protocol such as final temperature, in the formation of microstructure and their size distribution [116]. Due to the different thermal treatment protocol, there are discrepancies in both characteristic and transport properties between Han et al. [219] and Park et al. [116]. Although TR polymers are a hot topic in the membrane based gas separation area within five years,

there are only two simulation studies in the literature. Jiang et al. [227] determined the cavity size distribution and transport properties of six recently synthesized TR polymers and their precursors whereas Park et al. [228] analyzed the structure of TR polymers and their precursors. Park et al. [228] carried out their simulations for a broad range of temperatures in order to clarify the effect of temperature. There are big differences in FFV of simulation studies due to the calculation method of FFV. Jiang et al. were used CESA algorithm [233] which is based on energetic rather than geometric considerations. Park et al. preferred the Bondi's method [84] in where the simulated van der Waals volume was used in the calculation of FFV, and Hofmann-Heuchel method [234] according to the R_max approach. Calculated d-spacing values coincide with the experimental values. X-ray scattering patterns of 6FDA-bisAPAF and its corresponding TR polymer exhibit that these polymers are completely in an amorphous state without any crystalline phase.

Overall, the estimated structural properties agree quantitatively well with the experimental data, such as density, and d-spacing. However, some disagreement exists with respect to the literature values of FFV which had been calculated with different methods. The details of characterization simulations can be obtained from previous Chapter 2.

Table 8.1: Comparison of estimated properties of PIs with previously reported data.

Properties		6FDA-bisAPAF	TR polymer
d-spacing (Å)	Experimental	5.70[a1], 5.40[a2], 5.48[b]	6.40[a1], 5.80[a2], 6.00[b]
	This work	5.34	5.91
FFV	Experimental	0.190[a1], 0.170[a2], 0.159[b]	0.280[a1], 0.220[a2], 0.263[b]
	Simulation	0.106[c], 0.214[d1], 0.287[d2]	0.133[c], 0.251[d1], 0.303[d2]
	This work	0.186	0.231
FFV increase (%)	Experimental		48[a1], 29[a1], 65[b]
	Simulation		25.5[c], 17.2[d1], 5.6[d2]
	This work		24.2
Density (g/cm^3)	Experimental	1.47[a1], 1.49[a2], 1.536[b]	1.27[a1], 1.38[a2], 1.293[b]
	Simulation	1.491[d]	1.384[d]
	This work	1.517	1.403
Tg	Experimental	301[a1], 300[a2], 313[e], 291[f]	

[a]Ref. 219 ([1]thermal imidization, [2]azeotropic imidization), [b]Ref. 116 (thermally treated at 450ºC), [c]Ref. 227 (Fractional Cavity Volume), [d]Ref. 228 ([1]Park and Paul method, [2]Hofmann-Heuchel method), [e]Ref. 220, [f]Ref. 232.

8.3.2 Sorption simulations

GCMC simulations to predict the sorption of CO_2 and CH_4 gases in the model PI matrix and its TR polymer were carried out at different pressures. There are few experimental sorption coefficient data reported in the literature as listed in Table 8.2. It is well-known in the literature [230, 231] that while light gases such as CH_4, N_2, and H_2 do not plasticize polymer membranes CO_2 induces strong plasticization. Previous simulation studies reported in the literature [215-217] on CO_2 plasticization estimated sorption-induced volume swelling and FFV increase at experimentally obtained equilibrium concentrations. Figure 8.2 shows the convergence of the CO_2 concentration in 6FDA-bisAPAF PI and its TR polymer through the SRCs at 1, 10, 20, 30 and 40 atm. These cycles provided an estimation of the extent of CO_2 induced volume swelling and plasticization in both membrane materials. Due to its high resistance to plasticization, TR polymers become important especially in the CO_2/CH_4 separation [84, 234]. Neither Park et al. [7] nor Sanders et al. [223] did see any evidence of plasticization in their TR polymers up to 16 atm when they measured permeability as a function of feed pressure. Except these two experimental studies, there is not any experimental or simulation study about CO_2-induced plasticization effect on TR polymers.
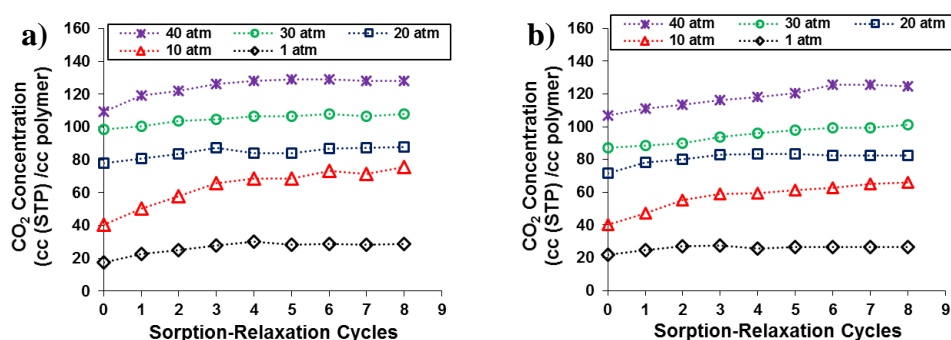
Figure 8.2 : Increase in the CO_2 concentration in a) 6FDA-bisAPAF and b) its TR polymer due to sorption induced plasticization at 35°C, 1, 10, 20, 30 and 40 atm.
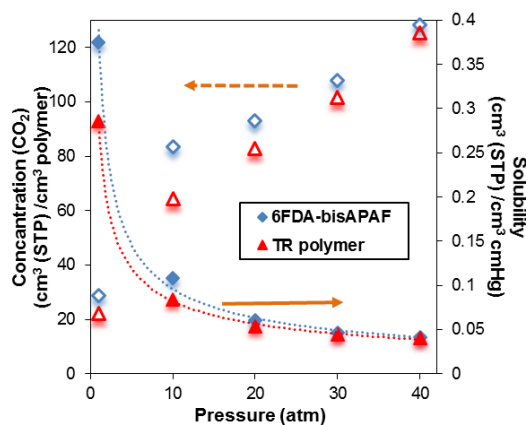
Figure 8.3 : CO_2 concentration and Solubility in 6FDA-bisAPAF and its TR polymer at 35°C.

Table 8.2 compares the sorption coefficients of CO_2 and CH_4 gases estimated in this simulation study with the experimental and simulation sorption coefficients reported in the literature [227, 229, 233]. As can be seen from Table 8.2, there is a big scatter in the sorption coefficients of TR polymer. But mainly, the calculated sorption coefficients of these light gases in the polyimides are generally in good agreement with the experimental data reported in the literature.

Table 8.2: Sorption coefficients of light gases in 6FDA-bisAPAF and its TR polymer.

	Sorption Coefficient (cm^3 (STP) / (cm^3 atm))		Sorption Selectivity (α_S)	
	CO_2^a	CH_4^a	CO_2/CH_4	Ref.
TR polymer	26.3	7.4	3.6	This study
	118	9.6	12.3	Exp.213[b]
	22	4.3	5.1	Exp.213[c]
	35.9±18.3	5.59±0.85	6.4	Sim.227
6FDA-bisAPAF	30.3	4.24	7.2	This study
	30.1	1.75	17.2	Exp.235
	28.6±8.5	1.95±0.68	14.7	Sim.227

[a] at 25°C and 1 atm;   [b] thermal imidization;   [c] azeotropic imidization.

In accordance with the differences in the flexibility of diamine–dianhydride linkages in PI backbone and linkage between the phenyl ring and a benzoxazole ring, (C-C-C-O) linkage, in TR polymer, the sorption-induced volume swelling is slightly higher in 6FDA-bisAPAF than TR polymer as presented in Table 8.3 and Figure 8.4, which indicates that polyimide underwent a more significant plasticization than its TR polymer. These results agree with Figure 8.5 where 6FDA-bisAPAF has a wide range of degree in torsion due to its flexible backbone while TR polymer was fixed in the between (-40) and 40 degrees due to the rigidity of the coplanar structure of

the polybenzoxazole ring. However, TR polymer gains a chance to change its conformation because of high free volume and can increase the FFV while the sorption of CO_2 due to the high probability of being around -180 and 180 degrees.

Table 8.3:   Relationship between the backbone flexibility ($\sigma|\phi|$), FFV increase and CO_2 solubility.

	$\sigma\|\phi\|$	FFV initial	FFV final	% increase	S_{CO2}[a,b]
6FDA-bisAPAF	40.1	0.186	0.238	28	7.097
TR polymer	11.3	0.231	0.269	16.5	6.360

[a] cc(STP)/cc polymer.atm, [b] at 35ºC and 10 atm.
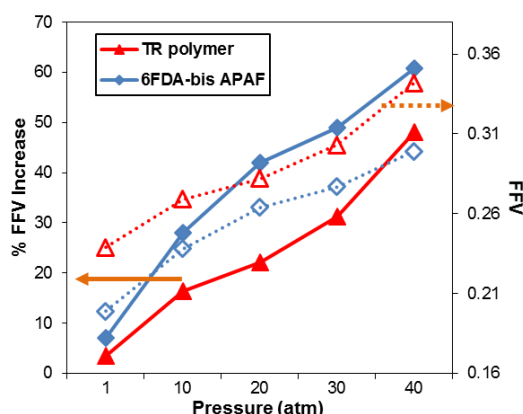
Figure 8.4 : FFV and FFV increase (%) in 6FDA-bisAPAF and its TR polymer at 35ºC.
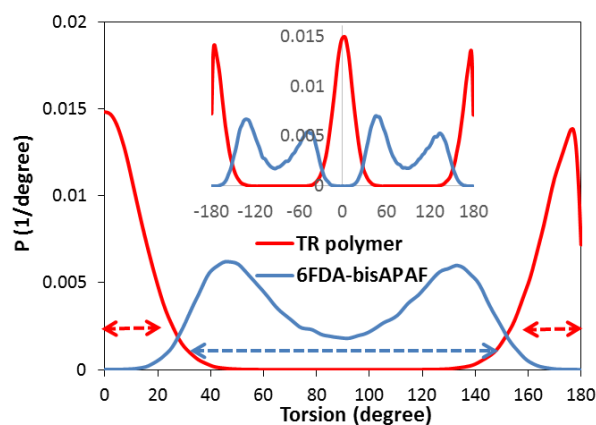
Figure 8.5 : Dihedral distribution of (C–N–C–C) linkage in 6FDA-polyimide and (C-C-C-O) linkage in its TR polymer.

8.3.3 Sorption-induced accessible free volume increase

Figure 8.6 compares FAV distribution as a function of probe size for 6FDA-bisAPAF and its TR polymer before and after saturation with CO_2. The increase in the FAV can be seen for a probe radius above 1.6 Å; and much more significantly for both PI and TR polymer above 2.0 Å, which is the first bigger radius than the kinetic

radius of CO_2 in range given in Figure 8.6. After SRCs were applied, the decrease in FAV percentage was obtained in both TR polymer and its precursor until probe radius of 2.0 Å. Due to the adsorption CO_2 in to the large radius than 2.0 Å and the interaction with the polymer matrices, it increases the FAV percentage, and by the way decreases the FAV percentage in small radiuses with the compression of them. The change in the FAV distribution before and after saturation with CO_2 is more drastic for 6FDA-bisAPAF due to its higher chain flexibility. The role of the sorbate-polymer interactions can be better understood with the help of RDFs.
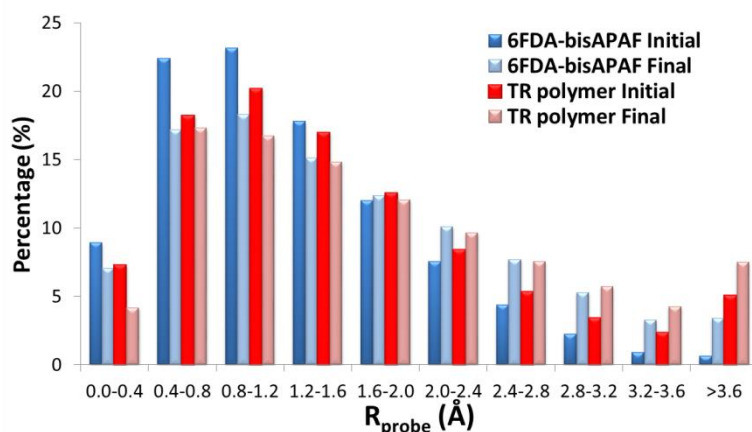
Figure 8.6 : Fractional accessible volume distribution in empty 6FDA-bisAPAF and its TR polymer before and after saturation with CO_2.

8.3.4 Radial distribution functions

RDFs can be used for an in-depth analysis of atomic interactions between penetrants and the PI matrices. Based on the location and intensity of the peaks in the RDF, one can determine the preferential sorption sites on the polymer chain for a particular sorbate. Figure 8.7 (a) presents the RDFs of CO_2 (with 140 CO_2 molecules which correspond to the equilibrium concentration at 10 atm and 35°C) around four typical atoms of the 6FDA-bisAPAF polymer chain: the oxygen and nitrogen in the imide, the fluorine in the -CF_3 group, and the oxygen in the hydroxyl bulky groups of diamine (labeled as O1, N, F, and O2, respectively). The distinct peaks at 3.1, 3.7 and 4.7 Å in the RDFs indicate that the oxygens and nitrogen are the preferential sorption sites for CO_2, but the fluorine atoms are not. Furthermore, the intensities of the peaks for the interactions of CO_2 with O1 and O2 are relatively higher indicating stronger attraction.

Figure 8.7 (b) presents the RDFs of CO_2 (with 119 CO_2 molecules at equilibrium concentration at 10 atm and 35°C) around three typical atoms of the TR polymer

chain: the oxygen and nitrogen in the benzoxazole ring and the fluorine in the -CF$_3$ group (labeled as O, N and F respectively). Two significant peaks that were observed in the RDFs corresponding to the CO$_2$-O and CO$_2$-N pairs, indicate the preferential sorption sites for CO$_2$ in TR polymer. When 6FDA-bisAPAF polyimide was thermally treated to the TR polymer, the intensity of the peaks for the interactions of CO$_2$ with the oxygens in the imide and the hydroxyl bulky groups, changed drastically from 1.74 (O1) and 2.01 (O2) to 1.34(O). Moreover, the interaction with the nitrogens in the imide was affected as revealed by the shift of the CO$_2$-N peak in the RDF from 4.7 to 3.9 Å indicating a relatively less restricted access to these sites, but with low intensity (changed from 1.77 to 1.56). The occupation of the sorption sites on the PI backbone by CO$_2$ molecules promotes plasticization by increasing the chain mobility. The interaction of CO$_2$ molecules with the O1 and O2 sites in 6FDA-bisAPAF exhibits this effect. RDF results show why the plasticization resistance of TR polymer arises from. Because there are some limitations in the interaction of oxygen sorption sites with the CO$_2$ penetrant molecule.
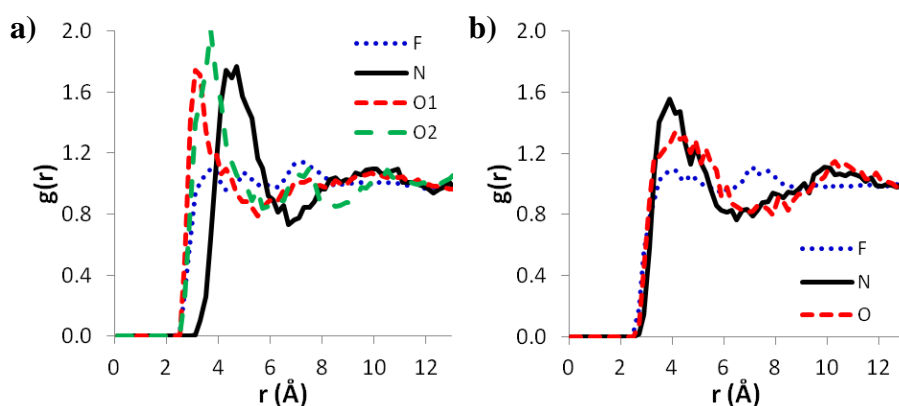
Figure 8.7 : Radial distribution functions (g(r)) of CO$_2$ in a) 6FDA-bisAPAF and b) TR polymer.

8.4   Summary

The structural properties of the investigated polymers were estimated in good agreement with the experimental data, which indicates that molecular simulation can be used successfully to characterize various PI structures.

Simulation of the sorption process of CO$_2$ successfully reproduced the plasticization behavior in all polymers through the sorption-relaxation cycles.

The structural properties, i.e. d-spacing, fractional free volume (FFV), cohesive energy density and glass transition temperature, of the PIs were estimated in good

agreement with the experimental data, which indicates that molecular simulation can be used successfully to characterize various PI structures.

6FDA-bisAPAF has a wide range of degree in torsion due to its flexible backbone while TR polymer was fixed in the between (-40) and 40 degrees due to the rigidity of the coplanar structure of the poly-benzoxazole ring. However, TR polymer gains a chance to change its conformation because of high free volume and can increase the FFV while the sorption of CO_2 due to the high probability of being around -180 and 180 degrees.

RDF results show why the plasticization resistance of TR polymer arises from. Because there are some limitations in the interaction of oxygen sorption sites with the CO_2 penetrant molecule. Moreover, the interaction with the nitrogen in the imide was affected as revealed by the shift of the CO_2-N peak in the RDF from 4.7 to 3.9 Å indicating a relatively less restricted access to these sites, but with low intensity (changed from 1.77 to 1.56).

9. CONCLUSIONS

9.1 Summary and Conclusions

Polyimide membranes have been widely applied for gas separations due to their attractive permeability, selectivity, and processing characteristics. Their use for natural gas and hydrocarbon separations is limited by plasticization-induced selectivity losses in feeds with significant partial pressures of CO_2 and C_3+ hydrocarbons. In this dissertation, the links between chemical structure of 6FDA-based polyimide gas separation membranes and sorption induced plasticization were examined via molecular simulation methods. The work addresses three types of polymeric materials namely, polyimides, copolyimides and thermally rearranged polymers.

The effect of the observed plasticization and the associated relaxations in the polyimide matrix was assessed by means of the change in the local structure and free volume of a polyimide. The effect of polymer structure and mechanism of structural relaxations are aimed to understood, as are the factors that influence solubility and mobility of the plasticizing penetrant. Hence, particular emphasis was given to tailoring the physical properties by systematic variations of monomers in order to see the sorption induced plasticization effect.

Several polymer structures were successfully prepared using Monte Carlo and Molecular Dynamics simulations. The accuracy of the method used to prepare the model polyimide matrices was verified by the comparison of the physical properties, i.e. density, d-spacing, fractional free volume (FFV), cohesive energy density and glass transition temperature, of the PIs, which were estimated from simulation study and present experimental studies in the literature. Consequently, the results of structural properties demonstrated that molecular simulation can be used successfully to characterize various PI structures.

The primary material property that we study is the fractional free volume, in other words, fractional free volume change through the sorption-relaxation cycles in order

to reproduce the plasticization behavior in the PIs. Estimated sorption coefficients of CO_2, propylene and propane through SRCs and CH_4, O_2 and N_2 in all polymers are within the same order of magnitude with the experimental data in the literature. Additionally, the most important analysis tool used is the radial distribution function which enables one to see the most preferential sites on the polymer structure for a particular sorbate. This study showed that it was possible to determine the effect of sorption induced plasticization on polymer perfermances with tailoring firstly FFV of polymeric membrane and secondly atomic interactions between penetrants and the PI matrices, and hence chemical structure of polymer.

Sorption simulation results reveal that the CO_2 sorption capacities of the PIs at 35°C and 10 bar are proportional the FFV of the swollen PI, with similar FFV values yielding similar CO_2 concentrations as seen in Figure 9.1. Thus, the sorption of the CO_2 molecules induces configurational changes in the polymer backbone and local relaxations of matrices through the particular interactions with the sorption sites, leading to an increase in the FFV associated with swelling and plasticization.
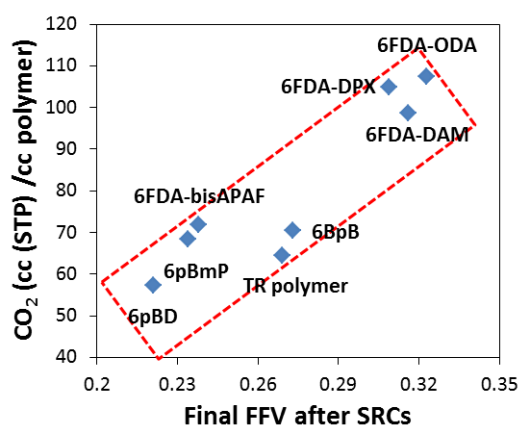
Figure 9.1 : Schematic illustration of relationship between CO_2 concentration and FFV.

Linear correlation between the FFV increase in CO_2 sorption and the standard deviation of the dihedral angle distribution of the diamine - dianhydride linkage which was used to provide an insight about backbone flexibility was proposed for polyimides whose FFV differs largely from each other. This relationship may be used to predict the FFV change, whence the degree of plasticization, of the PIs as a function of this standard deviation. Consequently, this may lead to an efficient screening of suitable combinations of diamine and dianhydride pairs among hundreds that are resistant to sorption-induced, which is a major problem for their

use in commercial gas separation applications as membrane materials. However, another conclusion was observed that the degree of plasticization or FFV increase may be differ when the backbone flexibility and FFV of the polyimides are similar or close to each other, depending to the functional groups attached to the side and backbone of the polymer chain. For instance, while the FFV of the three copolyimides are similar before sorption, after SRCs, FFV increase due to the CO_2 sorption changes dramatically. Therefore, it can be concluded that these two parameters such as the change in the backbone flexibility and the interactions between polymer structure and penetrant molecules should be taken into account in determination of degree of plasticization.

The dependence of sorption induced plasticization and swelling on both the backbone flexibility and the interactions between polymer structure and penetrant molecules was found in propylene/propane sorption simulations. CO_2 sorption capacity of PIs at 35°C and 10 bar depends on the FFV of the swollen PI, with similar FFV values yielding similar CO_2 concentrations. Thus, particular interactions between CO_2 and sorption sites have limited differential contribution on sorption capacity, as supported also by the RDFs. However, no such relationship was obtained for propane and propylene at 25°C and 1.13 bar due to changing site preferences, indicating the strength of sorbate-site interactions is significant on sorption capacity, as well as the FFV.

In addition, another interesting result that confirms above conclusion, was based on the study of 6FDA-bisAPAF and its TR polymer. 6FDA-bisAPAF has a wide range of degree in torsion due to its flexible backbone while TR polymer was fixed in the between (-40) and 40 degrees due to the rigidity of the coplanar structure of the poly-benzoxazole ring. Moreover, there are some limitations also in the interaction of oxygen sorption sites of TR polymer with the CO_2 which reduce the local relaxations due to the side group motions and hence the plasticization degree or % FFV increase. However, the interaction with the nitrogen in the imide was affected as revealed by the shift of the CO_2-N peak in the RDF from 4.7 to 3.9 Å indicating a relatively less restricted access to these sites, but with low intensity (changed from 1.77 to 1.56). The summary of this hypothesis can be given as in the Figure 9.2. However, TR polymer was expected to be in the right lower corner below 6FDA-DAM PI due to its rigid backbone and lack of interaction between CO_2 at 35°C and 10 bar. This may

be due to the limitations of Force Field to model the TR polymer. This may be minimized and some ideas are suggested to deal with this issue in the recommendations for future work.
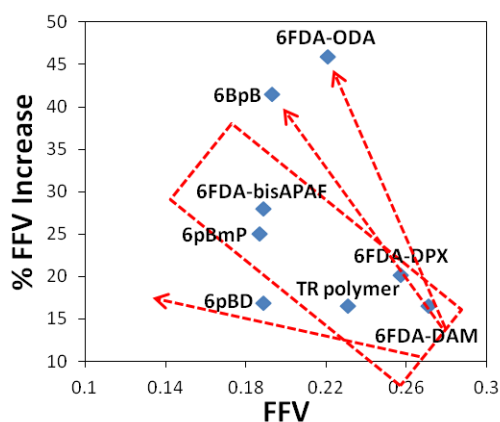
Figure 9.2 : Shcematic illustration of relationship between %FFV Increase and FFV.

Three component system such as polymer-solvent-sorbate were investigated and it was observed that in 6FDA-DAM and 6FDA-ODA PIs, residual solvents reduce CO_2 sorption capacity and alter CO_2/CH_4 selectivity. In addition, relationship between backbone rigidity and plasticization resistance is altered in the presence of solvents. Both plasticization effects of solvent and CO_2, and competition between plasticization tendency of CO_2 and anti-plasticization effect of solvent at small amounts were clearly observed in our molecular simulation study. However, as it is known those solvent-sorbate-polymer interactions are so complex and in order to prove our findings, simulations should be repeated at least three times. This recommendation will be stated in the next section.

Two different group contribution methods were examined in terms of their applicability to copolyimides to predict the permeability and selectivity coefficients. The predictions of the method of Alentiev et al. exhibited less error than the method of Park and Paul for the copolyimides which have data available in the literature and therefore was chosen as the method to carry out predictions for more than 2200 possible copolyimide structures. To ensure the reliability of the method and eliminate the any speculative results, these promising structures need to be experimentally synthesized and characterized to further test the predictive capability of the method used here.

The proposed copolyimide structures for CO_2/CH_4 separation were investigated by means of their plasticization resistance to CO_2 by molecular simulation and

successfully synthesized and characterized in order to compare with simulation results. Moreover, the plasticization behavior of these three copolyimides was investigated experimentally and CO_2 permeability did not change up to pressure 9 atm indicating that the plasticization effect did not observed. H-bonding arises from carboxylic acid group in DABA diamine was seen clearly in molecular simulation study and also identified with FTIR and TGA measurements experimentally.

9.2 Recommendations for Future Research

With the accurate estimation of the diffusivities and hence permeabilities of the PIs in the future, the simulation methodology applied here can be used to predict the effect of plasticization on transport properties of gases in different polyimides for which there are no experimental data to explore their potential use as membrane material.

It has been shown that plasticization is a major limitation to applying polyimide membranes in propylene/propane and CO_2/CH_4. The simulation approach presented in this work would likely be used in obtaining propylene/propane-induced plasticization for other polymeric gas separation membrane materials rather than polyimides. The addressed facilitated plasticization was observed in the investigation of binary mixture of propylene and propane where both components of a binary mixture show autoplasticization. Research on many other polymer structures in this area may provide more insight into how the facilitated plasticization effect of binary mixture of propylene and propane can be changed by tailoring polymer structure and how the material structure relates to competitive sorption at practically relevant to the operating conditions.

By working with high DABA contents in the copolyimide, the selectivity can be increased. The improved selectivity in mixed gas, due to the increased Langmuir sorption, should be even greater with higher DABA contents. In addition, DABA diamine has an ability to be crosslinking due to its carboxylic acid groups which also enables h-bonding. By the help of crosslinking, the selectivity can also be increased.

Mixed matrix composite membranes consist of molecular sieving domains (e.g. zeolites or carbon) embedded within a polymeric matrix. This approach can produce membranes with superior transport properties relative to pure polymers, while

retaining the processability of polymers. Mixed matrix membranes are being pursued for natural gas separations. With aggressive feed streams, plasticization-induced selectivity losses in the polymer phase are still expected to be problematic also in mixed matrix membranes. Advances in molecular modeling provide an opportunity to quantitatively investigate penetrant induced plasticization and understand the physics behind it. This approach can be used for the mixed matrix membranes. Especially, copolyimide with DABA diamine which may be tuned to optimize the interfacial bonding in mixed matrix membranes, can be a viable candidate for use in this area.

The sorption and diffusion interaction terms are likely to be significant at higher feed pressures, with higher sorbing components such as CO_2 and C_3+ hydrocarbons. So, permeability measurements for three copolyimide should also be performed at high feed pressures. Besides this, high pressure permeability measurements, rather than 10 bar, would be of vital interest for molecular simulations as well.

For H_2/CO_2 separation, 52 different copolyimide structures which exceed the 2008 upper bound have been identified by the help of group contribution methods. It would be of interest to further explore the proposed copolyimide structures for H_2/CO_2 separation by means of their plasticization degree in molecular simulation and experimentally.

To show the reliability of data obtained for three component system (polymer-solvent-sorbate) which is so complex, simulations should be repeated at least three times.

There are some disagreements in the result at low pressure corresponding to the TR polymer. This may be due to the limitations of Force Field to model the TR polymer. In order to see the effect of force field, different force field model which is also suitable for polymeric structures can be used. TR polymers are a new class of thermally-modified aromatic polyimides which has recently been presented as a prominent membrane material in gas separation area. Some parameters in force field model can not be best fitted to predict the possible interactions in polymer chain.

REFERENCES

[1]   **Bos, A., Punt, I. G. M., Wessling, M., Strathmann, H.** (1999). CO_2 induced plasticization phenomena in glassy polymers, *Journal of Membrane Science*, *155,* 67-78.

[2]   **Staudt-Bickel, C., Koros, W. J.** (1999). Improvement of CO_2/CH_4 separation characteristics of polyimides by chemical crosslinking, *Journal of Materials Processing Technology, 155,* 145-154.

[3]   **Ismail, A. F., Lorna, W.** (2002). Penetrant-induced plasticization phenomenon in glassy polymers for gas separation membrane, *Separation and Purification Technology, 27* (3), 173-194.

[4]   **Baker, R. W.** (2004). *Membrane Technology and Applications*. Menlo Park, California. : John Wiley & Sons, Ltd.

[5]   **Robeson, L. M.** (1991). Correlation of separation factor versus permeability for polymeric membranes, *Journal of Membrane Science, 62,* 165-185.

[6]   **Robeson, L. M.** (2008). The upper bound revisited, *Journal of Membrane Science*, *320*, 390-400.

[7]   **Park, H. B., Jung, C. H., Lee, Y. M., Hill, A. J., Pas, S. J., Mudie, S. T., Wagner, E. V., Freeman, B. D., Cookson, D. J.** (2007). Polymers with Cavities Tuned for Fast Selective Transport of Small Molecules and Ions, *Science*, *318*, 254-257.

[8]   **Rutta, V.** (1999). *Crystallization, Morphology, Thermal Stability and Adhesive Properties of Novel High Performance Semicrystalline Polyimides*. (PhD Thesis). Polytechnic Institute and State University, Faculty of Virginia, Blacksburg, Virginia.

[9]   **Yampolskii, Y., Pinnau, I., Freeman, B.** (2006). *Material Science of Membranes for Gas and Vapor Separation*. England. : John Wiley & Sons, Ltd.

[10]   **Scholes, C. A., Kentish, S. E. and Stevens, G. W.** (2008). Carbon dioxide separation through polymeric membrane systems for flue gas applications. *Recent Patents on Chemical Engineering, 1,* 52–66.

[11]   **Michaels, A. S., Vieth, W. R. and Barrie, J. A**. (1963). Solution of gases in polyethylene terephthalate, *Journal of Applied Physics., 34,* 1.

[12]   **Vieth, W. R. and Sladek, K. J.** (1965). A model for diffusion in a glassy polymer, *Colloid Science, 20,* 1014.

[13]   **Burns, R. L., Koros, W.J.** (2003). Structure property relationships for poly(pyrrolone-imide) gas separation membranes, *Macromolecules*, *36,* 2374-2381.

[14] **Raymond, R.Z., Gregory, K.F.** *"Theory", Chap. 3 in Membrane Handbook,* Eds: Winston, W.S., Kamalesh, K.S. : Chapman&Hall.

[15] **Wind, J. D., Sirard, S. M., Paul, D. R., Green, P. F., Johnston, K. P., Koros, W. J.** (2003). Relaxation dynamics of CO_2 diffusion, sorption, and polymer swelling for plasticized polyimide membranes, *Macromolecules, 36,* 6442–6448.

[16] **Punsalan, D., Koros, W. J.** (2005). Thickness-dependent sorption and effects of physical aging in a polyimide sample, *Journal of Applied Polymer Science*, *96,* 1115–1121.

[17] **Wessling, M., Lopez, M. L., Strathmann, H.** (2001). Accelerated plasticization of thin film composite membranes used in gas separation, *Separation and Purification Technology, 24,* 223–233.

[18] **Kesting, R. E.** (1990). The four tiers of structure in integrally skinned phase inversion membranes and their relevance to the various separation regimes, *Journal of Applied Polymer Science*, *41,* 2739–2752.

[19] **Dong, G., Li, H., Chen, V.** (2011). Plasticization mechanisms and effects of thermal annealing of Matrimid hollow fiber membranes for CO_2 removal, *Journal of Membrane Sci*ence, *369,* 206-220.

[20] **Okamoto, K., I., Tanaka, K., Shigematsu, T., Kita, H., Nakamura, A., Kusuki, Y.** (1990). Sorption and transport of carbon dioxide in a polyimide from 3,3',4,4'-biphenyltetracarboxylic dianhydride and dimethyl-3,7-diaminobenxothiophene-, 5,5'-dioxide, *Polymer*, *31,* 673.

[21] **Costello, L. M., Koros, W. J.** (1992). Temperature dependence of gas sorption and transport properties in polymers: measurement and applications, *Industrial Engineering Chemical Research, 31,* 2708.

[22] **Duthie, X., Kentish, S., Powell, C., Nagai, K., Qiao, G., Stevens, G.** (2007). Operating temperature effects on the plasticization of polyimide gas separation membranes, *Journal of Membrane Sci*ence, *294,* 40-49.

[23] **Reijerkerk, S. R., Nijmeijer, K., Ribeiro Jr., C. P., Freeman, B. D., Wessling, M.** (2011). On the effects of plasticization in CO_2/light gas separation using polymeric solubility selective membranes, *Journal of Membrane Sci*ence, *367,* 33-44.

[24] **Bos, A.** (1996). *High pressure CO_2/CH_4 separation with glassy polymer membranes aspects of CO_2-induced plasticization.* (Ph.D. Thesis). University of Twente, The Netherlands.

[25] **Kanehashi, S., Nakagawa, T., Nagai, K., Duthie, X., Kentish, S., Stevens, G.** (2007). Effects of carbon dioxide-induced plasticization on the gas transport properties of glassy polyimide membranes, *Journal of Membrane Science*, *298,* 147–155.

[26] **Liu, Y., Ding, M., Xu, J.** (1995). Gas permeabilities and permselectivity of photochemically crosslinked polyimides, *Journal of Applied Polymer Science, 58,* 485-489.

[27] **Kulkarni, S. S., Yates, S. F., Swamikannu, A. X.** (1990). *Cross-linked gas selective membranes.* Allied-Signal Inc.: United States.

[28] **Cao, C., Chung, T. S., Liu, Y., Wong, R., Pramoda, K. P.** (2003). Chemical cross-linking modification of 6FDA-2,6-DAT hollow fiber membranes for natural gas separation, *Journal of Membrane Science*, *216*, 257-268.

[29] **Liu, Y., Chung, T. S., Wang, R., Li, D. F., Chng, M. L.** (2003). Chemical cross-linking modification of polyimide/poly(ether sulfone) dual-layer hollow fiber membranes for gas separation, *Industrial & Engineering Chemistry Research, 42,* 1190-1195.

[30] **Tin, P. S., Chung, T. S., Liu, Y., Wang, R., Liu, S. L., Pramoda, K. P.** (2003). Effects of cross-linking modification on gas separation permformance of Matrimid membranes, *Journal of Membrane Science, 225*, 77-90.

[31] **Liu, Y., Wang, R., Chung, T. S.** (2001). Chemical cross-linking modification of polyimide membranes for gas separation. *Journal of Membrane Science, 189*, 231-239.

[32] **Ren, J., Wang, R., Chung, T. S., Li, D. F., Liu, Y.** (2003). The effects of chemical modifications on morphology and performance of 6FDA-ODA/NDA hollow fiber membranes for CO_2/CH_4 separation, *Journal of Membrane Science*, *222*, 133-147.

[33] **Bos, A., Punt, I., Strathmann, H., Wessling, M.** (2001). Suppression of gas separation membrane plasticization by homogeneous polymer blending, *AIChE J., 47* (5), 1088–1093.

[34] **Bos, A., Punt, I. G. M., Wessling, M., Strathmann, H.** (1998). Plasticization-resistant glassy polyimide membranes for CO_2/CH_4 separations, *Separation Purification Technology*, *14* (1/3), 27–39.

[35] **Maeda, Y., Paul, D. R.** (1987). Effect of Antiplasticization on Selectivity and Productivity of Gas Separation Membranes, *Journal of Membrane Science, 30,* 1-9.

[36] **Ruiz-Trevino, F.A., Paul, D. R.** (1998). Gas Permselectivity Properties of High Free Volume Polymers Modified by a Low Molecular Additive, *Journal of Applied Polymer Science, 68,* 403-415.

[37] **Ruiz-Trevino, F.A., Paul, D. R.** (1997). Modification of Polysulfone Gas Separation Membranes by Additives, *Journal of Applied Polymer Science, 66,* 1925-1941.

[38] **Larocca, N. M., Pessan, L. A.** (2003). Effect of Antiplasticisation on the Volumetric, Gas Sorption and Transport Properties of Polyetherimide, *Journal of Membrane Science, 218,* 69-92.

[39] **Wessling, M., Schoeman, S., Boomgaard T. v. d., Smolders, C. A.** (1991). Plasticization of gas separation membranes, *Gas Separation and Purification, 5,* 222- 228.

[40] **Houde, A. Y., Kulkarni, S. S., Kulkarni, M. G.** (1992). Permeation and plasticization behaviour of glassy polymers: a WAXD interpretation, *Journal of Membrane Science, 71*, 117.

[41] **Kazarian, S. G., Brantley, N. H., Eckert, C. A**. (1999). Applications of vibrational spectroscopy to characterize poly(ethylene terephthalate) processes with supercritical CO_2, *Vibrational Spectrosc*opy, *19, 277.*

[42] **Hachisuka, H., Sato, T., Imai, T., Tsujita, Y., Takizawa A., Kinoshita, T.** (1990). Glass transition temperature of glassy polymers plasticized by CO_2 gas, *Polymer Journal, (Tokyo), 22,* 77-79.

[43] **Smith, E., Mulder, M. H. V., Smolders, C. A., Karrenbeld, H., Van Eerden, J., Feil, D.** (1992). Modelling of the diffusion of carbon dioxide in polyimide matrices by computer simulation, *Journal of Membrane Science, 73,* 247-257.

[44] **Zhang, R., Mattice, W. L.** (1995). Atomistic modeling of the diffusion of small penetrant molecules in the bulk amorphous polyimide of 3,3′,4,4′-benzophenonetetracarboxylic dianhydride and 2,2-dimethyl-1,3-(4-aminophenoxy) propane, *Journal of Membrane Science, 108*, 15-23.

[45] **Hofmann, D., Fritsch, D., Ulbrich, J., Paul, D.** (1996). Molecular modelling simulation of gas transport in amorphous polyimide and poly(amide imide) membrane materials, *Polymer, 37*, 4773-4785.

[46] **Hofmann, D., Fritz, D., Ulbrich, J., Paul, D.** (2000). Molecular simulation of small molecule diffusion and solution in dense amorphous polysiloxanes and polyimides, *Computer Theory Polymer Science, 10*, 419-436.

[47] **Heuchel, M., Hofmann, D.** (2002). Molecular Modeling of Polyimide Membranes for Gas Separation, *Desalination*, *144*, 67-72.

[48] **Heuchel, M., Hofmann, D., Pullumbi, P.** (2004). Molecular modeling of small-molecule permeation in polyimides and its correlation to free-volume distributions, *Macromolecules, 37*, 201-214.

[49] **Neyertz, S., Brown, D.** (2004). Influence of System Size in Molecular Dynamics Simulations of Gas Permeation in Glassy Polymers, *Macromolecules*, *37*, 10109-10122.

[50] **Chang, K. S., Tung, C. C., Wang, K. S., Tung, K. L.** (2009). Free Volume Analysis and Gas Transport Mechanisms of Aromatic Polyimide Membranes: A Molecular Simulation Study, *Journal of Physical Chemistry B, 113*, 9821-9830.

[51] **Alentiev, A. Y., Loza, K. A., Yampolski, Y. J.** (2000) Development of the methods for prediction of gas permeation parameters of glassy polymers: polyimides as alternating co-polymers, *Journal of Membrane Science, 167*, 91-106.

[52] **Kotelyanskii, M., Theodorou, D. N.** (2004). *Simulation Methods for Polymers*. New York. : Marcel Dekker Inc.

[53] **Metropolis, N., Rosenbluth, A. W., Resenbluth, M. N., Teller, A. H. and Teller, E.** (1953). Equation of state calculations by fast computing machines. *Journal of Chemical Physics, 21*, 1087-1092.

[54] **McDonald, I. R.** (1972). NpT-ensemble Monte Carlo calculations for binary liquid mixtures. *Molecular Physics, 23*, 41-58.

[55] **Valleau, J. P., Cohen, L. K.** (1980). Primitive model electrolytes. I. Grand canonical Monte Carlo computations. *Journal of Chemical Physics, 72*, 5935-5941.

[56] **Ray, J. R.** (1991). Microcanonical ensemble Monte Carlo method, *Physics Review A, 44*, 4061-4064.

[57] **Andersen, H. C.** (1980). Molecular dynamics simulations at constant pressure and/or temperature, *Journal of Chemical Physics, 72*, 2384-2393.

[58] **Nose, S.** (1984). A unified formulation of the constant temperature dynamics methods, *Journal of Chemical Physics, 81,* 511-519.

[59] **Lo, C., Palmer, B.** (1995). Alternative Hamiltonian for molecular dynamics simulations in the grand canonical ensemble. *Journal of Chemical Physics, 102*, 925-931.

[60] **Li, T., Kildsing, D. O., Park, K.** (1997). Computer simulation of molecular diffusion in amorphous polymers, *Journal of controlled release, 48*, 57-66.

[61] **Martin, M. G.** (2006). Comparison of the AMBER, CHARMM, COMPASS, GROMOS, OPLS, TraPPE ve UFF force fields for prediction of vapor–liquid coexistence curves ve liquid densities, *Fluid phase equilibria, 248*, 50-55.

[62] **Mayo, S. L., Olafson, B. D., Goddard, W. A.** (1990). DREIDING: A generic force field for molecular simulation, *Journal of Physical Chemistry*, *94*, 8897-8909.

[63] **Katajisto, J., Linnolahti, M., Haukka, M., Pakkanen, T. A.** (2003). Development of a New Force Field for Property Prediction of Cyclo-Olefin Copolymers, *Journal of Physical Chemistry B, 108*, 2168-2172.

[64] **Sun, H., Mumby, S. J., Maple, J. R., Hagler, A. T.** (1994). An ab initio CFF93 all atom force field for polycarbonates, *Journal of the American Chemical Society, 116*, 2978-2987.

[65] **Hagler, A. T., Lifson, S., Dauber, P.** (1978). Consistent Force Field Studies of Intermolecular Forces in Hydrogen-Bonded Crystals. 2. A Benchmark for the Objective Comparison of Alternative Force Fields, *Journal of the American Chemical Society, 101*, 5122-5131.

[66] **Allen, M. P., Tildesley, D. J.** (1987). *Computer Simulation of Liquids*. Oxford : Oxford University Press.

[67] **Nosé, S.** (1984). A Molecular Dynamics Method for Simulations in the Canonical Ensemble, *Molecular Physics., 52*, 255.

[68] **Hoover, W. G.** (1985). Canonical Dynamics: Equilibrium Phase-Space Distributions, *Physical Review A, 31*, 1695.

[69] **Berendsen, H. J. C., Postma, J. P. M., van Gunsteren, W. F., DiNola, A., Haak, J. R.** (1984). Molecular-Dynamics with Coupling to an External Bath, *Journal of Chemical Physics, 81,* 3684.

[70] **Gear, C. W.** (1971). *Numerical initial value problems in ordinary differential equations.* Englewood Cliffs, NJ : Prentice-Hall.

[71] **Verlet, L.** (1967). Computer experiment on classical fluids. I. Thermodynamical properties of Lennard-Jones molecules, *Physical Review, 159*, 98-103.

[72] **Hockney, R. W.** (1970). The potential calculation and some applications, *Methods Computational Physics, 9*, 136-211.

[73] **Swope, W. C., Andersen, H. C., Berens, P. H., Wilson, K. R.** (1982). A computer simulation method for the calculation of equilibrium constants for the formulation of physical clusters of molecules: application to small water clusters, *Journal of Chemical Physics, 76*, 637-649.

[74] **Beeman, D.** (1976). Some multistep methods for use in molecular dynamics calculations, *Journal Compuational Physics, 20*, 130-139.

[75] **Van Kampen, N. G.** (1981). *Stochastic Processes in Physics and Chemistry.* North-Holland, Amsterdam : Prentice-Hall.

[76] **Frenkel, D., Smit, B.** (2002). *Understanding Molecular Simulation, From Algorithms to Applications,* San Diego, Californa, USA : Elsevier.

[77] Materials studio 5.0 edition. San Diego: Accelrys; 2009.

[78] Polymer User Guide, Amorphous Cell Section, Version 4.1; Molecular Simulations: San Diego, 2000.

[79] **Zhang, L., Xiao, Y., Chung, T. S., Jiang, J.** (2010). Mechanistic understanding of CO_2-induced plasticization of a polyimide membrane: A combination of experiment and simulation study, *Polymer*, *51*, 4439-4447.

[80] **Ohya, H., Kudryavtsev, V. V., Semenova, S. I.** (1996). *Polyimide Membranes: Applications, Fabrications, and Properties*. Tokyo, Japan : Gordon and Breach.

[81] **Shimazu, A., Miyazaki, T., Maeda, M., Ikeda, K.** (2000). Relationships between the chemical structures and the solubility, diffusivity, and permselectivity of propylene and propane in 6FDA-based polyimides, *Journal of Polymer Science: Part B: Polymer Physics*, *38*, 2525-2536.

[82] **Connolly, M. L.** (1983). Solvent-accessible surfaces of proteins and nucleic-acids, *Science*, *221*, 709.

[83] **Connolly, M. L.** (1983). Analytical molecular surface calculation, *Journal of Applied Crystals, 16,* 548.

[84] **Bondi, A.** (1968). *Physical properties of molecular crystals, Liquid and glasses.* New York : Wiley.

[85] **Koros, W. J., Hellums, M. W.** (2002). *Encyclopedia of Polymer Science and Technology, Transport Properties.* England : M. W. John Wiley & Sons, Ltd.

[86] **Chang, K. S., Tung, C. C., Wang, K. S., Tung, K. L.** (2009). Free Volume Analysis and Gas Transport Mechanisms of Aromatic Polyimide Membranes: A Molecular Simulation Study, *Journal of Physical Chemistry B*, *113*, 9821-9830.

[87] **Chang, K. S., Huang, Y. H., Lee, K. R., Tung, K. L.** (2010). Free volume and polymeric structure analyses of aromatic polyamide membranes: A molecular simulation and experimental study, *Journal of Membane Science, 354*, 93-100.

[88] **Ediger, M. D., Adolf, D. B.** (1994). *Atomistic Modeling of Physical Properties*. New York : Springer-Verlag.

[89] **Ghosh, M. K., Mittal, K. L.** (1996). *Polyimides: Fundamentals and Applications*. New York : Marcel Dekker.

[90] **Wind, J. D., Paul, D. R., Koros, W. J.** (2004). Natural gas permeation in polyimide membranes, *Journal of Membrane Science*, *228*, 227-236.

[91] **Wang, X., Li, Y., Zhang, S., Ma, S. T., Shao, Y., Zhao, X.** (2006). Synthesis and characterization of novel polyimides derived from pyridine-bridged aromatic dianhydride and various diamines, *European Polymer Journal, 42*, 1229-1239.

[92] **Tanaka, K., Islam, M. N., Kido, M., Kita, H., Okamoto, K.** (2006). Gas permeation and separation properties of sulfonated polyimide membranes, *Polymer*, *47*, 4370-4377.

[93] **Er, O. O., Sen, S., Atalay-Oral, C., Guner, F. S., Tantekin-Ersolmaz, S. B.** (2006). Copolyimide membranes for gas separation, *Desalination, 200*, 259-261.

[94] **Shang, Y., Fan, L., Yang, S., Xie, X.** (2006). Synthesis and characterization of novel fluorinated polyimides derived from 4-phenyl- 2,6-bis[4-(4'-amino-2'-trifluoromethyl phenoxy) phenyl]pyridine and dianhydrides, *European Polymer Journal*, *42*, 981-989.

[95] **Wang, Y. C., Huang, S. H., Hu, C. C., Li, C. L., Lee, K. R., Liaw, D. J., Lai, J. Y.** (2005). Sorption and transport properties of gases in aromatic polyimide membranes, *Journal of Membrane Science, 248*, 15-25.

[96] **Hofmann, D., Fritz, L., Ulbrich, J., Paul, D.** (1997). Molecular modelling of amorphous membrane polymers, *Polymer, 38*, 6145-6155.

[97] **Matsui, S., Sato, H., Nakagawa, T.** (1998). Effects of low molecular weight photosensitizer and UV irradiation on gas permeability and selectivity of polyimide membrane, *Journal of Membrane Science, 141*, 31-43.

[98] **Tsai, F. Y., Harding, D. R., Chen, S. H., Blanton, T. N.** (2003). High-permeability fluorinated polyimide microcapsules by vapor deposition polymerization, *Polymer, 44*, 995-1001.

[99] **Tanaka, K., Okano, M., Toshino, H., Kita, H., Okamoto, K.** (1992). Effect of Methyl Substituents on Permeability and Permselectivity of Gases in Polyimides Prepared from Methyl-Substitued Phenylenediamines, *Journal of Polymer Science, Part B; Polymer Physics*, *30*, 907-914.

[100] **Coleman, M. R., Koros, W. J.** (1990). Isomeric polyimides based on fluorinated dianhydrides and diamines for gas separation applications, *Journal of Membrane Science, 50*, 285-297.

[101] **Yeom, C. K., Lee, J. M., Hong, Y. T., Choi, K. Y., Kim, S. C.** (2000). Analysis of permeation transients of pure gases through dense polymeric membranes measured by a new permeation apparatus, *Journal of Membrane Science, 166*, 71-83.

[102] **Fritsch, D., Peinemann, K. V.** (1995). Novel highly permselective 6F-poly(amide-imide)s as membrane host for nano-sized catalysts, *Journal of Membrane Science, 99*, 29-38.

[103] **Tanaka, K., Kita, H., Okamoto, K.** (1993). Sorption of carbon dioxide in fluorinated poyimides, *Journal of Polymer Science: Part B: Polymer Physics*, *31*, 1127-1133.

[104] **Neyertz, S., Brown, D., Pandiyan, S., van der Vegt, N. F. A.** (2010). Carbon Dioxide Diffusion and Plasticization in Fluorinated Polyimides, *Macromolecules*, *43*, 7813-7827.

[105] **Macchione, M., Jansen, J. C., De Luca, G., Tocci, E., Longeri, M., Drioli, E.** (2007). Experimental analysis and simulation of the gas transport in dense Hyflon® AD60X membranes: Influence of residual solvent, *Polymer, 48*, 2619-2635.

[106] **Burns, R. L., Koros, W. J.** (2003). Structure-property relationships for poly(pyrolone-imide) gas separation membranes, *Macromolecules, 36*, 2374-2381.

[107] **Gusev, A. A., Suter, U. W.** (1991). Theory for solubility in static systems, *Phyical Review A*, *43*, 6488-6494.

[108] **Greenfield, M. L., Theodorou, D. N.** (2001). Coarse-Grained Molecular Simulation of Penetrant Diffusion in a Glassy Polymer Using Reverse and Kinetic Monte Carlo, *Macromolecules*, *34*, 8541-8553.

[109] **Tanaka, K., Kita, H., Okano, M., Okamoto, K.** (1992). Permeability and Permselectivity of Gases in fluorinated and Non-Fluorinated Polyimides, *Polymer*, *33*, 585-591.

[110] **Sato, S., Suzuki, M., Kanehashi, S., Nagai, K.** (2010). Permeability, diffusivity, and solubility of benzene vapor and water vapor in high free volume silicon- or fluorine-containing polymer membranes, *Journal of Membrane Science, 360*, 352-362.

[111] **Pandiyan, S., Brown, D., van der Vegt, N. F. A., Neyertz, S.** (2009). Atomistic models of three fluorinated polyimides in the amorphous state, *Journal of Polymer Science, Part B: Polymer Physics*, *47*, 1166-1180.

[112] **Chiou, J. S., Barlow, J. W., Paul, D. R.** (1985). Plasticization of glassy polymers by CO_2, *Journal of Applied Polymer Science, 30* (6), 2633-2642.

[113] **Hirayama, Y., Yoshinaga, T., Kusuki, Y., Ninomiya, K., Sakakibara, T., Tamari T.** (1996). Relation of gas permeability with structure of aromatic polyimides I, *Journal of Membrane Science, 111*, 169-182.

[114] **Sun, H.** (1998). COMPASS: An ab Initio Force-Field Optimized for Condensed-Phase Applications Overview with Details on Alkane and Benzene Compounds, *Journal of Physical Chemistry B., 102*, 7338-7364.

[115] **Koros, W. J., Burns, R. L.** (2003). *Patent US 6,602,415 B2.* Polymeric membrane for separation of fluids under elevated temperature and/or pressure conditions, US.

[116] **Park, H. B., Han, S. H., Jung Lee, C. H. Y. M., Hill, A. J.** (2010). Thermally rearranged (TR) polymer membranes for CO_2 separation, *Journal of Membrane Science, 359*, 11–24.

[117] **Staudt-Bickel, C., Koros, W. J.** (2000). Olefin/paraffin gas separations with 6FDA-based polyimide membranes, *Journal of Membrane Science, 170*, 205.

[118] **Tanaka, K., Taguchi, A., Hao, J. Q., Kita, H., Okamoto, K.** (1996). Permeation and separation properties of polyimide membranes to olefins and paraffins, *Journal of Membrane Science, 121*, 197.

[119] **Okamoto, K., Noborio, K., Hao, J., Tanaka, K., Kita, H.** (1997). Permeation and separation properties of polyimide membranes to 1,3-butadiene and n-butane, *Journal of Membrane Science, 134*, 171.

[120] **Krol, J. J., Boerrigter, M., Koops, G. H.** (2001). Polyimide hollow fiber gas separation membranes: preparation and the suppression of plasticization in propane/propylene environments, *Journal of Membrane Science, 184*, 275.

[121] **Das, M., Koros, W. J.** (2010). Performance of 6FDA–6FpDA polyimide for propylene/propane separations, *Journal of Membrane Science, 365*, 399-408.

[122] **Burns, R. L., Koros, W. J.** (2003). Defining the challenges for C_3H_6/C_3H_8 separation using polymeric membranes, *Journal of Membrane Science, 211*, 299.

[123] **Shimazu, A., Miyazaki, T., Katayama, S., Ito, Y.** (2003). Permeability, Permselectivity, and Penetrant-Induced Plasticization in Fluorinated Polyimides Studied by Positron Lifetime Measurements, *Journal of Polymer Science: Part B: Polymer Physics, 41*, 308-318.

[124] **Chan, S. S., Wang, R., Chung, T. S., Liu Y.** (2002). C_2 and C_3 hydrocarbon separations in poly(1,5-naphthalene- 2,2'-bis(3,4-phthalic) hexafluoropropane) diimide (6FDA-1,5-NDA) dense membranes, *Journal of Membrane Science, 210*, 55–64.

[125] **Heb, S., Scharfenberger, G., Staudt-Bickel, C., Lichtenthaler, R. N.** (2002). Propylene/propane separation with copolyimides containing benzo-15-crown-5-ether to incorporate silver ions, *Desalination, 145*, 359-364.

[126] **Hess, S., Staudt-Bickel, C., Lichtenthaler, R. N.** (2006). Propene/propane separation with copolyimide membranes containing silver ions, *Journal of Membrane Science, 275,* 52–60.

[127] **Visser, T., Wessling, M.** (2008). Auto and mutual plasticization in single and mixed gas C3 transport through Matrimid-based hollow fiber membranes, *Journal of Membrane Science*, *312,* 84–96.

[128] **Jiang, L. Y., Chung, T. S., Rajagopalan, R.** (2008). Dehydration of alcohols by pervaporation through polyimide Matrimid® asymmetric hollow fibers with various modifications, *Chemical Engineering Science, 63*, 204 – 216.

[129] **Du, N., Dal-Cin, M. M., Pinnau, I., Nicalek, A., Robertson, G. P., Guiver, M. D.** (2011). Azide-based Cross-Linking of Polymers of Intrinsic Microporosity (PIMs) for Condensable Gas Separation, *Macromolecular Rapid Commuications, 32*, 631–636.

[130] **Mozaffari, F., Eslami, H., Moghadasi, J.** (2010). Molecular dynamics simulation of diffusion and permeation of gases in polystyrene, *Polymer, 51*, 300–307.

[131] **Zheng, T., Fried, J. R.** (2001). Monte carlo simulation of the sorption of pure and mixed alkanes in poly[1-(trimethylsilyl)-1-propyne], *Separation Science and Technology*, *36* (5&6), 959–973.

[132] **Pan, F., Ma, J., Cui, L., Jiang, Z.** (2009). Water vapor/propylene sorption and diffusion behavior in PVA–P(AA-AMPS) blend membranes by GCMC and MD simulation, *Chemical Engineering Science, 64*, 5192-5197.

[133] **Velioğlu, S., Ahunbay, M. G., Tantekin-Ersolmaz, S. B.** (2012). Investigation of CO_2-induced plasticization in fluorinated polyimide membranes via molecular simulation *Journal of Membrane Science, 417*, 217-227.

[134] **Semenova S. I.** (2004). Polymer membranes for hydrocarbon separation and removal, *Journal of Membrane Science*, *231*, 189-207.

[135] **Chng, M. L., Xiao, Y., Chung, T. S., Toriida, M., Tamai, S.** (2009). Enhanced propylene/propane separation by carbonaceous membrane derived from poly (aryl ether ketone)/ 2,6-bis(4-azidobenzylidene)-4-methyl-cyclohexanone interpenetrating network, *Carbon, 47*, 1857-1866.

[136] **Joly, C., Le Cerf , D., Chappey, C., Langevin, D., Muller, G.** (1999). Residual solvent effect on the permeation properties of fluorinated polyimide film, *Separation and Purification Technology*, *16*, 47–54.

[137] **Fu, Y. J., Hu, C. C., Qui, H. Z., Lee, K. R., Lai, J. Y.** (2008). Effects of residual solvent on gas separation properties of polyimide membranes, *Seperation and Purification Technology, 62*, 175-182.

[138] **Kruczek, B., Matsuura, T.** (2003). Effect of Solvent on Properties of Solution-Cast Dense SPPO Films, *Journal of Applied Polymer Science, 88*, 1100–1110.

[139] **Guan, R., Dai, H., Li, C., Liu, J., Xu, J.** (2006). Effect of casting solvent on the morphology and performance of sulfonated polyethersulfone membranes, *Journal of Membrane Science, 277*, 148–156.

[140] **Tung, K. L., Lu, K. T., Ruaan, R. C., Lai, J. Y.** (2006). MD and MC simulation analyses on the effect of solvent types on accessible free volume and gas sorption in PMMA membranes, *Desalination*, *192*, 391–400.

[141] **Recio, R., Palacio, L., Pradanos, P., Hernandez, A., Lozano, A. E., Marcos, A., de la Campa, J. G., de Abajo, J.** (2007). Gas separation of 6FDA–6FpDA membranes, Effect of the solvent on polymer surfaces and permselectivity, *Journal of Membrane Science*, *293*, 22–28.

[142] **Chang, K. S., Hsiung, C. C., Lin, C. C., Tung, K. L.** (2009). Free Volume Analysis and Gas Transport Mechanisms of Aromatic Polyimide Membranes: A Molecular Simulation Study, *Physical Chemistry B, 113*, 10159-10169.

[143] **Zhang, L., Fang, W., Jiang, J.** (2011). Effects of Residual Solvent on Membrane Structure and Gas Permeation in a Polymer of Intrinsic Microporosity: Insight from Atomistic Simulation, *Journal of Physical Chemistry C, 115*, 11233-11239.

[144] **Yampolskii, Y., Freeman, B.** (2010). *Membrane Gas Separation*. United Kingdom : John Wiley & Sons Ltd.

[145] **Robeson, L. M., Smith, C. D., Langsam, M.** (1997). A group contribution approach to predict permeability and permselectivity of aromatic polymers, *Journal of Membrane Science*, *132*, 33-54.

[146] **Park, J. Y., Paul, D. R.** (1997). Correlation and prediction of gas permeability in glassy polymer membrane materials via a modified free volume based group contribution method, *Journal of Membrane Science, 125*, 23-39.

[147] **Shao, L., Chung, T. S., Wensley, G., Goh, S. H., Pramoda, K. P.** (2004). Casting solvent effects on morphologies, gas transport properties of a novel 6FDA/PMDA-TMMDA copolyimide membrane and its derived carbon membranes, *Journal of Membrane Science*, *244*, 77-87.

[148] **Yampolskii, Y., Shishatskii, S., Alentiev, A., Loza, K.** (1998). Group contribution method for transport property predictions of glassy polymers: focus on polyimides and polynorbornenes, *Journal of Membrane Science*, *149*, 203-220.

[149] **Bogdanic, G.** (2006). Group Contribution Methods for Estimating the Properties of Polymer Systems, *Hemijska Industrija, 60*, 287-305.

[150] **Van Krevelen, D. W.** (1990). *Properties of Polymers*. Amsterdam, The Netherlands : Elsevier.

[151] **Salame, M.** (1986). Prediction of gas barrier properties of high polymers, *Polymer Engineering Science, 26*, 1543.

[152] **Laciak, D. V., Robeson, L. M., Smith, C. D.** (1999). *Group contribution modeling of gas transport in polymeric membranes*, in: B.D. Freeman, I. Pinnau (Eds.), Polymer Membranes for Gas and Vapor Separation, ACS Symposium Series 733, Washington, DC : American Chemical Society.

[153] **Meares, P.** (1954). The diffusion of gases through polyvinyl acetate, *Journal of American Chemical Society, 76*, 3415.

[154] **Staudt-Bickel, C.** (2003). Cross-linked copolyimide membranes for the separation of gaseous and liquid mixtures, *Soft Material, 1*, 277-293.

[155] **Chan, S. S., Chung, T. S., Liu, Y., Wang, R.** (2003). Gas and Hydrocarbon (C-2 and C-3) transport properties of co-polyimides synthesized from 6FDA and 1,5-NDA (napthalene) /Durene diamines, *Journal of Membrane Science, 218*, 235-245.

[156] **Yoshino, M., Nakamura, S., Kita, H., Okamoto, K. I., Tanihara, N., Kusuki, Y.** (2003). Olefin/paraffin separation performance of asymmetric hollow fiber membrane of 6FDA/BPDA-DDBT copolyimide, *Journal of Membrane Science, 212*, 13-27.

[157] **Liu, S. L., Wang, R., Liu, Y., Chng, M. L., Chung, T. S.** (2001). The physical and gas permeation properties of 6FDA-durene/2,6-diaminotoluene copolyimides, *Polymer, 42*, 8847-8855.

[158] **Li, Y. S., Wang, X. Q., Ding, M. X, Xu, J. P.** (1996). Effects of molecular structure on the permeability and permselectivity of aromatic polyimides, *Journal of Applied Polymer Science, 61*, 741-748.

[159] **Barsema, J. N., Kapantiadakis, G. C., Van der Vegt, N. F. A., Koops, G. H., Wessling, M.** (2003). Preparation and characterization of highly selective dense and hollow fiber asymmetric membranes base on BTDA-TDI/MDI co-polyimide, *Journal of Membrane Science, 216*, 195-205.

[160] **Lin, H. W., Vora, R. H., Chung, T. S.** (2000). Gas transport properties of 6FDA-durene/1,4-phenylenediamine (pPDA) copolyimides, *Journal of Polymer Science Part B: Polymer Physics, 38*, 2703-2713.

[161] **Lin, H. W., Vora, R. H., Chung, T. S.** (2001). Gas transport properties of 6FDA-durene/1,3-phenylenediamine (mPDA) copolyimides, *Journal of Polymer Science art B: Polymer Physics, 81*, 3552-3564.

[162] **Sen, S.,** 2004. *Gas separation with copolyimide membrane.* (Master Thesis). I.T.U. Institute of Science and Technology, Istanbul.

[163] **Kim, J. H., Koros, W. J., Paul, D. R.** (2006). Effects of CO_2 exposure and physical aging on the gas permeability of thin 6FDA-based polyimide membranes, Part1: Without cross-linking, *Journal of Membrane Science, 282*, 21-31.

[164] **Liu, S. L., Wang, R., Chung, T. S., Chng, M. L., Liu, Y., Vora, R. H.** (2002). Effect of diamine composition on the gas transport properties in 6FDA-durene/3,3'-diaminodiphenyl sulfone copolyimides, *Journal of Membrane Science, 202*, 165-176.

[165] **Er, Ö.O.** (2006). *Synthesis and characterization of 6FDA-based copolyimides.* (Master Thesis). I.T.U. Institute of Science and Technology, Istanbul.

[166] **Xiao, S., Feng, X., Huang, R. Y. M.** (2008). Synthetic 6FDA-ODA copolyimide membranes for gas separation and pervaporation: correlation of separation properties with diamine monomers, *Polymer Engineering and Science, 12*, 796-805.

[167] **Xiao, S., Feng, X., Huang, R. Y. M.** (2007). Synthesis and properties of 6FDA-MDA copolyimide membranes: Effects of diamines and dianhydrides on gas separation and pervaporation properties, *Macromolecular Chemistry and Physic*s, *208*, 2665-2676.

[168] **Xiao, S., Feng, X., Huang, R. Y. M.** (2007). Synthetic 6FDA-ODA copolyimide membranes for gas separation and pervaporation: Functional groups and separation properties, *Polymer*, *48*, 5355-5368.

[169] **Niwa, M., Nagaoka, S., Kawakami, H.** (2006). Preparation of novel fluorinated block copolyimide membranes for gas separation, *Journal of Applied Polymer Science*, *100*, 2436-2442.

[170] **Wang, L., Cao, Y., Zhou, M., Ding, X., Liu, Q., Yuan, Q.** (2008). The gas permeation properties of 6FDA-2,4,6-trimethyl-1,3-phenylenediamine (TMPDA)/1,3-phenylenediamine (mPDA) copolyimides, *Polymer Bulletin, 60*, 137-147.

[171] **Wang, L., Cao, Y., Zhou, M., Ding, X., Liu, Q., Yuan, Q.** (2008). Gas transport properties of 6FDA-TMPDA/MOCA copolyimides, *European Polymer Journal*, *44*, 225-232.

[172] **Kotov, B. V., Gordina, T. A., Voishchev, V. S., Kolninov, O. V., Pravednikov, A. N.** (1977). Aromatic polyimides as charge transfer complexes, *Polymer Science U.S.S.R., 19*, 711–716.

[173] **Vinh-Thang, H., Kaliaguine, S.** (2013). Predictive Models for Mixed-Matrix Membrane Performance: A Review, *Chemical Review, 113*, 4980−5028.

[174] **Konietzny, R., Barth, C., Harms, S., Raetzke, K., Koelsch, P. and Staudt, C.** (2011). Structural investigations and swelling behavior of 6FDA copolyimide thin film, *Polymer International*, *60*, 1670–1678.

[175] **Schmeling, N., Konietzny, R., Sieffert, D., Rölling, P., and Staudt, C.** (2010). Functionalized copolyimide membranes for the separation of gaseous and liquid mixtures, *Beilstein Journal Organic Chemistry, 6*, 789–800.

[176] **Kraftschik, B., Koros, W. J., Johnson, J. R., Karvan, O.** (2013). Dense film polyimide membranes for aggressive sour gas feed separations, *Journal of Membrane Science, 428*, 608–619.

[177] **Chung, T. S., Lin, W. H., Vora, R. H.** (2001). Gas Transport Properties of 6FDA-Durene/1,3- Phenylenediamine (mPDA) Copolyimides, *Journal of Applied Polymer Science*, *81*, 3552–3564.

[178] **Kratochvil, A. M., and Koros, W. J.** (2008). Decarboxylation-Induced Cross-Linking of a Polyimide for Enhanced CO_2 Plasticization Resistance, *Macromolecules*, *41*, 7920-7927.

[179] **Qiu, W., Chen, C. C., Xu, L., Cui, L., Paul, D. R., and Koros, W. J.** (2011). Sub-Tg Cross-Linking of a Polyimide Membrane for Enhanced CO_2 Plasticization Resistance for Natural Gas Separation, *Macromolecules, 44*, 6046–6056.

[180] **Wind, J. D., Staudt-Bickel, C., Paul, D. R. and Koros, W. J.** (2003). Solid-State Covalent Cross-Linking of Polyimide Membranes for Carbon Dioxide Plasticization Reduction, *Macromolecules, 36*, 1882-1888.

[181] **Chen, X. Y., Kaliaguine, S.** (2013). Mixed Gas and Pure Gas Transport Properties of Copolyimide Membranes, *Journal of Applied Polymer Science*, *128,* 380-389.

[182] **Li, Y., Ding, M., Xu, J.** (1997). Gas Permeation Properties of Copolyimides from 1,4-Bis(3,4-dicarboxyphenoxy) benzene Dianhydride and 2,2-bis(3,4-dicarboxyphenyl) hexafluoroisopropane Dianhydride, *Polymer International*, *42*, 121-126.

[183] **Maya, E. M., Lozano, A. E., de Abajo, J., de la Campa, J.G.** (2007). Chemical modification of copolyimides with bulky pendent groups: Effect of modification on solubility and thermal stability, *Polymer Degradation and Stability*, *92*, 2294-2299.

[184] **Maya, E. M., Lozano, A. E., de Abajo, J., de la Campa, J.G.** (2007). Partially pyrolyzed membranes (PPMs) derived from copolyimides having carboxylic acid groups. Preparation and gas transport properties, *Journal of Membrane Science, 349*, 385-392.

[185] **Mikawa, M., Nagaoka, S., Kawakam, H.** (1999). Gas transport properties and molecular motions of 6FDA copolyimides, *Journal of Membrane Science*, *163*, 167–176.

[186] **Piroux, F., Espuche, E., Mercier, R., Pineri, M.** (2002). Sulfonated copolyimides: influence of structural parameters on gas separation properties, *Desalination, 145*, 371-374.

[187] **Inoue, H., Sasaki, Y., and Ocawa, T.,** (1996). Properties of Copolyimides Prepared from Different Tetracar boxylic Dianhydrides and Diamines, *Journal of Applied Polymer Science, 62*, 2303-2310.

[188] **Wang, L., Cao, Y., Zhou, M., Qiu, X., Yuan, Q.** (2009). Synthesis, characterization, and gas permeation properties of 6FDA-2,6-DAT/mPDA copolyimides, *Frontiers of Chemistry in China*, *4* (2), 215–221.

[189] **Pinel, E., Brown, D., Bas, C., Mercier, R., Alberola, N. D., and Neyertz, S.** (2002). Chemical Influence of the Dianhydride and the Diamine Structure on a Series of Copolyimides Studied by Molecular Dynamics Simulations, *Macromolecules*, *35*, 10198-10209.

[190] **Halitoglu, S., Tantekin Ersolmaz, S.B.** (2007). Prediction of gas permeability coefficients of copolyimides by group contribution methods, *NAMS*, Orlando, Florida : May 12-16.

[191] **Menczel, J. D., Prime, R. B.** (2009). *Thermal Analysis of Polymers*. England : Wiley**.**

[192] **Menard, K. P.** (1999). *Dynamic Mechanical Analysis*. New York : CRC Press.

[193] **Kertik, A.** (2010). *Gas purification using polymer/zeolite composite membranes*. (M.Sc. Thesis). I.T.U. İstanbul, Turkey**.**

[194] **Reid, B. D., Ruiz-Trevino, F. A., Musselman, I. H., Balkus, K. J. Jr., Ferraris, J. P.** (2001). Gas Permeability Properties of Polysulfone Membranes Containing the Mesoporous Molecular Sieve MCM-41, *Chemical Material, 13*, 2366-2373.

[195] **Zornoza, B., Irusta, S., Tellez, C., and Coronas, J.** (2009). Mesoporous Silica Sphere-Polysulfone Mixed Matrix Membranes for Gas Separation, *Langmuir, 25* (10), 5903–5909.

[196] **Krishnana, P. S. G., Vora, R. H., Veeramania, S., Goh, S. H., Chung, T. S.** (2002). Kinetics of thermal degradation of 6FDA based copolyimides—I, *Polymer Degradation and Stability*, *75*, 273–285.

[197] **Cui, L., Qiu, W., Paul, D. R., Koros, W. J.** (2011). Physical aging of 6FDA-based polyimide membranes monitored by gas permeability, *Polymer*, *52*, 3374-3380.

[198] **Park, S. H., Kim, K. J., So, W. W., Moon, S. J., and Lee, S. B.** (2003). Gas Separation Properties of 6FDA-Based Polyimide Membranes with a Polar Group, *Macromolecular Research*, *11*, 157-162.

[199] **Hirayama, Y., Yoshinaga, T., Nakanishi, S., Kusuki, Y.** (1999). *In Polymer Membranes for Gas and Vapor Separation*: Chemistry and Materials Science; Freeman, B. D., Pinnau, I., Washington, DC. : American Chemical Society.

[200] **Hasanain, F., Wang, Z. Y.** (2008). New one step synthesis of polyimides in salicylic acid, *Polymer*, *49***,** 831-835.

[201] **Kawakami, H., Nakajima, K., Shimizu, H., Nagaoka, S.** (2003). Gas permeation stability of asymmetric polyimide membrane with thin skin layer: effect of polyimide structure, *Journal of Membrane Science*, *212*, 195–203.

[202] **Kawakami, H., Mikawa, M., Nagaoka, S.** (1997). Formation of surface skin layer of asymmetric polyimide membranes and their gas transport properties, *Journal of Membrane Science*, *137*, 241-251.

[203] **Kim, Y. K., Lee, J. M., Park, H. B., Lee, Y. M.** (2004). The gas separation properties of carbon molecular sieve membranes derived from polyimides having carboxylic acid groups, *Journal of Membrane Science*, *235*, 139–146.

[204] **Koros, W. J.** (1985). Simplified analysis of gas/polymer selective solubility behavior, *Journal of Polymer Science, Part B: Polymer Physics Edition, 23*, 1611.

[205] **Bondar, V. I., Freeman, B. D., Pinnau, I.** (1999). Gas sorption and characterization of poly (ether-b-amide) segmented block copolymers, *Journal of Polymer Science, Part B: Polymer Physics, 37*, 2463.

[206] **Lin, H., Freeman, B. D.** (2005). Materials selection guidelines for membranes that remove CO_2 from gas mixtures, *Journal of Molecular Structure, 739*, 57–74.

[207] **Vieth, W. R.** (1988). *Membrane Systems: Analysis and Design*, USA : Oxford University Press.

[208] **Yampolskii, Y.** (2012). Polymeric Gas Separation Membranes, *Macromolecules, 45,* 3298−3311.

[209] **Plate, N. A., Yampolskii, Yu. P.** (1994). *In Polymeric Gas Separation Membranes;* Paul, D. R., Yampolskii, Yu.P., Boca Raton, FL. : Eds.; CRC Press.

[210] **Tullos, G. L., Mathias, L. J.** (1999). Unexpected thermal conversion of hydroxy-containing polyimides to polybenzoxazoles, *Polymer, 40,* 3463-3468.

[211] **Choi, J. I., Jung, C. H., Han, S. H., Park, H. B., Lee, Y. M.** (2010). Thermally rearranged (TR) poly(benzoxazole-co-pyrrolone) membranes tuned for high gas permeability and selectivity, *Journal of Membrane Science, 349,* 358-368.

[212] **Han, S. H., Lee, J. E., Lee, K. J., Park, H. B., Lee, Y. M.** (2010). Highly gas permeable and microporous polybenzimidazole membrane by thermal rearrangement, *Journal of Membrane Science, 357,* 143-151.

[213] **Han, S. H., Misdan, N., Kim, S., Doherty, C. M., Hill, A. J., Lee, Y. M.** (2010). Thermally Rearranged (TR) Polybenzoxazole: Effects of Diverse Imidization Routes on Physical Properties and Gas Transport Behaviors, *Macromolecules, 43,* 7657-7667.

[214] **Jung, C. H., Lee, J. E., Han, S. H., Park, H. B., Lee, Y. M.** (2010). Highly permeable and selective poly(benzoxazole-co-imide) membranes for gas separation, *Journal of Membrane Science, 350,* 301-309.

[215] **Hodgkin, J. H., Liu, M. S., Dao, B. N., Mardel, J., Hill, A. J.** (2011). Reaction mechanism and products of the thermal conversion of hydroxy-containing polyimides, *European Polymer journal, 47,* 394-400.

[216] **Calle, M., Lee, Y. M.** (2011). Thermally Rearranged (TR) Poly(ether-benzoxazole) Membranes for Gas Separation, *Macromolecules, 44,* 1156-1165.

[217] **Wang, H., Liu, S., Chung, T. S., Chen, H., Jean, Y. C., Pramoda, K. P.,** (2011). The evolution of poly(hydroxyamide amic acid) to poly(benzoxazole) via stepwise thermal cyclization: Structural changes and gas transport properties, *Polymer, 52,* 5127-5138.

[218] **Wang, H., Chung, T. S.** (2011). The evolution of physicochemical and gas transport properties of thermally rearranged polyhydroxyamide (PHA), *Journal of Membrane Science, 385-386,* 86-95.

[219] **Han, S. H., Kwon, H. J., Kim, K. Y., Seong, J. G., Park, C. H., Kim, S., Doherty, C. M., Thornton, A. W., Hill, A. J., Lozano, A. E., Berchtold, K. A., Lee, Y. M.** (2012). Tuning microcavities in thermally rearranged polymer membranes for CO_2 capture, *Physical chemistry chemical physics,14,* 4365-4373.

[220] **Calle, M., Chan, Y., Jo, H. J., Lee, Y. M.** (2012). The relationship between the chemical structure and thermal conversion temperatures of thermally rearranged (TR) polymers, *Polymer, 53,* 2783-2791.

[221] **Calle, M., Lozano, A. E., Lee, Y. M.** (2012). Formation of thermally rearranged (TR) polybenzoxazoles: Effect of synthesis routes and polymer form, *European Polymer journal, 48*, 1313-1322.

[222] **Smith, Z. P., Sanders, D. F., Ribeiro, C. P., Guo, R., Freeman, B. D., Paul, D. R., McGrath, J. E., Swinnea, S.** (2012). Gas Sorption and Characterization of Thermally Rearranged Polyimides Based on 3,3'-dihydroxy-4,4'-diamino-biphenyl (HAB) and 2,2'-bis-(3,4-dicarboxyphenyl) Hexafluoropropane Dianhydride (6FDA), *Journal of Membrane Science, 415-416,* 558-567.

[223] **Sanders, D. F., Smith, Z. P., Ribeiro, C. P., Guo, R., McGrath, J. E., Paul, D. R., Freeman, B. D.** (2012). Gas Permeability, Diffusivity, and Free Volume of Thermally Rearranged Polymers Based on 3,3′-dihydroxy-4,4′-diamino-biphenyl (HAB) and 2,2′-bis-(3,4-dicarboxyphenyl) hexafluoropropane dianhydride (6FDA), *Journal of Membrane Science*, *409-410*, 232-241.

[224] **Kim. S., Lee, Y. M.** (2012). Thermally rearranged (TR) polymer membranes with nanoengineered cavities tuned for CO_2 separation, *Journal of Nanoparticle Research, 14*, 949.

[225] **Ong, Y. K., Wang, H., Chung, T. S.** (2012). A prospective study on the application of thermally rearranged acetate-containing polyimide membranes in dehydration of biofuels via pervaporation, *Chemical Engineering Science, 79*, 41-53.

[226] **Kim. S., Han, S. H., Lee, Y. M.** (2012). Thermally rearranged (TR) polybenzoxazole hollow fiber membranes for CO_2 capture, *Journal of Membrane Science*, *403-404*, 169-178.

[227] **Jiang, Y., Willmore, F. T., Sanders, D., Smith, Z. P., Ribeiro, C. P., Doherty, C. M., Thornton, A. W., Hill, Freeman, B. D., Sanchez, I. C.** (2011). Cavity size, sorption and transport characteristics of thermally rearranged (TR) polymers, *Polymer, 52*, 2244-2254.

[228] **Park, C. H., Tocci, E., Lee, Y. M., Drioli, E.** (2012). Thermal Treatment Effect on the Structure and Property Change between Hydroxy-Containing Polyimides (HPIs) and Thermally Rearranged Polybenzoxazole (TR-PBO), *Journal of Physical Chemistry B, 116*, 12864-12877.

[229] **Vogel, H., Marvel, C. C.** (1961). Polybenzimidazoles, new thermally stable polymers, *Journal of Polymer Science, 50*, 511.

[230] **Iwakura, Y., Uno, K., Imai, Y.** (1964). Polyphenylenebenzimidazoles, *Journal of Polymer Science, Part A, Polymer Chemistry, 2*, 2605.

[231] **Kubota, T., Nakanishi, R.** (1964). Preparation of fully aromatic polybenzoxazoles, *Journal of Polymer Science, Part B: Polymer Letters*, *2*, 655.

[232] **Hodgkin, J. H., Buu N. D.** (2009). Thermal conversion of hydroxy containing polyimides to polybenzoxazoles. Does this reaction really occur?, *European Polymer Journal, 45*, 3081–3092.

[233] **In't Veld, P. J., Stone, M. T., Truskett, T. M., Sanchez, I. C.** (2000). Liquid structure via cavity size distributions, *Journal of Physical Chemistry B*, *104*, 12028-12034.

[234] **Heuchel, M., Böhning, M., Hölck, O., Siegert, M. R., Hofmann, D.** (2006). Atomistic Packing Models for Experimentally Investigated Swelling States Induced by CO_2 in Glassy Polysulfone and Poly(ether sulfone), *Journal of Polymer Science, Part B: Polymer Physics, 44*, 1874.

[235] **Baker, R. W., Lokhandwala, K.** (2008). Natural gas processing with membranes: an overview, *Industrial Engineering Chemical Research, 47*, 2109-2121.

APPENDICES

APPENDIX 1: The RDFs before and after the SRCs in 6FDA-DAM

APPENDIX 2: The RDFs before and after the SRCs in 6FDA-DPX

APPENDIX 3: Radial Distribution Function for Propane and Propylene

APPENDIX 1 : The RDFs before and after the SRCs in 6FDA-DAM
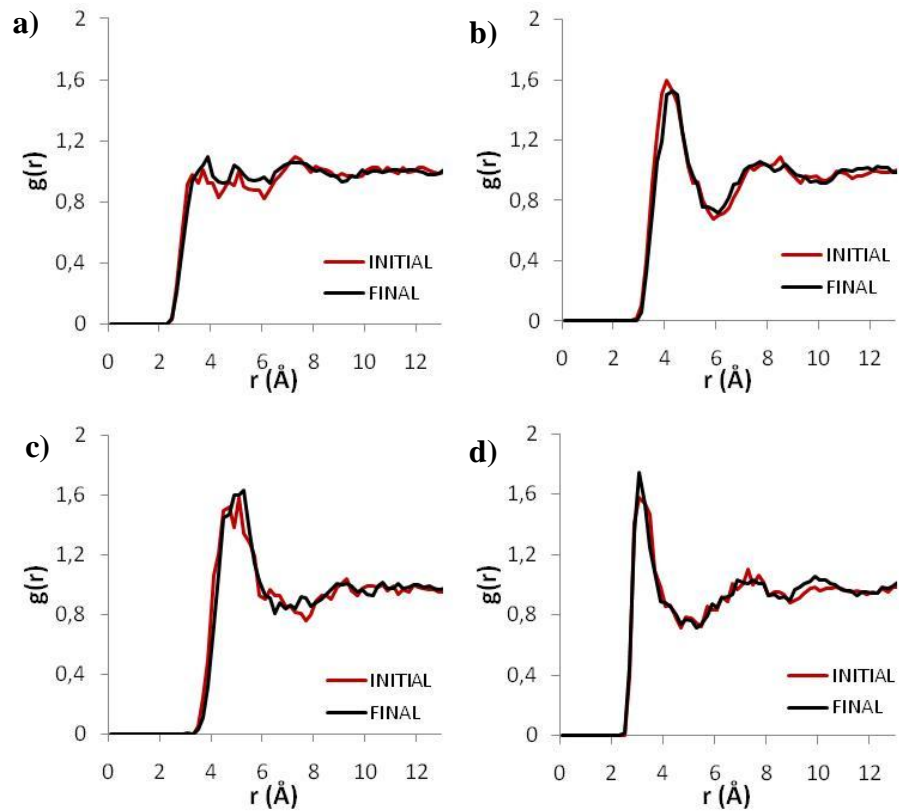
Figure A.1 : Radial distribution functions g(r) of CO_2 around a) F, b) C1, c) N1, and d) O1 atoms in 6FDA-DAM at the initial and final stages of the sorption process.

APPENDIX 2 : The RDFs before and after the SRCs in 6FDA-DPX
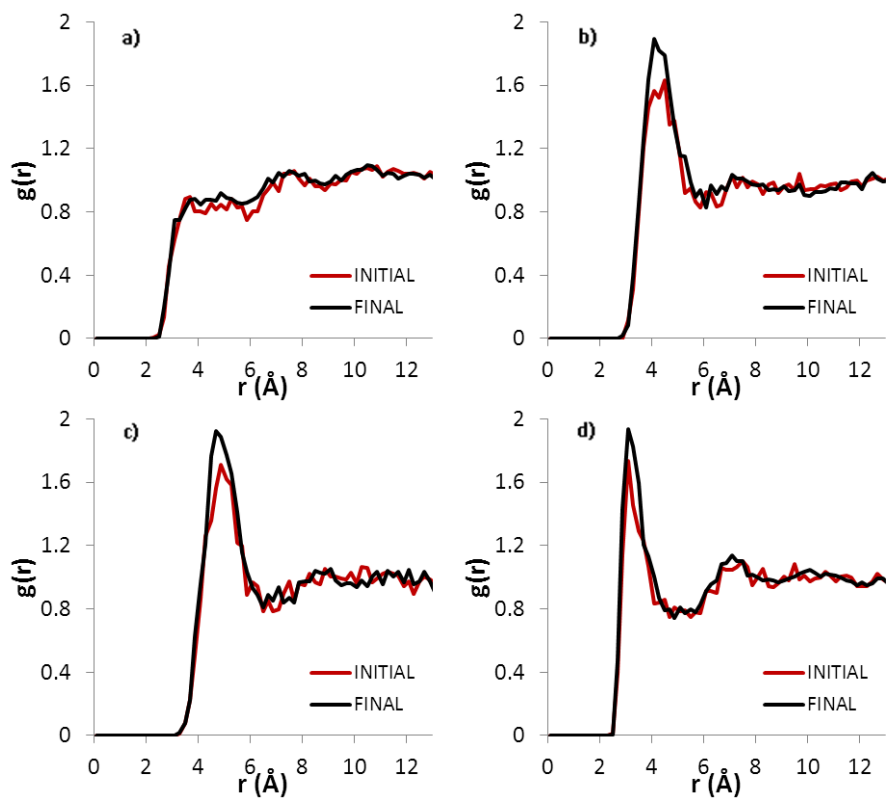
Figure A.2 : Radial distribution functions g(r) of CO_2 around a) F, b) C1, c) N1, and d) O1 atoms in 6FDA-DPX at the initial and final stages of the sorption process.

APPENDIX 3 : Radial distribution function for propane and propylene

The RDFs of pure propane (43 molecules/simulation cell) and propylene (72 molecules/simulation cell) around the four typical atoms such as the oxygen and nitrogen in the imide, the fluorine in the -CF$_3$ group, and the oxygen in the ether linkage (labeled as F1, N1, O1 and O2, respectively) in the saturated 6FDA-ODA are presented in Figure A.3. The RDFs show that the preferential sorption site for propane is the backbone N1 atoms, even though they are the least accessible, followed by the O1 and O2 sites; and F1 is the weakest sorption site. The position of the first peak of RDF around the O2 site indicates the access of propylene molecules to this site is also significantly restricted. On the other hand, the RDFs for propylene show that O1 and N1 sites have affinity to propylene with the O1 atoms being the most preferential sorption sites. Comparison of the RDFs belonging to the initial and final stages (Figure A.3, A.4) of the SRC procedure indicates that the propylene and propane molecules exhibit almost same and higher preference for all groups except F1 site on the backbone of 6FDA-ODA at the initial stage of the sorption, which may explain the substantial increase in the FFV and plasticization induced by both penetrants. However, at the final stage of the sorption, N1 site for propane and O1 site for propylene become most preferential sorption sites. From this result, one may conclude that, the change in propylene concentration and FFV will be much higher due to the interaction with more flexible site, O1, compared to N1 which is in the backbone.
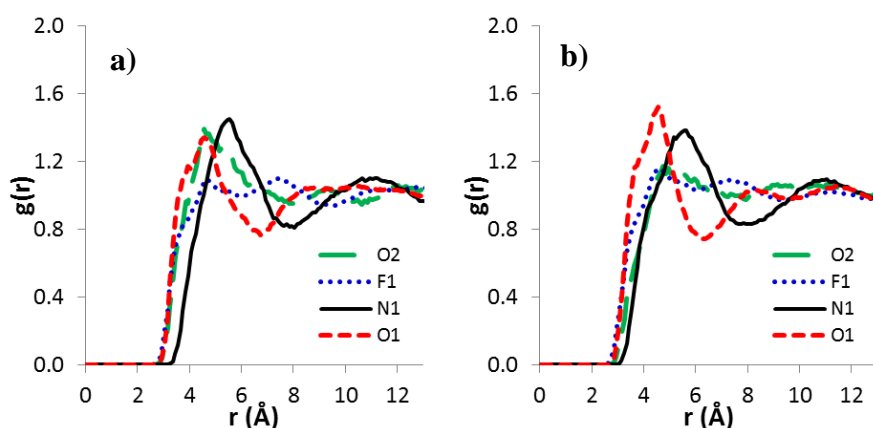
Figure A.3 : g(r) of **a)** propane and **b)** propylene (single gas) around sites of 6FDA-ODA for *final stages*.
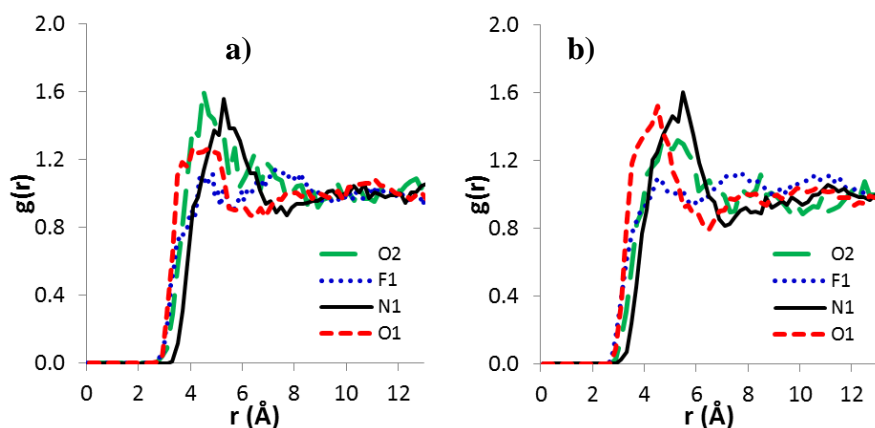
Figure A.4 : g(r) of a) propane and b) propylene (single gas) around sites of 6FDA-ODA for *initial stage*.

Figure A.5 shows the RDFs corresponding to the sorption of a binary mixture of propane and propylene (P_{C6H8}:P_{C6H6} = 50:50) in 6FDA-ODA, in which the simulation cell contains 18 propane and 28 propylene molecules. Comparison of RDFs of hydrocarbons belonging to the initial stages of the SRC procedure indicates that the propylene and propane molecules exhibit almost same affinity for all groups on the backbone of 6FDA-ODA. Moreover, O2 sites show slightly high performance compared to other sites for both penetrants. However, at the final stage of the mixed gas sorption, while the interaction between propylene and O2 site increases considerably, for propane instead of O2 site again N1 site take places as in single gas sorption measurements. The RDFs exhibit significant variation for both species with respect to pure component RDFs. The increased peak for propane in the RDF of the N1 site indicates the preferential occupation of these sites in the presence of propylene. Propylene, on the other hand, occupies more preferentially the O2 sites on the diamine moiety due to its smaller size, and to a lesser extent the N1 sites to the expense of the F1 sites on the dianhydride moiety, which is more favorable to propane. Since both penetrants affect the backbone atoms in 6FDA-ODA PI, the change in total FFV increase in mixed gas sorption measurements is nearly the same with single propane sorption measurements.
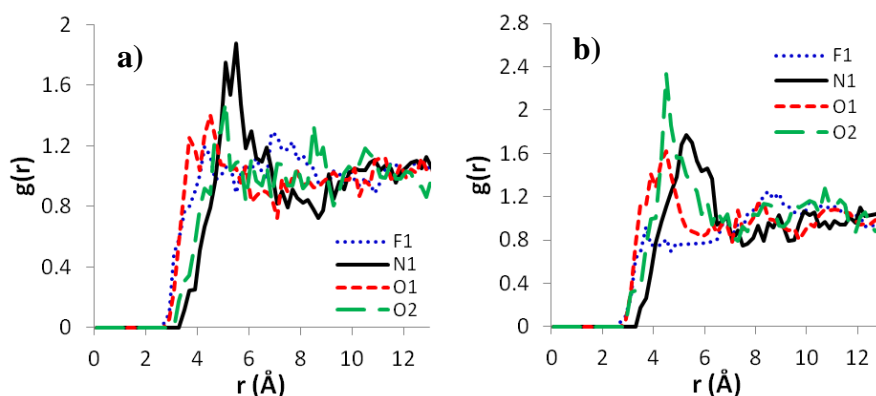
Figure A.5 : g(r) of a) propane and b) propylene (binary gas) around sites of 6FDA-ODA for *final stages*.
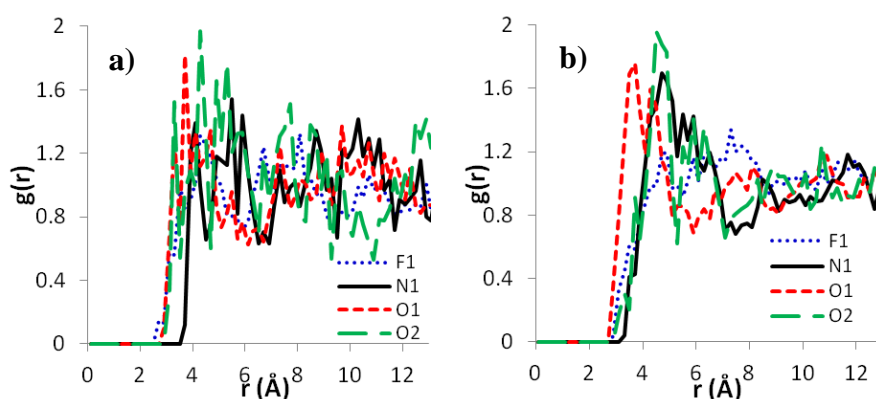
Figure A.6 : g(r) of a) propane and b) propylene (binary gas) around sites of 6FDA-ODA for *initial stages*.

The RDFs of pure propane (55 molecules/simulation cell) and propylene (70 molecules/simulation cell) around the O1, N1, F1, and C1 atoms of the 6FDA-DPX are shown in Figure A.7. The intensities of the peaks indicate that at the initial stage, the C1 atoms are the most preferential sorption sites for propane and propylene, followed by the N1 and O1 sites. Comparison of the RDFs belonging to the initial and final stages of the SRC procedure indicates that both propylene and propane molecules maintain their high preferences to the C1 sites at the final stage of the sorption. Moreover, there is little difference in N1 sorption site between propane and propylene, while the other sorption sites are almost same at the final stage of propane and propylene.
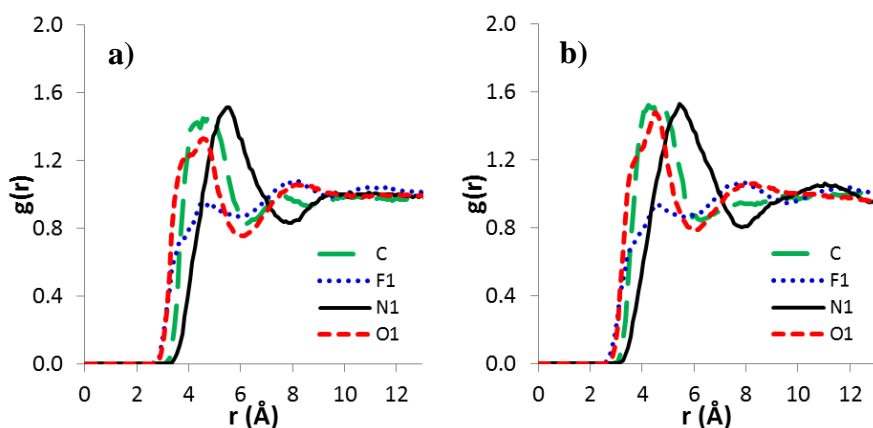
Figure A.7 : g(r) of a) propane and b) propylene (single gas) around sites of 6FDA-DPX for *final stages*.
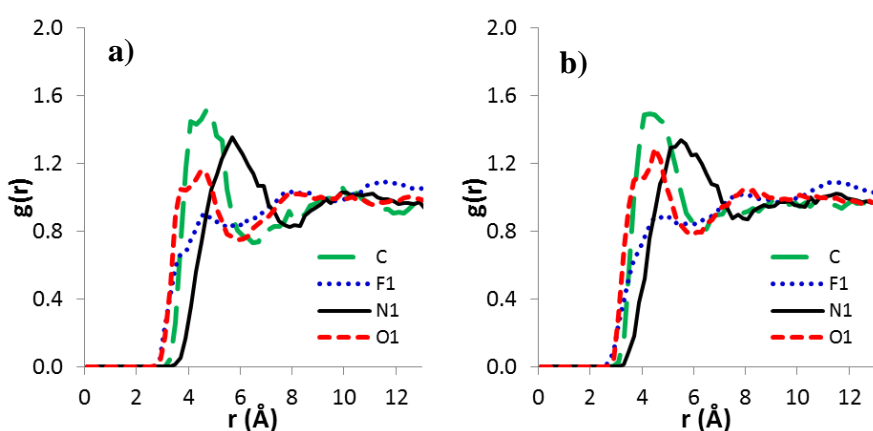
Figure A.8 : g(r) of a) propane and b) propylene (single gas) around sites of 6FDA-DPX for *initial stages*.

Figure A.9 shows the RDFs corresponding to the sorption of a binary mixture of propane and propylene (P_{C6H8}:P_{C6H6} = 50:50) in 6FDA-DPX, in which the simulation cell contains 21 propane and 42 propylene molecules. Comparison of the RDFs of penetrants belonging to the initial stage (Figure A.10) of the SRC procedure indicates that propane exhibits higher affinity for C1 and N1 sites compared to propylene. However, at the final stage of the mixed gas sorption, while propane interaction with adsorption sites (C1 and N1) decreases in the presence of propylene, propylene interaction increases compared to the single gas sorption measurements. One can conclude that propylene overshadows the affinity of propane molecules to the sorption sites in the mixed gas sorption condition. The RDFs do not exhibit significant variation for both species with respect to pure component RDFs. However, there is slight increase in propylene affinity to C1 site between the single and mixed gas sorption measurements, while the opposite situation is available for propane with the increased N1 affinity. Although the interaction of both penetrants

with sorption sites changes slightly between the single and mixed gas sorption in 6FDA-DPX PI, there is big difference in FFV increase.
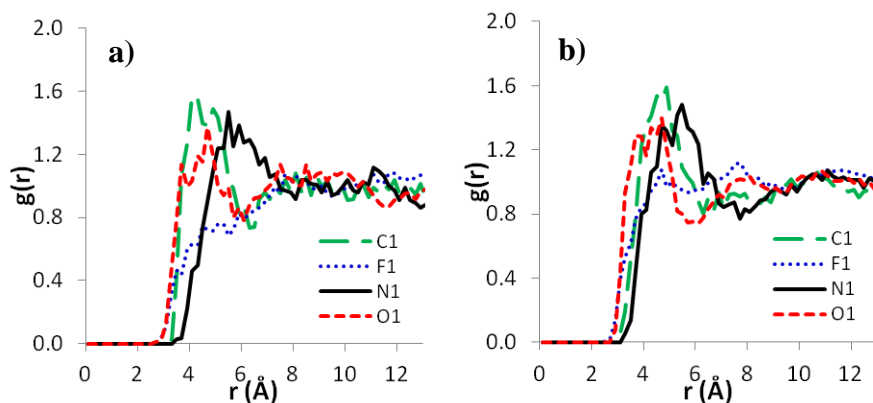
Figure A.9 : g(r) of a) propane and b) propylene (binary gas) around sites of 6FDA-DPX for *final stages*.
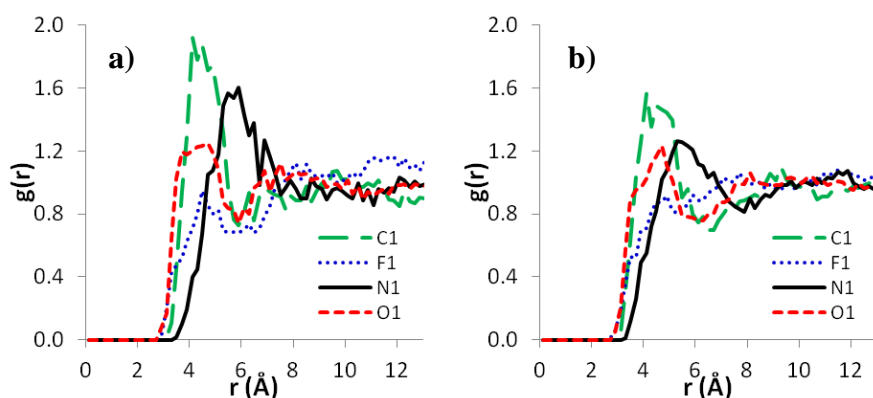
Figure A.10 : g(r) of a) propane and b) propylene (binary gas) around sites of 6FDA-DPX for *initial stages*.

The RDFs of pure propane (61 molecules/simulation cell) and propylene (92 molecules/simulation cell) around the O1, N1, F1, and C1 atoms of the 6FDA-DAM are shown in Figure A.11. The intensities of the peaks indicate that the N1 atoms are the most preferential sorption sites for propane and propylene, followed by the C1 and O1 sites, with the C1 and O1 atoms having relatively stronger affinity to propylene than propane. Moreover there is not any significant change in the RDFs of both hydrocarbons obtained in the initial and final stages (Figure A.11, A.12) of the SRC procedure, thus the site preferences of these hydrocarbons do not change with concentration. This may be explained by the higher rigidity of the 6FDA-DAM backbone and the limited rearrangement of the polymer chain due to increased concentration.
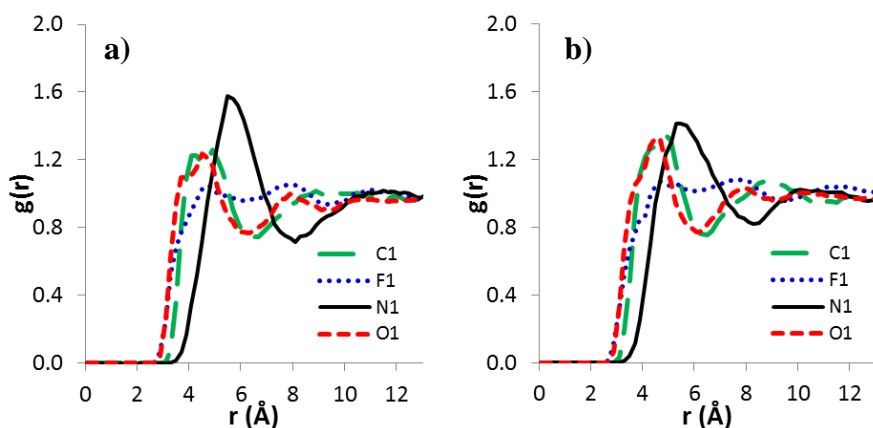
Figure A.11 : g(r) of a) propane and b) propylene (single gas) around sites of 6FDA-DAM for *final stages*.
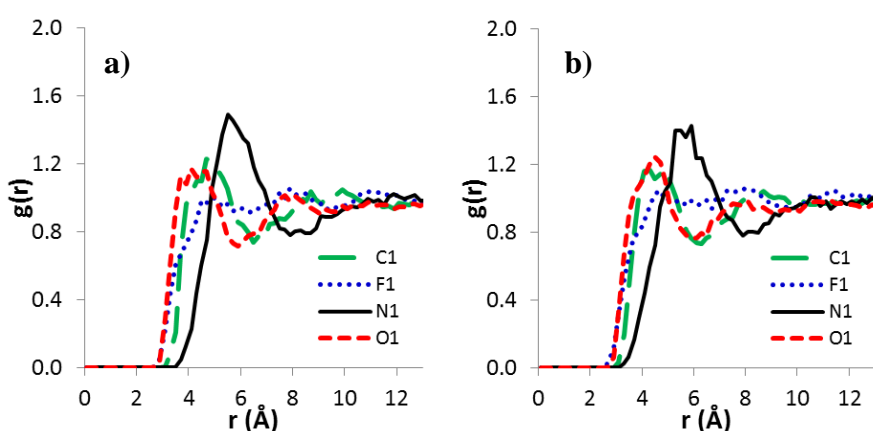
Figure A.12 : g(r) of a) propane and b) propylene (single gas) around sites of 6FDA-DAM for *initial stages*.

The RDFs for the binary mixture of propane and propylene ($P_{C6H8}:P_{C6H6}$ = 50:50) in 6FDA-DAM are presented in Figure A.13. The concentrations of propane and propylene at the simulated conditions are 27 and 56 molecules/simulation cell, respectively. The intensities of the peaks indicate that the N1 atoms are the most preferential sorption sites for both hydrocarbons at two stages. However there are some small changes in the intensity of other sorption sites. While the affinity of propane in the mixture increases for the O1 atoms with respect to initial stage, the affinity of propylene increases for C1 slightly. Additionally, the preference of the propane molecules for the F1 atoms is higher in the mixture with respect to propylene in the mixture as well as pure propane. In mixed gas sorption measurements of 6FDA-ODA PI, the affinity of propylene to the sorption site shifted from side groups (O1) to the backbone atoms (O2) and high FFV increase could not be observed. However, when the 6FDA-DAM PI is concerned, the affinity of hydrocarbons increased for side groups (C1, O1 and F1 as explained above) and did

not change for backbone atoms (N1). So in the mixed gas sorption measurements, the FFV increase are in the middle of the pure gas sorption measurements.
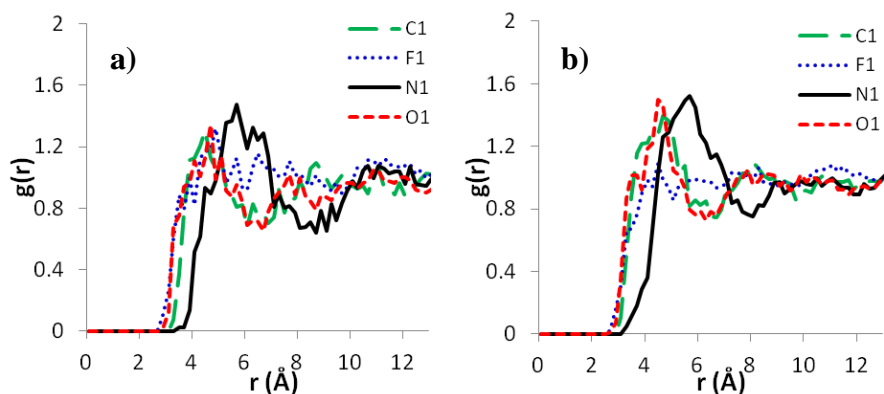
Figure A.13 : g(r) of a) propane and b) propylene (binary gas) around sites of 6FDA-DAM for *final stages*.
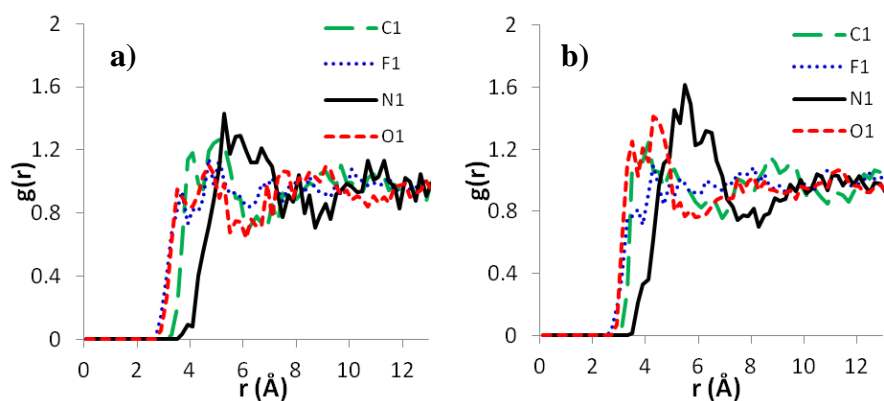
Figure A.14 : g(r) of a) propane and b) propylene (binary gas) around sites of 6FDA-DAM for *initial stages*.

CURRICULUM VITAE

Name Surname: Sadiye VELİOĞLU

Place and Date of Birth: ŞUMNU, 30.08.1982

E-Mail: sadiyehalitoglu@gmail.com, halitoglu@itu.edu.tr

EDUCATION:

BSc: Istanbul Technical University, Department of Chemical Engineering, Chemical Engineering Programme

MSc: Istanbul Technical University, Department of Advanced Technologies, Material Science and Engineering Programme

> **Advisors:** Prof. Dr. Birgül TANTEKİN-ERSOLMAZ &
>
> Assoc. Prof. Dr. Göktuğ AHUNBAY
>
> **Dissertation title:** Molecular Simulation of Polyimide Gas Separation Membranes.

PhD: Istanbul Technical University, Department of Material Science and Engineering, Material Science and Engineering Programme

> **Advisors:** Prof. Dr. Birgül TANTEKİN-ERSOLMAZ &
>
> Assoc. Prof. Dr. Göktuğ AHUNBAY
>
> **Dissertation title:** Investigation of Sorption Induced Plasticization in Polymeric CO_2 Separation Membranes

PROFESSIONAL EXPERIENCE

- **Teaching Assistant**
  [January 2009-December 2014]
  Istanbul Technical University, Faculty of Chemical and Metallurgical Eng., Dept. of Chemical Engineering, Maslak, Istanbul.

  Thermodynamics II, Mass Transfer, Mathematical Modelling in Chemical Engineering, Chemical Engineering Design II, Chemical Engineering Lab. I (Mass Transfer Experiment), Numerical Methods, Fluid Mechanics, Industrial Chemistry and Lab.

- **Internship**
  [June 2005-July 2005]
  Mercedes-Benz Türk A.Ş., Hosdere, Istanbul

- **Internship**
  [June 2004-July 2004]
  Atakoy ISKI Biological Treatment Plants, Atakoy, Istanbul

COMPUTER / LANGUAGE SKILLS

- Computer Operating Systems : MS Office, Linux, Windows.
- Programming Languages : Fortran, C, Matlab
- Chemical Engineering Design Program : ChemCad
- Molecular Simulation Programs : Accelrys Materials Studio 5, LAMMPS (Large-scale Atomic/Molecular Massively Parallel Simulator)

PROFESSIONAL EXPERIENCE AND AWARDS:

- *"Best Student Poster Presentation Award."* **Halitoğlu S.,** Ahunbay M. G., Tantekin-Ersolmaz S. B., Molecular simulation of the sorption behavior of gases in polyimide membranes, *Engineering with Membranes 2008*, Membrane Processes, 26 May 2008, Algarve, Portugal.

- "Scholorship" from "The Scientific and Technological Research Council of Turkey" (TUBITAK) for 2214/A International Doctoral Research Fellowship Programme. 6 months (25 August 2013 – 25 February 2014), Blaise Pascal Univeristy, Institute of Chemistry of Clermont-Ferrand, Thermodynamics and Molecular Interactions Laboratory, Clermont-Ferrand, FRANCE.

- *"Excellent Poster Award."* **Velioglu-Halitoglu S.,** Ahunbay M. G., Tantekin-Ersolmaz S. B., Simulation of propylene/propane plasticization in 6FDA-based polyimide membranes, *The 10th International Congress on Membranes and Membrane Processes, ICOM-2014,* 20-25 July 2014, Suzhou, China. (Poster Presentation)

PUBLICATIONS, PRESENTATIONS AND PATENTS:

- **Velioğlu S.,** Ahunbay M. G., Tantekin-Ersolmaz S. B., 2012: Investigation of CO_2-induced plasticization in fluorinated polyimide membranes via molecular simulation, *Journal of Membrane Science*, **417**, 217-227.

- **Sadiye Velioğlu,** S. Birgul Tantekin-Ersolmaz, Prediction of Gas Permeability Coefficients of Copolyimides by Group Contribution Methods. **DOI:10.1016/j.memsci.2015.01.012**

- **Sadiye Velioglu**, Xun Yao, Julien Devémy, M. Goktug Ahunbay, S. Birgul Tantekin-Ersolmaz, Alain Dequidt, Margarida F. Costa Gomes, Agílio A.H. Pádua, Solvation of a Cellulose Microfibril in Imidazolium Acetate Ionic Liquids: Effect of a Co-Solvent. The journal of physical chemistry B 12/2014; **DOI: 10.1021/jp508113a.**

- **S. Velioğlu**, M. G. Ahunbay, S. B. Tantekin-Ersolmaz, Investigation of Propylene/Propane Plasticization Effect Iin Polyimide Membranes via Molecular Simulation Methods. (**in preparation**)

- **S. Velioğlu,** M. G. Ahunbay, S. B. Tantekin-Ersolmaz, CO_2-Induced Plasticization in Copolyimides Containing a Sulfone Group. (**in preparation**)

- **S. Velioğlu**, M. G. Ahunbay, S. B. Tantekin-Ersolmaz, "Why TR polymers does not plasticize?" : Investigation of CO_2 Sorption-Induced Plasticization in Thermally Rearranged (TR) Polymers. (**in preparation**)

INTERNATIONAL CONFERENCES ATTENDED AND ABSTRACTS PUBLISHED IN THE PROCEEDINGS

- **Halitoğlu S.,** Tantekin-Ersolmaz S. B., Prediction of gas permeability coefficients of copolyimides by group contribution methods, May 12-16 2007, NAMS (North American Membrane Society), Orlando, Florida, USA. (Poster Presentation)

- **Halitoğlu S.,** Ahunbay M. G., Tantekin-Ersolmaz S. B., Molecular simulation of the sorption behavior of gases in polyimide membranes, Engineering with membranes 2008, Membrane processes, 26 May 2008, Algarve, Portugal. (Poster Presentation)

- **Halitoğlu S.,** Ahunbay M. G., Tantekin-Ersolmaz S. B. Synthesis, Gas Permeability, and Molecular Simulation of Copolyimide Membranes Containing Sulfone Groups, North American Membrane Society (NAMS) 2009, June 20-24, 2009, Charleston, South Carolina, USA. (Poster Presentation)

- **Halitoğlu S.,** Ahunbay M. G., Tantekin-Ersolmaz S. B., Molecular simulation of the sorption behavior of gases in copolyimide membranes, Euromembrane 2009, September 6-10, 2009, Montpellier, France. (Poster Presentation)

- **Halitoğlu S.,** Ahunbay M. G., Tantekin-Ersolmaz S. B., Synthesis, characterization, and molecular simulation of 6FDA/BTDA-pBAPS copolyimide membrane for CO_2/CH_4 separation, Euromembrane 2009, September 6-10, 2009, Montpellier, France. (Oral Presentation)

- Erpek E., Ozkale B. A., **Halitoğlu S.,** Atalay-Oral C., Ahunbay M. G., Tantekin-Ersolmaz S. B., Polymer-zeolite-additive three-component mixed matrix composite membrane for CO_2/CH_4 separation, Euromembrane 2009, September 6-10, 2009, Montpellier, France. (Oral Presentation)

- **Halitoğlu S.,** Kabacaoğlu I., Ahunbay M. G., Tantekin-Ersolmaz S. B., Assessment of Structure-Solubility Relationship for Copolyimide Gas Separation Membranes via Molecular Simulation, AIChE 2010, Minneapolis, MN, November 7-12, Salt Lake City, UT. (Oral Presentation)

- **Halitoğlu S.,** Ahunbay M. G., Tantekin-Ersolmaz S. B., Investigation of Propylene/ Propane Plasticization Effect in Polyimide Membranes via Molecular Simulation Methods, ICOM 2011, Amsterdam, July 23-29. (Oral Presentation)

- **Halitoğlu S.,** Ahunbay M. G., Tantekin-Ersolmaz S. B., Investigation of CO_2-induced plasticization in Sulfone Group Containing Copolyimides via Molecular Simulation, ICOM 2011, Amsterdam, July 23-29. (Poster Presentation)

- Avci A. H., Hoppenbrouwer F., **Halitoğlu S.,** Ahunbay M. G., Tantekin-Ersolmaz S. B., Mixed-Gas Permeation and CO_2 Plasticization Behavior of Ternary Mixed-Matrix Membranes, ICOM 2011, Amsterdam, July 23-29. (Poster Presentation)

- **Velioğlu S.,** Kabacaoğlu I., Ahunbay M. G., Tantekin-Ersolmaz S. B., Residual Solvent Effect on CO_2-Induced Plasticization of Polyimide Membranes, AIChE 2011, Minneapolis, MN, October 20, Salt Lake City, UT. (Oral Presentation)

- **Velioğlu S.,** Ahunbay M. G., Tantekin-Ersolmaz S. B., Residual Solvent Effect on CO_2-Induced Plasticization of Polyimide Membranes, 12 American Institute of Chemical Engineers (AIChE) Annual Meeting, Pittsburgh, PA, USA October 28- November 3, 2012. (Oral Presentation)

- **Velioğlu S.,** Ahunbay M. G., Tantekin-Ersolmaz S. B., CO_2-Induced Plasticization in Copolyimides Containing a Sulfone Group, 12 American Institute of Chemical Engineers (AIChE) Annual Meeting, Pittsburgh, PA, USA, October 28- November 3, 2012. (Poster Presentation)

- **Velioğlu S.,** Ahunbay M. G., Tantekin-Ersolmaz S. B., Simulation of Propylene/Propane Plasticization in 6FDA-Based Polyimide Membranes. 13 American Institute of Chemical Engineers (AIChE) Annual Meeting, San Fancisco, CA, USA, November 3-8, 2013. (Oral Presentation)

- **Velioğlu S.,** Ahunbay M. G., Tantekin-Ersolmaz S. B., Investigation of CO_2 Sorption-Induced Plasticization in Thermally Rearranged (TR) Polymers via Molecular Simulation Methods, 13 American Institute of Chemical Engineers (AIChE) Annual Meeting, San Fancisco, CA, USA, November 3-8, 2013. (Poster Presentation)

- Padua A. A. H., **Velioglu S.,** Devemy J., Andanson J. M., Costa-Gomes M. F., Cellulose in ionic liquids: Dissolution experiments in the presence of a co-solvent and solvation of a microfibril by molecular simulation, 248th ACS National Meeting, San Francisco, CA, USA, August 10-14, 2014. **(Invited talk, presented by Padua A. A. H)**

- **Sadiye Velioglu,** Xun Yao, Emilie Bordes, Julien Devemy, Jean-Michel Andanson, Margarida F. Costa Gomes, Agilio A.H. Padua, The solvation of cellulose in ionic liquids: experiments and simulation of a microfibril, ILSEPT - 2nd International Conference on Ionic Liquids in Separation and Purification Technology, The Westin Harbour Castle, Toronto, Canada, June 29 – July 2, 2014. **(Keynote lecture, presented by Padua A. A. H)**

- **Velioglu-Halitoglu S.,** Ahunbay M. G., Tantekin-Ersolmaz S. B., Investigation of Propylene/ Propane Plasticization Effect in Polyimide Membranes via Molecular Simulation Methods, ICOM 2014, Suzhou, China, July 20-25, 2014. (Poster Presentation)

- **Velioglu-Halitoglu S.,** Ahunbay M. G., Tantekin-Ersolmaz S. B., Prediction of plasticization resistance of 6FDA-based polyimide membranes via molecular simulation, ICOM 2014, Suzhou, China, July 20-25, 2014. (Oral Presentation)

- Marcel Balçık, **Sadiye Velioğlu,** M. Göktuğ Ahunbay, S. Birgül Tantekin-Ersolmaz, CO_2-Induced Plasticization in Copolyimides Containing a Sulfone Group, 14 American Institute of Chemical Engineers (AIChE) Annual Meeting, Atlanta, USA, November 16-21, 2012. (Oral Presentation)

NATIONAL CONFERENCES ATTENDED AND ABSTRACTS PUBLISHED IN THE PROCEEDINGS

- **Halitoğlu S.,** Tantekin-Ersolmaz S. B., Kopoliimid membran malzemelerinin gaz geçirgenliklerinin grup katkısı yöntemi ile teorik olarak hesaplanması, 7th National Chemical Engineering Congress, 5 September 2007, Eskisehir, Turkey. (Poster Presentation)

- **Halitoğlu S.,** Ahunbay M. G., Tantekin-Ersolmaz S. B., April 24-25 2008, 8th Chemical Physics Congress, Istanbul, Turkey. (Poster Presentation)

- **Halitoğlu S.,** Ahunbay M. G., Tantekin-Ersolmaz S. B., Poliimid Membranlarda Gaz Adsorpsiyonunun Moleküler Düzeyde Modellenmesi, 8th National Chemical Engineering Congress, 26-29 August 2008, Malatya, Turkey. (Oral Presentation)

- **Halitoğlu S.,** Tantekin-Ersolmaz S. B., Ahunbay M. G., Screening Copolyimide Gas Separation Membranes via Molecular Simulation, 5.Ulusal Nanobilim ve Nano Teknoloji Konferansı (5th National Nanoscience and Nano Technology Conference) 2009, 8-12 June 2009, Eskisehir, Turkey. (Poster Presentation)

- **S. Halitoglu-Velioglu,** M. G. Ahunbay, S. B. Tantekin-Ersolmaz, "Screening Copolyimide Gas Separation Membranes via Molecular Simulation", EMCC-6, Antalya, Türkiye, 7-12 March 2010. (Poster Presentation)

- **Velioğlu S.,** Ahunbay M. G., Tantekin-Ersolmaz S. B., Sülfon Grubu İçeren Kopoliimid Membranlarda CO_2 Plastizasyonunun İncelenmesi, 10th National Chemical Engineering Congress, Istanbul, September 3-6, 2012, Turkey. (Oral Presentation)

- **Velioğlu S.,** Ahunbay M. G., Tantekin-Ersolmaz S. B., Poliimid Gaz Ayırma Membranlarının Plastizasyon Direncinin Moleküler Simülasyon Yöntemleriyle Belirlenmesi, 11th National Chemical Engineering Congress, Eskişehir, September 2-5, 2014, Turkey. (Oral Presentation)

TRAINING COURSES ATTENDED:

- Nanostructured Materials and Membrane Modeling and Simulation Course, FORTH/ICE-HT, 18-27 June 2008, Patras, Greece. (http://ina.unizar.es/cursos/EF2%20leaflet.pdf)

- Collaborative Computational Project (CCP5) Summer School 2009, 5-14 July 2009, Sheffield, England. (http://www.cecam.org/workshop-890.html)

- TUBITAK 2237, Proje Hazırlama, Yazma ve Yürütme Eğitimi, Antalya 2014, 24-26 October 2014.

INSTRUMENTAL ANALYSIS EXPERIENCE:

Experienced in the use of:
- Gel Permeation Chromatography (GPC)
- Scanning Electron Microscopy (SEM) (JEOL JSM-6390LV)
- Intelligent Gravimetric Analyser (IGA) (Hiden Isochema, UK)
- Fourier Transform Infrared Spectroscopy (Perkin-Elmer Spectrum One)
- Thermo-Gravimetric Analysis (TGA) (Perkin-Elmer Diamond TG/DTA)
- Differential Scanning Calorimetry (DSC) (Perkin-Elmer 4000 Series)
- Dynamic Mechanical Analysis (DMA) (Perkin-Elmer Diamond)
- Constant - volume variable - pressure single and mixed gas permeability measurements.